LASER CLADDING

BY

JOHN POWELL B.Sc. M.Sc.

A THESIS PRESENTED FOR THE DEGREE OF DOCTOR OF PHILOSOPHY OF THE UNIVERSITY OF LONDON.

J. PERCY RESEARCH GROUP
DEPT. OF METALLURGY
IMPERIAL COLLEGE OF SCIENCE
AND TECHNOLOGY
LONDON SW7.

1983.

CONTENTS

CHAPTER 4 PRE PLACED POWDER CLADDING

CHAPTER 5

The Blown Powder Cladding ,Cladding-Surface Alloying ,of Exhaust Valves

VIBRO LASER CLADDING

CHAPTER 7

SUMMARY

APPENDICES

ABSTRACT

The new subject of laser cladding is investigated. The important processing parameters governing the morphology and quality of metal clad deposits on metal substrates are identified both theoretically, and in practice. Cladding metal is either preplaced on a substrate as a powder prior to laser irradiation or blown, in powder form, into a laser produced weld pool on the substrate surface. Cracking and porosity in clad deposits was reduced by ultra sonic vibration of the substrate (now a patented process). The direction for future work is indicated and commercial viability is investigated.

CHAPTER 1

AIMS AND OBJECTIVES OF THIS WORK

1.1. INTRODUCTION

The coating or cladding of one metal or alloy with another is an important aspect of industrial metallurgy. The benefits of tailoring material combinations to any given application are numerous and, of course, include corrosion protection and improved erosion and wear resistance.

The laser is a relatively new industrial tool which is capable of producing a hot spot on the surface of a material which, according to the operating parameters can be used as an energy source for heat treatment, welding or cutting.

The aim of this present work is to investigate the mechanisms involved in welding a new surface onto a substrate using a high power laser as the energy source. This process, laser cladding, is of great interest to industry and has already found industrial application even in the absence of a thorough understanding of how the laser-substrate-cladding metal interactions create the finished product.

1.2 METHODS OF LASER CLADDING

The two methods of laser cladding investigated in this work are:

A. Pre placed powder cladding: A set amount of the cladding metal powder is placed on a substrate and the laser beam with a chosen energy density distribution travels over the powder,

melting it and welding it to the surface of the substrate.

B. Blown on powder cladding: Cladding metal powder is continuously blown into a weld pool created on the surface of the substrate by the impingment laser beam. This powder is melted and incorporated into a surface weld.

Both methods have been tried in industry with varying degrees of success and it is obvious that a deeper understanding of the mechanisms will facilitate the application of either process to future engineering problems. This thesis attempts to identify the effects of the various process variables upon the quality of the clad surface. This analysis involves a combination of theoretical and practical results and the completion of this initial investigation should pave the way towards an optimisation of the process in future applications.

1.3 AIMS AND OBJECTIVES

The aims and objectives of this thesis are ennumerated below with indications showing where the various aspects are tackled in the text.

1. The completion of a literature survey covering the various aspects of laser surface treatments (chapter 2 and appendix A) and the major competitive cladding processes (appendix G).
2. The development of theoretical models of both pre placed and blown on powder cladding and the laser-material interactions involved (chapter 3).
3. An investigation into the effect of the processing parameters on the quality of the clad deposit for both processes,

(Quality refers to porosity, cracking, dilution and morphology), (Chapter 4 and 5).

4. After identification of the flaws possible in a deposit and the reasons therefore, develop methods to reduce their likelihood (Chapter 6 appendices B, C and F).

It is of course impossible to cover all the ground in one thesis but many major points are covered and the direction to be taken by new work is made clear.

CHAPTER TWO

LITERATURE SURVEY

2.1. INTRODUCTION

The literature survey which follows begins with an explanation of laser physics and the basics of laser-material interactions. A subject as new as laser cladding requires this basic introduction to facilitate the readers' understanding of the points raised later. There follows an indepth review of the small amount of previous work on laser cladding. Laser cladding itself is compared and contrasted with closely associated techniques. If the reader requires further information about non laser cladding in order to put laser cladding into context, a full review of competitive techniques is included in this thesis as Appendix G .

2.2. CARBON DIOXIDE LASERS AND THEIR INTERACTIONS WITH MATERIALS

2.2.1 THE PHYSICS OF CO_2 LASERS

2.2.1.1 GENERAL

The word laser is an acronym for 'Light Amplification by the Stimulated Emission of Radiation'. A triatomic

molecule such as CO_2 has several meta-stable excited vibrational states in which it can exist under the correct energy conditions and it is the relaxation of the molecule from such an energy state to a more stable condition which results in a photon of energy being emitted. Figure 2.1 shows the three major vibrational modes of the CO_2 molecule, a large number of quantised possible transitions exist over the band 9μm - 11μm with a mean value of approximately 10.6μm (31). The particular vibrational state of a molecule is designated by three integral numbers. The first number is the quantum level or excitation number of the symmetric mode; the second number is the excitation number of the bending mode; and the third number is the excitation number of the asymmetric mode. Only the energy levels of the pure modes are given in Fig 2.1, but all of the mixed vibrational states are further subdivided into series of levels due to the gross rotation of the vibrating molecule. These levels are also quantised and are designated by J, the rotational quantum number.

2.2.1.2. STIMULATED EMISSION AND POPULATION INVERSION

Stimulated emission is the reverse process of the absorption which is the more usual result of a photon impinging upon an atom or molecule. In the case of stimulated emission the incoming photon induces a downward energy transition in the molecule which liberates a further photon (See Fig 2.1). In order that this stimulated photon emission becomes the dominant feature of the photon - molecule interactions it is necessary that the gas (in this case) is in the thermodynamically unusual state

FIGURE 2.1

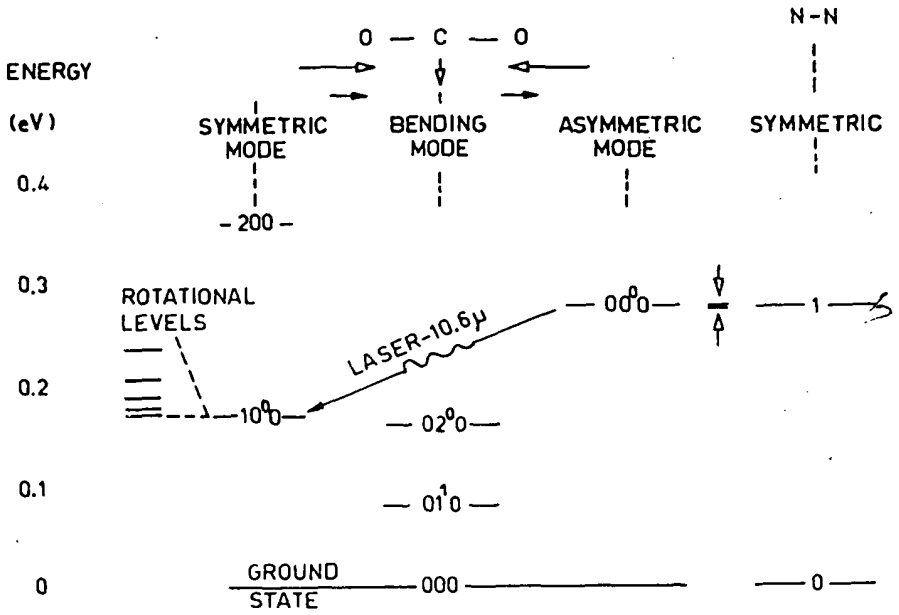

Energy levels diagram of the CO_2 - N_2 - system

FIG·2.2.

Non Lasing to Lasing

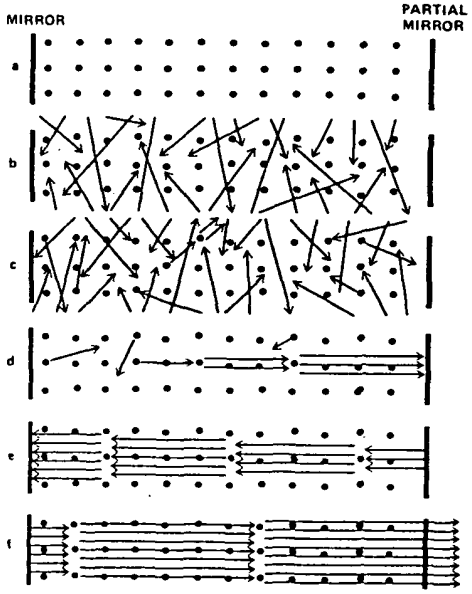

referred to as population inversion.

One of the precepts of the laws of thermodynamics is that for a temperature T, the distribution of the population of gas molecules between the two energy states E and $E + \Delta E$ is given by:

$$\frac{P(E + \Delta E)}{P(E)} = e^{-\Delta E / KT}$$

ie the majority of a population of molecules at temperature T will be in the lowest of two possible energy states.

Under certain conditions, in this case inside an electric discharge, it is possible to arrange matters so that the majority of molecules are in the higher, meta-stable energy state. This 'population inversion' is a necessary feature of a system within which a 'lasing' action is to operate.

2.2.1.3. THE ROLE OF N_2 AND He IN A CO_2 LASER

The excitation of CO_2 molecule by direct electron impact within the arc is a rather inefficient process and it is a combination of this direct energy trasnmission and the indirect excitation of CO_2 by means of collision with electrically excited N_2 which makes the production of high power CO_2 lasers possible. In a typical glow discharge about 15% of the electron energy goes into pumping the CO_2 upper laser level directly and up to 85% goes into pumping the various vibrational levels of N_2 (32). The upper N_2 levels then act as an energy reservoir which collisionally couples energy into the CO_2 (001) lasing level via the

first vibrational N_2 level as indicated in Fig21.

To extract this stored energy with high efficiency it is important that the 100/020 lower lasing levels should not be heavily populated, and He is often used in the lasing gas mixture to enhance their collisonal depopulation to the ground state. At high discharge powers however, it becomes difficult to ensure that the gas temperature remains below about 500^{o} K to avoid excessive thermal population of these lower levels. At powers below IKW this waste heat disposal problem is adequately dealt with by passing the discharge gas along the optical cavity relatively slowly but the total discharge length must be long, because the laser output is limited to about 45 Wm^{-1}. In industrial lasers the overall length of such devices is kept manageable by 'folding' the discharge tube and using appropriate mirrors to keep the laser discharge aligned with the tube. When the gas flow is increased to near sonic velocities the laser power generated per metre of discharge increases dramatically. (The 2KW control laser machine used in this work has gas flow velocities of up to 500 m/s). Commercial machines using this fast axial flow system are available with powers ranging from 500W to 6KW, the specific output power being approximately 500 Wm-1. The reason why fast axial flow lasers achieve higher outputs than the similar slow axial flow machines is because the waste heat dissipation method changes from conduction in the slow flow case to convection in the fast flow case.

2.2.1.4. LASER OPTICS AND THEIR EFFECT ON THE STIMULATED EMISSION IN THE ARC

The laser cavity is the name given to describe the glass tubes and water cooled gold plated copper mirrors which contain the laser discharge. Materials such as germanium, gallium arsenide, cadmium telluride, zinc selenide and sodium or potassium chloride are transparent to the laser radiation emitted by CO_2 lasers (wave length 10.6μm) and can be used to transmit or focus the beam. The mirror at one end of the optical cavity is partially transparent to the beam to allow it to be used. (In the case of the control laser machine used in this work the'output window' is made of ZnSe which has a reflectivity of about 35% for 10.6μm radiation.)

The build up of stimulated emission to produce a coherent laser beam within the optical cavity is shown in Fig 2.2. Initially spontaneous random emissions occur. Those whose direction is along the axis of the laser have the longest path length in the laser medium and are more likely to stimulate further emission.

This is turn is amplified by the mirrors at either end of the laser cavity.

2.2.1.5. PULSED CO_2 LASERS

Although high power CO_2 lasers are most commonly used as continuous output machines the output can be pulsed, that is to say the electrical discharge is alternately switched off and on to produce an intermittant output of regulated high power pulses. The peak power of each pulse is greater

than the mean power achieved by a continuous beam but the overall power output is governed by the pulse shape, width (or duration) and the pulsing rate. Typical values for pulsing a normally 5KW(cw) machine are (32):

Power	=	10^5 W peak, 100 W average
Pulse length	=	10-100m sec
Pulse rate	=	up to 100 pps

Work in the field is still at an early stage and application advantages are under investigation.

Pulses can em it energies because the laser gas is cold and therefore more efficient, also there is an electrical surge when the lasing arc is struck.

2.2.2. FUNDAMENTALS OF LASER-SOLID INTERACTIONS

The basic and dominent physical mechanism of laser interaction with absorbing media is heating. The temperature rise is determined by the laser power, interaction time, absorption co-efficient, specific heat and thermal diffusivity. (33). In metals, light is absorbed by interaction with electrons. A quantum of optical energy is absorbed by an electron, which is raised to a higher energy state in the conduction band. The excited electrons collide with lattice phonons and with other electrons to give up their energy. These collision processes govern the transfer of heat within the material.

There are three regimes of laser-material interaction, listed in order of ascending power input as:

a) Heating with no melting.
b) Heating with a solid-liquid phase change

c) Heating with a solid-liquid phase change combined with plasma formation

The power input to the surface of a component during laser irradiation is often described by the useful compound parameter P/VD where;

P = Laser beam power
V = The laser spot-workpiece relative velocity
D = Laser spot diameter on the workpiece surface

Basically, if the value of P/VD is increased then the effect of the laser beam on the material is more profound, although the actual relationship between the two can be complex.

In this and all subsequent discussion in this work the only thermal regime to be discussed will be: b/ heating with a solid-liquid phase change.

The physics of the laser-material interaction is different for each regime but types 'a' and 'c' are not directly relevant to the field of laser cladding or surface alloying.

The reflectivity of all metals at ambient temperatures is high in the long infrared. For wavelengths greater than 5μm, almost all metals have a reflectivity greater than 90% (34). At wavelengths greater than 5μm, the reflectivity is dependent on the electrical conductivity. Metals with high electrical conductivity have the highest values of infrared reflectivity.

The amount of light absorbed by a metallic surface is proportional to 1-R, where R is the reflectivity.

At the CO_2 laser wavelength of 10.6μm, where R is close to unity, 1-R becomes small which means that only a small fraction of the incident energy is absorbed and is available for melting.

The differences in values of 1-R are important in the context of the CO_2 laser metalworking. For silver or copper the value of 1-R for 10.6μm radiation is approximately 0.02 at ambient temperatures. The comparable figure for steel is 0.05 which accounts to some extent for the comparitive ease with which steel is melted compared to copper or silver. At the shorter wavelengths attained by Nd:YAG lasers (1.06μm) the value of 1-R for steel is approximately 0.35 which indicates a seven fold increase in initial absorption and therefore these lower powered machines can in some cases compete with the multikilowatt CO_2 machines.

The reflectivity of metals decreases with heating from the initial very high values already mentioned to a low value comparable with that of a black body when considering a typical weld pool with its pool of molten metal covered by a cloud of vapour. The importance of these considerations will become apparent in Chapter 3 which deals with a theoretical analysis of the subject.

2.2.3. TYPES OF CO_2 LASERS

The major differences in CO_2 laser system designs are those due to the differences in the arrangements of the

electrical excitation unit and the gas flow direction relative to the optical axis.

Duley (1976) (35) listed the various system design arrangements as follows:

1) The axial system: In this case, the electrical field (ie the direction of electrical discharge) is co axial with the optical axis which is the same as the gas flow direction.

2) Transverse Discharge system: The gas flow direction is the same as the electrical discharge direction and this direction is perpendicular to the optical axis.

3) Transverse Gas Flow System: The optical axis coincides with the electrical discharge axis which is perpendicular to the gas flow direction.

4) Transverse Gas and Transverse Discharge: The optical axis the gas flow axis and the electrical discharge axis are mutually orthogonal (ie they each follow one of the XY or Z axis with respect to each other.)

The laser system used throughout this work was a fast axial 2KW CO_2 laser supplied by Control Laser Limited (formerly BOC Limited Industrial Power Beams Division).

The lasers can be used in either the continuous wave or the pulsed mode.

2.3. LASER APPLICATIONS

2.3.1. LASER SURFACE TREATMENTS

Laser surface treatments at present under investigation for commercial use include:

a) Transformation hardening.

b) Surface homogenisation.

c) Laser glazing.

d) Cladding.

e) Surface alloying.

A general view of these subjects was the subject of a recently published paper co written by the present author and Dr W M Steen. This paper has been included in this thesis as appendix A.

Further discussion would involve going into the subjects in depth which would be inappropriate and would render this literature review unduly bulky.

2.3.2. LASER CLADDING AND CLOSELY ASSOCIATED TECHNIQUES

2.3.2.1. LASER CLADDING

In order to distinguish between laser cladding and other methods of producing a new surface on a substrate using a laser, it is necessary to include here an appropriate definition of laser cladding. The definition has to be approximate because laser cladding overlaps in many respects

with such techniques as laser surface alloying and laser vapour deposition. As a basic guideline then, laser cladding can be said to be; the laser fusing of a cladding material to a substrate producing a substantial ($\sim$.5mm+thick) deposit with a low level of substrate-deposit dilution ($\leq$10%). The usual form the cladding material takes is a metallic powder and, in general, the substrate is a metal block with surface properties inferior to those required. The very fact that a weld must exist between the two means that an amount of substrate-deposit dilution is concomitant with the process but this is generally regarded as a drawback as it often results in a reduction in effectiveness of the finished product (except in cases where this dilution is planned = see the section on laser surface alloying).

Published material dealing specifically with aspects of laser cladding is scarce, although reference to it as a viable process is usually made in general papers on laser processing, eg (36) (37) (38) (39).

The first patent relating to the process (40) was initially filed in the USA, by the Caterpillar Tractor Company. This patent claims the invention of 'a method for fusibly bonding a substantially solid powder coating material to a metal article' by 'depositing a band of powder onto a surface of the metal article; rapidly melting said coating material and said surface of the metal article by focusing a continuous wave laser beam thereon' to provide 'a solidified surface layer having properties based on said coating material with a thin region of interstitched bond between it and the metal article'. The application example cited is one which has aroused a great deal of interest in laser cladding from an industrial point of view; that of the

cladding of the wear surface of engine valves. The method in this case was to continuously pre-place the cladding powder on the surface to be clad as the valve was rotated under the laser beam (see Fig2.3). Valves of austenitic chrome nickel silicon steel were clad with Stellite 6, a cobalt based hard facing alloy. The results quote an example of a valve clad to a depth of 1.27mm with a uniform cross section and an excellent interstitched bond. The electron probe results shown in figure compare the dissolution gradient of a laser clad valve and a gas welded valve. In the case of the laser clad specimen, the smoothness of the trace indicates the fine grain structure of the coating and the narrow interfacial dilution zone is clearly shown. In the case of the gas welded specimen the interstitched bond is approximately 0.5mm thick which compares poorly with the laser clad specimen with a bond thickness of 0.05mm approximately. Iron from the steel embrittles and reduces the oxidation resistence of stellite 6 and dilution is therefore to be avoided. Another disadvantage of the gas welded sample is shown by the coinciding peaks and valleys in the Cr, Co and C scan lines. This effect is indicative of the presence of large crystals, such as chromium carbides produced by the high heat input and slow cooling rates associated with gas welding. The hardness of the laser clad deposit was found to be Rc 65-67 as compared to the gas welded deposit readings of Rc 62-65, this being another point in favour of the laser cladding process. Finally, the authors of the patent claim that 'by utilising the manufacturing method of the present invention to apply the hard alloy layer on the engine valve, the hard facing portion of the cost of the valve can be reduced to approximately half that of gas welding techniques'.

Fig - 2.3. Laser cladding
(Caterpillar tractor Co)

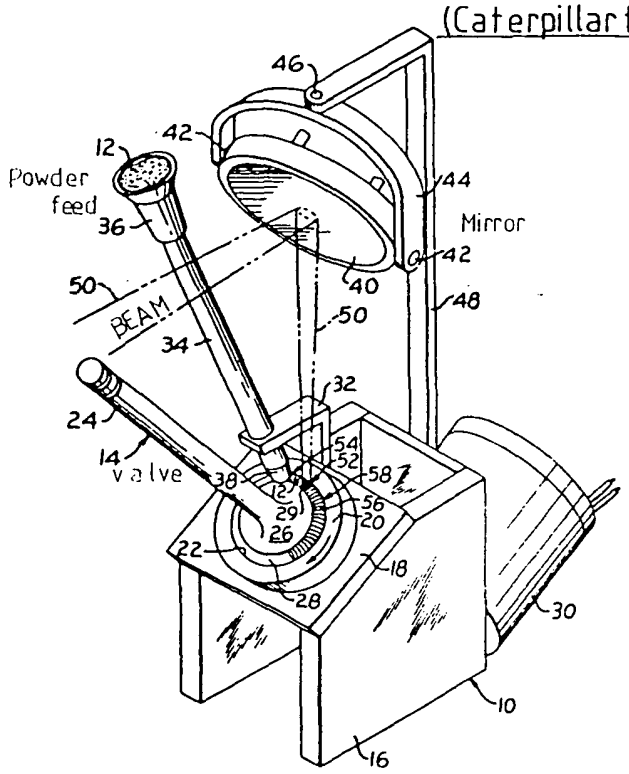

FIGURE. 2.4.
Laser cladding (Rolls Royce)

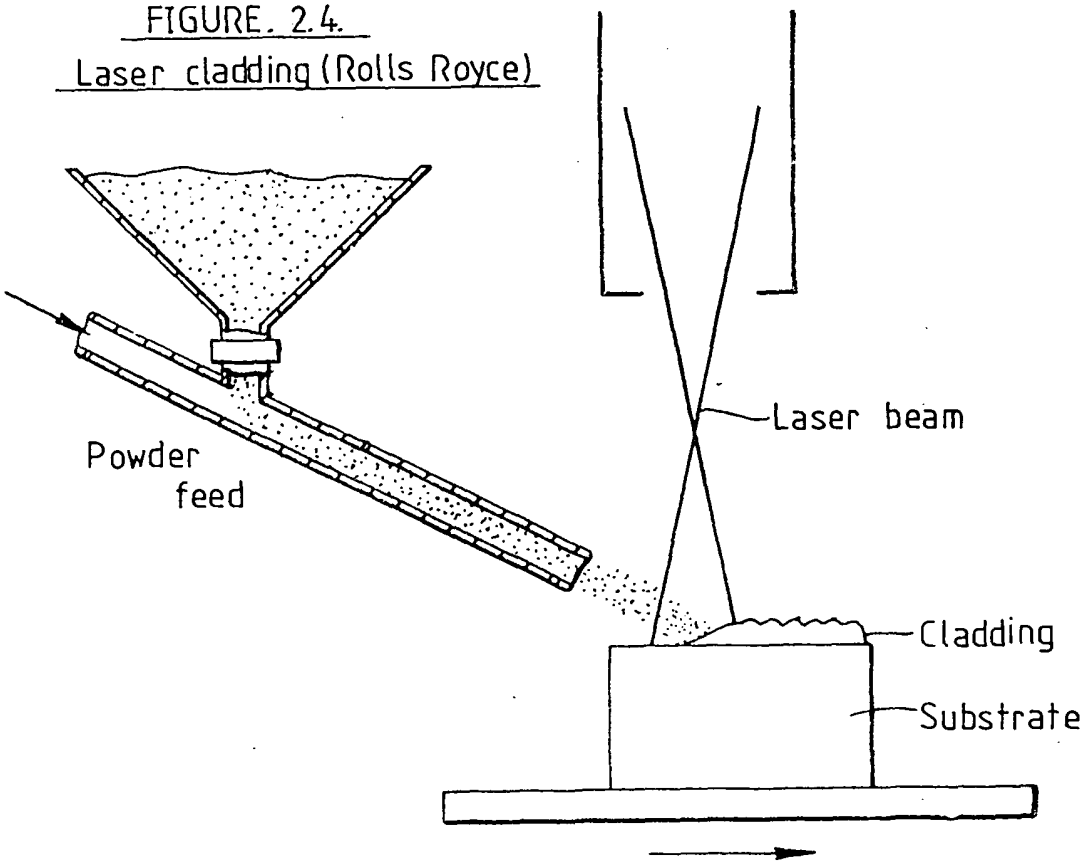

A more recent patent(41), was brought out by Rolls Royce Ltd in 1980. In this case powder cladding by the blown powder process was documented, rather than the earlier pre-placed powder laser cladding. A schematic diagram of the method is shown in figure2.4. A shallow molten pool is created on the substrate surface and into this area is blown the cladding powder which melts and leaves a track of clad material across the substrate as the substrate is moved in the x or y direction. This process, being the most commonly used in the experimental part of this thesis, will be described in great detail later in this work. The range of the various production parameters were given in the Rolls Royce patent as follows:

a) Laser beam spot diameter at the substrate: 1-4mm

b) Relative velocity of beam and substrate: 4-20mm/sec

c) Carrier gas flow rate: 2-5mg/sec

d) Powder delivery rate: 45-55mg/sec

e) Carrier gas: Argon

f) Laser power 800-2250 Watts

The material combination employed as an example in this case were a Nimonic 75 substrate and a Stellite 12 cladding powder. Stellite 12 has the following composition:

Constituent	% by weight
Carbon	1.70 - 1.95
Silicon	1.5 max

Constituent	% by weight
Manganese	1.5 max
Aluminium	1.0 max
Chromium	27-31
Iron	2.5 max
Molybdenum	2.5 max
Nickel	1.5 max
Titanium	1.0 max
Tungsten	8-10
Cobalt	Balance

(As cast hardness = 546 HV)

Using the experimental parameters mentioned earlier, successful tracks of depths of between 0.35 and 1.9mm thick were deposited having hardnesses in the range 450 to 600 HV.

Work carried out at Imperial College by Steen and Courteney in 1979 (42) involved an investigation of the same Nimonic 75 - Stellite 12 combination. The powder was, in this case, not blown into the weld pool but was pre-placed on the substrate prior to laser irradiation.

The experimental programme involved attempting to clad the substrate with the following variables:

Laser power levels of 1600, 1800 and 2000W. (P)

Two powder thicknesses : 0.5 and 1.00mm

(Powder density 50% solid)

Beam diameters at substrate : 2.0, 3.3 and 4.7mm (D)

Substrate-Beam relative velocity : 3 - 30mm/sec (V)

The Nimonic 75 substrate was in the form of 1.18mm thick sheet and the Stellite 12 was 300 mesh powder.

The results showed that a weld between the substrate and molten powder was formed only when the average energy per unit area exceeded approximately 23 J/mm^2 for a 0.5mm deep powder layer and 2 J/mm^2 for the 1.0mm deep layers.

The hardness of the deposited Stellite 12 was found to be in the 600 - 650 HV range, an increase on the as cast hardness of 546 HV attributable to the rapid cooling associated with the process. The relationships between the operating parameters and the condition of the finished clad surface were investigated and this led to the production of operating charts relevant to individual beam diameters(Appedix.A,Fig13). The figure shows the relationship between the Power P and the velocity V and the width of the deposited track.

There is a cut off on the right of the graph showing the P/DV levels above which the substrate is melted throughout and the weld pool, instead of being supported from below, is joined to solid material only at its sides. The cut off levels

on the left indicate the operating regime beyond which the powder may or may not be melted but this is not combined with welding to the substrate. Between these two limiting parameters (which change with D) the width of the deposited track was found to be linerly related to the parameter $^{P}/_{V}$ irrespective of beam diameter or powder depth. This effect is to be expected as the $^{P}/_{V}$ value measures the amount of energy absorbed per unit length by the powder-substrate combination, an increase in energy absorption being accompanied by increased melting of both the powder and the substrate. As the total amount of melting increased with $^{P}/_{V}$ it was also observed that the substrate was more effected by the increase than the powder and thus, the dilution increased in a linear manner with $^{P}/_{V}$ (eg dilution for 0.5mm powder at $^{P}/_{V}$ = 50 J/mm = ~ 2 % and at $^{P}/_{V}$ = 100 J/mm = ~ 16%).

Track widths in the range 1-4mm with thickness of 0.75 - 1.25mm were obtained during this experimental programme, a typical coverage rate being the production of a 2mm wide track, 1mm thick at a rate of 22mm/s. (with a laser power of 2KW).

Work carried out by Gnanamuthu (43), using a 15KW (max power) c.w. CO_2 laser has shown good results with the following substrate-cladding combinations:-

Tribaloy alloys on Steel : Tribaloy cobalt based alloys are well known cladding materials for wear and corrosion resistence.

Using a pre-placed powder bed 6mm deep and a laser power of 12.5KW, a cladding thickness of 6 to 7mm and width of almost 10mm was achieved in a single sweep of the beam. Dilution of the cladding alloy with the substrate was less than 5% by weight and the hardness of the deposit was R_c 58. The beam diameter used was 14mm and the processing speed was 1.27mm/s.

The powder was applied as a slurry and the reason why the depth of the solid deposit is the same as the powder thickness has to do with the fact that the powder is melted in a wider track than the width of the cladding-substrate interfacial weld, the surface tension of the weld pool then draws it into a truncated cycloid area on either side of the clad track. In the case of massive deposits (and in this case) it is quite common for the cross section of the clad layer to be more than a semi cycloid and thus there is deleterious undercut at the deposit-substrate interface.

This will be discussed at length in the experimental discussion of this thesis.

Stellite alloys on Steel : This system met with similar success. The cobalt based Stellite 1 was clad at a rate of 1kg/h using

3KW of laser power. The Stellite was laid on the substrate in the form of 3mm diameter cast rods and these were welded onto the substrate with a 6.4mm diameter beam at a processing speed of 4.23mm/s. As before, the dilution levels were excellent, being less than 5%, and the hardness was higher than the as-cast value at R_c60.

Tungsten Carbide in Iron on Steel : A mixture of coarse (nominal particle size of 0.5mm) tungsten carbide particles and iron powder (44mm) was applied to a steel (AISI.1018) surface without a binder and was processed with the following parameters: laser power 12.5KW, beam diameter 12mm and processing speed 5.5mm/sec.

The WC particles were not melted during the operation but were distributed in the iron which melted and was welded to the steel. The surface which results from this type of processing is similar to that of a laser assisted particle injected surface (see section 2.3.2.4.5).

Alumina on Aluminium : Alumina powder was melted onto a 2219 aluminium alloy resulting in a very hard surface. The parameters used were: Laser power 12.5KW, laser beam size 6.4 x 19mm (Rectangular, Oscillating at 690H_z), Processing speed 8.47mm/sec. It is not clear how well the alumina is bonded to the substrate and some cracking was evident but the process shows promise.

An interesting cladding technique was developed by Koji etc at (44) involving the cladding of a rhenium film onto a permalloy substrate. The difficulty in this case is the disparity between the melting points of the rhenium cladding powder (Mpt. 3180°C) and the substrate (Mpt 1480°C). The finished product must have a surface layer of pure rhenium and because of the difficulties of dilution in a case where the substrate has a much lower melting point than the cladding material, straightforward single pass laser melting/welding was inappropriate. The problems were overcome by use of a multiple pass method: The rhenium powder was pressed into a tightly packed layer on the substrate and was then exposed to a pulsed laser beam from a Nd-YAG laser. The depth of the powder layer is 50μm and its density is almost 70% of that of bulk rhenium. The first exposure of this pow der layer to the laser beam results in the melting of a thin skin on the surface of the powder layer so that the substrate-powder sandwich becomes a substrate-powder-solid rhenium skin sandwich. Subsequent laser heating results in the melting of the substrate by conduction through the powder layer. This molten substrate flows into the gaps between the powder Particles and thus, the finished product consists of a substrate-powder dispersion in substrate-pure rhenium film sandwich. The optimum power density for the primary irradi ation was found to be: 1.4×10^5

W/cm^2 which resulted in a melted depth of 20 microns. If a greater power density is employed the surface is damaged by scattering of liquid rhenium particles. The time for each pulse was 0.2ms and the spotradius was 0.1mm. In the case of the secondary irradiation a lower surface temperature for a longer time was required as the heat has to be conducted through to the substrate without melting the existing pure rhenium skin. To this end the parameters used were : 0.9×10^5 W/cm^2 power density with 1.0ms pulse width and a spot diameter of 0.5mm.

Finally, one novel method of laser cladding is described by Shaefer and Ayers in their laser spraying patent (45). In this method, the powder is introduced into the beam above the substrate and is propelled towards the substrate by the evaporation caused on the upper surface of each particle by exposure to the laser beam. The particles thus accelerated , upon impingement on the surface of the substrate can clad, alloy or imbed the surface. The particles must have certain properties for the phenomenon of evaporation induced propulsion to be realised. The vapour pressure of the particles must be from about 10^{-2} to about 10^{-1} atmospheres greater than the ambient pressure (which can be adjusted by use of an atmospheric chamber). Generally, this vapour pressure should be reached at a temperature from about the melting point of the powder particles to about five hundred degrees Celsius above the melting point. The second critical property of the particles is the coefficient of heat absorption

which is defined by :

$$\alpha = \frac{P_A}{\pi r^2 P}$$

PA = amount of power absorbed by the particle

r = particle radius

P = power density of the laser beam

Values for the coefficient required to give a sufficient rate of heating for laser spraying are from 0.2 to 1.0. A sufficient rate of heating is one that raises the temperature of the particles to one at which their vapour pressure exceeds the ambient pressure by 10^{-2} to 10^{-1} atm. in a period of time of not more than 10^{-2}sec.

Examples of suitable cladding materials include metal oxides such as Al_2O_3, Cr_2O_3, TiO_2 ; metals of bw to moderate density (sp. gr. 10) such as Al, Ti, Cr, Fe ; metal carbides, cemented carbides and nitrides.

Although this laser cladding method is being investigated, actual results from feasibility studies of various cladding-substrate combinations have not yet been reported.

It is clear that a great deal of work remains to be carried out into the scientifically and industrially very promising field

of laser cladding, and it is towards this end that the work in this thesis was carried out.

2.3.2.2. LASER SURFACE ALLOYING

Laser surface alloying is an extension of laser cladding in that it is the same process carried out with an increased laser power input to the 'cladding' pool. This increase in power input leads to substantial melting of the substrate and the mixing of the substrate metal and the cladding material creates a new alloy on the surface of the substrate.

The added elements may be in powder or solid form ie rods, wires or sheet, and can be pre-placed on the component or added while the melting is in progress.

The mixing of the additional material and the substrate is aided by the presence in the weld pool of strong convective forces, within the weld pool. (46).

At the central point of impingement of the laser beam, the temperature is highest and the surface tension lowest. The temperature decreases and the surface tension increases along a line from the centre to the edge of the pool (the temperature coefficient of the surface tension is positive for most materials). Thus, any volume element of the surface experiences a net force

parallel to the surface causing it to move from the centre to the edge of the weld pool. This mixing, present in nearly all laser metal working process, results in an alloyed layer which is of uniform composition and is made up of fine grains.

There are two main areas of application of laser alloying, one being the laser alloying of a substrate to achieve superior mechanical, physical or chemical properties on a surface or part of a surface, the other being laser alloying for electrical characteristics used in the production of various electronic components. These two fields can be roughly labelled 'macro' and 'micro' laser alloying respectively.

In the case of macro laser alloying for improved mechanical, physical or chemical surface properties, materials studies have been reported. (43) (47), detailing the successful alloying of low carbon and low alloy steels with a range of elements (Cr, C, Ni, W, V, Mn). The laser alloying process is still being researched and although several applications have been assessed, there are no reports of the use in production as yet. However, it is likely that the process will be important to the automotive, aerospace and possibly the domestic appliance industry, since the method can be employed as an on-line process for high volume production. Aluminium-silicon alloys can be strengthened locally by increasing the silicon level (48) and this has obvious attractions

for the weight conscious automotive industry. Work on hardening aluminium valve seats, power steering assemblies and piston rings by laser alloying has been carried out and a cast iron diesel engine valve seat has been suggested as a suitable laser alloying application (56). The operating temperature of a steel exhaust valve seat may exceed the tempering temperature of a transformation hardened layer, resulting in a softening of the seat. If the seat is alloyed with chromium, hardness is maintained at elevated temperatures.

Work carried out at Imperial College by Bennett and Steen (49) investigated the feasability of applying thin surface alloyed coatings to Nimonic alloy substrates. The substrate used was Nimonic 75 and the alloying powders were Tribaloys 100 and 400.

The application of the alloying powders to the substrate in the form of a paste after mixing them with a binder was found to give very poor results. The reasons for this failure, which has been noted in other projects include :

1. There is a difficulty in loading the binder with sufficient powder whilst at the same time avoiding the possibility of non homogeneous mixtures.
2. The products of combustion (vapours and gasses) resulting from the inter action of the laser beam and the binder tended to blow away the powder/binder paste ahead of the laser beam.

3. The tendency for some binders to curl up when heated and thus avoid being struck by the beam.

The use of a pre-placed dry powder technique gives much better results and resulted in the production of uniform alloy beads although in the case of Tribaloy 100 transverse cracking was a problem.

The commercial viability of 'macro laser surface alloying ' is obvious and the near future should bring the process, which has been justified in many contexts, on to the production lines of many engineering concerns.

Micro surface alloying is not very relevant to this thesis, suffice it to say here that Q switched ruby and Nd:YAG lasers have been used to alloy ohmic contacts on GaAs epilayers and workers in the field have concluded that the process is in some respects preferable to the more usual thermal alloying techniques.

2.3.2.3. THE CONSOLIDATION OF SPRAYED COATINGS BY LASER RE-MELTING

2.3.2.3.1 Introduction

The various techniques of spraying a new surface onto a substrate are discussed in Appendix G, where it is noted that the finished product has a tendency to porosity and poor clad layer-

substrate adhesion.

Experimental programmes have been carried out into the subject of laser re-melting plasma and flame sprayed coatings ((50), (51)) and the results proved to be very encouraging.

2.3.2.3.2. LASER CONSOLIDATION OF PLASMAS SPRAYED COATINGS

2.3.2.3.2.1 General

In the case of plasma sprayed coating , corrosion resisting coatings of titanium and 316L stainless steel on steel substrates have been laser melted with good results (50). After laser processing, these initially porous coatings were pore free and exhibited good surface quality. Results with wear resisting surfaces showed good consolidation but a propensity to cracking initiated by the thermal stresses encountered during cooling.

2.3.2.3.2.2. The Effect of Retained Gasses

When a laser beam heats porous plasma sprayed samples from ambient temperature to above the melting point of the coating, gasses trapped within pores in the coating experience increases in absolute temperature which range from about fourfold in the case of low melting point alloys (eg Met co 16c) to more than sixfold for Ti.If, as is often the case, the pores are closed and at

atmospheric pressure before the laser processing, the dramatic increase in pressure on laser heating can often result in the explosive ejection of metal from the surface of the weld pool. Another problem associated with these pores is that they can be trapped in the remelted layer with deleterious results. The research team at the Amercican Naval Research Lanoratory (50) decided to obviate these problems by minimising the amount of gas trapped in the coating by plasma spraying in a vacuum. This method was found to have benefits which extended well beyond that of ·ing trapped gasses.

The lesser degree of oxidation in the vacuum sprayed coatings was at least as beneficial in improving laser remelted coating properties as was the reduction in trapped gasses. For example, individual powder particles of the 316L stainless steel sprayed in air are covered in a thin coat of chromium rich oxide which hampers consolidation during laser melting. Hastelloy C, when plasma sprayed in air oxidises less than 316L or titanium but the small percentage of oxide present agglomerated during laser melt consolidation yielding undesirably coarse oxide particles.

2.3.2.3.2.3 Thermal Stress Effects

Thermal stress effects caused by the thermal cycle of the irradiated zone, result in cracking which is the most serious limitation of the laser consolidation process. The cracks can

classified into four types:

a) cracks in the coating

b) cracks in the substrate

c) cracks at the coating-substrate interface

d) cracks which traverse the interface

a) cracks in the coating: cracks in the coating can be further grouped according to whether they are located; i/ in the melt pass ii) in the as sprayed coating or iii) within both the melted and unmelted portions of the coating. Cracks of type 1 are most frequently encountered when very steep thermal gradients are a feature of the process. (High power densities and rapid sample speeds). eg Ti was successfully consolidated with a laser beam diameter of 1mm, a power of 8KW and a translation speed of 30 cm/sec, but cracking occurs when it is melted at the same speed with a 4KW beam and a 0.5mm spot. The melting of bulk Ti can be carried out under much more severe conditions without cracking, the inferiority of sprayed Ti in this case being attributed to a high interstitial content which leads to embrittlement.

Cracks of group ii, those restricted to the unmelted portion of the coating, are relatively common when the melted portion of the coating is stronger than the unmelted portion. Under these conditions a linear crack can form in the sprayed metal along the edge of the melt pass. Where multiple overlapping melted passes

are being carried out to cover a surface these cracks are eliminated. Cracks of type iii, which traverse the melt interface, occur more frequently than any other type. The problem is severe with wear resisting alloys for example; vacuum plasma sprayed Ferro-TiC cm. This material, which consists of TiC particles in a steel matrix is extremely hard and is unable to accomodate the strains necessary to prevent cracking during cooling.

Type b cracks, those which are localised in the substrate, are not found in metallic substrates because of their resistance to thermal shock. Such cracking might be expected with metallic coatings laser consolidated on ceramic substrates and future work may well give evidence of this effect.

Type c cracks, at the coating-substrate interface, are found in the metal-metal system under two circumstances: 1/ when melt passes part way through the sprayed coating were repeated and overlapped to cover a sizable surface. Under these circumstances there is sometimes enough accumulated stress to peel the coating free from the substrate. This effect can be obviated by melting through the sprayed layer and the surface of the substrate to produce an interfacial weld. The effecacy of this welding has to be weighed against the often deleterious effects of the resultant substrate-coating dilution. Melting only a thin surface layer of the coating can also present peeling because of the lower stress levels produced.

A second mechanism of interfacial cracking involves the production of brittle intermetallics at a welded coating-substrate interface. This is the case with such combinations as titanium on steel. Cracking in this case can only be avoided by avoiding penetration of the melt zone into the substrate or by the use of an interlayer which is compatible with both materials.

Cracks of type d, which traverse the interface are unusual and can be expected only when both the substrate and the coating are of limited ductility and a strong bond is formed between them.

The large thermal stresses which result from laser consolidation severly limit the viability of the process when hard wear resistant materials form the coating. Slowly moving beams and the use of substrate pre-heating reduce and can eliminate cracking (52) but such an approach offers no significant advantage over traditional means of weld cladding. It is reasonable, however, to conclude that effective laser remelt consolidation of many ductile coatings can be readily accomplished if the coatings are not excessively oxidised during spraying and if the amount of trapped gasses is sufficiently low.

2.3.2.3.3 Laser Consolidatin of Sprayed Coatings

The previous section outlines the problems and advantages of

plasma sprayed coating consolidation by laser melting and all the general points therein are, of course, directly applicable to the discussion on flame sprayed coatings. All that remains to be said is that test results (51) have shown that the combination of flame spraying and laser fusing can produce high quality coatings. Existing self fluxing alloys are ideal for the process and the rates for the fusing of thin coatings with a 10KW laser are over ten times faster than the alternative oxy-acetylene torch fusing process. This rate of processing is comparable to the flame spraying rates in some cases eg Metco 15E self fluxing alloy (29.5%Ni, 17% G, 4% Fe, 4% Si, 3.5% B and 1% C:- used as a hard facing cladding material) laser fused at a rate of 2.4 cm^2 sec^{-1} to a depth of .2mm. The spraying rate for a .2mm deep layer is approximately $7cm^2/sec$ (51).

The hardness of this alloy was similar to that of the torch fused coatings but the surface was found to be rougher. One big advantage of the laser process was the fact that there was no need to heat the substrate to any appreciable degree if this was considered to be undesirable.

2.3.2.4 SURFACE HARDENING BY THE INJECTION OF CARBIDE PARTICLES INTO THE LASER WELD POOL

This method consists of injecting hard carbide particles into a shallow molten zone established by a high power laser beam.

Processing conditions and materials are chosen such that the injected particles dissolve as little as possible before the substrate solidifies and it is in this respect that the process differs from laser surface alloying where the melting and dissolving of the impinging powder is required.

A great deal of work has been carried out in this field at the American Naval Research Laboratory (refs (53) (54) (55) and (56). The work has resulted in the production of carbide injected layers from 100 to 700mm thick with a volume fraction of carbide particles in the melted zone of up to 50%.

The range of experimental variables was as follows:-

Laser powers: 3 to 10KW (cw CO_2 laser)

Substrate velocities: 5 to 15 cm/sec

Weld pool diameter: 3mm approx

Powder flow: He propelled powder (Tic or WC) flow rate; 1-2 g/sec Powder size; 50-100mm

Metals which have been hardened by this method include 304 Stainless steel Inconel X-750, Ti - 6AI-4V and 5052 Aluminium.

A fundamental practical difficulty with the process exists in

the conflicting energy requirements of the substrate and the powder ie the substrate needs to be substantially melted to facilitate powder entrapment, but melting of the powder itself is undesirable to the finished product and dilution often results in embrittlement. Three further drawbacks to the industrialisation of the process are that:

a) The as hardened surface is rough and has to be ground flat.

b) The post treatment thermal stress combined with the presence of stress concentrations at the substrate-particle interfaces result in cracking often initiated by the hard, brittle carbide particles.

c) There is a certain amount of porosity in the finished trace, thought to be gas trapped during theentry of the particles into the weld pool.

Reference (55) outlines a research programme which involved injecting Ti-6AL-4V with TiC particles to reduce the co-efficient of friction of the Titanium alloy which is very high. The kinetic coefficient of friction was reduced from an original value of $U_k = 0.40$ to a post injection treated value of only 0.16 which gradually increased to 0.26 with repeated testing. The carbide particles stood proud of the matrix and thereby reduced the contact area with the steel slider used in the U_k tests. It was also noted that dissolution of the carbide particles hardened the substrate from an initial diamond pyramid hardness (DPH) of 341 to an as treated value of 447. This increase in hardness

results from the partial dissolution of the injected Tic particles (which have a DPH of 3270) followed by the formation of a dispersion of very fine Tic particles upon the rapid solidification of the laser weld pool.

The process reduces the wear experienced by the Titanium alloy in applications which involve sliding and fretting and could, in the future, renew interest in the use of titanium in light weight machinery.

The American experimental programme into the general field of carbide particle injection into laser weld pools found that the final surface structure is independant of the laser power/sample speed combinations chosen (54). Operating with a laser power of 15KW and a sample speed of 15cm/sec can yield calculated cooling rates approaching 10^5 $^{o}C/sec$. These conditions produce melt duration times of approximately 0.05 seconds and cooling rates of the order of 10^3 $^{o}C/sec$. In an iron or nickel based alloy considerable dissolution of WC can occur in 0.05 seconds and so other means must be found to prevent matrix embrittlement if the process is to become used commercially.

Work is still being carried out to refine this process which does produce a hard surface layer which is securely bonded to the substrate of which it is an extension.

LASER CHEMICAL VAPOUR DEPOSITION

Laser chemical vapour deposition (LCVD) utilises the thermal energy of a laser beam to heat specific areas of the surface of a substrate which is in an environment of a thermally degradable vapour. The vapour thus degrades above the heated areas and precipitates the required surface onto the substrate. The process therefore requires a vapour which is non absorbing to the laser radiation and a substrate which is absorbing. One such combination which resulted in the controlled deposition of TiC on carbon steel was investigated by Mazumber and Allen (57).

The chemical degradation initiated by the CO_2 laser heating of the steel substrate was :

$$Ti\ Cl_4 + CH_4 = TiC + 4HCl$$

The deposition of TiC using conventional CVD is well known (see Appendix A).

Takahashi and Itoh (58) reported that TiC films obtained by the usual CVD methods tend to peel off or crack. The use of a laser in this context offers several advantages :

a) Spatial resolution and control

b) Limited distortion of the substrate

c) The possibility of cleaner films because of the smaller area heated

The thickness of deposit is dependant on both the laser power and irradiation time as would be expected. The temperatures of the substrate during irradiation were in the order of 1000 ^{o}C (The reaction is favoured between 900 and 1100^{o}C) and the irradiation times were up to one second resulting in a fine micron thick deposit for a 400W laser. The diffusion layer between the TiC surface and the steel substrate was found to be minimal.

The conclusions drawn from this experimental programme were as follows:-

1) Extremely fine grained films may be deposited.

2) Hardness values exceeding 2000 KHN were observed

3) By controlling the irradi ation parameters the TiC deposit thickness may be varied

4) There is a threshold irradication time for a particular laser power

5) Deposition rate increases with power

6) Deposition thickness increaes with time but the rate of increase decreases after an optimum time

An experimental programme carried out at the University of

Southern California involved the cladding of quartz substrates with metals and insulators (59). It is possible to generate deposits of almost any material which can be deposited by conventional C.V.D and research continues into the applicability of lasers to the various processes.

In the case of metallic deposition by means of CO_2 laser heating of a fused quartz substrate a striking feature of the process was found to be its self limitation. Once a metallic film was deposited to a limiting extent subsequent laser radiation was reflected by the new surface. For example; the maximum thickness of film achieved for Ni deposition from $Ni(CO)_4$ was 550 A. This particular film having a resistivity of $\leq 4 \times 10^{-5}$ ohm-cm ($\leq$ 5 times its bulk resistivity). The self limiting phenomenon is also observed in the diameter of the deposited Ni films. The resolution achievable with LCVD deposition is greater than the diffraction limited resolution of the laser beam itself. The diameter of the deposited film is dependant on the irradi ation conditions and is always less than half the laser spot diameter. ($D_{1/e} = 1.1mm$). This good resolution will be important in the production of semi-conductor devices by this process. The adhesion of the deposited film can be enhanced by pre-cleaning the substrate with a laser scan of sub threshold (for deposition) power.

The investigation carried out at U.S.C into the deposition of a

representative dielectric substantiated the findings of the Mazumder investigation described earlier in this section but also showed that the thickness profile of the deposit could be tailored with correct processing. It was discovered that for laser generated surface temperature only slightly above the threshold for the deposition reaction, the resulting films showed a flat, uniform thickness profile which could be built thicker by multiple pulses. In this way, in one case a deposit thickness of 1000 A was built up with twenty pulses. Normal, prolonged irradiation techniques of building up deposits resulted in a deposit with a thickness which increases rapidly towards the centre. Steen (60) investigated the deposition of cobalt oxide from cobalt acetyl acetonate onto soda glass. This work also involved the development of a mathematical model of the process analysing both the thermal and mass transfer. An outline of the results is as follows:-

a) The effect of incident power/spot diameter ($^{P}/_{D}$)

Steen showed mathematically that $^{P}/_{D}$ and not $^{P}/_{D^2}$ (the power density) is the significant power parameter for a given substrate. This can be elegantly proved in practice by printing an image with a variable area (by means of masking the beam) where it is found that the larger areas print preferentially. If the substrate surface temperature (and therefore the deposition rate) depended on the power density ($^{P}/_{D^2}$) a uniform image would

be printed. If the temperature (related to P/D^2 is high enough, some thermally induced movement of the glass substrate and deposit can occur. Initially this results in a central pinching producing a peak but if the temperature is high enough to soften the glass, the thermally induced stress cycle will result in a central crater. The mathematical model showed the relationship of the diameter of the deposit to the 150°C isotherm which is the decomposition temperature of cobalt acetyl acetonate. Other relationships identified were ; a) the production of central black zones of heavy deposition, related to the isotherm at which mass transfer is the dominant influence on deposition and b) the production of central blue zones (indicating the dissolution of some cobalt into the glass substrate) associated with the - 950°C isotherm, a temperature at which the soda glass substrate becomes soft enough to flow.

The effect of deposition time : The deposition rate was found to be linear with time, as expected, although there is an initial induction period. The effect of vapour concentration : Increasing the vapour concentration has the effect of speeding up the rate depositions and produces a crisper image since the isotherms related to the central and outer zones are closer together for more concentrated vapours. Also, the more concentrated the vapour is, the shorter the heating time for a given thickness. Since this results in less thermal spread it helps to contribute to the image clarity.

The effect of substrate thermal conductivity and refectivity: The higher the thermal condutivity of the substrate, the more effectively the heated surface is cooled by heat dissipation into the body of the material. This means that a higher thermal conductivity material needs a higher energy input into it's surface to maintain a required surface temperature profile eg deposit formation is possible on glass in 120 secs (k glass = 0.84 W/M ^{o}K) with a value of $^{P}/_{D}$ of 7 W/cm. For a similar deposit on quartz (spectrosil k = 1.38 W/M ^{o}K) in the same time, a $^{P}/_{D}$ of II W/cm is required and for copper (k = 38.5 W/M ^{o}K), a similar deposition would be possible at 570 W/cm assuming a 50% reflectivity for the copper. The surface reflectivity is assumed to change during deposition. Such changes will be associated with the thickness or mode of deposition and will therefore be located at the dentre of the deposit thrreby having no effect on the diameter of the deposit but possible effects on the thickness. By correct control of production parameters it is clear that well defined substantial deposits can be clad onto substrates by the LCVD method.

It is obvious from the results accrued from the various experimental programmes that LCVD has a great deal of industrial potential, both in the field of hard facing and in the production of semiconductor devices. Although this is a laser cladding technique, the range of applications will in general differ from those related to the macro laser cladding which is the subject of the present authors research. Thus LCVD is really to be considered as a

complimentary technique rather than a competing one.

2.3.2.6 LASER VAPOUR DEPOSITION

2.3.2.6.1 General

Laser physical vapour deposition (LPVD) can be divided into two sections, one dealing with the condensation of a vapour created by laser heating and the other dealing with the substrate interaction with a laser produced plasma consisting of both liquid and vapour phases. The latter involves the sudden heating of a material surface to temperatures in excess of its boiling point and results in the explosive release of material whilst the former method merely employs laser heating as a method of melting and heating the melt to temperatures at which it gives off a substantial amount of vapour.

2.3.2.6.2 Vapour phase LPVD

This tranquil method results in good quality even coverage of a substrate and involves heating the cladding material (in the form of powder or bar) to temperatures well in excess of it's melting point. This evaporation takes place inside an evacuated chamber which also contains the substrate to be clad.

Most conventional evaporation sources consist of resistence heated W, Ta or Mo wires strips or boats containing or supporting the evaporant. Such sources are simple, but they have the disadvantage that they react with the various types of evaporants, especially oxides. This results in the deposition of decomposed or contaminated films. Direct heating of the material avoids this contamination and is also more suitable for the evaporation of high melting point materials such as Pt or Ir.

The fabrication of beam lead silicon integrated-circuit devices involves the vapour deposition of platinum. A method of achieving this using a 20W cw YAG laser was investigated by Hess and Milkosky (61). They found that a stable. easily controlled deposition process could be maintained and that the resulting platinum film was uniform and composed of small randomly orientated crystallites. Economical deposition rates of 100 A/min were not achieved during the course of the experiments but this failure was wholly attributable to the use of a laser of too low a maximum power.

The LPVD of dielectric and semi conductor films by a CO_2 laser has been investigated by Hass and Ramsey (62). Their prime areas of interest were films of Silicon oxides and films of Magnesium Fluoride.

2.3.2.6.2.1 Silicon Oxide Films

a) Silicon monoxide : Films produced by high vacuum evaporation of silicon monoxide are used extensively as optical coatings and protective layers. This material was found to be easily evaporated with a laser beam. Using a 60 W CO_2 laser, deposition rates of about 150 A/sec could be obtained and the properties of the films were found to be identical to those produced by conventional methods.

Silicon Dioxide : This is another material of great optical interest. It is transparent from the [illegible] uv to the near Ir, has a low refractive index and is, in addition, extremely hard and chemically durable. At the high temperatures required for its evaporation SiO_2 reacts with resistance heated boats and so it has not, until recently, been used as an optical protective layer, an application to which it is ideally suited. The first successful cladding with SiO_2 was carried out using an electrogun as a means of evaporation. Excellent results for the LPVD of SiO_2 were achieved, the deposit being of high purity and uniformity.

2.3.2.6.2.2 Magnesium Fluoride Films

Films of MgF_2 with their rather low index of refraction play an important role as single layer antireflections films and as a film component in multilayer anti reflection coatings (63). This

material is a good absorber of 10.6 wavelength radiation in the same way as the other materials in this section are and is thus easily evaporated by CO_2 laser radiation.

MgF_2 films were deposited onto quartz glass substrates at rates of 1000 - 1500 A/min at pressures of 1 -2 X 10^{-6} Torr. The refractive indexes of the films prepared in this way were identified by Hass and Ramsey and were found to be in close agreement to earlier vacuum deposited information published by Hall (64). Thus the laser deposited films were found to be identical to the established vacuum deposited films.

2.3.2.6.2.3. Film Materials

Experimentation exploring the adaptibility of the LPVD process toa wide range of materials has shown great promise. As mentioned by Smith and Turner (63), the deposition of films by means of a laser located outside the vacuum system offers several unique advantages. The technique is especially suitable for producing extremely clear coatings under ultra high vacuum conditions using a thoroughly baked out vacuum system without electric leads for an electron gun or for directly heated evaporation sources. Evaporation from the surface without extensively heating the container of the evaporant also further assures the deposition of clean films.

2.3.2.6.3 Plasma Condensation LPVD

The experimental arrangement is identical to that needed for vapour phase LPVD except that the process uses pulsed solid state lasers to deliver a short burst of high energy to the material to be deposited. The plasma which results from this sudden absorption of laser radiations consists of ionised and non ionised vapour as well as liquid phase material. Two factors contribute to the roughness of the surface finish obtained from this method of cladding (65 (66);

a) Liquid phase sputtering of the substrate

b) Etching of the surface by the impingement of high energy ions from the plasma.

This method is not used as a cladding method but is used as a method of creating thin films for assessment of their properties.

A particular feature of the laser condensates of W, Mo and Cr was found to be (66) that their resistivity ρ, at room temperature is in order of magnitude greater than the corresponding values for massive specimens ρ_0, while the values of the temperature coefficient of resistivity α, in the range 273 -373 K, on the other hand are several times lower than for the massive specimens α_0. The reasons for these changes are not yet known but this work is typical of that carried out on laser plasma condensation films. This technique, therefore, is shown to be a reasearch tool rather than an industrial application of lasers.

CHAPTER 3 THEORETICAL ANALYSIS

3.1 INTRODUCTION

The work carried out for this thesis investigated two distinct methods of cladding one metal with another using a laser energy source, these are;

A/ Pre placed powder cladding

and B/ Blown on powder cladding

The laser-material interactions are different for each of these and so two independant theoretical models of the processes were developed. The trends envisaged by each model were found to correlate closely with the practical results collected and presented in Chapters 4,5 and 6.

3.2 THEORETICAL ANALYSIS OF PRE PLACED POWDER CLADDING

3.2.1 General Theory

The theory developed for use in this work is best described by the following series of interaction stages:

1. A layer of solid metal powder rests on a substrate with no laser irradi ation. The powder (of known depth, density and composition) and the substrate (of known composition etc) are both at ambient temperature.

2. Laser irradiation begins, the surface powder particles heat up but are assumed not to conduct heat to the particles below them because of the low level of inter particle contact

(ie the bulk of the powder is assumed to be an insulator).

3. The insulated, irradiated surface particles melt and in the molten state can conduct heat but only to neighbouring particles experiencing wet contact. (ie the powder layer more than 2 Rp distance from the molten front is an insulator :- Rp = particle radius).

4. The molten front progresses through the insulating powder layer. This process is much faster in the vertical direction than in the horizontal because the liquid flow is gravity assisted.

5. Contact is established between the molten front and the substrate.

6. Contact with the substrate changes the energy balance from:

A. Laser Energy in = (Temperature rise + phase change (solid-liquid)
+ (Radiated loss from the melt surface)
+ (Convective loss from the melt surface)

to:

B. Energy in = (Temperature rise of melt nearest the surface)
+ (Radiated loss from the melt surface)
+ (Convective loss from the melt surface)
+ (Conducted temperature rise of substrate)
- (Temperature drop of once molten material and phase change (Liquid-solid)

(For equations A + B see page 56)

This chilling effect of the substrate leads to a reversal in the directions of travel of the melt front which now approaches the laser irradiated surface which, because of its distance from the

chilling effect is still being heated.

Depending on the conditions, a number of phenomena are now possible:

7A. The laser irradi ation is stopped or has moved on to the next element in the lateral direction . . the solidification is completed giving cladding with only interfacial instantaneous melting i.e. no dilution.

7B. The quenching capabilities of the substrate outweigh the energy inputs from the laser and the liquid-solid phase change, . . solidification is completed even if the laser continues to irradiate. On solidification the energy input is from the laser alone and remelting is rendered unlikely.

7C. The molten pool is quenched rapidly at first and then more and more slowly as the temperature gradients become shallower. This has the effect of establishing an equilibrium depth of melt which is much smaller than the pre substrate-contact melt depth.

7D. The molten pool is quenched rapidly at first (as in 7C) but after a certain amount of solidification the thermalgradient and energy balance favour the interruption of the solidification followed by slow re-melting. This re-melting takes place at an ever decreasing rate until an equilibrium melt depth (smaller than the original melt depth) is established.

7E. The molten front goes through the same cycle as in 7D but the established melt depth is greater than the original melt depth and thus dilution of the cladding material with the

substrate occurs.

The theory can be summarised by the following chart:

Fig 3.2.1 flow chart of pre placed powder-cladding.

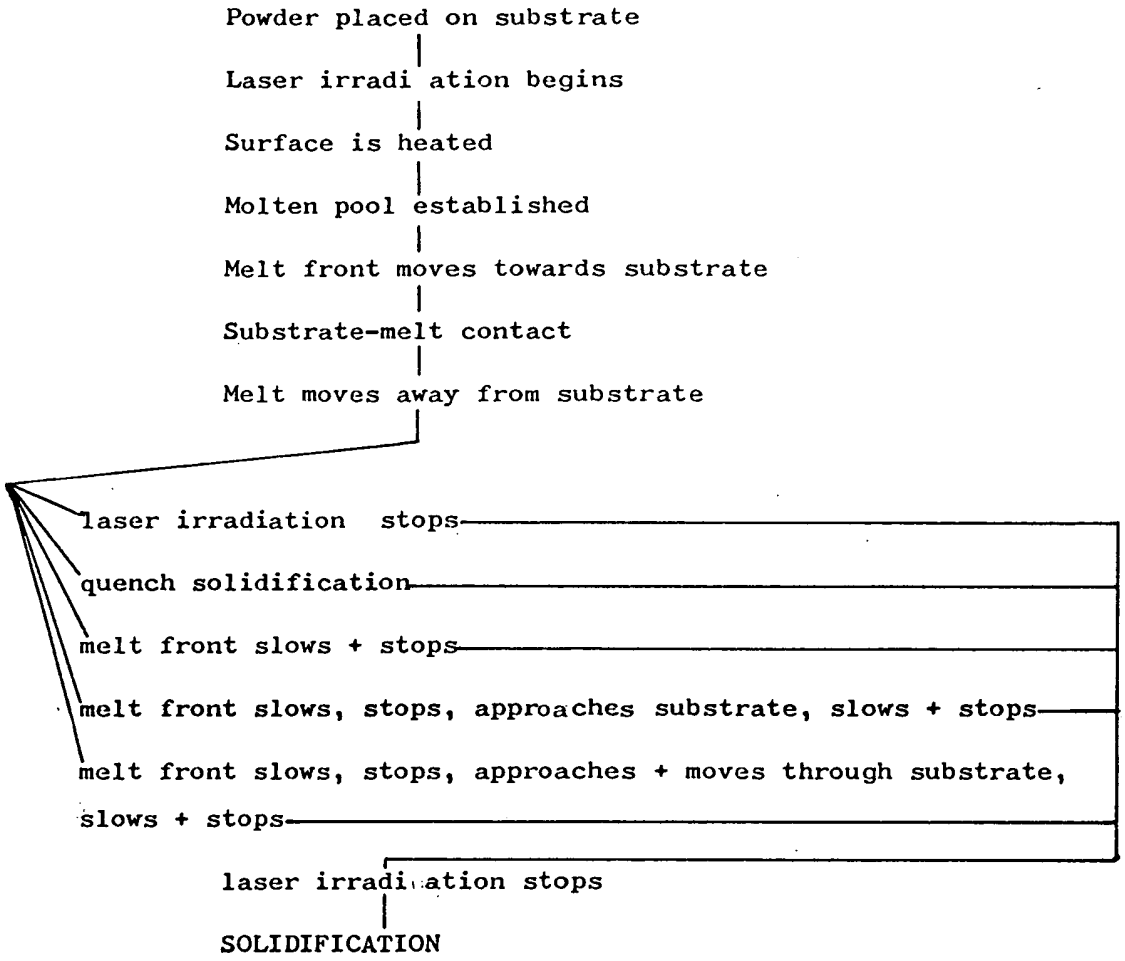

In practice the process can be interrupted at any point by removing the laser irradiation and so it is possible to tailor the position of the melt front prior to the start of the final solidification and thus avoid or control any dilution effects.

3.2.2 COMPUTER AIDED STUDY OF THE THEORY

A computer programme was constructed to test and quantify the theory of pre placed powder cladding just described. The logic behind the programme is put forward in Fig 3.2.2 which is a

flow diagram of the calculation steps taken by the computer. It is assumed for ease of calculation that the powder is a material with the same physical properties as its bulk material except for its thermal conductivity which is assumed to be zero.

On contact between the molten front and the substrate the method of calculating the temperature change of any element with time is changed to include a thermal conductivity factor.

The computer programme itself is presented in appendix D of this thesis. Figure 3.2.3.gives the graphical analysis of the information presented in a typical computer read out.

Equations A+B from page 53

A.

$$H = (C_\rho V \Delta T + Q \Delta V_\rho) + [(\sigma A (T_s^4 - T_a^4)) + (hA (T_s - T_a))] dt$$

B.

$$H = (C_\rho V \Delta T + Q \Delta V_\rho) + [(\sigma A (T_s^4 - T_a^4)) + (hA (T_s - T_a))] dt + KA \left[\frac{dT}{dx}\right] dt$$

Where

H = Heat imput to element of surface area A and volume V.
C = Specific heat
Q = Latent heat of melting
T_s = Surface temp
T_a = Ambient temp
h = Heat transfer coef.
σ = Stefan-Boltsmann const.
K = Thermal conductivity.
V = Volume
ρ = Density

FIGURE.3. Flow diagram of the computer model for preplaced powder cladding.

CALCULATION A

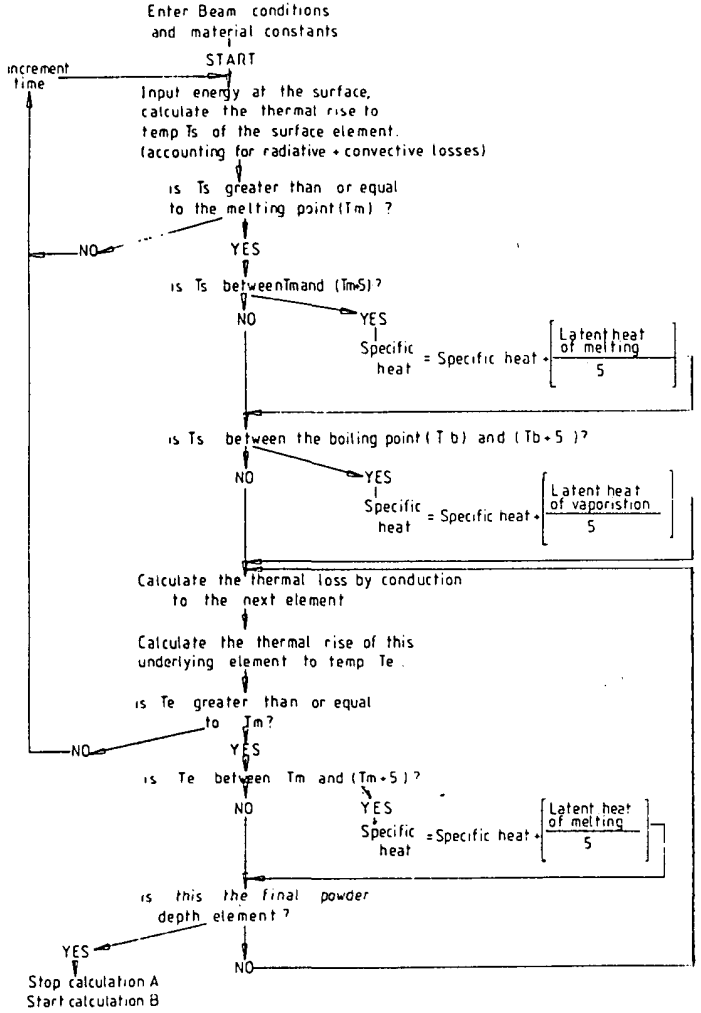

CALCULATION B

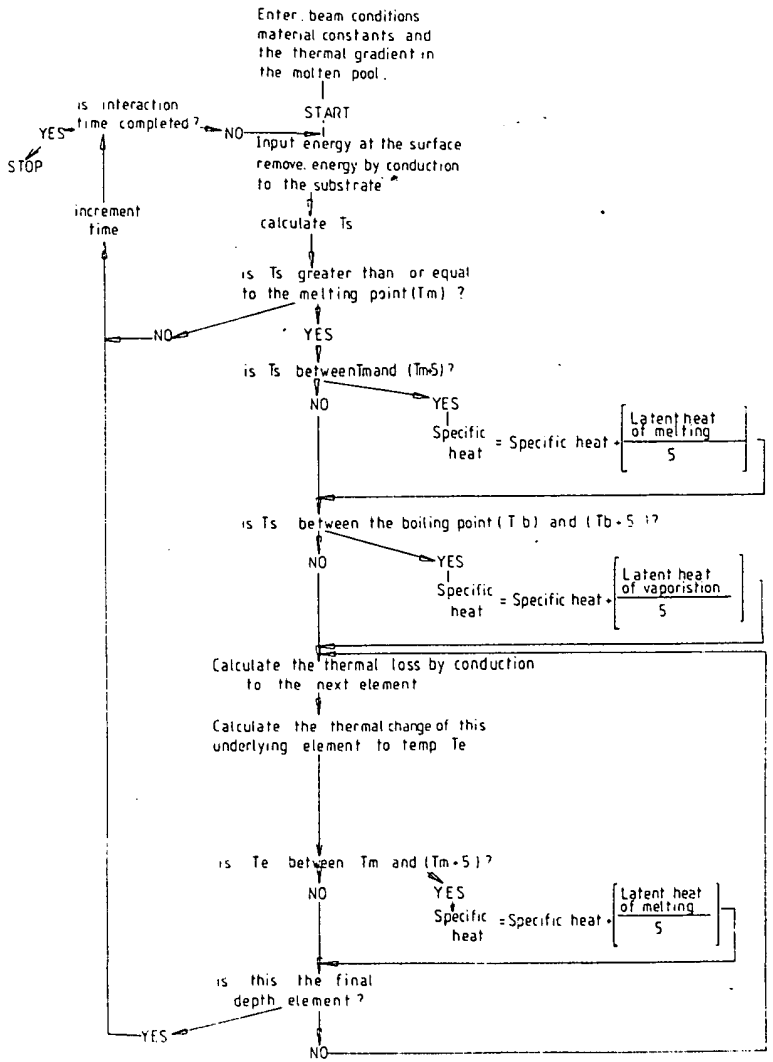

FIGURE.3.2.3. Graphical representation of the computer generated results.

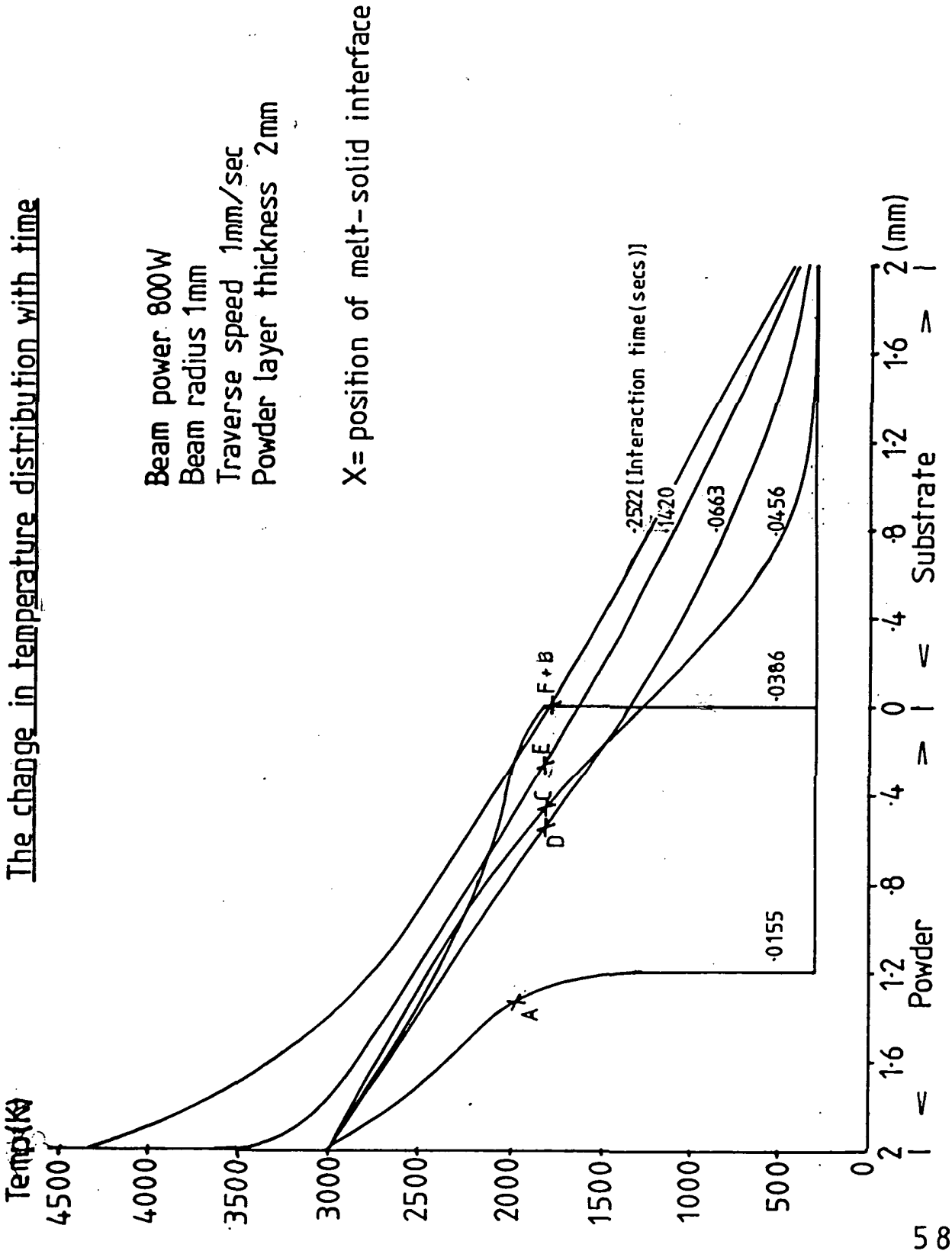

It can be seen that the computer model basically generates a complex Schmidt plot or thermal relaxation plot, the complexity being, to some extent, a result of the continued laser irradiation of the surface.

3.2.3 ANALYSIS OF THE COMPUTED RESULTS

The most important information available on the computer read out was the position of the melt front at any time (t) Figs 3.2.4 and 3.2.5 show the movement of the melt front with time for differing incident laser powers and powder depths. The trends postulated in the original theory can be easily identified, in the case of Fig 3.2.4 the varied parameter was the incident power from the laser.

The parameters used were:-

Depth of Powder	=	2.0mm
Melting point	=	1812 K
Latent heat of fusion	=	269000 J/kg
Boiling point	=	3000 K
Latent heat of vaporisation	=	9000000 J/kg
Density	=	7860 kg/m^3
Specific heat	=	438 J/kg/K
Thermal conductivity of material	=	80 W/m/k

Laser beam powers = 50, 100, 200, 400, 800 and 2000W.

For ease of calculation the powder was assumed to be consolidated (with a porosity of zero) and to have no thermal conductivity as bulk powder. Referring back to the earlier explanation of

FIGURE. 3.2.4.

The movements of the melt front with changing laser power.

Beam radius	= ·001m
Traverse speed	= ·001m/s
Interaction time	= 1 sec.

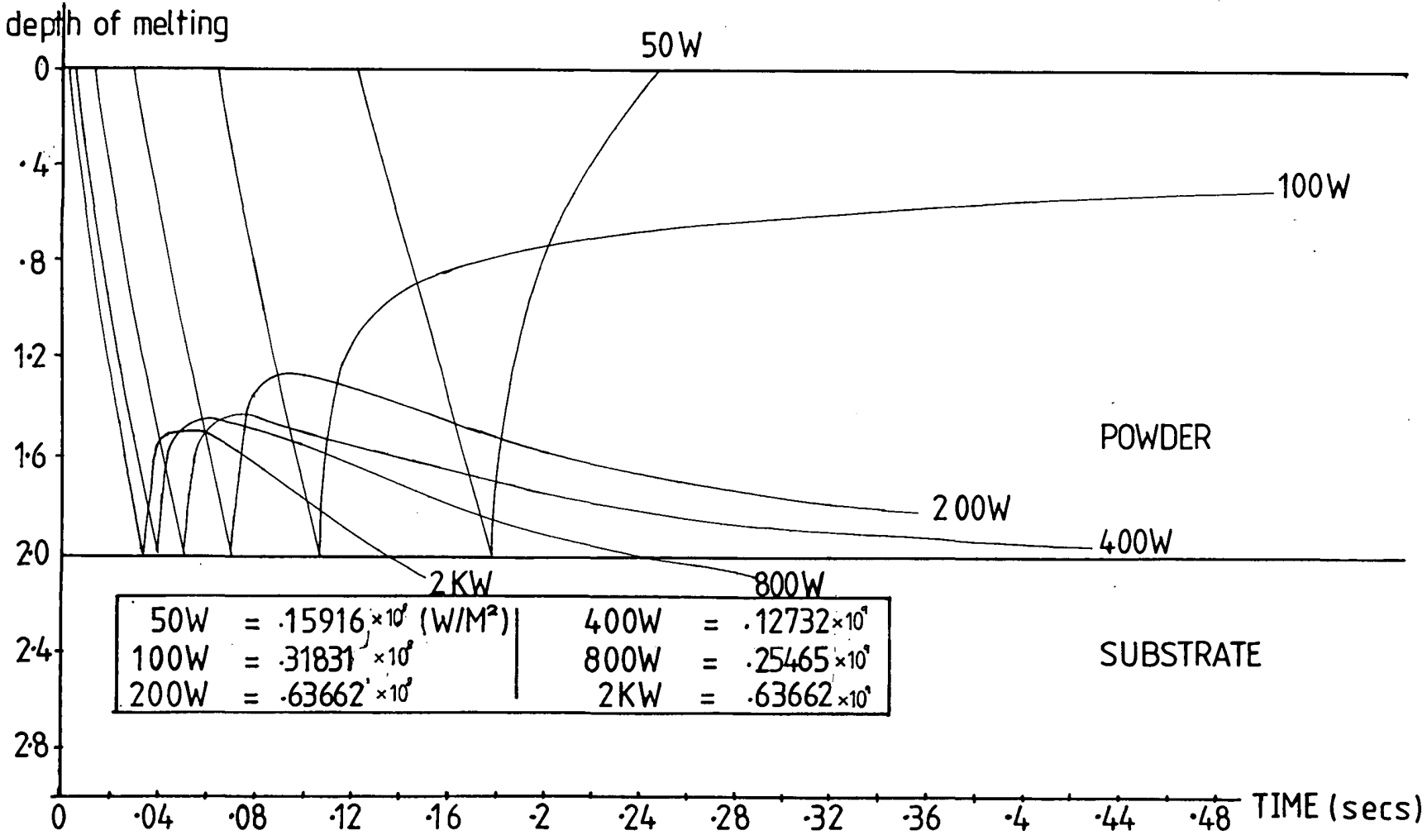

FIGURE. 3.2.5.
The movements of the melt front with changing powder depth.

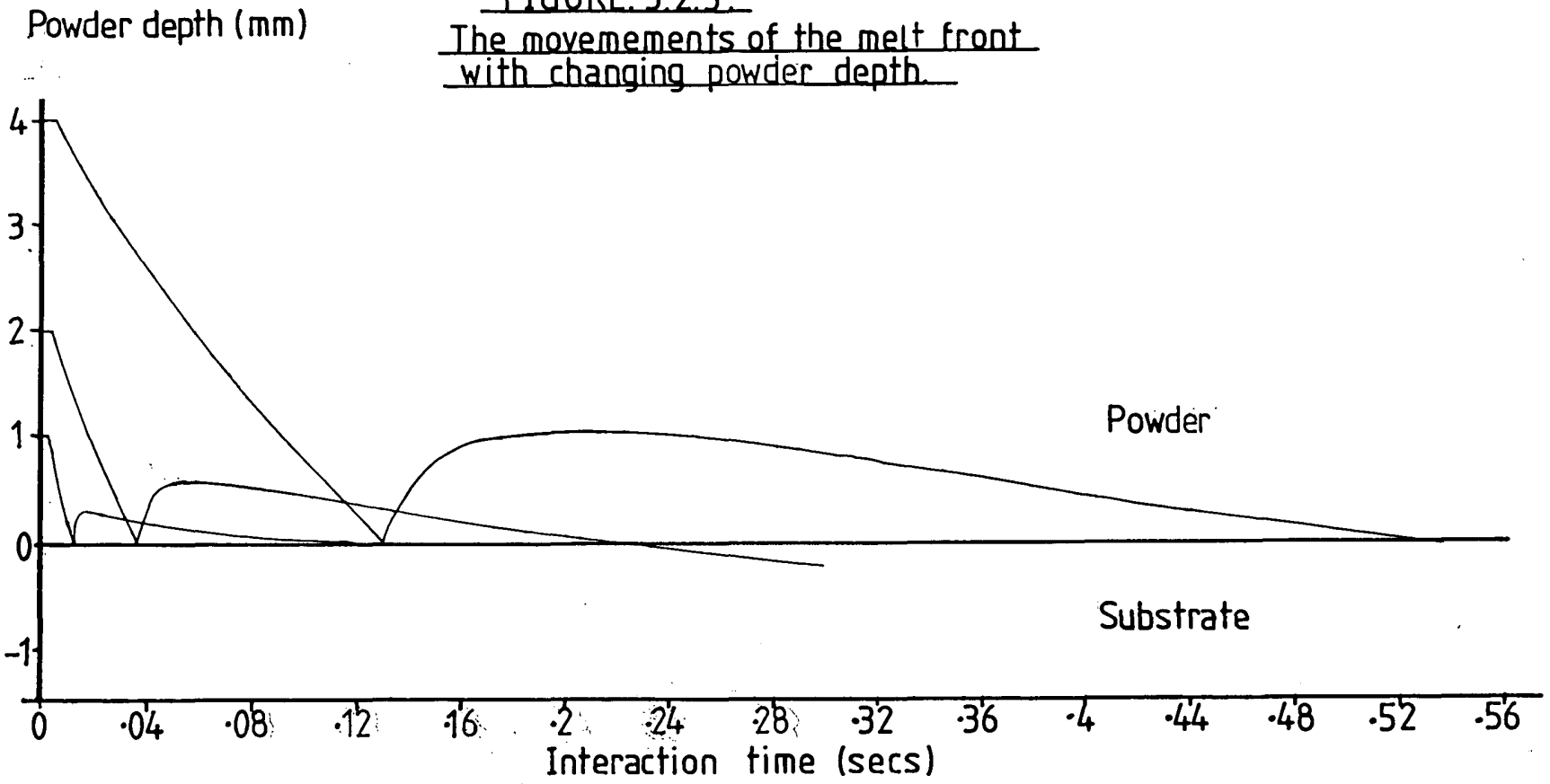

the theory, the lines on the graph can be identified with the relevant interaction combination. Assuming that all the samples underwent interaction stages 1-6, the lines can be correlated with the different kinds of stage 7 as follows:

Laser Power	Interaction Type
50 W	7B
100 W	7C
200 W	7D
400 W	7E
800 W	7E
2000 W	7E

It is important to note that even in the case of the 2KW interaction there is a substantial period of time between the first melting of the substrate and the second. This effectively means that there is a wide range of interaction times within which a non-dilute deposit will be clad onto the substrate, a phenomenom which was observed in practice.

Figure 3.2.5 shows the effect of cladding three depths of powder with the same energy density. This effect is similar to that of reducing the incident power in that, although the interaction type remains "7E", the time to melt and remelt as far as the interface increases with increasing powder depth. The position of 'turn round' of the melt pool (from solidifying to melting) is a function of the total depth of the melt (d) and in this case is approximately $d/4$ from the cladding - substrate interface.

If the maximum possible interaction time for no dilution is compared with the minimum required for melt - substrate contact time;

powder depth	tmin	tmax	$\frac{tmax-tmin}{tmax}$
1mm	.012	.092	.87
2mm	.037	.208	.82
4mm	.13	.516	.75

the value $\frac{tmax-tmin}{tmax}$ gives the proportion of tmax within which a non dilute clad deposit will result. Although there is a small downward trend (as a result of a cooler melt surface releasing less energy from the system by radiation and convection) it can be seen that more than three quarters of the maximum non dilution interaction time has no effect on the dilution of the finished deposit, carrying out the same analysis for the changing power graph (Fig 3.2.4):

Laser power	tmin	tmax	$\frac{tmax-tmin}{tmax}$
2KW	.032	.133	.76
1KW	.037	.208	.82
800W	.05	.24	.79
400W	.07	.49	.86

Here once again, more than three quarters of the maximum interaction time is 'safe working time' within which non dilute deposit is the result.

This large difference between tmin and tmax is of great use to industry because it means that if for example $\frac{tmin + tmax}{2}$ is chosen as the nominal interaction time for a commercial application a great deal of leeway is available in the choice, accuracy and stability of the operating parameters. As an example of this, consider a process attempting to get an undilute cladding with

a 2mm deep 'powder' layer and a one kilowatt beam with a radius of 1mm.

$$\text{Nominal interaction time} = \frac{t_{min} + t_{max}}{R} = .12 \text{ seconds.}$$

Assuming the amount of powder is constant, the power can be more than doubled or taken down to less than 10% of nominal. The interaction time can be increased to 170% of the nominal or decreased to 30%. These values take, of course a rather optimistic view of the trends as they deal only with an ideal situation, in practice such large changes in processing parameters would illustrate various faults within the theoretical model as follows:

A. It has been assumed that on interfacial contact of the melt and substrate enough energy is transferred to produce a weld. This will not be the case in some instances as the possibility of welding being completed depends upon the temperature distribution in the molten layer immediately before contact with the substrate. Figure 3.2.6 shows the thermal gradients extant in pools produced by different laser powers and powder thicknesses immediately prior to substrate contact.

These temperature gradients constitute an effective energy density available to the interface. It can be seen that above a certain limiting energy density (in this case approximately 500W for a 1mm radius beam) the thermal gradient within the 10% of the pool nearest the substrate assumes a constant value of, in this case 765°C per mm. This standardisation of the energy input available close to the interface is reflected in the following list of figures showing the thermal rise of the first space element (.2mm deep) of the substrate after liquid pool - substrate contact of .0002 and .0071 seconds duration.

FIGURE.3.2.6. Thermal gradients of molten pools prior to substrate contact.

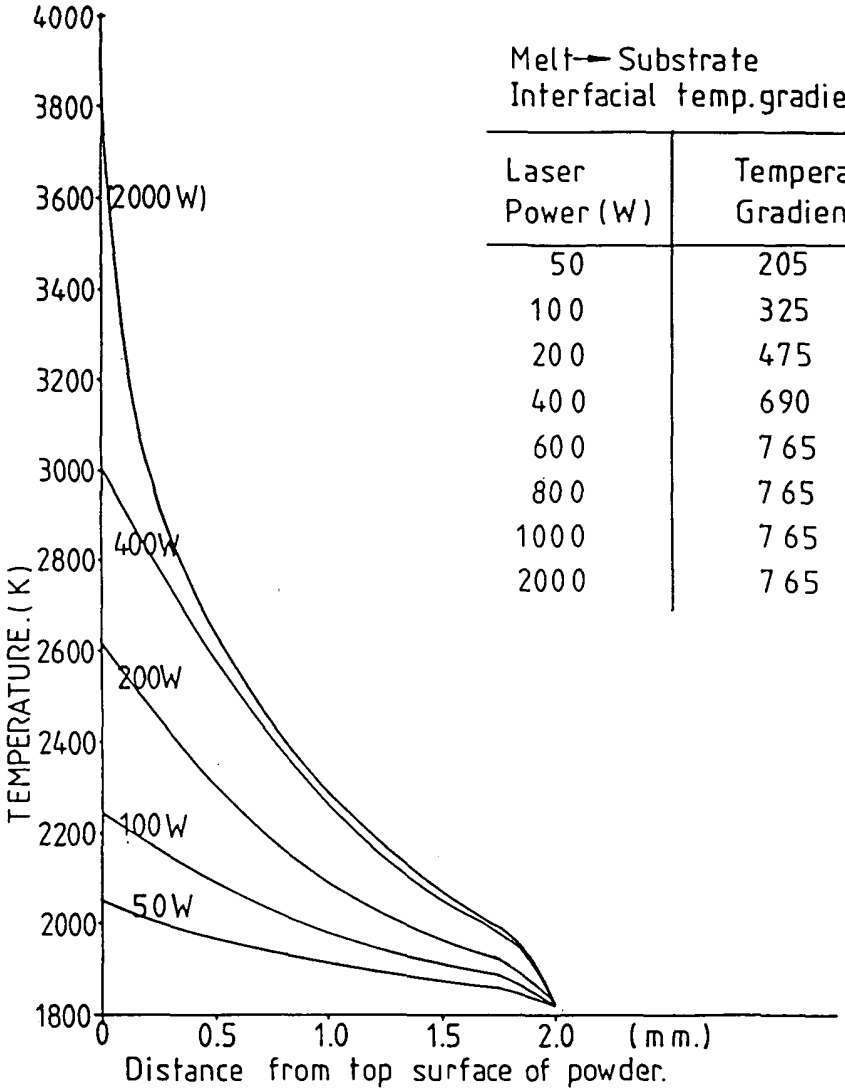

Melt→Substrate
Interfacial temp.gradients

Laser Power (W)	Temperature Gradients.(°C/mm)
50	205
100	325
200	475
400	690
600	765
800	765
1000	765
2000	765

Fig 3.2.7 THERMAL RISE OF FIRST 'WAFER' OF SUBSTRATE WITH TIME

TOTAL LASER POWER	INTERACTION TIME .0002 secs	INTERACTION TIME .0071 secs
	Temperature °C	
2KW	439	1030
1.5KW	439	1030
1.0KW	439	1030
.8KW	439	1030
.6KW	439	1030
.4KW	439	1022
.2KW	438	996
.1KW	437	976
.05KW	437	963

The differences, even below the limiting case are very small in comparison to the changes in input energy but it is to be assumed that in some cases the effect is large enough to prevent enough energy crossing the liquid-solid interface to produce a weld.

B. The model does not take into account the vigorous stirring experienced by an laser weld pool (see Chapter 5, section3.2.3.). This convection within the melt distributes the energy in the pool more evenly than has been postulated here. The result of this will be that as the average temperature of the weld pool increases so does the thermalgradient adjacent to the melt front (which must of course remain at the melting point). This will have an effect on the probability of weld production. A second practical upshot of this liquid movement is the entrapment of powder particles adjacent to the pool in the lateral direction and their incorporation into the pool which increases in size with greater energy inputs.- an effect which will be described in Chapter 4.

C. Surface tension effects, which determine the morphology of the weld pool have been ignored. If an even source of energy, restricted to a certain area were employed (as assumed in the computer model) the melt front approaching the substrate would be curved in a manner which would mean that the centre of the pool would be nearer the substrate than the peripheral melt. The effect of this would be to initially chill the melt from one central point resulting in very complex heat flow and a weld bead suffering from undercut. The energy input to the powder was, in this case, tailored to try and defeat this effect (see Chapter 4).

3.2.4 Summary

In summary it can be postulated that pre placed laser cladding can be divided into several classes in order of increasing total energy input.

A. Powder heating but no melting.

B. Powder melting but melt does not progress as far as the substrate.

C. Melt contacts substrate and is subsequently solidified but interfacial energy conditions are not sufficient to produce a weld.

D. Melt contacts substrate and is partially or fully solidified on contact, an interfacial weld is created, solidification is completed on removal of the irradiation.

E. Melt contacts substrate and is partially solidified but subsequently remelted without the melt reaching the substrate surface. Solidification : on removal of the irradiation.

F. Melt contacts substrate and is partially solidified but melting is re started, the melt front crossing into the substrate producing a dilute deposit. Solidification : on removal of the irradiation.

Analysis of these stages has shown that classes D and E, the most commercially interesting ones, cover a surprisingly large range of processing parameters and dilution (F) can easily be avoided.

3.3 THEORETICAL ANALYSIS OF "BLOWN ON POWDER" LASER CLADDING

3.3.1 MATHEMATICAL ANALYSIS

3.3.1.1 General

Figure 3.3.1 shows the theoretical view of blown on powder cladding. In the case of blown on powder cladding, powder is propelled towards a cladding weld pool which consists mostly of already melted powder and to some extent of melted substrate. As the powder travels towards the weld pool it is heated in its passage through the laser beam. The hot particles are then impingent upon the surface of the weld pool where conduction from the molten mass combined with exposure to the incident beam bring about melting and consolidation into the weld pool. A combination of conduction from the molten pool and direct (but occluded) laser radiation bring about substrate melting. The powder propellant is an inert gas (usually Argon) which, to some extent, shields the weld pool from oxidation.

The initial beam assumptions concerning the theoretical treatment of the process are as follows:-

A The Laser Beam

1. Although the beam is diverging during its approach to the weld pool in practice, it is assumed to be neither converging nor diverging.

Fig. 3.3.1.

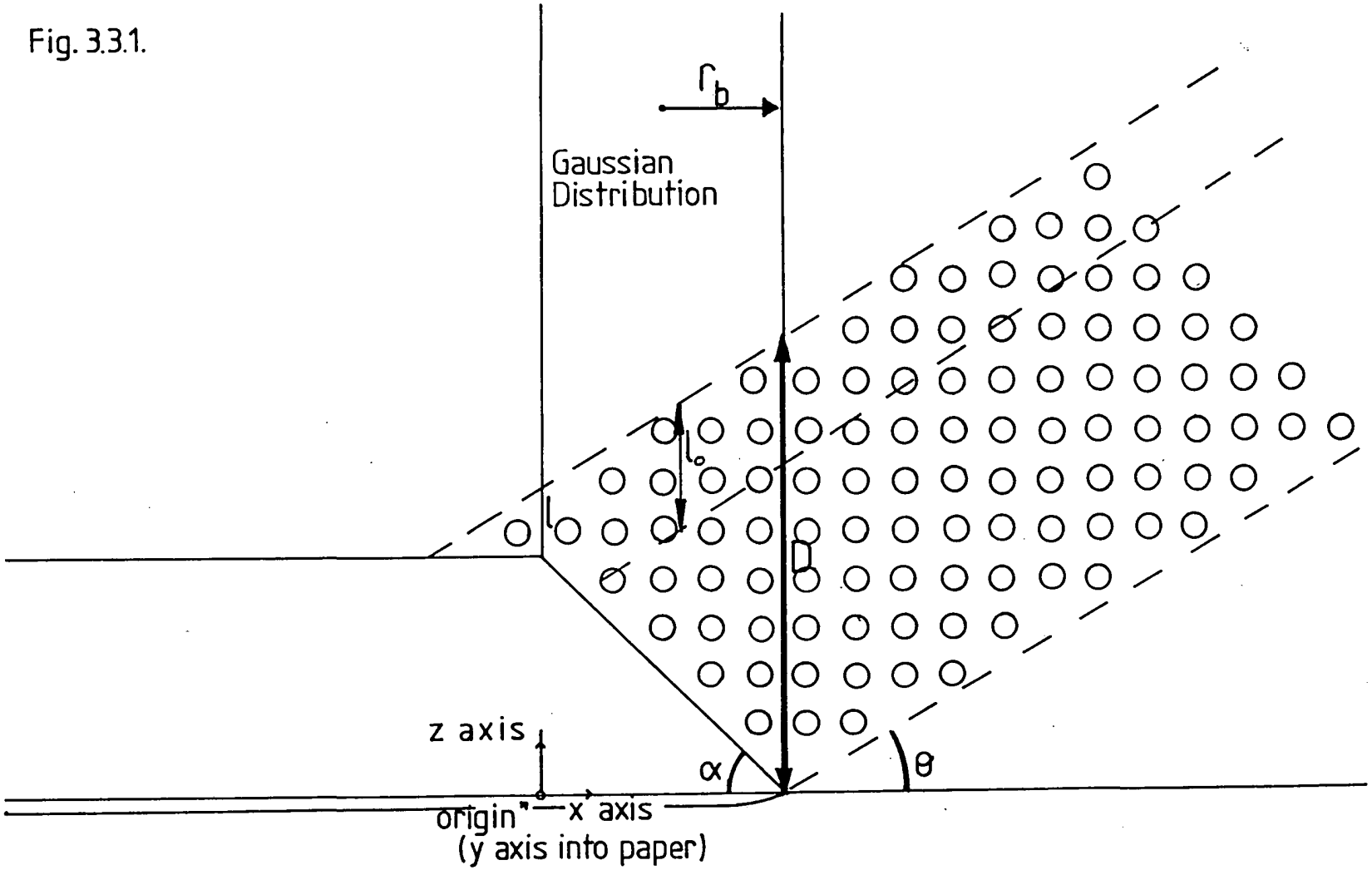
r_b
Gaussian
Distribution
l_o
l
D
z axis
α
θ
origin
x axis
(y axis into paper)

2. The power distribution across the beam is assumed to be Gaussian.

3. Although a Gaussian beam would have an infinite radius, a radius (R_B) for the beam is stipulated. This radius is taken as being that at which the intensity of the beam is $1/e$ of the central intensity (See Ref35).

B The Powder

1. The powder particles are assumed to be spherical and of a radius ρ_p.

2. The powder density in the cloud is assumed to be uniform.

3. The particles are assumed to be moving with the same, constant, velocity (V) along a straight path at an angle θ to the horizontal.

4. The depth of the moving particle cloud (D) is assumed to be constant in the vertical direction.

3.3.1.2 LASER BEAM ABSORPTION BY THE POWDER CLOUD

Taking these assumptions, the powder cloud can be said to absorb the incident energy in the manner described by the Bier-Lambert equation , ie

$$P_{(l_0)} = P_{(i)} \exp(-\beta l_0) \qquad (1)$$

where $P_{(l_0)}$ = remaining power after a powder depth, l_0.

$P_{(i)}$ = incident power

β = Bier-Lambert coefficient

As the beam has a Gaussian energy distribution $P_{(i)}$ in equation (1) must be expressed in the following way:-

$$P_r = \frac{P_{(tot)}}{\pi r_b^2} e^{-r^2/r_b^2} \qquad (2)$$

NB For r_b defined to the $1/e$ position.

where P_{tot} = Total beam power

P_r = Beam power at a distance r from the beam centre

r_b = Beam radius (see beam assumption No 3)

From equations (1) and (2) it is possible to express the residual power available after the beam has penetrated a powder cloud depth l_o.

$$P_{(l_o r)} = \frac{P_{tot}}{\pi r_b^2} \exp\left(\frac{r^2}{r_b^2}\right) \exp\left(-\beta l_o\right) \qquad (3)$$

Figure 3.3.1 shows that as the particles all travel in the same direction the height of powder above any particle remains constant throughout its flight through the laser beam. Thus, equation 3 gives a description of the energy field available to any plane of flight.

The Bier-Lambert coefficient β is a measure of the occlusion characteristics of the cloud, that is to say the energy absorption per unit depth.

This coefficient can be calculated in terms of the amount of powder under the beam and the size of the powder particles.

If the proportion of the total powder cloud which is unoccupied by particles is referred to as the voidage (ε), then the following is true:-

Total volume of particles

per unit volume $= 1-\varepsilon = n \frac{4}{3}\pi r_p^3$ (4)

$$n = \frac{3(1-\varepsilon)}{4\pi r_p^3} \quad (\text{per } m^3) \quad (5)$$

where n = number of particles per cubic metre

and r_p = the particle radius

If the powder cloud is assumed to consist of a set of layers of thickness 2rp in the vertical direction, the energy absorption of a set of these layers can be calculated. Although the surface area of the particle exposed to the incident laser radiation is equal to the top half of a sphere (i.e. $2\pi r_p^2$), the absorption of the beam is only equal to the shadow cast by a particle and this is equal to πr_p^2. Thus, for a layer 2rp deep and $1M^2$ the volume of the layer is: $2 r_p \ m^3$ (6)

From equation 5 and 6

The number of particles in the layer $= \frac{2 r_p \ 3(1-\varepsilon)}{4\pi r_p^3}$

$$= \frac{6\ (1-\varepsilon)}{4\pi r_p^2} \quad (7)$$

The beam absorbing area of this layer

$$= \frac{6\ (1-\varepsilon)}{4\pi r_p^2} \quad \pi r_p^2$$

$$= \frac{3\ (1-\varepsilon)}{2} \quad (8)$$

The proportion of the beam unaffected by the layer

$$I = 1 - \left(\frac{3(1-\varepsilon)}{2}\right) \quad (9)$$

Going back to equatin (1)

$$I = I_0 \exp(-\beta l)$$

where I_0 = original intensity

I = intensity after absorption

l = depth of absorbing layer

If $I_0 = 1$

I = equation 9 after $l = 2r_p$

So/

$$1 - \left(\frac{3(1-\varepsilon)}{2}\right) = \exp(-\beta 2 r_p) \qquad (10)$$

$$\ln\left[1 - \left(\frac{3(1-\varepsilon)}{2}\right)\right] = -\beta 2 r_p \qquad (11)$$

$$\beta = \frac{-\ln\left[1 - \left(\frac{3(1-\varepsilon)}{2}\right)\right]}{2 r_p} \qquad (12)$$

where ε = voidage

r_p = particle radius

3.3.1.3 RADIANT POWER DENSITY ON WELD POOL SURFACE

It is now possible to express the power density experienced by the surface of the weld pool. Fig 3.3.1 shows that it is assumed that the weld pool is, in the horizontal plane, a circle with the same dimensions as the laser beam. The surface of the weld pool is actually elliptical as it is inclined at an angle α to the horizontal. Powder cloud cover of the weld pool is illustrated by figure 3.3.1. It can be seen to consist of a powder layer of constant thickness which represents the common feature of over-shooting powder, and a wedge of powder which increases in thickness with (x) distance from the top of the weld pool.

From these considerations the thickness of the weld pool at a

distance x from the top of the weld pool is equal to:-

$$l_0 = l + (x \tan\theta) + (x \tan\alpha) \qquad (13)$$

Expressing equation (3) in terms of x and Y:

$$P_{(x,y)} = \frac{P_{tot}}{\pi r_b^2} \exp\left[\frac{-[(x-r_b)^2 + y^2]}{r_b^2}\right] \exp(-\beta l_0) \qquad (14)$$

Substituting in lo from equation (13) and B from equation (12)

$$P_{(xy)} = \frac{P_{tot}}{\pi r_b^2} \exp\left[\frac{-[(x-r_b)^2 + y^2]}{r_b^2}\right] \exp\left[\frac{\ln\left[1-\left(\frac{3(1-\varepsilon)}{2}\right)\right]}{2 r_p}(l + x\tan + x\tan\alpha)\right] \qquad (15)$$

This term defines the power input profile over the weld pool but does not take into account the fact that the weld pool is elliptical and not circular. This increase in the absorbing area has the effect of reducing the incident power density (which is of course inversly proportional to the absorbing area). The power density on the weld surface as a result of laser radiation P_w, is equal to $P_{(xy)} \cos\alpha$ i.e.

$$P_{(xy)} = \frac{P_{tot}\cos\alpha}{\pi r_b^2} \exp\left[\frac{-[(x-r_b)^2 + y^2]}{r_b^2}\right] \exp\left[\frac{\ln\left[1-\left(\frac{3(1-\varepsilon)}{2}\right)\right]}{2 r_p}(l + x\tan + x\tan\alpha)\right] \qquad (16)$$

Figure 3.3.2 shows the effect on the weld pool incident energy with changing voidage keeping all other variables stable. It can be seen that the wedge of powder 'casting a shadow' over the weld pool has the effect of decreasing the energy density over the pool but also moves the peak energy density to the left of the graph. This skewing of the Gaussian distribution is to be expected from the occlusion factor in equation 16 which of course shows that as the depth of powder increases with x so does the powder clouds ability to absorb the beam. It is also abvious that if the voidage remains constant but the value of rp is increased (which means that there are fewer, larger particles) then the value of β will decrease (see eqa 12) and so the effect will be similar

Fig. 3.3.2.A.

Power distribution on weld surface with changing ε (Voidage).

PTOT = 1000W
α = 45°
θ = 45°
r_p = ·05mm. l = 1mm. r_b = 1mm.

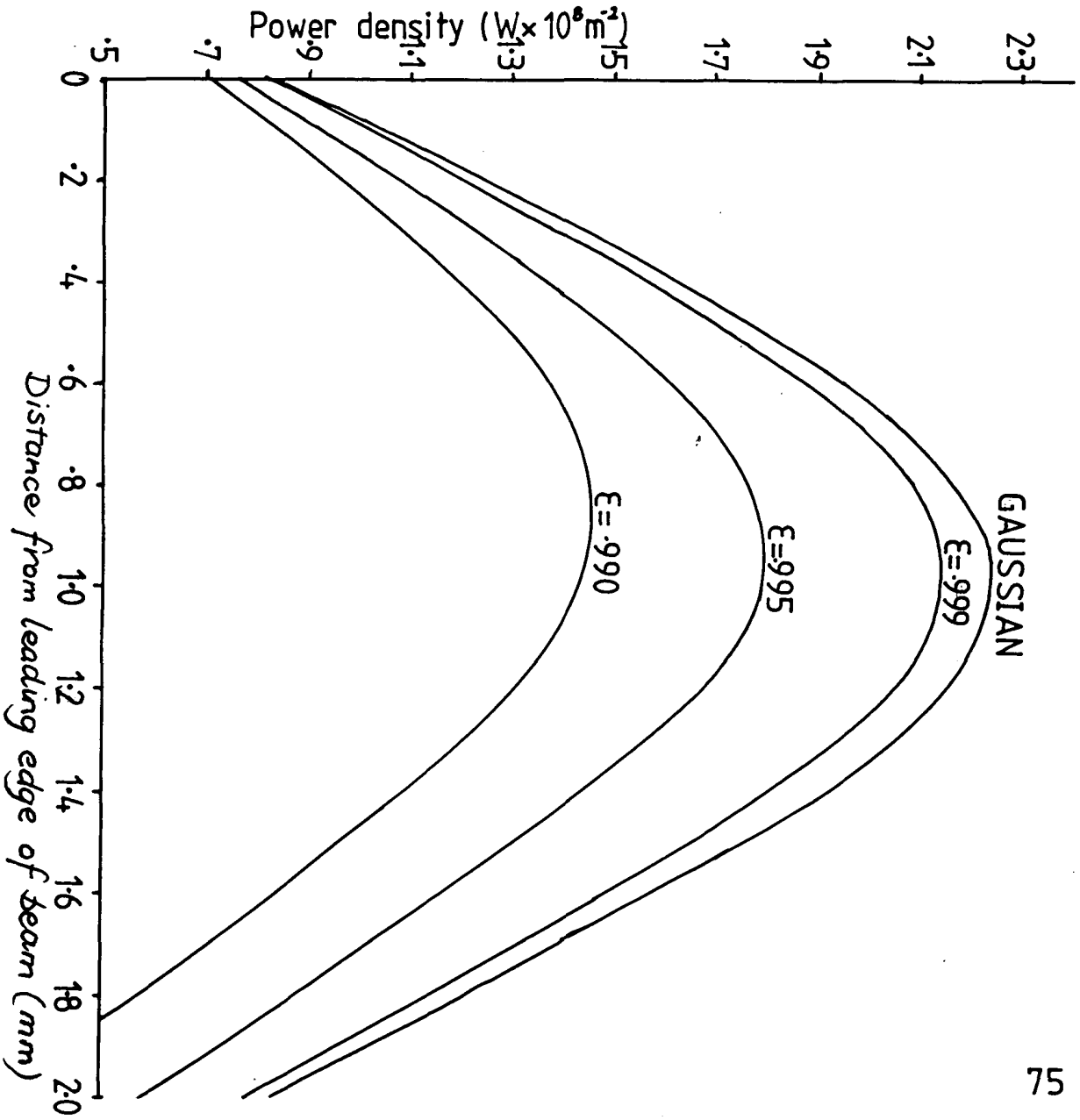

Fig. 3.3.2.B

Power distribution on weld with changing Γ_p.

PTOT = 1000W

α = 45 θ = 45

l = 1mm

Γ_b = 1mm

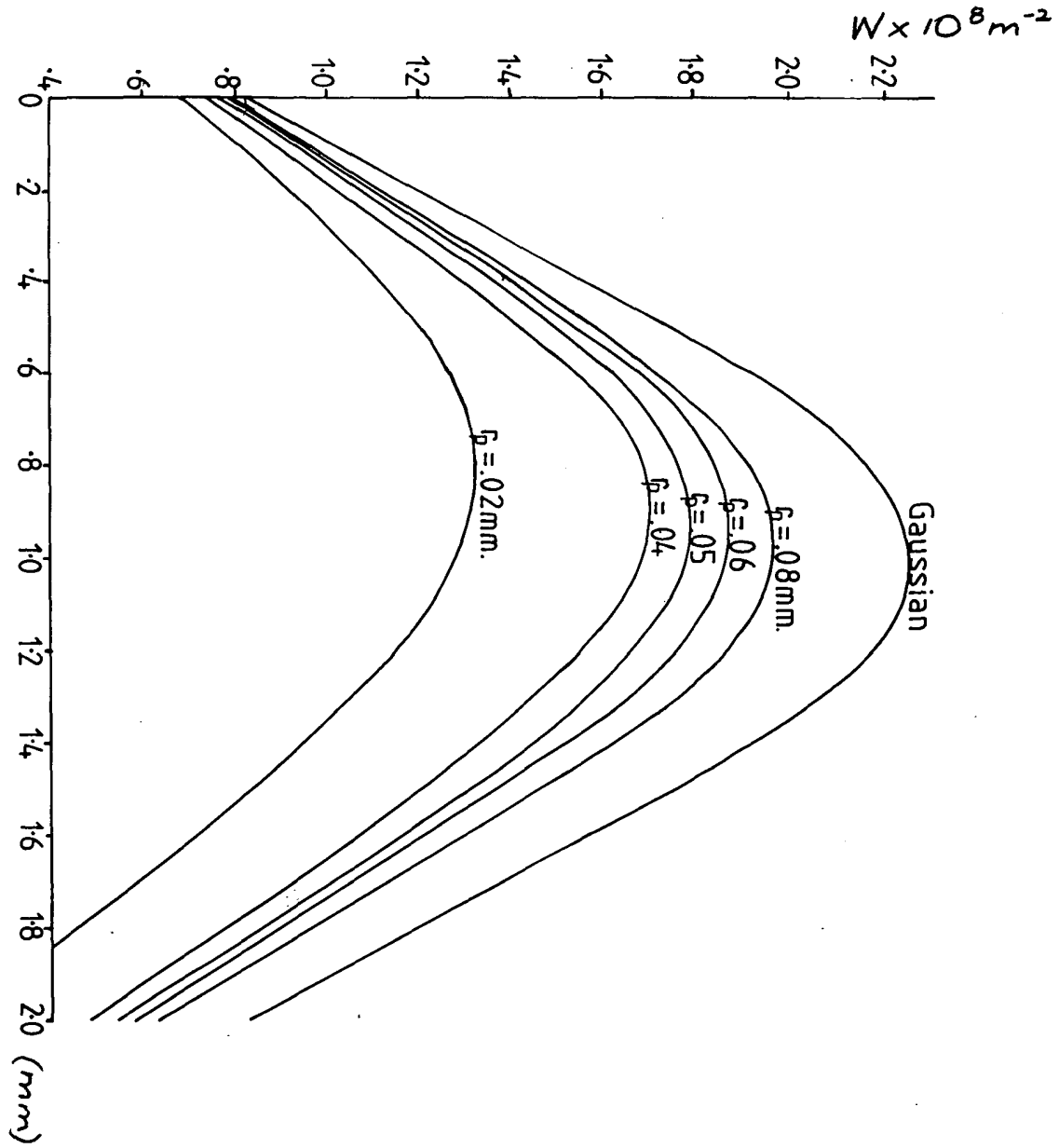

to increasing the voidage in figure 3.3.2. The same trend could be achieved by decreasing the value of θ or α or both as this would decrease the volume of the wedge over the weld pool and the maximum height of the powder cloud.

The effect of changing the particle radius is demonstrated in figure 3.3.2.B.

3.3.1.4 HEAT BALANCE ON A POWDER PARTICLE

The following calculations derive an expression for finding the temperature of any particle in the powder cloud at any position along its flight path to the weld pool.

Assuming the particle is at a uniform temperature T.

Heat in = Heat out plus Heat accumulated.

or/

$$\left[\begin{array}{l}\text{Laser energy absorbed} \\ [(1-r_f) P_{(xy)} (A\,dt)]\end{array}\right] = \left[\begin{array}{l}\text{Radiant loss} \\ [A^* \sigma (T_p^4 - T_a^4)\,dt]\end{array}\right] + \left[\begin{array}{l}\text{Convected loss} \\ [A^* h (T_p - T_a)\,dt]\end{array}\right] + \left[\begin{array}{l}\text{Temperature rise} \\ [\rho C_p V\,dt]\end{array}\right] \quad (17)$$

r_f = Average reflectivity
$A = \pi r_p^2$
$A^* = 4\pi r_p^2$
T_p = Particle temp.
T_a = Ambient temp.
σ = Stefans const.
h = Heat transfer coeff.
ρ = Particle material density.
C_p = Specific heat of particles.
V = Particle volume

Analysing each term separately:

Laser Energy Absorbed

This term is constructed in the following way;

The local energy input, after absorption of the beam by the powder above the particle in question is multiplied by the absorbing area of the particle (πr_p^2) and this is in turn multiplied by the absorption factor which is equivalent to $(1-r_f)$ where r_f is the reflectance of the material.

Thus, laser energy absorbed by a particle $= (1-r)\ P_{(r)}\ A dt$

expanding fromequation (3):

$$= (1-r_f)\frac{P_{tot}}{\pi r_b^2}\ \exp\left(\frac{-r^2}{r_b^2}\right)[\exp(-\beta l_o)]\pi r_p^2\ \frac{dx}{v.\cos\theta} \qquad (18)$$

NB $dt = \frac{dx}{v.\cos\theta}$ where dx is the distance travelled in the x direction of the particle with velocity v in the direction of flow.

Expressing this in terms of x and y with the Y axis at the left hand side of the beam radius (thus making x always positive as in the weld pool equation):

$$\text{laser energy absorbed } P_{(x,y)} = (1-r_f)\frac{P_{tot}}{r_b^2}\ \exp\left(\frac{(x-r_b)^2+y^2}{r_b^2}\right)[\exp(-\beta l_o)]\pi r_p^2\frac{dx}{v\cos\theta} \qquad (19)$$

$$\text{where } \beta = \frac{-\ln\left(1-\left(\frac{3(1-\varepsilon)}{2}\right)\right)}{2r_p} \quad \text{(from eq12)}$$

Radiant Loss

$$= A^*\sigma\,(T_p^4 - T_a^4)\,dt$$

Where A^* = total surface area of a sphere ($4\pi r_p^2$)

σ = Stephan Boltzmanns constant ($5.69 \times 10^{-8} W^{-2} K^{-4}$)

Tp = Particle temperature ^oK

Ta = Ambient temperature ^oK

$$\text{Radiant loss} = \frac{4\pi r_p^2\sigma(T_p^4 - T_a^4)\,dx}{v\cos\theta} \qquad (20)$$

Convective loss

$= A \cdot h\,(T_p - T_a)\,dt$

expressed in terms of X and T as before.

$$\text{Convective loss} = \frac{4\pi r_p^2 h\,(T_p - T_a)\,dx}{v\cos\theta} \qquad (21)$$

where h is the heat transfer coefficient for the material - gas system, defined for a sphere by Froessling as:

$$h = \frac{2K}{D} + \frac{0.6K}{D}\left[\left(\frac{C_p\mu}{K}\right)^{\frac{1}{3}}\left(\frac{Du\rho}{\mu}\right)^{\frac{1}{2}}\right]$$

where K = thermal conductivity of the gas

D = particle diameter

Cp = specific heat capacity of the gas

μ = viscosity of the gas

u = particle - gas relative velocity

ρ = particle density

For the sake of simplicity it willbe assumed in this work that there is no particle-gas relative velocity. This assumption is based on the fact that as the powder cloud escapes from the blowing nozzle the gas is travelling faster than the particles. With expansion into the atmosphere the gas slows down but the momentum of the particlescarries them forward at much the same velocity as their nozzle escape velocity if gravity is ignored. If gravity is considered the effect is that the particles accelerate with distance from the nozzle whereas the gas slows down. In the case of u=o :

$$h = {}^{2K}/_{D} \qquad (22)$$

Temperature rise.

$$= \rho C_p V_b dT$$

where ρ = density

C_p = specific heat

V_b = volume

$$= C_p \tfrac{4}{3}\pi r^3 dT \qquad (23)$$

Thus, the full expansion of eq.17. can be expressed by combining eqs.19, 20, 21, 22, + 23 :

$$(1-f)\frac{P_{tot}}{\pi r_b^2}\left[\exp\frac{-((x-\xi_b)^2+y^2)}{r_b^2}\right]\left[\exp(+\beta L_b)\right]\pi r_b^2 \frac{dx}{v\cos\theta} = \frac{4\pi r_b^2\sigma(T_b^4-T_a^4)dx}{v\cos\theta} + \frac{4\pi r_b^2 h(T_b-T_a)dx}{v\cos\theta} + \rho C_p \tfrac{4}{3}\pi r_b^3 dT \qquad (24)$$

Dividing throughout by πr_b^2 and taking $\check{P} = (1-f)\frac{P_{tot}}{\pi r_b^2}\exp(-\beta L_b)$

$$\check{P}\left[\exp\frac{-((x-\xi_b)^2+y^2)}{r_b^2}\right]\left[\frac{dx}{v\cos\theta}\right] = \frac{4\sigma(T_b^4-T_a^4)dx}{v\cos\theta} + \frac{4h(T_b-T_a)dx}{v\cos\theta} + \rho C_p \tfrac{4}{3} r_b\, dT \qquad (25)$$

$$\therefore dT = \frac{\check{P}\left[\exp\frac{-((x-\xi_b)^2+y^2)}{r_b^2}\right]\frac{dx}{4v\cos\theta} - \frac{(T_b^4-T_a^4)dx}{v\cos\theta} - \frac{h(T_b-T_a)dx}{v\cos\theta}}{\rho C_p \frac{1}{3} r_b} \qquad (26)$$

Taking $\check{V} = \rho C p \frac{1}{3} r_p v \cos\theta$;

$$\frac{dT}{dx} = \left[\frac{\check{P}}{\check{V}}\left[\exp\frac{[(x-r_b)^2+y^2]}{r_b^2}\right]\right] - \left[\frac{\sigma(T_p^4 - T_a^4)}{\check{V}} - \frac{h(T_p - T_a)}{\check{V}}\right] \qquad (27)$$

A numerical solution for this equation was developed and used as the basis of a computer analysis. For this analysis the factors concerning heat loss from the particle were considered to be negligable. The reasons for considering the heat loss to be negligable as compared to the heat gain of the particle are as follows:-

For the sake of simplicity, consider an incoming energy beam of uniform power impinging on a small spherical particle (see figure 3.3.3): considering the power input and output of the particle:

$$\text{power in} = \frac{(1-r)P_{tot}}{\pi r_b^2}\pi r^2 = (1-r)P_{tot}\left(\frac{r^2}{r_b^2}\right)$$

power out = radiated loss and convected loss

$$= \sigma(T_p^4 - T_a^4)A + h(T_p - T_a)A$$

Assuming the following representative values for the various

variables for small nickel particles at a temperature of 1020°C:

P_{tot} = 2000W

r_p = .00005 m

r_b = .0015 m

$(1-r)$ = .5

T_a = 293 K

T_p = 1293 K

σ = 5.67 x 10-8 W m^{-2} K^{-4}

h = 692.4: W/m/K

∴ Power in = .5 (2000) (.1 x 10^{-3}) = 1.0W

Radiated loss = 5.67 x 10^{-8} (1000^4) 4π (.00005)^2 = 1.78 x 10^{-3}W

Convected loss = 692.4 (1000) 4π (.00005)^2 = .022 W

∴ Power retained = 9.76W or 97.6 % of original.

It is obvious from the above that the input to the particle is only slightly affected by the radiated and convected losses and these can therefore be considered negligable, giving us an approximate equation :

$$\frac{dT}{dx} = \frac{\check{P}}{4\hat{V}}\left[\exp\frac{[(x-r_b)^2+y^2]}{r_b^2}\right]$$

from eqa 27.

3.3.1.5 COMPUTER MODELLING OF POWDER CLOUD HEATING

The numerical solution to this function was used on the basis of a computer programme (appendix E) which gave values for the temperature of any particle which having travelled through the beam, had arrived at a point x,y (in the horizontal plane). Thus, a particle temperature array at the surface of the weld pool was

obtained for a number of laser beam powers, voidages, beam radii particle velocities etc and it was found that exceptional circumstances would have to arise before any particles would impinge upon the weld pool in a molten state. A representative sample of these temperature arrays are presented in fig 3.3.3 and it can be seen that temperature rises are small in comparison to the melting point of, in this case, Nickel ($1450^{o}C$) . Combining the facts that melting and consolidation do take place at the surface of the weld pool and the incoming particles can be assumed to be solid, it can be postulated that the incoming cladding powder has a cooling rather than a heating effect on the weld pool and that melting takes place by conduction from the existing overheated weld pool to the cool particles.

3.3.2 SUMMARY

The theories constructed in the previous analysis form the basis of the discussion presented in Chapter Five of this thesis where it is shown that in this case, the energy distribution on the surface of the weld pool is approximately the same as that in the 'pre powder absorption' laser beam. For voidages less than .999 which will be the case as more effective powder delivery guns are developed, the skewing of the surface energy density towards the leading edge of the laser beam may have important effects upon the clad product. It should be borne in mind that the powder cloud has a double skewing effect, one attributable to absorption (removal of energy from the beam) and the other due to the transport of the energy absorbed towards the leading edge of the weld pool (ie the hottest particles are those which lead nearest to the 0,0 position see figure 3.3.3.

For the purpose of the experimental work in this thesis the mechanism of cladding can be approximated to:

A 'Gaussian' energy distribution laser beam is impingent upon a sloping weld pool which is being continuously cooled by incoming powder particles which are melted by conduction from the irradiated molten surface.

Figure 3.3.3 The computer generated temperature array for particles arriving at a position x y below the laser beam after travelling a distance x through the beam

Beam diameter = 3 mm Particle diamter = .1 mm

Beam power = 1800 W Particles speed = 1m/s

Material constants as for Ni. Voidage = .999

Temp in ^{o}C

Distance y. from beam centre (mm)

Distance x. from leading edge of beam	0	.2	.4	.6	.8	1.0	1.2	1.4
0	1030	983	945	807	664	524	395	244
.2	941	936	915	788	664	524	395	244
.4	880	860	832	674	632	515	395	244
.6	815	805	752	623	547	471	395	244
.8	740	732	705	572	498	424	334	244
1.0	677	665	640	520	448	76	291	240
1.2	603	586	573	460	397	334	255	187
1.4	544	532	498	405	343	281	213	145
1.6	480	473	441	347	292	235	156	82
1.8	417	411	367	299	241	184	115	47
2.0	345	340	289	246	193	144	83	21
2.2	267	259	228	191	141	97	35	20
2.4	205	188	162	132	83	52	20	20
2.6	147	137	107	83	44	23	20	20
2.8	84	76	53	31	20	20	20	20
3.0	20	20	20	20	20	20	20	20

Chapter 4

PRE PLACED POWDER CLADDING

4 1. GENERAL

Section 3.2 in Chapter 3 defined the process of melting and welding a pre placed powder layer to a substrate. Although the process has drawbacks, which will be discussed later, the ease of experimentation afforded by the lack of additional equipment needed to carry it out, means that such effects as rastering the laser beam can be easily studied. In this series of experiments various processing parameters were systematically changed to allow an analysis of their effects on the finished product but in all cases the basic exp erimental aim was to traverse a laser beam over a layer of powder on a substrate and to analyse the effect thereof.

4.2. EQUIPMENT USED

At this stage in this thesis it is appropriate to give a general description of the basic equipment available to the work.

4.2.1 THE IMPERIAL COLLEGE HIGH POWER LASER LABORATORY

4.2.1.1 The Layout of the Laboratory

Figure (4.1) shows the general layout of the laboratory. The two lasers (described later) can be used separately or in conjunction at any of the work stations depending

FIGURE. 4.1 . Schematic of the Imperial college high power laser laboratory.

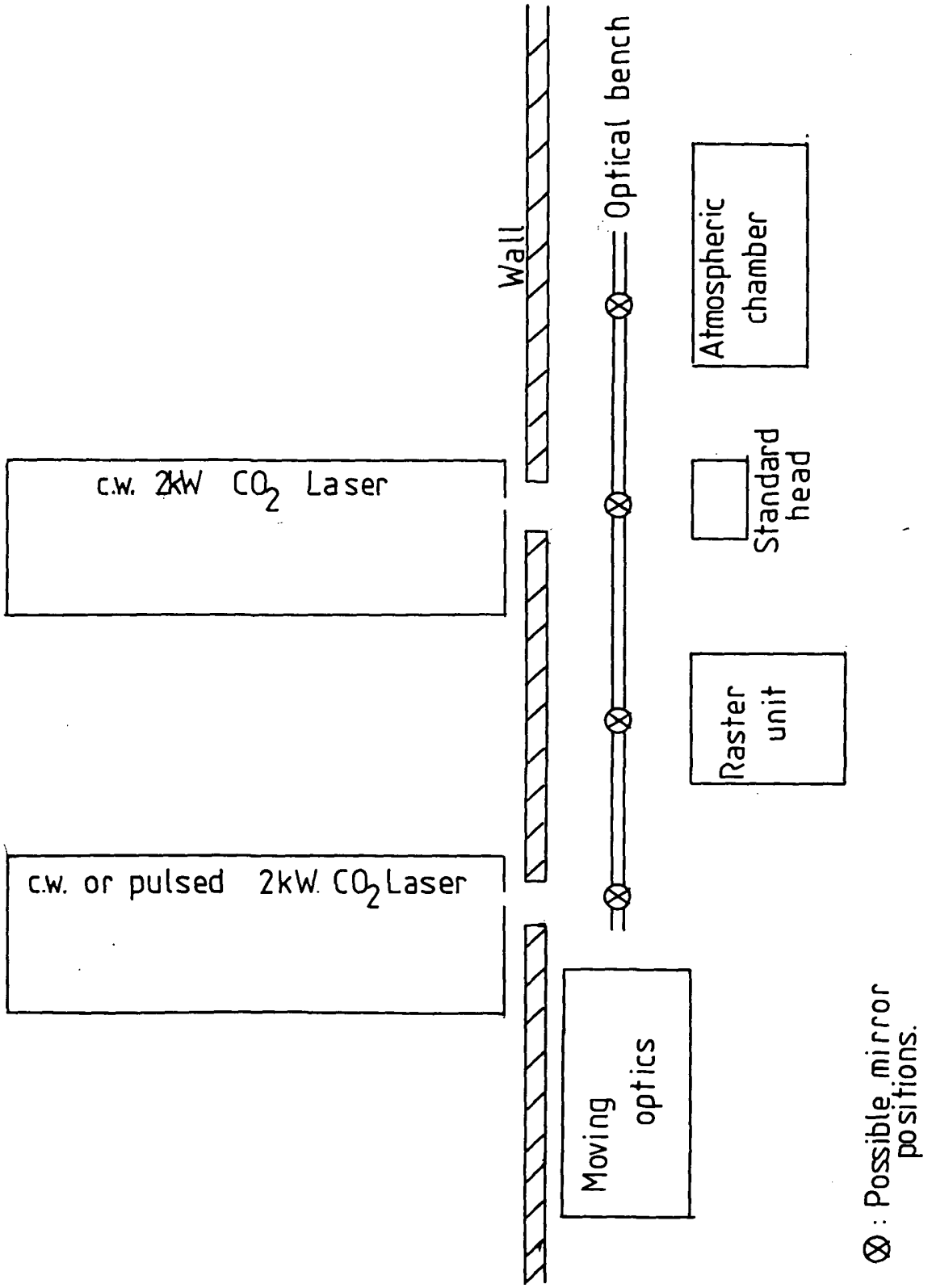

on how the emitted beams are deflected by the gold plated water cooled copper mirrors on the optical bench. It is also possible to use one of the lasers as an amplifier of the emitted beam of the other laser. All the work carrried out for this thesis uses either the standard laser head or the raster unit, both of which will be fully described shortly. As neither the computer controlled moving optics nor the atmospheric chamber were utilised a description of their operation will be left to other workers.

When setting up, for example, the'cw or pulsed' laser for operation at the raster head it is necessary to align the main beam with a coaxial heliumneon laser beam. This is done by first producing a beam print on a piece of asbestos a distance away from the output window and then turning the mainbeam off. By means of a 90^{o} prism placed directly in front of the output window a helium neon beam is introduced along the same path. Adjustment by means of small foot screws on the He-Ne laser allows the red spot to be centralised on the original beam print and the two beams can be assumed to be co-axial. The red beam is then reflected off two of the water cooled gold plated mirrors and they are adjusted until the spot is central on all the mirrors in turn, including the mirrors in the raster system itself. The He-Ne laser can now be switched off and taken out of the system by removal of the prism. The main beam will now follow the pre arranged path for processing work. Positioning of work pieces before processing can be facilitated by re introducing the red He-Ne beam prior to irradiation with the main CO_2 laser beam.

4.2.1.2 THE CONTINUOUS WAVE CO_2 LASER

Figure 4.2. is a schematic diagram of the control laser 2KW cw CO_2 laser (model 901), developed by control laser (formally BOC Industrial Power Beams Division) and the Welding Institute.

Typical gas composition and consumption data is shown in the following table:-

TABLE 4.1

Gas consumption and composition for the cw CO_2 laser

Gas	Composition Wt %	Typical gas consumption at full power with re-circulator engaged (litre/hr)
Helium	75-85	170
Nitrogen	10-14	50
CO_2	5-10	6

(From Control Laser Technical Literature)

A roots blower circulates the gas through the plasma tubes and the fast axial design makes it possible torealise high gas velocities (up to approx 500 m/s). Discharge stability at such high gas velocities is achieved by shock stabilisation.

A combination of low current (700 mA DC max) and high voltage (30KW open circuit) electrical discharge results in the excitation of the gas mixture (as described previously) to yield 10.6mm laser radiation. This radiation is strongly

FIGURE. 4.2. The 'Control laser' 2kW.(cw).CO_2 laser

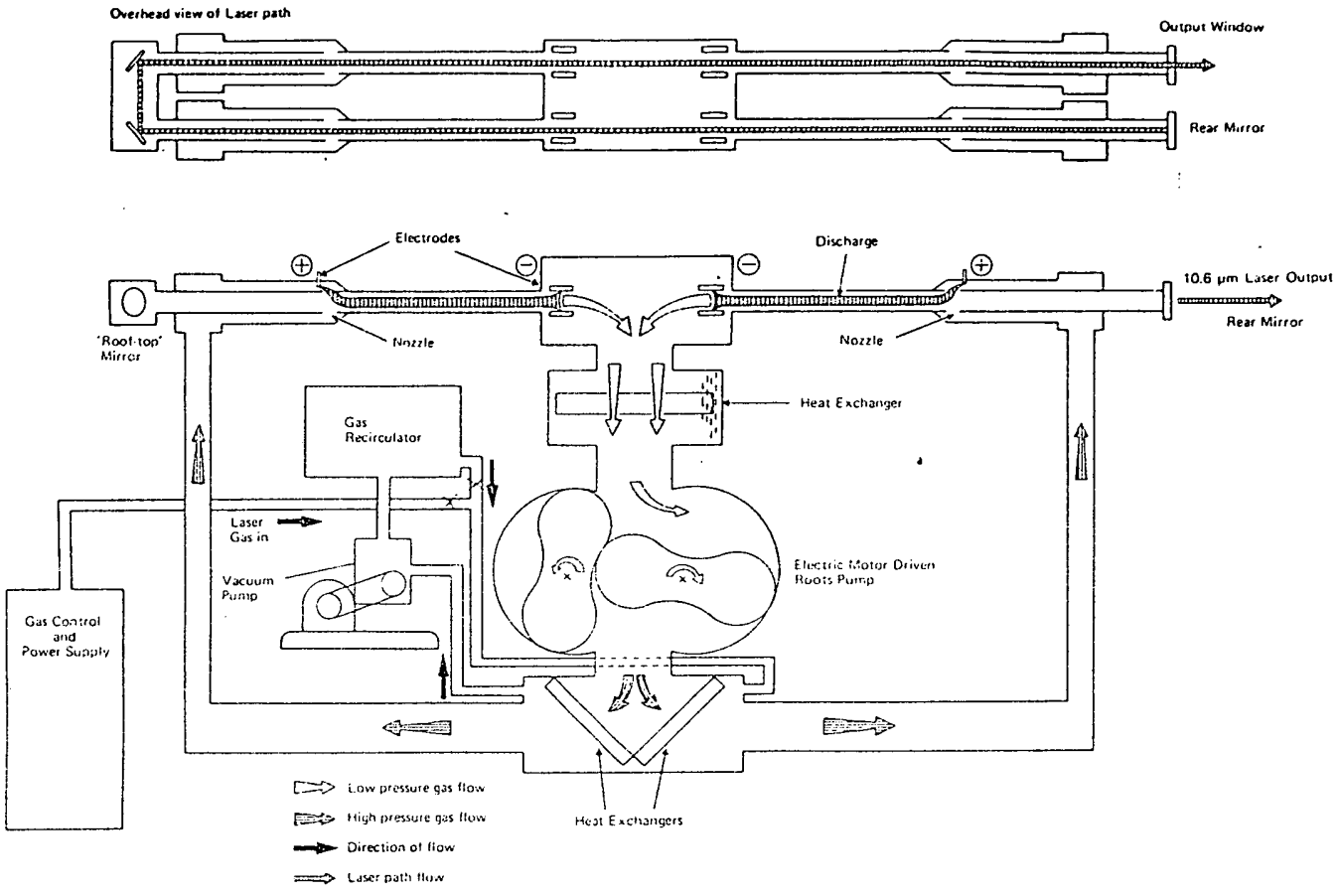

BOC 2kw CO_2 Laser – Gas and Discharge Paths

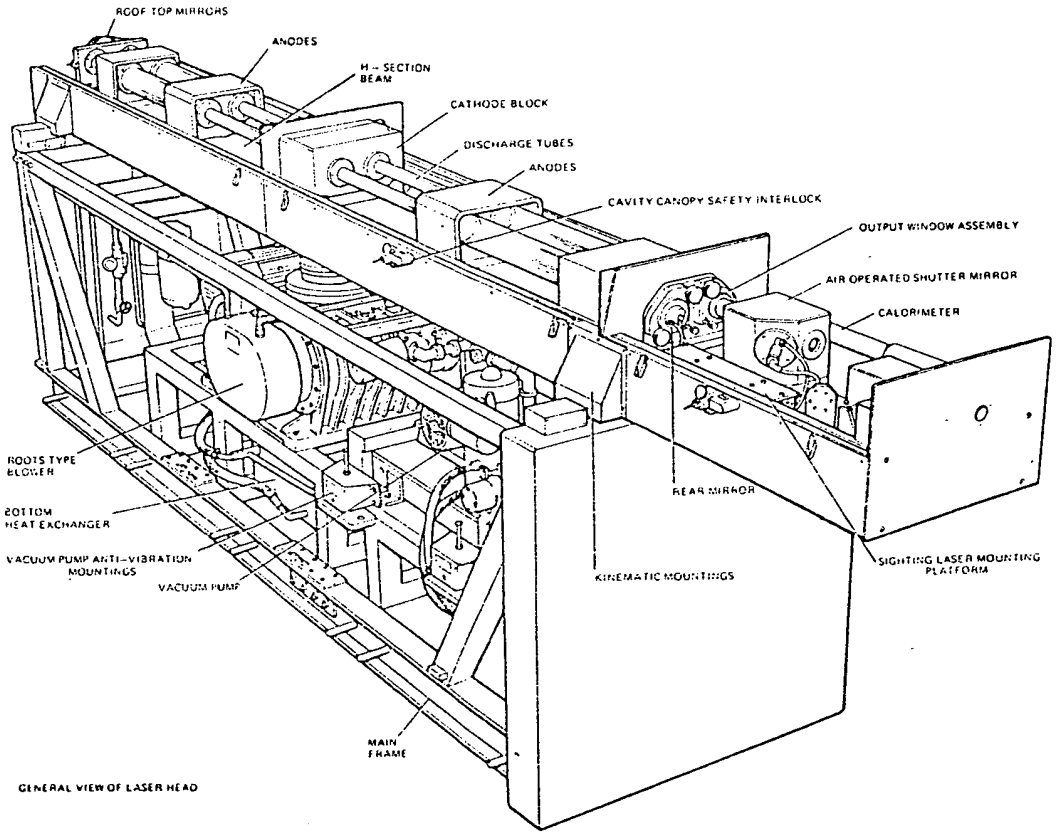

GENERAL VIEW OF LASER HEAD

absorbed by many materials and so it is necessary to use specialised unsusceptable materials for the construction of CO_2 laser optics.

To contain and direct the beam, water cooled, gold plated copper mirrors are used. Beam transmission or focussing is achieved by the use of 10.6mm wavelength transparent media including : germanium, gallium arsenide, cadmium telluride, zinc selenide and sodium or potassium chloride. The control laser 2KW machine utilises an output window made of water cooled GaAs which has a reflectivity of about 35% for 10.6mm radiation. The lenses used for focussing the beam are generally made of potassium chloride.

The total optical cavity in 8 meters long folded in the middle and a pneumatically operated on-off shutter beyond the output window directs the beam into a water cooled calorimeter when the beam is not in use.

The temperature of the water in the calorimeter is related to the power output of the beam and the digital display of the power level is taken directly from a calibrated thermocouple reading of this temperature.

4.2.1.3 THE cw/PULSED CO_2 LASER

This laser differs from the earlier model only in its ability to produce a pulsed output.

It is possible to change the pulse repetition rate, duration and shape. The pulsing is achieved by simple electrical

switching of the HT arcs. It is well known that prior to the ignition of the arcs the potential difference between the anode and cathode is greater (35KV) that when the arcs are struck (25KV). This drop in voltage on ignition is part of the design of the machine but does not happen quite instantaneously and so for a short time the arc energy is greater than nominal and this boosts the laser output momentarily. Combining this with the fact that a 'cool' lasing gas is more efficient than a steady state excited gas in producing laser light it can easily be seen that intermi ttent high energy (approx 3 x nominal at peak) pulses can be emmitted by the laser if the HT arcs are switched on and off. The response time of the electrical and gas systems limit the proximinity of the pulses to each other and the average output will be, in general, lower than the nominal cw output for the same electrical conditions. Intermittent high energy pulses were found, during the course of this work, to have no beneficial effect on cladding and if the pulsing was spaced widely enough to make each pulse an individual event the energy input was not sufficient for cladding.

4.2.1.4 THE STANDARD LASER HEAD

The standard laser head mentioned in section 4.2.1.1 as part of the layout of the laboratory is basically a means of holding a KCl (or similar suitable material) lens, focussing the beam through a small nozzle through which is propelled a gas which determines the atmosphere in the laser spot - substrate interaction zone. The gas can be inert, to prevent excessive reaction of hot or molten metal with the air, or reactive, for example;

O_2 is employed to aid the ablation process when cutting mild steel(67).

Figure 4.3 is a cross section of such a laser head showing the lens, lens mount, lens height adjustments, heater, gas inlet, x-y nozzle movement and the nozzle itself. The lens height adjustment varies the position of the focal point of the lens with respect to the nozzle.

The x-y nozzle movement is necessary because the lenses are held between rubber O rings for gas tightness and a clearance is allowed in the lens holder to allow for thermal expansion when the beam is being transmitted. It is therefore very difficult to position and x-y movement of the nozzle is necessary for centralising the focussed spot.

The heater incorporated into the head is there to prevent the KCl lens reacting with atmospheric moisture and becoming 'fogged'. At this point it should be mentioned that there must always be a co-axial gas flow even if it is not necessary from the materials interactions point of view. This is because the gas flow keeps the lens clean, one speck of dust on the KCl lens leads to the creation of a hot spot through beam absorption, resulting in cracking and eventual melting of the lens and damage to the inside of the laser head.

4.2.1.5 THE RASTER UNIT

Figure 4.4. shows the raster unit employed during the study of pre-placed powder cladding. The sinusoidal oscillation of mirror 'A' results in x direction rastering

FIGURE 4,3. The standard laser head

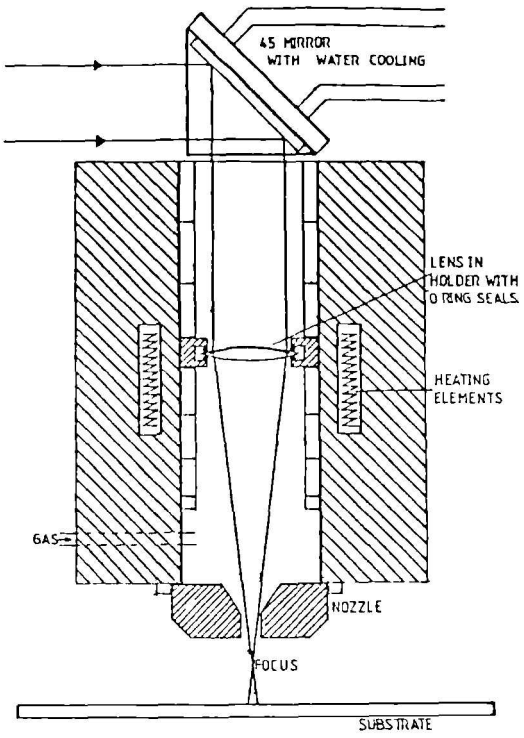

FIGURE 4,4. The raster unit

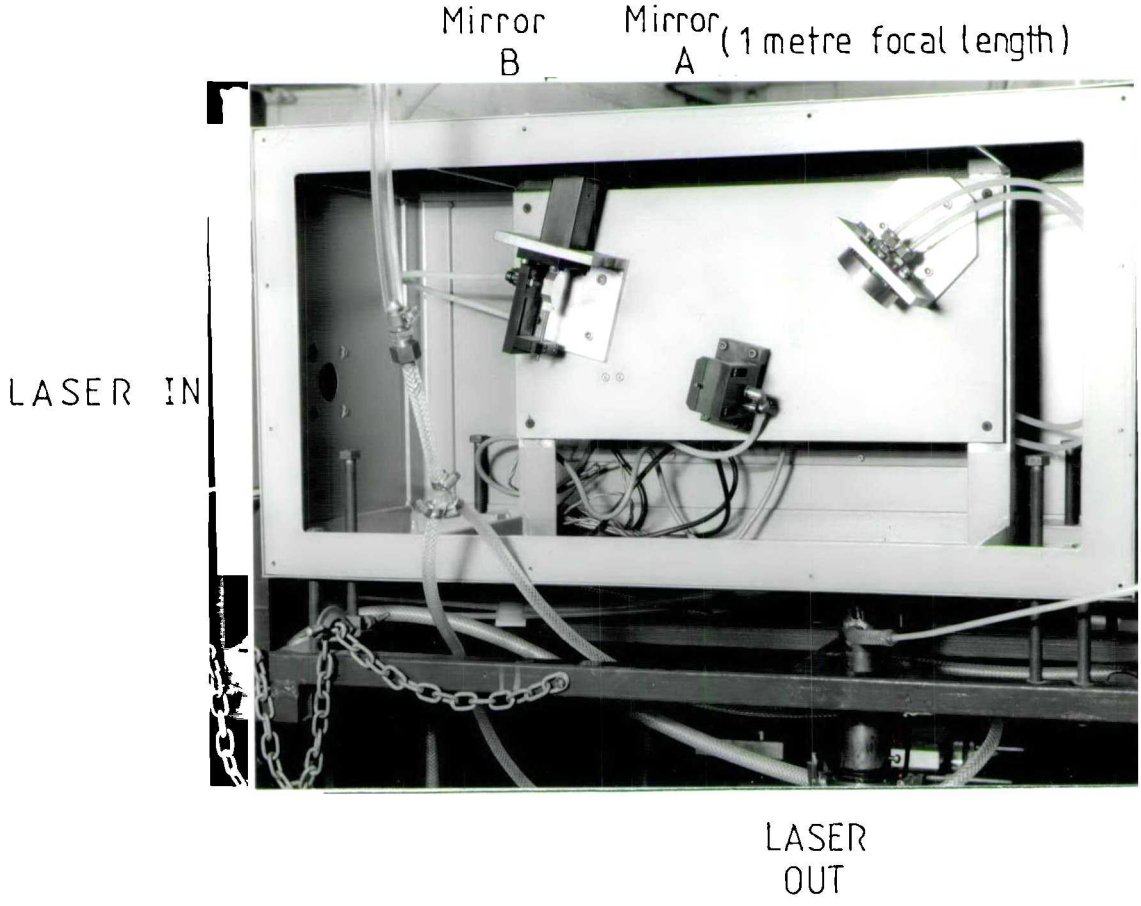

of the beam ie. rastering in the plane of the paper. The movement of substrates was always into or out of the photograph and so if mirror A was turned on alone, the effect on the substrate would be similar to being exposed to a broad, thin source of energy. Vibration of mirror 'B' results in the production of a 'line source' of energy into and out of the figure ie in the direction of travel of the substrate. The effect of this on a substrate would be similar to being exposed to a reduced power stationary spot for a prolonged time.

Oscillation of both mirrors at the same time results in a block source of energy on the surface of the substrate the dimensions and energy profile of which are determined by the amplitudes and frequencies of the mirrors movement (both mirrors are independently controlled). The other factor affecting the energy density on the sample surface is of course the distance from the focussing mirror to the powder layer, a factor which effects the size of spot which is experiencing the rastering. The calibration chart for the rastering mirrors is included here as Figure 4.5.

The effect on the energy distribution of dwell times will be discussed and the practical consequences investigated later in this chapter.

It is, of course, impossible to have a small laser nozzle providing an inert atmosphere protection for the cladding weld pool if a rastered beam is being employed. For this reason the special 'head' shown in Fig 4.6 was used. The

FIGURE. 4.5.
Raster unit calibration

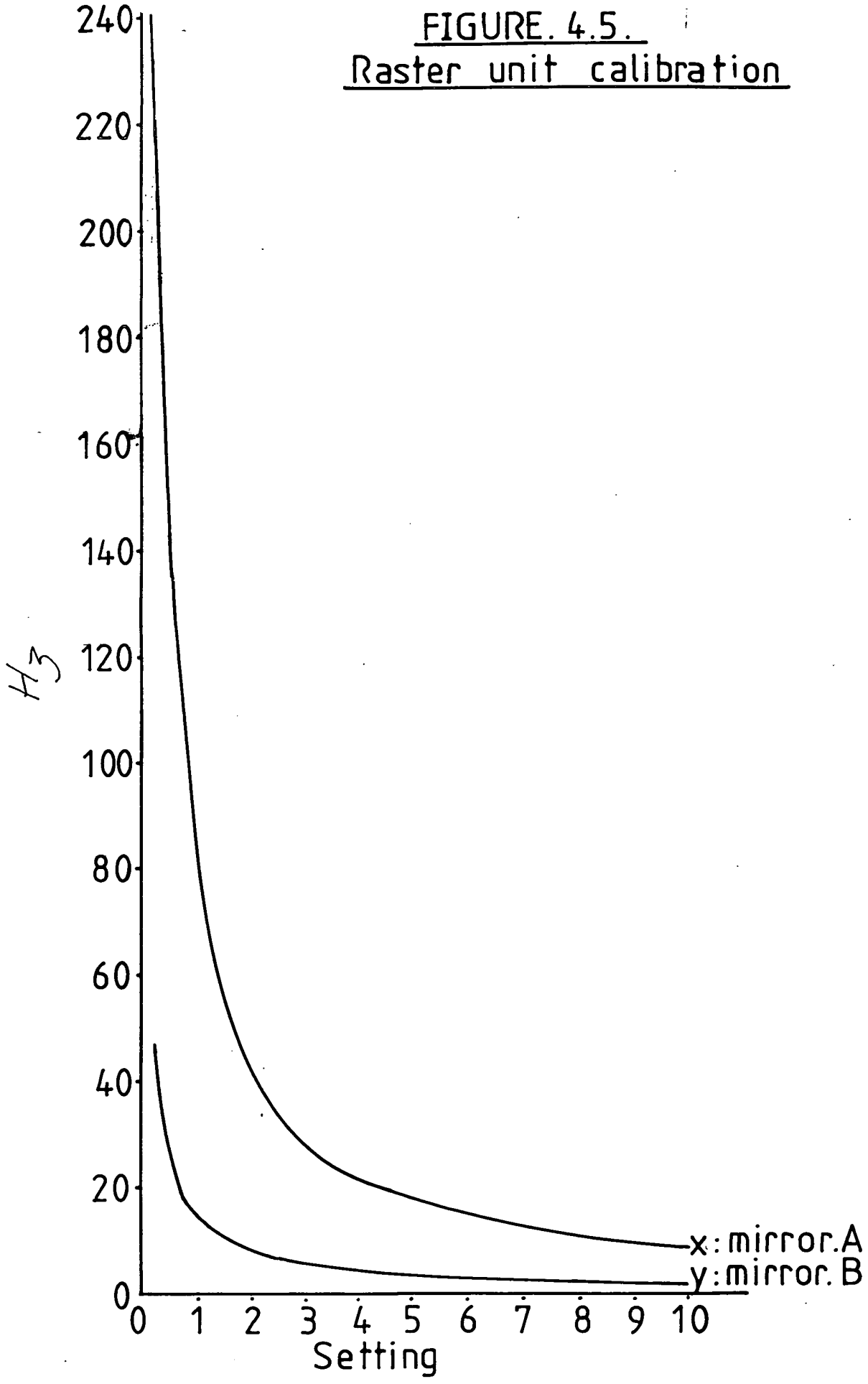

top end was gas sealed with a KCl flat, Ar was pumped into the tube (the diameter of which was larger than any raster configuration used) and expelled from the bottom, covering the weld pool.

4.2.2 THE X-Y TABLE

The hydraulically powered x-y table used throughout this work had the following capabilities:-

A/	X direction speeds	:-	0-350 mm/sec
B/	X direction stroke	:-	380mm
C/	Y direction speeds	:-	0-10 mm/sec
D/	Y direction stroke	:-	152mm
E/	Height adjustment	:-	±150 mm

Two valves controlled the rate of oil supply to the X and Y cylinders and thus the rate of traverse. The Y movement was usually used for positioning and the faster, longer X movement was used for processing. Mechanically actuated interlocks prevented the table from reaching the end of its traverse at high speed. When processing with the table, only the central portion of the movement should be studied to prevnt processing speed anomalies caused by the starting up and slowing down of the table.

An electronic timer attached to the table measured directly the time taken for the table to traverse the central ten centimeters of its X movement. The digital display was then recorded after each run and used to calculate the processing speed.

the valve controls for the hydraulic fluid flow and thus the processing speed were infinately variable making it very difficult to re-set a processing speed previsouly used, this will be mentioned later in the experimental work.

4.3 EXPERIMENTAL PROCEDURE

Figure 4.6 is a schematic representation of the experimental set up used for these experiments. The bulk of this work was carried out in the following manner:-

1. A cut to size (3" x 1" x $\frac{1}{2}$") mild steel substrate would be placed between the fixed spacers.

2. The top of this substrate would be uniformly covered by a deep layer of stainless steel powder.

3. A steel edge would be slowly moved across the bed of powder whilst being in firm contact with the spacers which have thereby fixed the depth of powder remaining (3.25mm) on the surface of the substrate.

4. The speed of the X movement of the X-Y table would be set.

5. The sample would be passed under the laser beam, the following parameters having been pre-set and noted:

   a) Beam power

   b) Rastering conditions ie

      i X direction raster amplitude and frequency

      ii Y direction raster amplitude and frequency

FIGURE.4.6.
Experimental set up for pre placed powder cladding.

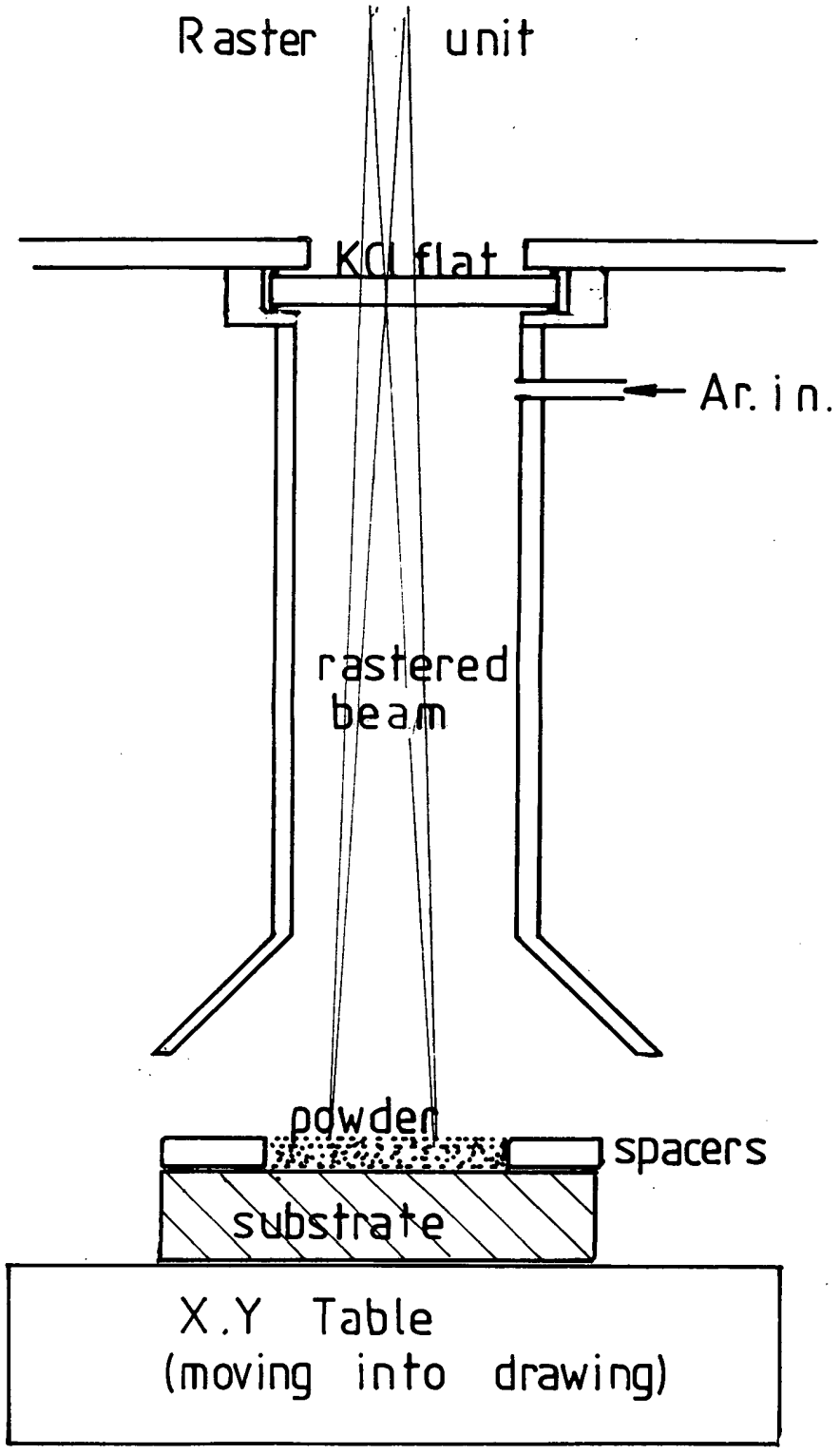

c) The sample would then be electrically engraved with an identifcation number ready for metallographic examination.

Thus, the effects of the following variables on the process were investigated:

a) Rastering characteristics:

i Spot source (no rastering)

ii X direction rastering (different raster amplitudes)

iii Combined X and Y rastering

b) Beam power

c) Processing speed

The samples collected from this series of experiments were sectioned, polished and optically examined. Hardness testing was carried out but the results from the hardness survey were found to be disappointingly uninformative (see next section).

Photomicrographs of the deposited stainless steel were similar in all cases and it was decided to omit all but a representative few from the report. The interesting information accrued from these experiments was taken from measurements obtainedfrom photomicrographs. The relationships between the parameters and the size and shape of the deposit cross sections was of great interest.

4.4 RESULTS AND DISCUSSION

4.4.1 The Effect on Deposit Morphology of Raster Configuration

4.4.1.1 The Effect of Changing from Spot to Line to Block Source at Different Raster Amplitudes

Figure 4.7 shows the change in deposit cross section attributable to the change in incident energy source from the unrastered spot size (.5 mm radius) to an X direction rastered line source (ie a line at 90° to the direction of travel) to a simultaneously X and Y directions rastered block source. The dimensions of the X and Y amplitudes are marked on the figure adjacent to the relevant cross section together with any other change in processing parameters. (all tracing at X15).

Table 4.2 below gives the physical dimensions of the cross sections:

Table 4.2 cross section dimension for the spot-line block source experiments.

Cross Section I.D. Letter	Energy Source Type + Dimension (mm)	Processing Speed mm/sec	Cross Section Area mm^2	Base Width mm	Max Width mm	Comments
A	Spot (1mm x 1mm)	3.3	7.15	2.2	2.3	
B	Line (4mm x 1mm)	3.3	8.40	3.4	3.7	
C	Block(4mm x 4mm)	3.3	9.05	3.1	3.8	
D	Spot (1mm x 1mm)	3.3	7.30			
E	Line (5mm x 1mm)	3.3	8.90	4.4	Base	
F	Block(5mm x 4mm)	3.3	8.70	4.3	Base	

Cross Section I.D. Letter	Energy Source Type + Dimension (mm)	Processing Speed	Cross Section Area mm^2	Base Width mm	Max Width mm	Comments
G	Spot (1mm x 1mm)	3.3	7.40	2.1	2.9	
H	Line (7mm x 1mm)	3.3	4.85+ 3.95	1.8 + 1.8	2.3 2.2	Two beads produced
I	Block(7mm x 4mm)	3.3	No Cladding			
J	Spot (1mm x 1mm)	2.5	9.00	1.4	3.7	
K	Line (4mm x 1mm)	2.5	11.20	3.6	4	
L	Block(4mm x 4mm)	2.5	11.10	3.5	4	
M	Spot (1mm x 1mm)	2.0	10.20	2.1	3.8	.7mm^2 substra melted
N	Line (7mm x 1mm)	2.0	12.90	6.0	Base	
O	Block(7mm x 4mm)	2.0	13.10	6.0	Base	

FIGURE. 4.7. The effect of changing from spot to line to block source at different raster amplitudes.

(×15)

(See table 4.2)

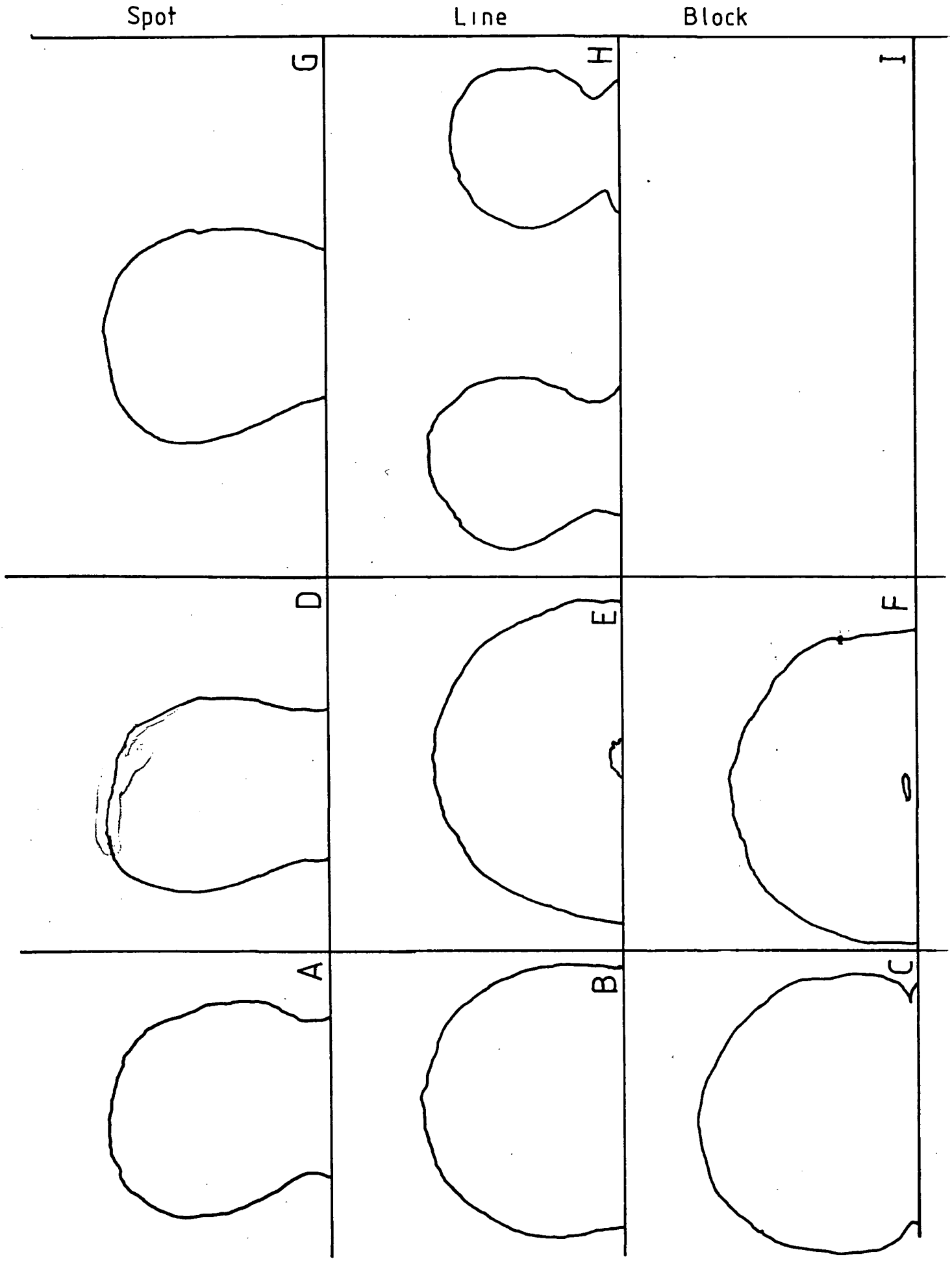

FIGURE 4.7. Continued.

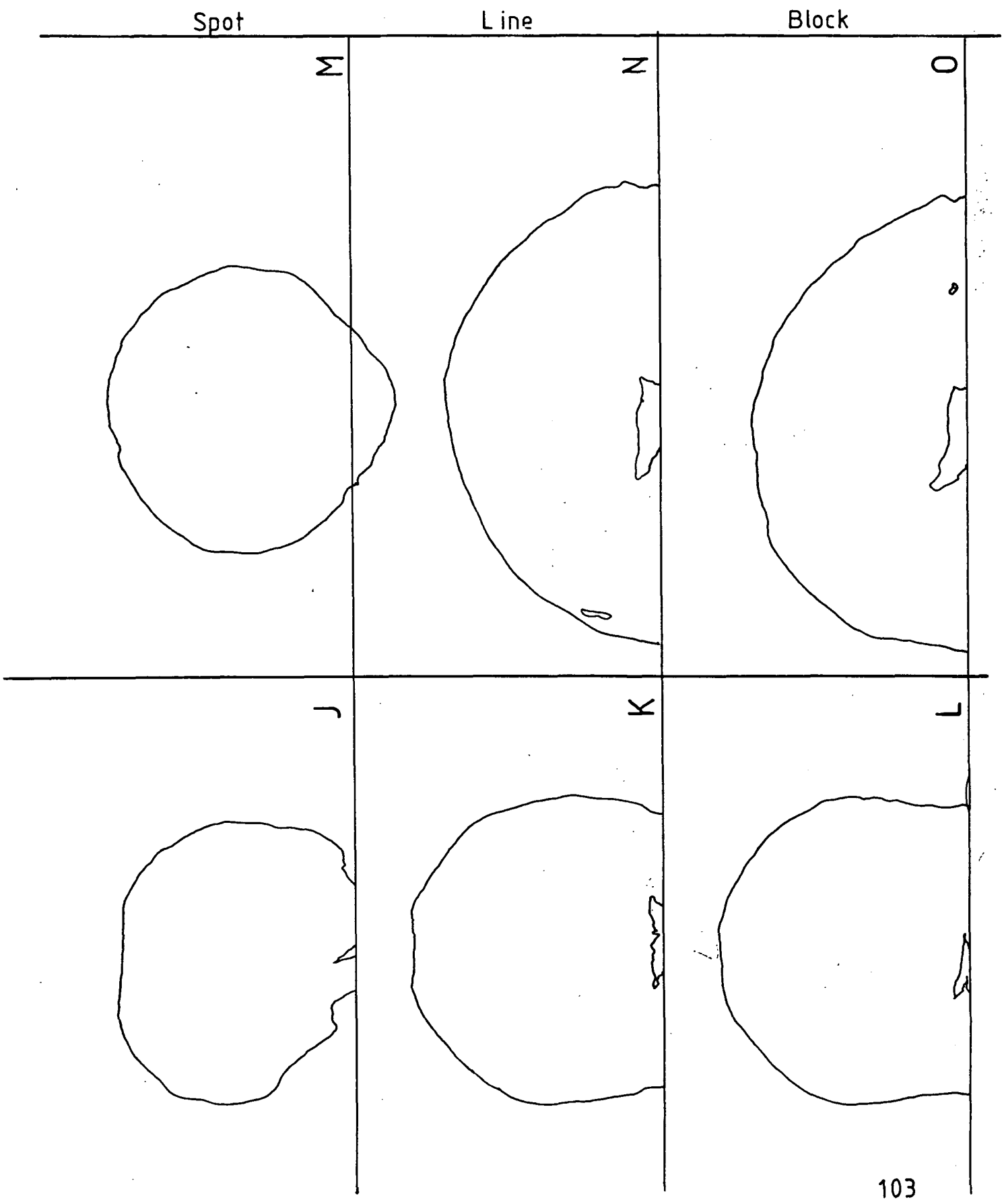

The tracings and the readings make it possible to analyse the morphologies of the different weld pools produced by a range of energy distributions impingent upon the powder bed. The processing parameters which were kept unchanged throughout the series of runs were as follows:

Powder depth = 3.25mm

Laser power = 1500 W

Raster frequencies = Maximum in both X and Y direction

Considering cross sections A to I it is clear that the changes are due to differences in the energy densities and their interaction times. In chapter 3 it was explained that the process is capable of producing good quality cladding over a wide range of processing parameters. Good quality, in this case, refers to the production of a good interfacial weld with no dilution and it can be observed that this is the case in cross sections A to G although H and I need further explanation. Runs A to G obviously fall within range, A D and B being produced under identical (spot source) conditions, B and E with line sources of 4mm and 5mm total length (NB 4mm line source length describes 3mm rastered movement of a 1mm diameter spot), and C and F with block energy sources of dimensions 4mm x 4mm and 5mm x 4mm respectively.

There is only a slight difference between the line and block source samples because although a block source has a lower energy density than a line, its interaction time with any powder element is greater, in this case (C and F) the energy density is one quarter of the line source case (B and E) but the interaction time is four times as large (1.2 secs instead of

.3 secs). Thus the total energy input remains the same and, when samples comfortably inside the good cladding parameter range are considered, the finished product remains fundamentaly unchanged. Further analysis of these cross sections requires some information about the energy densities experienced by the weld pools. Figure 4.8 shows the output from the computed relative energy densities of a gaussian energy distribution beam of radius .5mm undergoing simple harmonic oscillation of differing amplitudes. The peaks at the end of the movement reflect the high deceleration and acceleration, low velocity parts of the SHM movement and the low energy density at the centre of the movement is due to the naximum traverse velocity being found there. Movement of the energy densities at the peaks and in the centre of the movement (Fig 4.8) shows that as the amplitude is increased the difference between the maximum and minimum increases ie the peaks become more profound. It is this effect which resulted in cross section H being split into two. The melt front in the powder bed which approaches the substrate will bear a resemblance to the energy density which created it although the effect will be damped out by convective flow and surface tension forces. Four different types of laser-liquid-solid interaction are illustrated in figure 4.9 as a possible mechanism of cladding which satisfys the experimental evidence.

Interaction Type 1 : A defocussed gaussian beam is impingent on the powder producing a molten pool whose shape is governed mainly by surface tension forces and is approximately circular in cross section. This weldpool contacts the substrate and is frozen by, initially, point contact and, as the liquid collapses onto the substrate, area contact. The clad product of such an interaction will have a great deal of undercut

Fig. 4.8.

Power distributions
with changing raster widths.

Beam radius = 1mm.

RASTER WIDTH	MAX P_f	MIN P_f	MIN/MAX
2	373	308	·8
4	251	144	·57
6	201	96	·48
8	175	70·5	·4
10	155	58·5	·37
16	115	52	·45

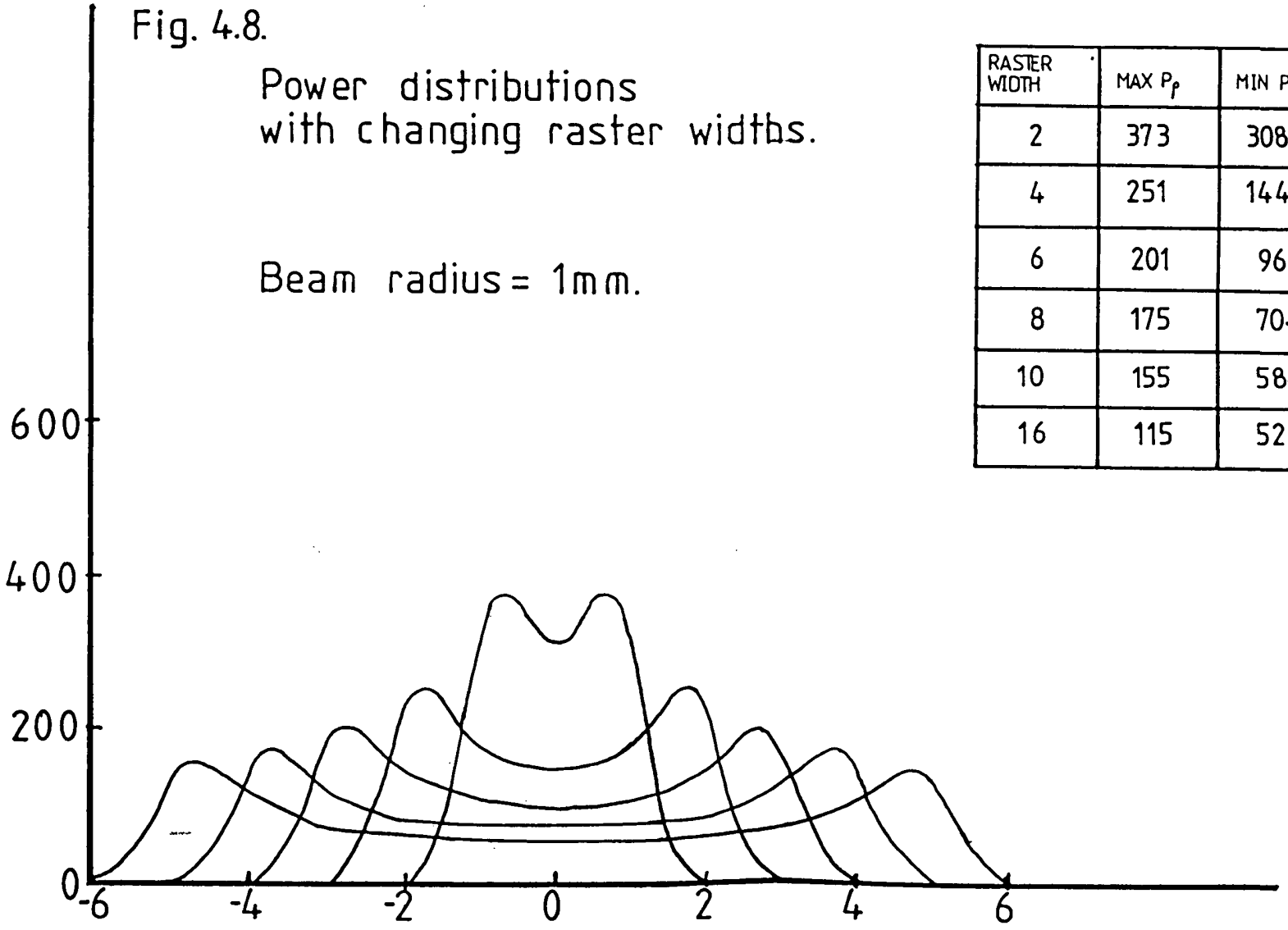

FIGURE.4.9. BEAM-MELT-SUBSTRATE INTERACTIONS.

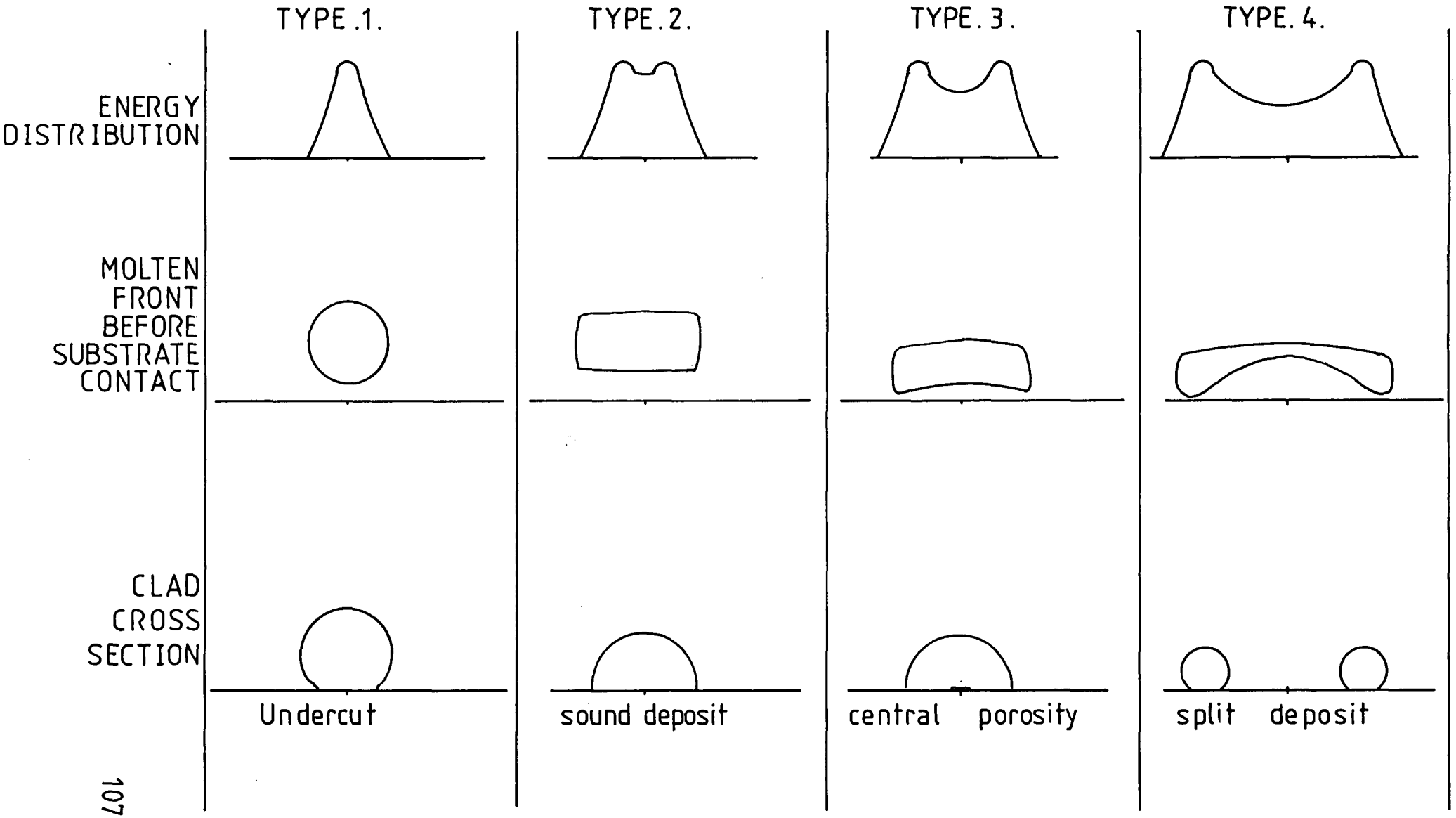

because the liquid-solid contact solidifies the melt before the liquid can wet the substrate extensively. All clad tracks carried out with a spot source energy input had an unacceptable (to industry) level of undercut, eg A D and G.

Interaction Type 2 : A rastered beam attempts to introduce a velocity gradient across the melt front by melting the powder more effectively, both in the initiation and propogation stages, at the extremes of its SHM, but the effect is counter acted by surface tension effects attempting to draw the melt into a circular cross section. The result is a 'square' melt front which contacts the substrate evenly resulting in an approximately semi circular cross section deposit (eg B) with no undercut.

Interaction Type 3 : The same struggle exists between the uneven energy input and the surface tension as in type 2 but in this case the increased separation of the energy peaks and the increase in the difference between max and min energy densities (see Fig 4.8) means that the outer edges of the melt contact the substrate first.

Thus the solidification begins at the edges of the deposit trapping the small amount of still unmelted powder in the centre. This powder is subsequently melted into the pool as the pool is solidifying but the air in this powder bed is trapped at the liquid-solid interface and a central pore is evident in the deposit. (see sample E). With prolonged laser-pool interaction this interfacial pore can have time to float free of the interface and appear above the centre of the clad-substrate interface. (see sample F).

Interaction Type 4 : Energy distribution effects become dominant and the melt front approaches the substrate as two peaks joined by a thin bridge of melt (bearing a strong resemblance to the energy density). The two peaks contact the substrate and adhere and solidification begins during which the surface tension effects are strong enough to break the molten link between the two peaks. Solidification is then completed in the same way as in type 1 leaving two similar type 1 deposits, the distance between which is determined by the raster amplitude.

These four types of interactions will be referred to later as they explain most of the results collected in this investigation.

The reason why no sample exists for cross section I is because the energy density available (1500 W over a 4 x 7mm square) was not capable of initiating melting in the interaction time available (1.2 secs) . The theory in chapter 3 showed that at low energy densities the time taken to initiate melting can be much greater than the time to reach the substrate once melting has been initiated and this is demonstrated by increasing the interaction time to 2.0 seconds (cross section O) where not only has melting been initiated and completed but the melt has been heated sufficiently to prevent being split into two by minimal central melting.

Although the subject of processing speed (interaction time) and its effect on deposit morphology will be dealt with in the next section, cross sections J to O have been included here as a demonstration that the principles governing samples A to I are generally applicable. Slowing down the processing time has much the same effect as increasing the total power and this

has led to K and L being more energy distribution dependant than before (B and C) and so the central pore has become more prominent.

N and O are the longer interaction time (2 rather than 1.2 seconds) versions of H and I and it can be seen that the more effective coupling of the energy, particularly in the centre, has produced type 3 clads rather than type 4. This is because the thinness of the bridge joining the two peaks during the production of H was to a large extent attributable to the long initiation time related to the central energy density. This initiation time (see chapter 3) reduces rapidly with increasing power at low power densities but changes little with high power densities so although the weld pool at the edges of the rastering will grow faster than in the middle the melting, initiation is now approximately simultaneous and the cladding becomes type 3.

Sample M is of interest because it is one of the very few samples produced with any dilution of the deposit with the substrate. It will be noted that this sample experienced the maximum energy density.(1500 W over a .5mm radius circle) for the longest interaction time (.5 seconds) for a spot. In this case the melt was produced, semi solidified and remelted through to the substrate within that time (see chapter 3).

In summary it can be said that, for this process the energy density/interaction time experienced by H is totally unsuitable as is the interaction experienced by M*. Between this two extremes which are, as was postulated earlier in chapter 3,

widely separated, acceptable surface welded, no dilution, deposits are possible with varying degrees of central porosity and undercut.

* NB

H : line dimensions : 6mm x 1mm, interaction time .3 secs

M : spot dimensions : 1mm x 1mm (dia), interaction time .5 secs ($.785mm^2$)

Laser power 1500W powder depth 3.25mm

4.4.1.2 THE EFFECT OF CHANGING PROCESSING SPEED

Fig 4.10 shows the changing cross sections of deposits clad with changing processing speed for two sets of samples, one set carried out with a 7mm line source of energy and the other with a 4mm line source. The theoretical model in chapter 3, dealing as it does with a one dimensional argument does not imply that a change in processing speed would result in a change in the amount of material clad but this is obviously the case in practice. Considering figure 4.10A (the 4mm line source) first, this phenomenon of cross section increase with decreasing cladding speed can be explained.

The amount of powder directly under the line source of energy is small in comparison to the actual amount of material melted. In this case the nominal amount of material under the beam would result in a clad cross sectional area of:

4mm (the width) x 3.25mm (the depth) x (3.4×10^{-3}) (Powder density; g mm^{-3}) $\div$ (7.8×10^{-3}) (density of stainless steel ; g mm^{-3}) = 5.67 mm^2

FIGURE. 4.10.A. The effect of changing the processing speed.

(×15)

(1500W)

4mm rastered beam.

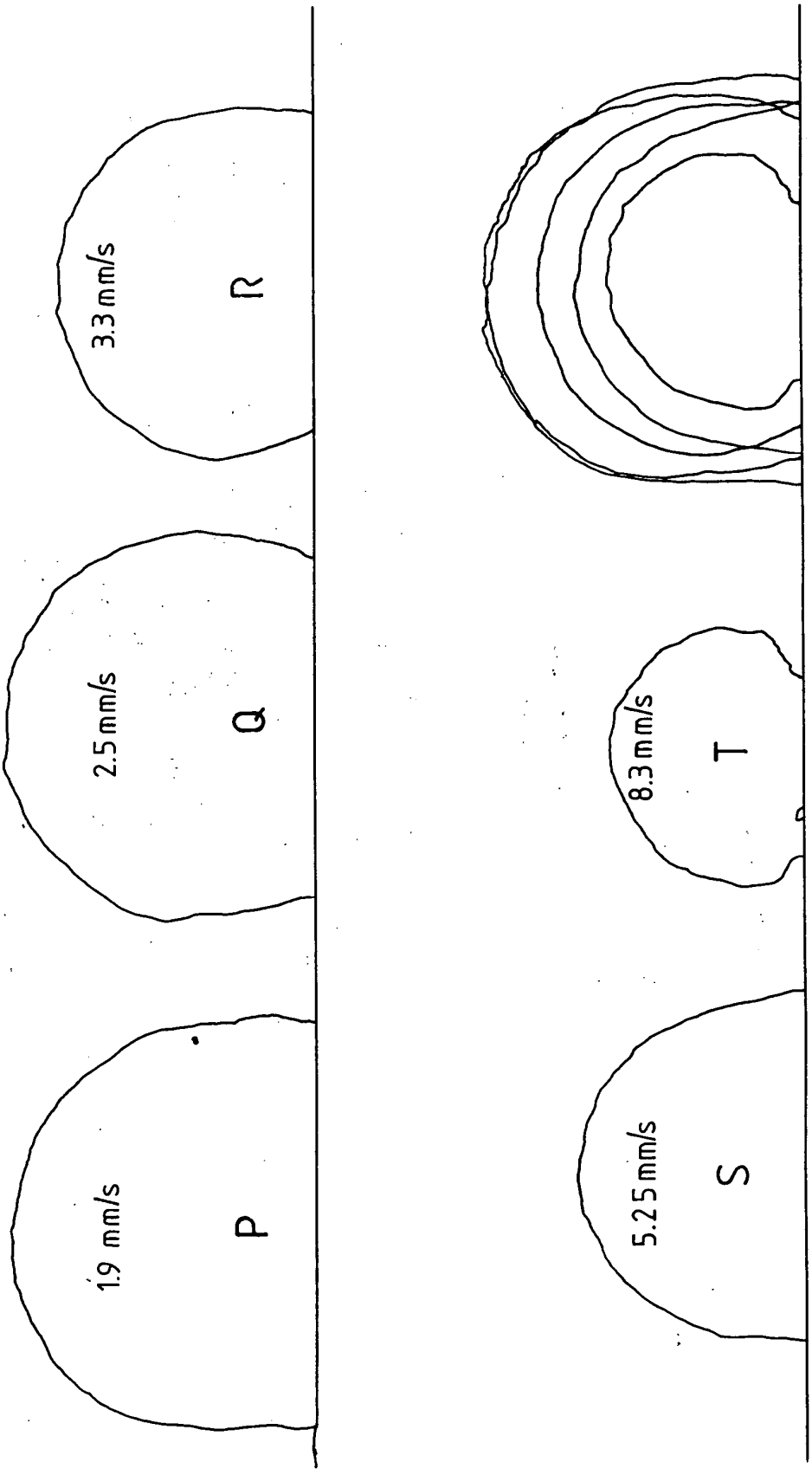

FIGURE. 4.10.B. The effect of changing the processing speed.

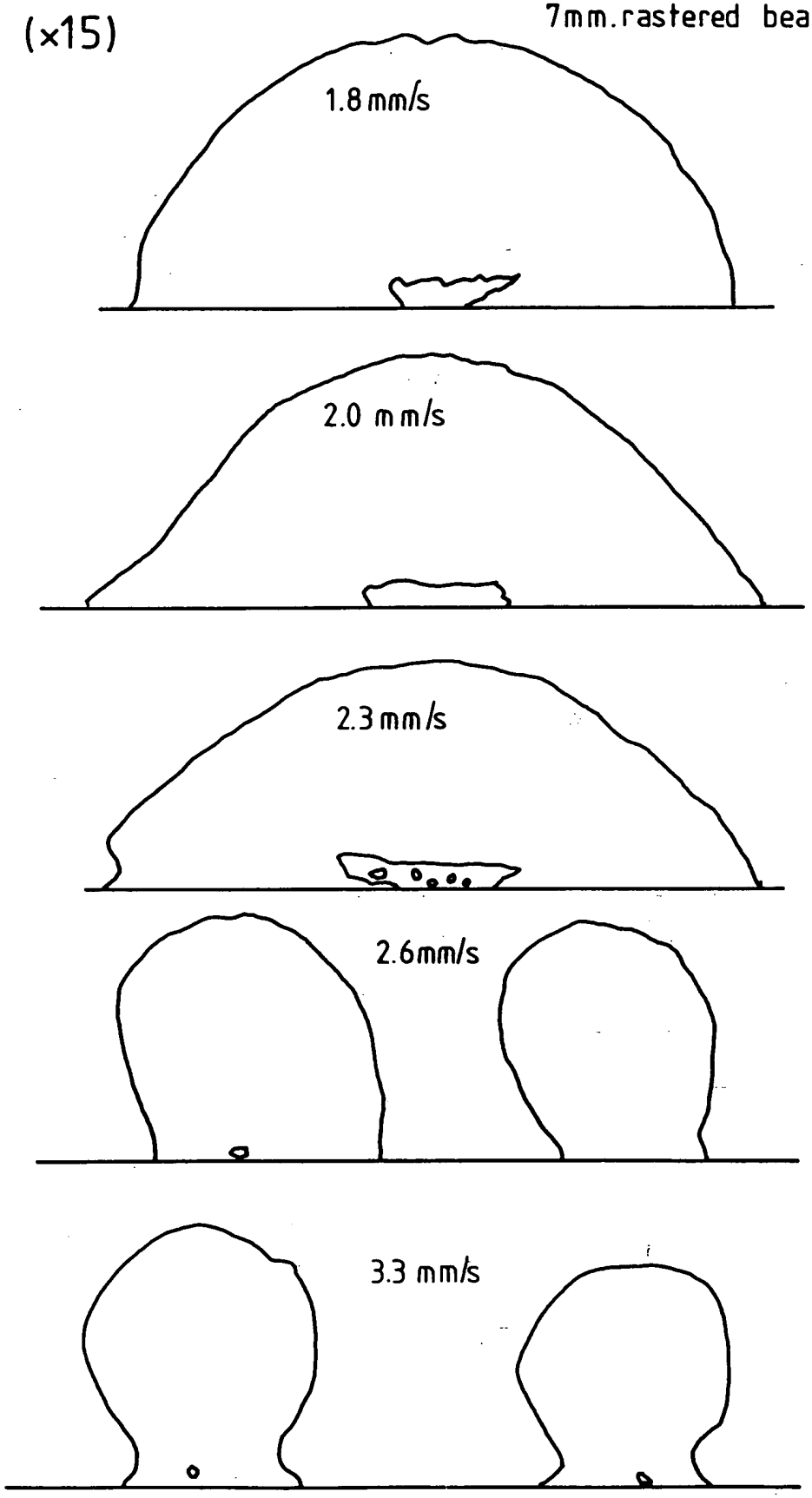

All except the smallest trace are larger than this in cross section area, a result which is easily understood if it is considered that the powder on each side of the weld pool collapses into it leaving denuded areas on each side. The extent of this gathering of surrounding powder is affected by the speed of processing which governs the base width and average temperature of the melt. At high processing speeds (T) the amount of material melted is low as a result of the low energy input. This small melt has its morphology governed by surface tension forces and becomes a type 1 (see earlier) deposit dropping through the powder bed with a basically circular cross section. The melt is short lived and has a rather low average temperature in comparison with the other melts to be discussed and thus does not interact with the surrounding powder bed very effectively. Any incorporated powder will cool the surface of the melt still further and help to chill the rapidly solidifying melt.

As processing speeds are decreased (S,R) the increased laser material interaction not only melts more material but tends to combat the surface tension forces and spread the pool in the direction of rastering. This hotter more extensive pool incorporates a certain proportion of the incoming powder by the method postulated in figure 4.11 until the combination of the lasers removal and the cooling effects of the substrate and incoming powder solidify the melt.

At even slower processing speeds the base width of the pool is similar to that of the raster width (see cross sections P and Q) and the powder on each side of the melt is allowed to collapse and be incorporated into the melt until the denudation of the surrounding area means there is no longer

FIGURE.4.11. Powder collapse into the melt.

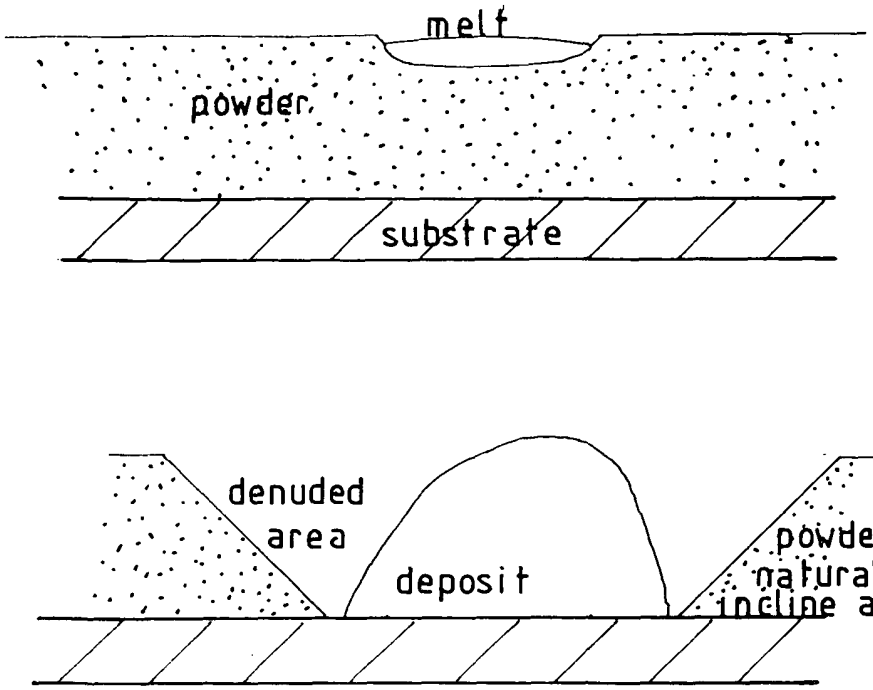

FIGURE.4.12. Increase in X-sect. area with interaction time.

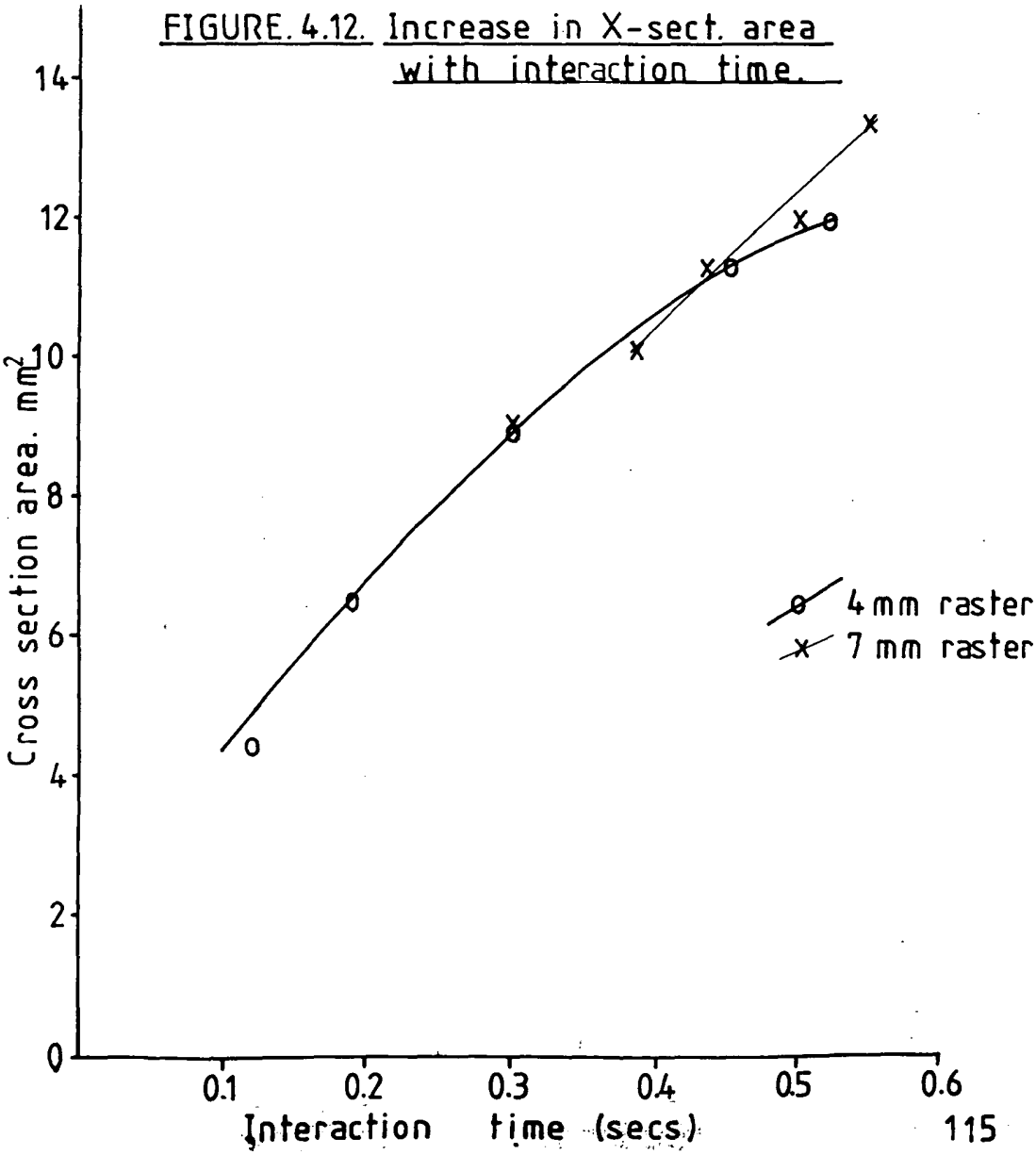

a reservoir of powder available.

These trends are reflected in figure 4.12 where it can be noted that after an initial linear rise of cross section area with interaction time the curve levels out as a larger and larger percentage of the available surrounding powder is incorporated into the melt.

Considering the samples covered by figure 4.10B it can be seen that at slow processing speeds (U, V and W) the above arguments are directly applicable. At high speeds however, the surface tension effects, enhanced by the cooler weld pools separate the deposit into two parralell tracks. The increase in total cross sectional area still follows a basically linear trend (figure 4.12) but the deposits are slightly larger than would be expected. This slight increase is attributable to the fact that the melt, in separating, is approaching the surrounding powder.

4.4.1.3 THE EFFECT OF CHANGING THE LASER POWER

Observation of figure 4.13 and 4.14 shows that increasing the laser power is closely analagous to increasing the laser material interaction time. Figure 4.12 shows that the limiting cross section for this powder bed and raster width (4mm) is in the region of thirteen mm^2, the linear trend being disturbed only above eleven mm^2 by lack of available powder this linearity is shown in figure 4.14 and it is unfortunate that at the time of these experiments the laser had a maximum reliable power of 1700W otherwise the levelling out of the curve at the limiting cross section could once again have been observed.

FIGURE.4.13. The effect of changing the laser power.

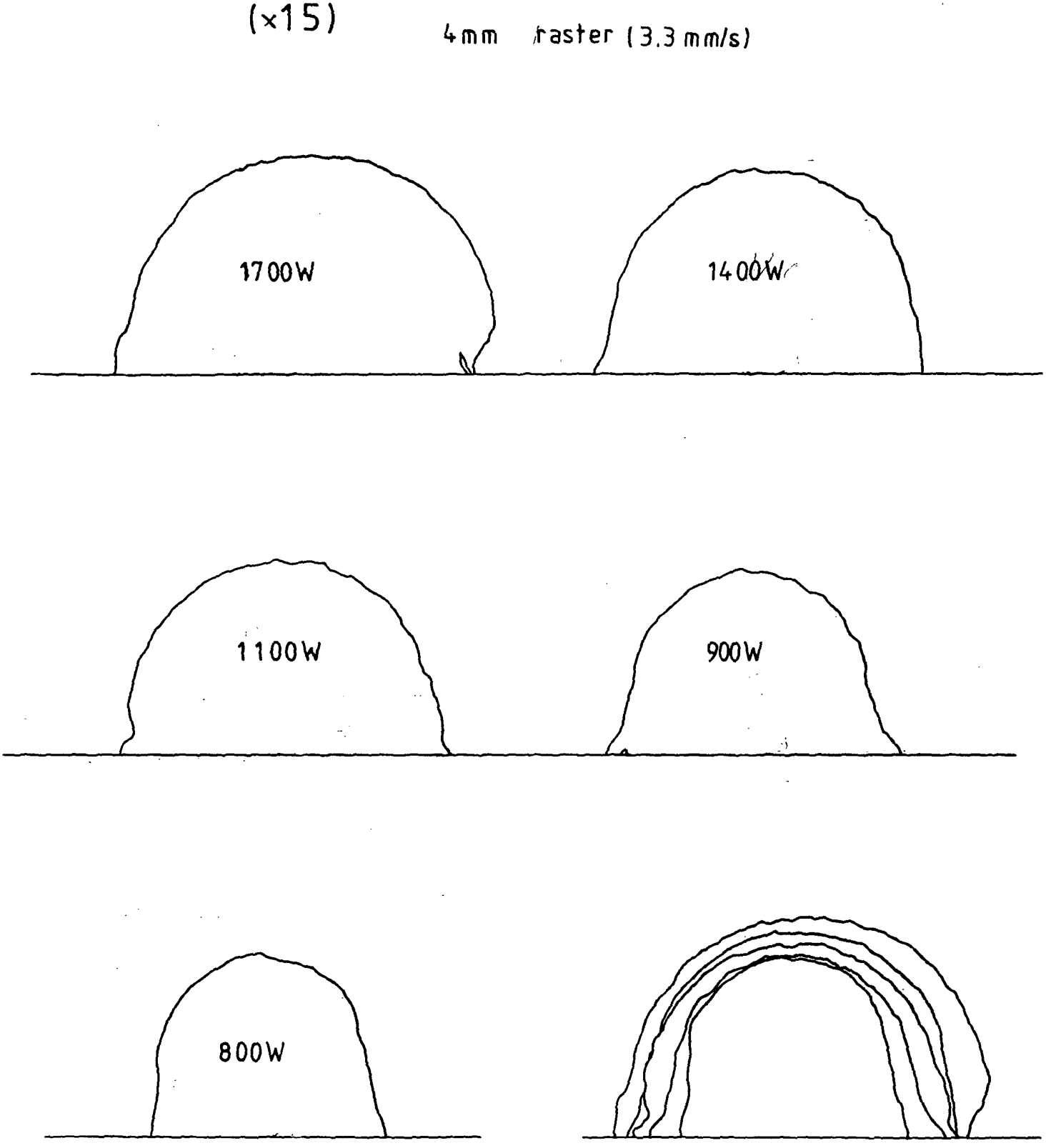

FIGURE 4.14. Cross section variation with power

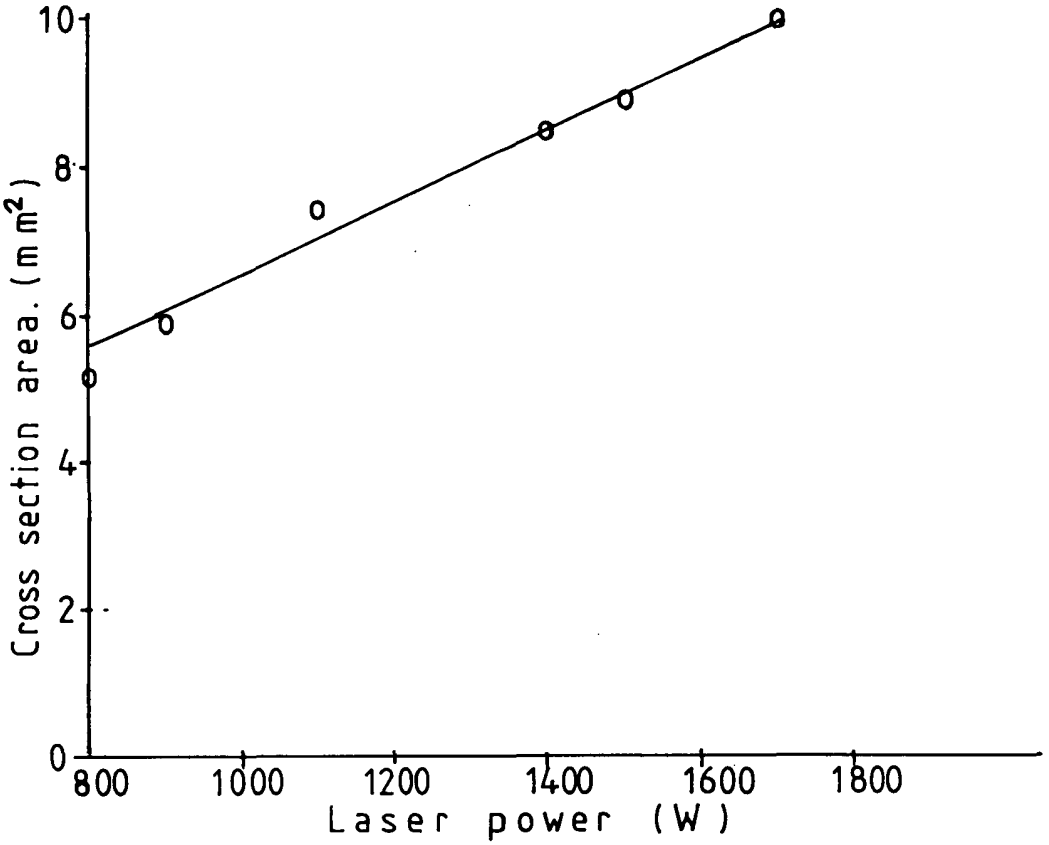

FIGURE. 4.15. P/V: X sect. area

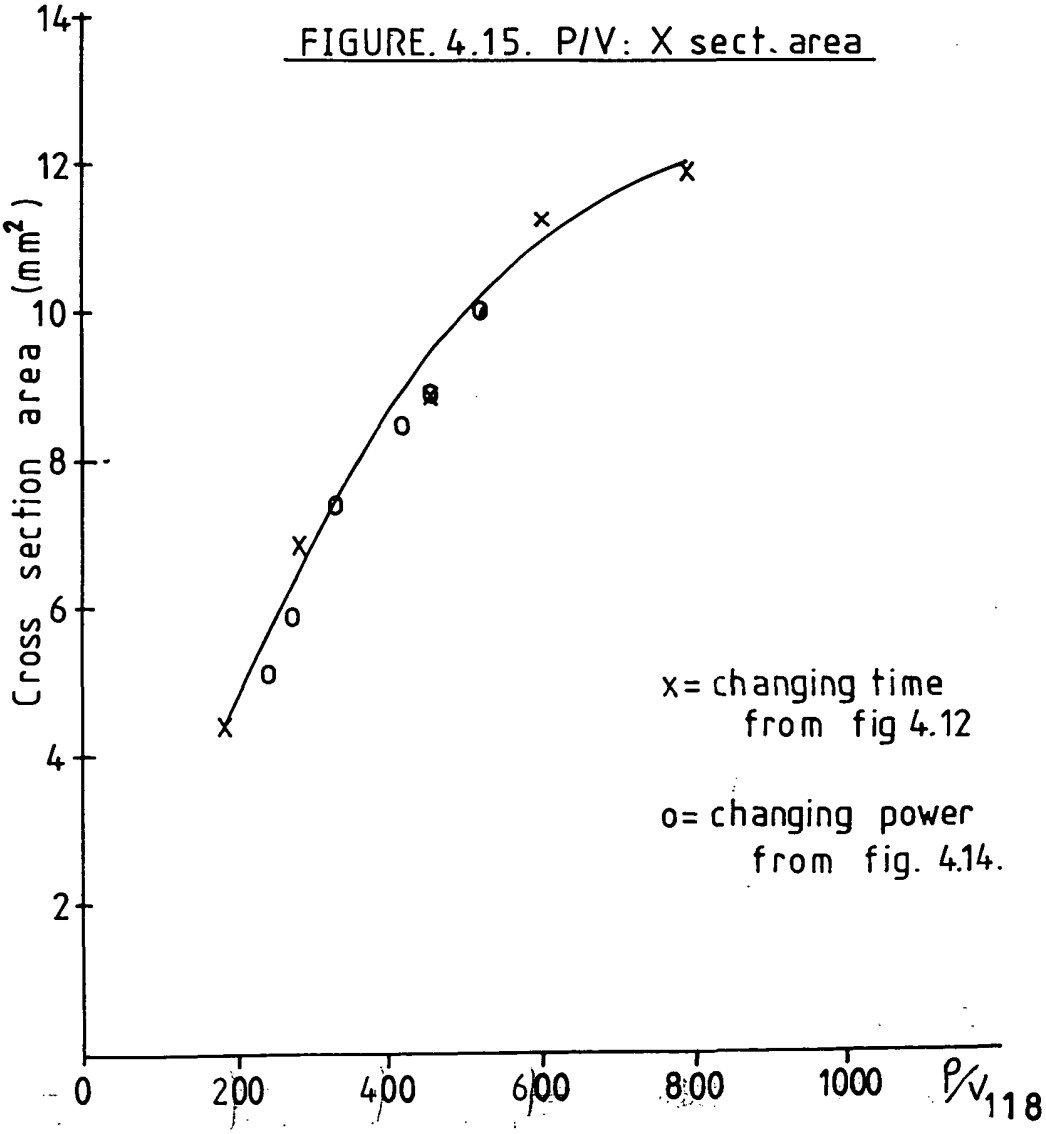

Figure 4.15 combines 4.14 and 4.12 by plotting cross sectional area against laser power/processing speed (energy input). The correlation is striking and so, the validity in this context of using the combined parameter P/VD

P = laser power

V = processing speed

D = beam diameter

often used in laser processing circles is obvious.

In this case, of course, D is no longer a simple measure of the beam diameter but is related to both the beam diameter and the raster configuration. The ennumeration of a 'D' term capable of expressing not only the different sizes of raster configuration and beam diameters but the effects related to the altered energy profile (figure 4.8 etc) should be the aim of future work, but at the moment only runs carried out under identical raster and spot size conditions can be directly compared.

4.4.2 THE EFFECT ON DEPOSIT MORPHOLOGY OF DEPTH OF POWDER BEING CLAD

Figures 4.16 to 4.20 show the results of an experimental programme carried out to investigate the effects of differing depths of cladding powder on the final deposit. Stainless steel (316) powder was layed on the annealed high carbon (.7%C) steel substrate in a wedge so that, during processing the laser encountered an ever increasing depth of powder. The type of deposit which resulted from this process is shown in figure 4.16. It can easily be seen that the nature of the deposit cross section changes radically and to

FIGURE 4.16.

The type of deposit produced by cladding a wedge of powder with a rastered beam.

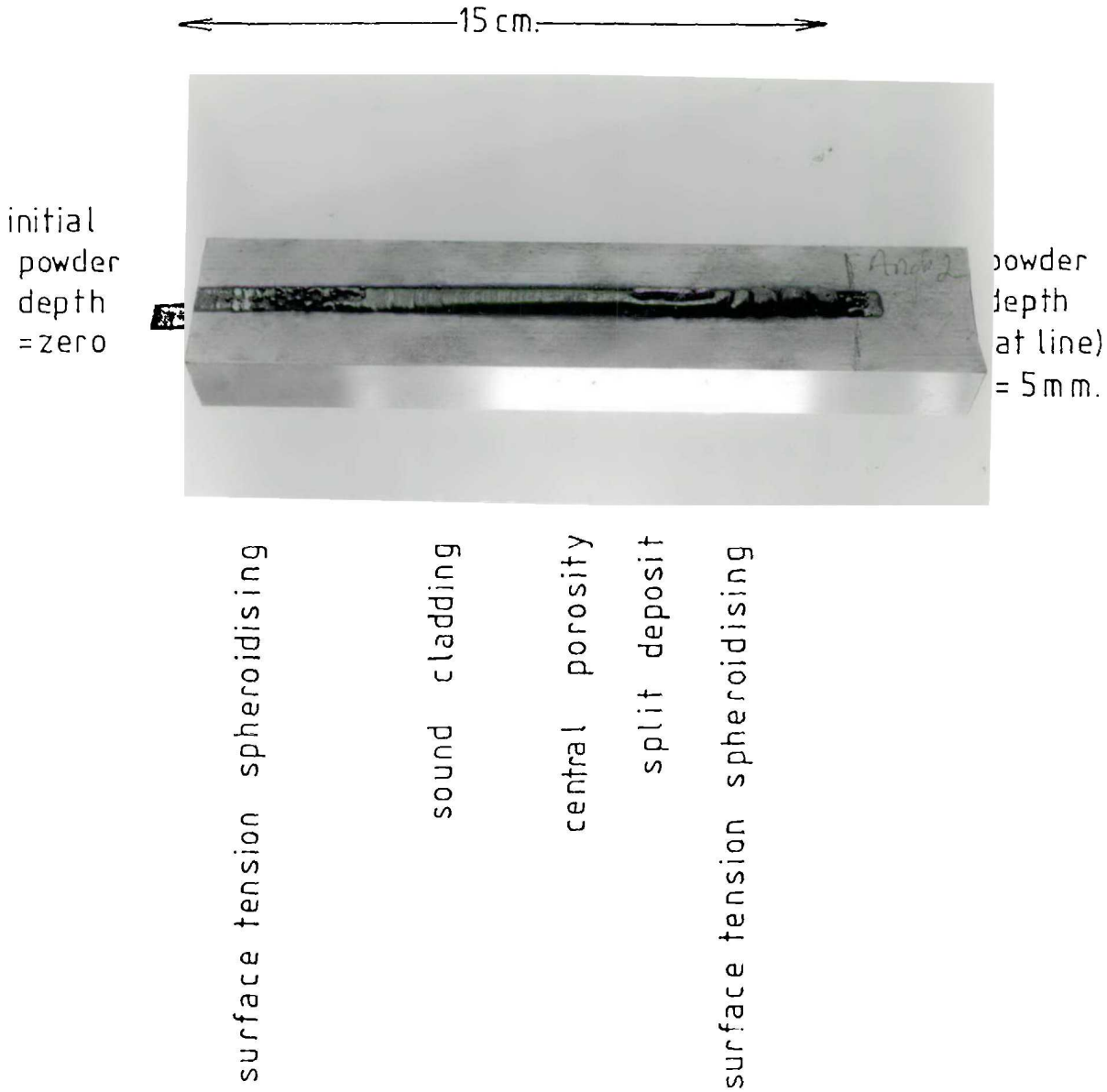

FIGURE. 4.17. The cross section variation with powder depth.

(×15)

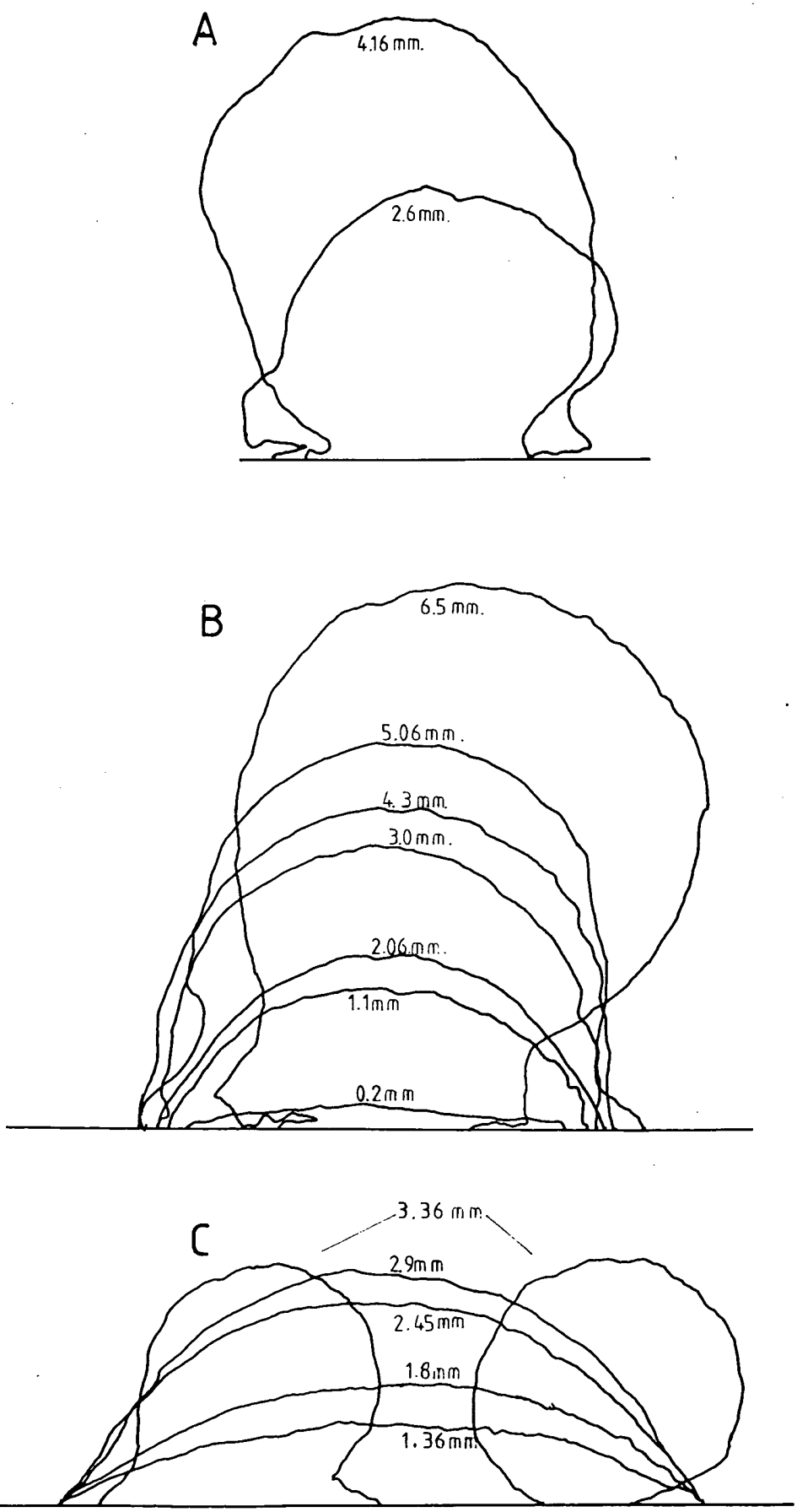

(Nominal powder depth shown)

investigate this effect the specimens were sectioned and their cross sections traced as before (See figure 4.17 A B and C). The processing parameters relevant to the production of these cross sections were as follows:-

Fig 4.17A

Unrastered spot (1mm radius)

Powder wedge depth Omm ——5mm in 15cm

Fig 4.17B

Line source (5mm x 1mm)

Powder wedge depth Omm——7.5mm in 225 cm

Fig 4.17C: (also fig 4.16 and further metallography)

Line source (7mm x 1mm)

Powder wedge depth Omm——5mm in 15cm

NB Line source (9mm x 1mm) was attempted but cladding failed.

The set processing parameters were

Laser power 1500 W

Speed of traverse 3.3 mm/sec

The numbers by each outline represent the nominal powder depth where the cross section was taken. Figure 4.18 compares the cross sectional areas of the deposits with the nominal powder depths and shows the expected linear trend between the two.

This information once again supports the theoretical view (chapter 3) that a wide range of operating parameters exist within which cladding is possible with no dilution. As the powder is increased in depth the surface tension of the weld pool becomes an increasingly dominant factor in determining the shape of the eventual cross section. This is clearly shown in figure 4.17 B and C if the maximum nominal powder depth

FIGURE. 4.18. Nominal powder depth inflences on X section area.

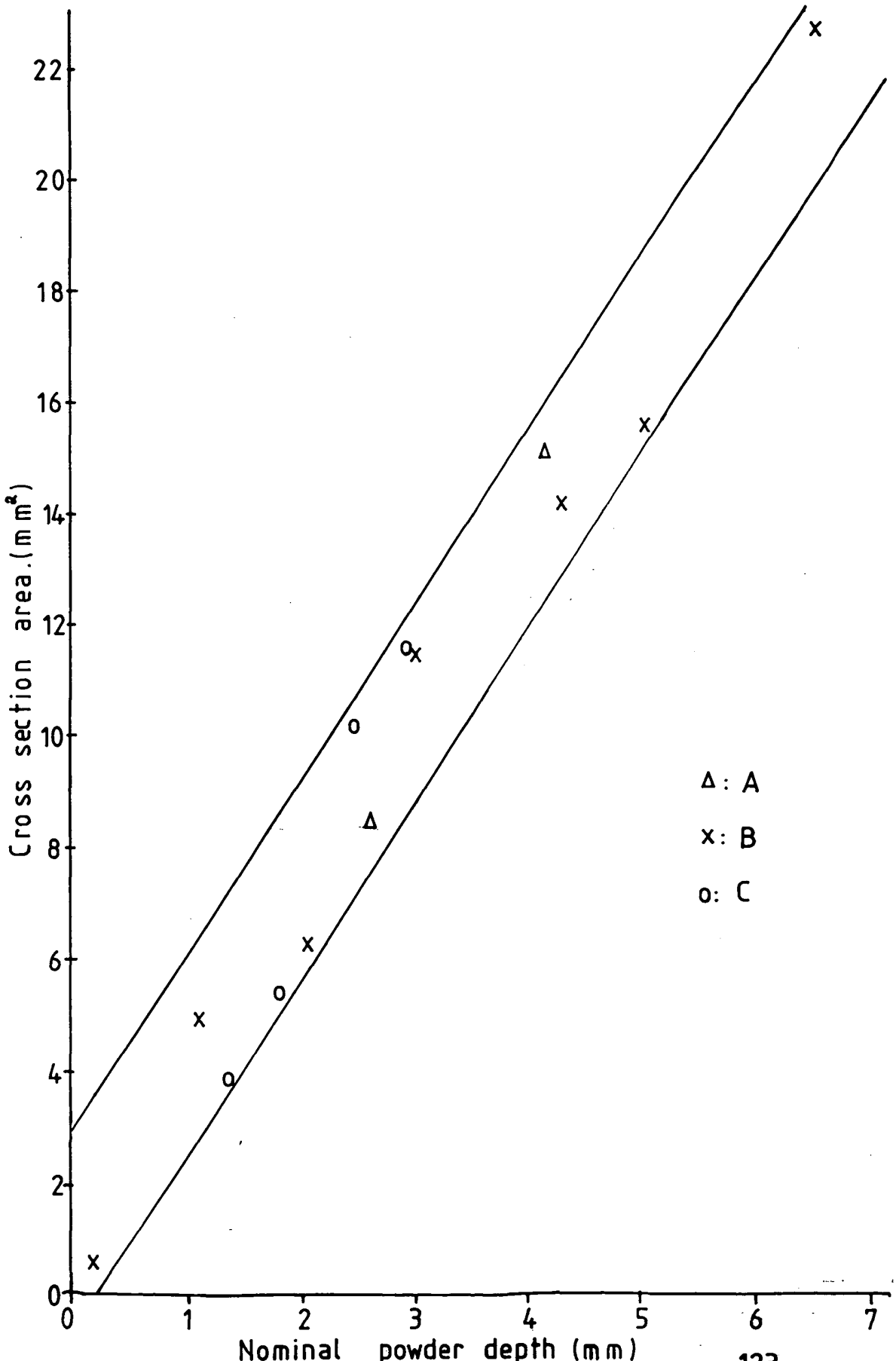

outlines are compared with the lines immediately below them. In the case of the smaller line source (4.17B) the increased surface tension, a result of the weld pool being cooler, causes the cross section to tend to the circular (Type 1) and undercut is the result. The weld pool is cooler (prior to substrate contact) than the smaller cross section pools because the power input is constant and the amount of powder melted is increased with increasing powder depth. The surface tension effect in figure 4.17C causes the development of a type 4 deposit (see figure 4.9).

The most informative sample is that described by figure 4.17C and observed in figure 4.16 and this was chosen for further study as the arguments concerning it are relevant to many aspects of the process in general.

The macrographs in figure 4.19 (photos 1-10) show the growth and deterioration of the clad cross section as the depth of powder (nominal) increased, taking these in turn; figure 4.19 photo 1; The martensitic heat treated zone is a reflection of the energy distribution in the beam although the difference between the depth at the edges of the rastering and the centre will be damped out by thermal conduction within the general area. The beam energy density is not sufficient to initiate melting of the substrate at this processing speed (3.3mm/sec).

Figure 4.19 photo 2; The very small amount of powder on the substrate has been melted by the laser beam but the molten particles have consolidated with their neighbours to produce small molten spheroids whose shape is determined by the high surface to volume ratios associated with small bodies. These

FIGURE. 4.19 Macroscopic investigation of cladding different powder thicknesses.

(× 5.6)

martensite-

·7 %C steel (annealed)—

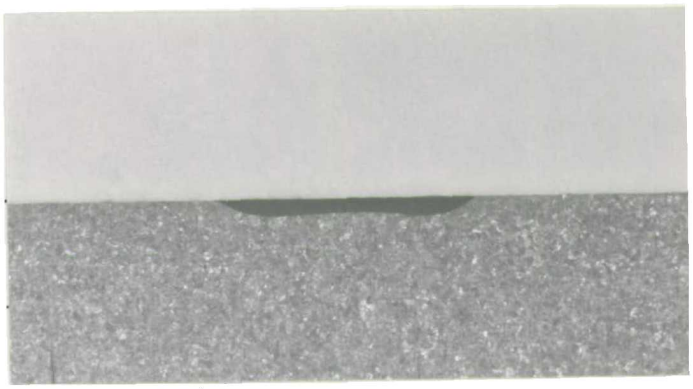

1

no powder

stainless steel—
martensite—

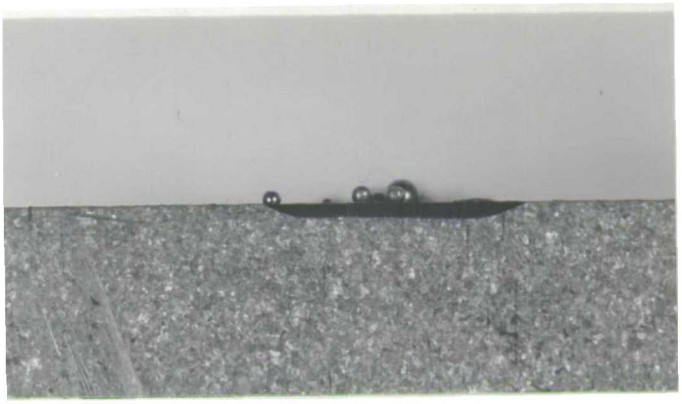

2

nominal powder depth = ·2 mm.

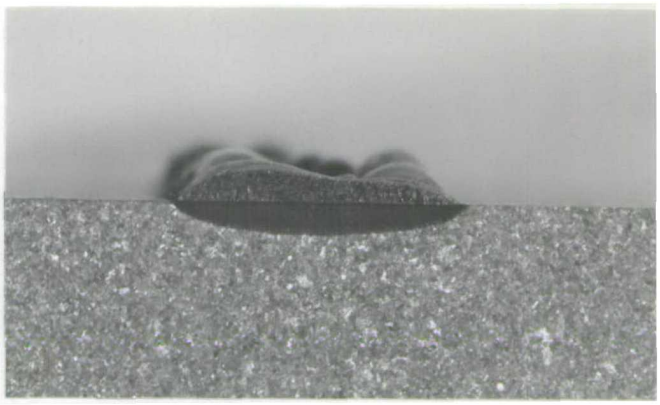

3

n.p.d. = 1.25mm.

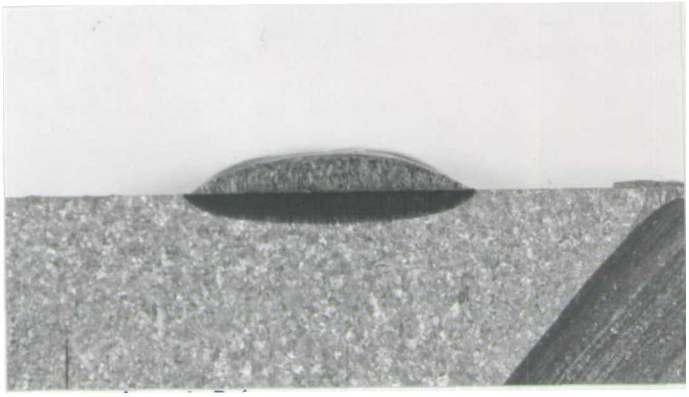

4

n.p.d. = 1.36 mm.

FIGURE 4.19 Continued

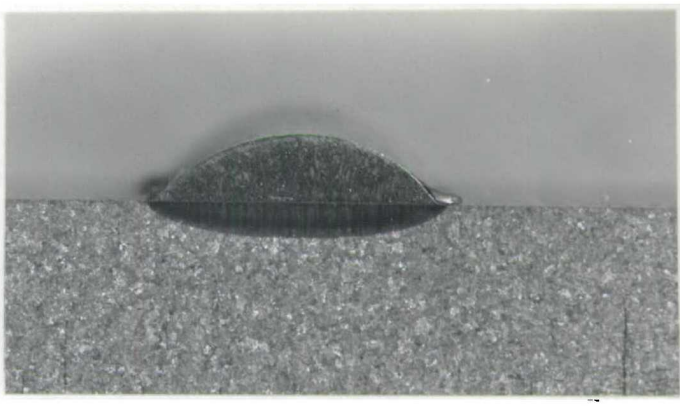

5 nominal powder depth = 1.8 mm.

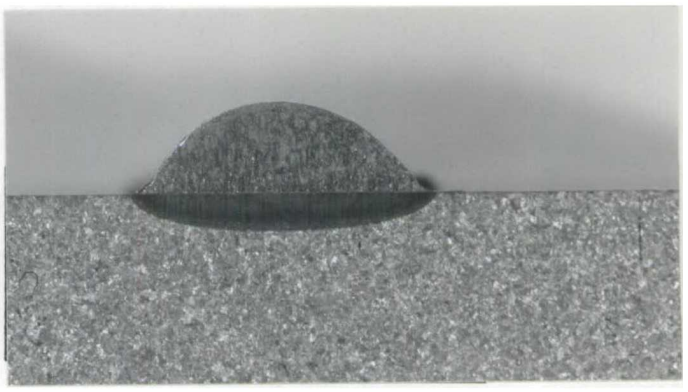

6 n.p.d.= 2.43 mm.

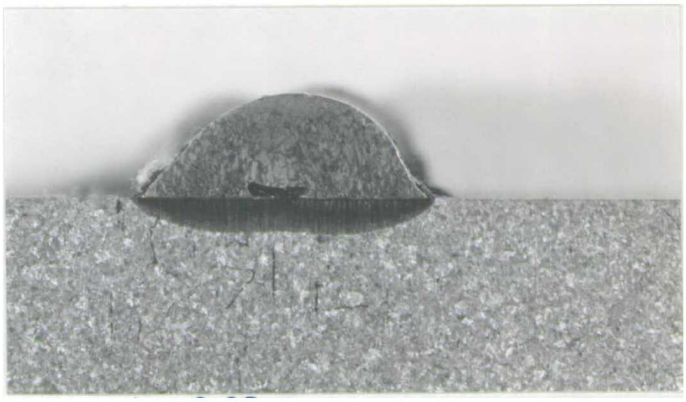

7 n.p.d. = 2.93 mm.

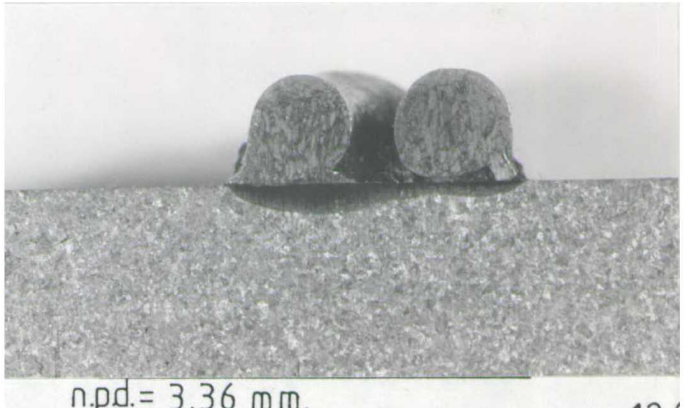

8 n.p.d.= 3.36 mm.

FIGURE. 4. 19. Continued.

(×5.6)

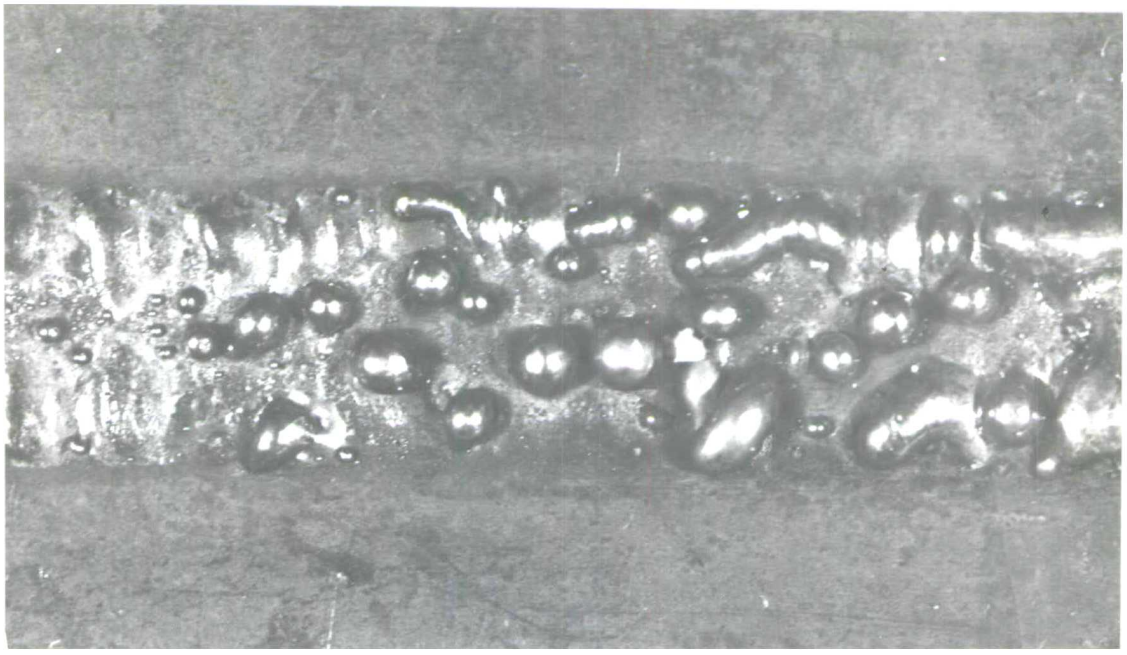

9. Spheroidised deposit. (powder increases →)

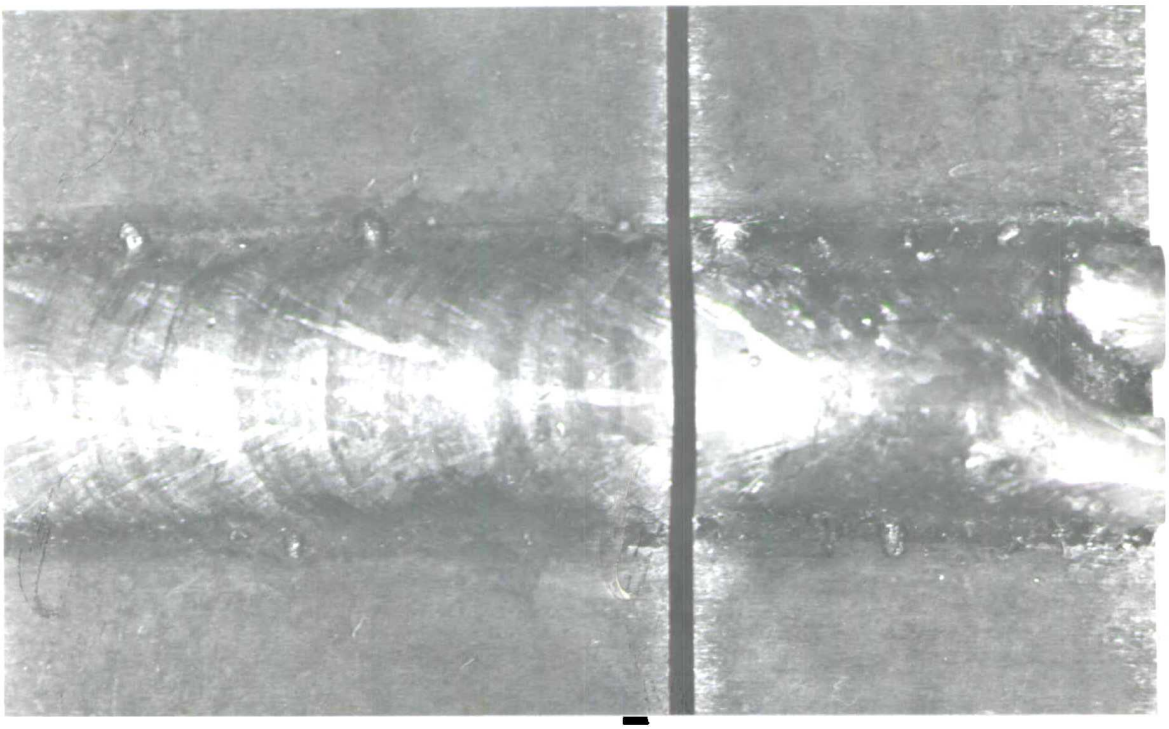

10. Sound cladding → split deposit. (close to the top surface the direction of solidification is less influenced by the chilling effect of the substrate and tends to follow the beam travers direction →.)

high surface to volume ratios means that the major effect controlling the morphology of the deposit is surface tension which, of course tends to form spheroids to reduce the surface free energy (see also photo 9).

Figure 4.19 photo 3; Surface tension effects are reduced due to decreased surface to volume ratio but more importantly the coalescence of neighbouring particles does not sufficiently denude the surrounding area of powder completely so the whole melt is unified and cladding is possible although accelerated melting at the sides of the raster sweep have led to a build up of material at the sides (see also photo 9).

Figure 4.19 photos 4, 5 and 6: Acceptable cladding of the type 2 sort with linear increase of melt with powder depth (see earlier sections). The grain size of the stainless steel grows coarser indicating slower cooling rates, this can be attributed to lower average temperatures of melt due to more material being melted by a constant power input.

Figure 4.19 photo 7; Central porosity (type 3 cladding) indicating that the powder melting process has trapped an appreciable amount of unmelted powder in the centre (see earlier notes). It is interesting to note that the pore acts as an insulator to heat transfer resulting in equiaxed rather than columnar (chill cast) grains in the stainless steel and a reduction in the extent of the heat affected zone in the high carbon steel substrate at the centre (see photo 10)

Figure 4.19 photo 8; Type 4 cladding, the speed of melting at the sides of rastering is higher than at the centre and the quenching begins at the extremes of the raster movement freezing the melt into two parallel tracks (see also photo 10).

Note the coarser grain structure and small heat affected zone of the right hand track as a result of poor melt-substrate contact.

Beyond this depth of powder the melt formed into large lumps (see figure 4.16) as a result of the high surface tension forces associated with the cooler melt.

Figure 4.20 shows the heat affected zones of the unrastered spot (1mm x 1mm) and a 7mm x 1mm rastered spot. Comparison of these with figure 4.19 photo 1 clearly demonstrates two features of the theoretical treatment of chapter 3 and earlier this chapter (figure 4.8 and 4.9) vis:

A. A beam of a given power distribution can clad a powder bed of considerable depth onto a substrate even if it is incapable of melting the substrate directly. The melted cross section of the substrate for the unrastered beam was a minimal .1mm^2 compared to the maximum recorded powder melt cross section of 15.1mm^2, the rastered beams did not melt any substrate but could melt sustantial amounts of powder.

B. If the separation of the extremes of the raster movement is large in comparison to the unrastered spot size the energy input approximates to a dual, separated gaussian rather than step function source (see figures 4.8 and 4.9).

4.5 GENERAL CONCLUSIONS

The results accrued here indicate that the theoretical approach of chapter 3 section 2 combined with the theory postulated in figure 419 for dividing the deposits into types, are applicable directly to the practical considerations of pre placed powder cladding. The morphology of any clad deposit is affected by a number of factors the main ones being the energy density and configuration of the beam and the surface tension of the pool. By controlling the operating parameters of the process it is possible to get a wide range of sound

clad deposits with no dilution problems.

The major drawbacks to the process are:-

A. It is difficult to get a reproducable density of powder bed.

B. Complex shapes cannot be clad because powder cannot be pre placed prior to, for example, rotation in the vertical plane.

C. The overlapping of tracks to produce a completely clad surface is very difficult because any track denudes the area on either side of it and can often be of a greater height than that of the powder bed needed for its production.

The process lends itself to the production of single, hard faced, tracks on flat components and future work should study the possibilities of overfilling a pre cut groove with powder with the intention of producing flush to the surface hard tracks for wearing surfaces.

FIGURE. 4 20.

(×5 6)

Unrastered (5mm rad) spot on .7%C steel.

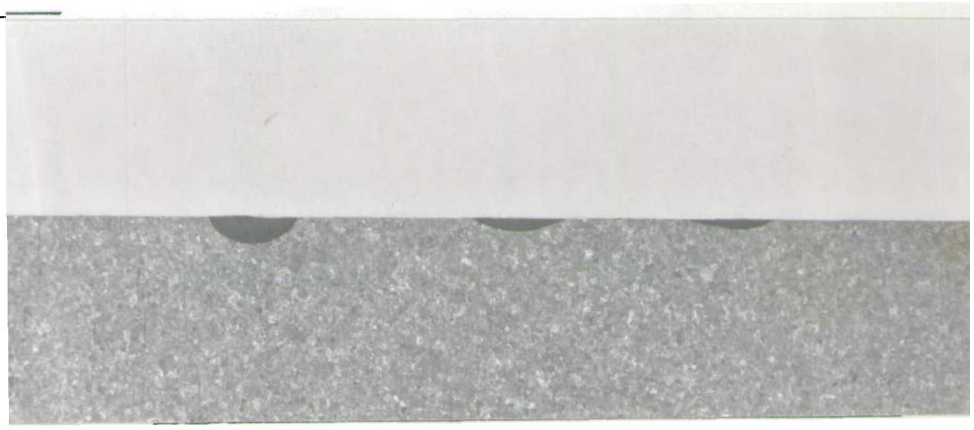

7mm rastered spot. (dwell times only effect substrate)

CHAPTER 5

THE BLOWN POWDER CLADDING/SURFACE ALLOYING OF EXHAUST VALVES

The cladding or surface alloying of the wearing surface of exhaust valves is a subject of considerable commercial interest. The utilisation of a laser as the heat source for this process has been of interest to many industrial concerns including Fiat, AVCO and British Leyland

The present work involved rotating the valve under the stationary, partially focussed laser beam and propelling hard facing powder onto the molten weld pool produced. Thus, a line of new material was deposited on the valves wearing surface, reducing its susceptability to corrosion, erosion and wear.

5.2 EXPERIMENTAL PROCEDURE AND RESULTS

5.2.1 EQUIPMENT USED

The laser used was the control laser model 901, (cw only) using the standard laser head described in the previous chapter.

A variable speed D.C motor was used to turn the valve during the cladding process (see Figure 5.1) and the powder was delivered in a stream of Argon from a Deloro stellite gravity-fed spray gun. The spheroidised SF40 powder is a Nickel based hard facing alloy with the following nominal composition :

FIGURE 5.1 Experimental arrangement for laser valve cladding.

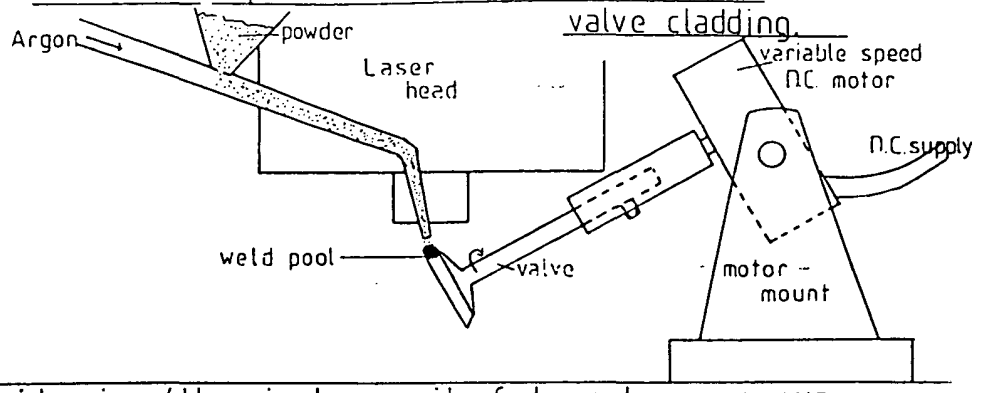

A. side view. (the simple, gravity fed powder spray gun is shown in cross section).

B. front view (partial).

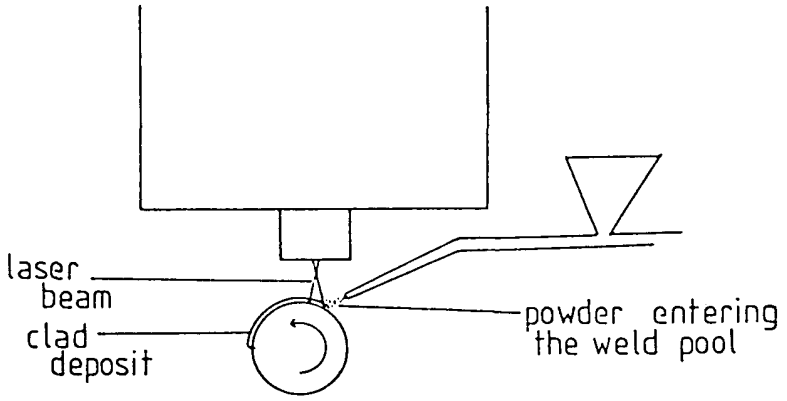

note: the weld pool is to one side of the central axis of the valve to provide the best powder catchment conditions.

FIGURE 5.2. Cross section of valve (scale = 1:1)

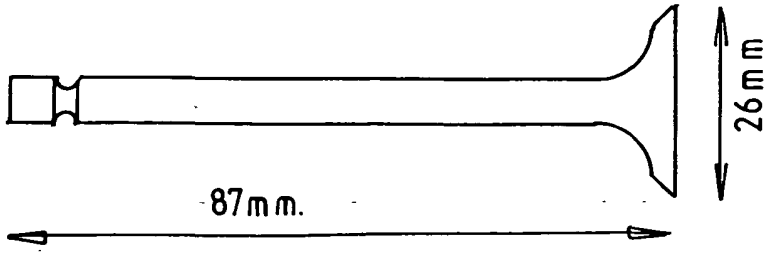

Table 5.1

THE COMPOSITION OF STELLITE SF40

Element	Cr	C	Fe	Si	B	Ni
Percentage	7.5	0.3	1.5	4.0	1.5	85.0

The valves were supplied by British Leyland and Figure 5.2 is a full size drawing of a cross section. The composition of the valve material was not given but E.P.M.A traces indicate that basic components were as follows:-

Fe 65% Cr20% Mn 9% Ni 4% Si.25% C .65% (Wt %)

5.2.2 EXPERIMENTAL PROCEDURE

The laser power having been set and allowed to stabilise, a valve was inserted into the holder attached to the variable speed DC motor (see Figure 5.1). The speed of rotation was then timed and the surface to be clad carefully positioned under the laser beam and powder flow. The rotation of the valve was initiated, followed by the flow of powder propelling Argon. When conditions were stable, the laser was fired during the execution of one revolution of the valve. The valve was then removed, the next positioned, and one of the parameters changed before the next run.

The main variables examined were:-

a. The rotation speed of the valve; 16,8,4,2 seconds/rev

b. The laser power; 1500 or 1800 W

c. The Argon flow rate; 6,8 or 10*

(* - Rotameter readings corresponding to increasing gas and powder flow rates - see Figure 5.7)

Each sample thus produced was sectioned and a macrograph prepared.

Selected samples were analysed by electron probe micro analysis (EPMA) to measure the level of dilution, and by optical microscopy to inspect the metallurgical features present.

5.2.3 RESULTS

The production parameters together with some comments accrued from inspection of the relevant macrographs are presented in Table 6.2.

The graphs which constitute Figure 5.3 relate to the physical dimensions and proportions of the deposits. It should be mentioned at this stage that 'deposit' in this case refers to the whole of the solidified weld pool, which includes melted substrate as well as cladding material. The graphs show the relationships between the operating parameters and the clad deposit width, depth, cross sectional area, dilution level and the amount of powder melted into the weld pool.

A selection of the macrographs showing the deposit cross sections are shown in Figure 5.4. Figures 5.4 A and B illustrate the trends shown by the graphs whilst C and D show special cases of keyholing and excessive porosity. The magnification of the macrographs is in most cases X10 and is otherwise

stipulated if this is not the case.

Figure 5.5 presents the results of the electron probe micro analysis (EPMA) carried out on three samples together with the relevant micrographs. Each sample was EPM analysed for Ni, Fe + Cr. The micrographs are printed at a magnification of X220 or as otherwise stated and are shown in Figure 5.6.

TABLE 5.2

Production parameters and comments on valves clad with Stellite SF40

SAMPLE	LASER POWER (WATTS)	ARGON FLOW READING	ROTATION TIME (SECS)	DILTUION %	POROSITY %	MAX 'DEPOSIT' DEPTH	'DEPOSIT' WIDTH	'DEPOSIT' X. SECT AREA	NEW MATERIAL X. Sec. AREA	COMMENTS
1	1500	6	2.0	80	0	.12	0.9	.105	.021	
2	"	"	3.0	50	0	.20	1.4	.175	.087	
3	"	"	4.0	50	0	.24	1.6	.280	.140	
4	"	"	5.0	45	0	.30	1.8	.340	.187	
5	"	"	6.0	50	0	.32	1.9	.380	.190	
6	"	"	9.0	40	0	.35	2.0	.550	.330	
7	"	"	10.5	30	0	.40	2.1	.680	.476	
8	"	"	15.0	40	0	.50	2.2	.890	.534	
9	"	8	1.7	50	0	.05	0.4	.010	.005	See Macro's
10	"	"	3.5	25	0	.22	1.5	.195	.146	See Macro's, Mic + EPMA
11	"	"	4.0	30	0	.22	1.4	.220	.154	
12	"	"	5.0	40	0	.25	1.6	.280	.168	
13	"	"	6.5	35	0	.28	1.65	.310	.201	See Macro's

SAMPLE	LASER POWER (WATTS)	ARGON FLOW READING	ROTATION TIME (SECS)	DILUTION %	POROSITY %	MAX 'DEPSOIT' DEPTH	'DEPOSIT' WIDTH	'DEPOSIT' X SECT AREA	NEW MATERIAL X SEC. AREA	Comments
14	"	"	8.0	15	0	.30	1.7	.370	.314	
15	"	"	9.0	20	0	.30	1.8	.490	.392	
16	"	"	17.0	15	1	.50	1.9	.730	.620	See Macro's
17	"	10	1.7	50	0	.15	1.0	.110	.055	See Macro's
18	"	"	3.5	30	0	.23	1.4	.250	.182	See Macro's
19	"	"	4.0	25	0	.30	1.55	.320	.240	
20	"	"	5.0	30	0	.32	1.6	.325	.244	
21	"	"	7.0	10	0	.35	1.7	.450	.405	See Macro's
22	"	"	8.0	10	0	.40	1.6	.530	.477	
23	"	"	9.0	10	0	.50	1.65	.610	.549	
24	"	"	15.0	10	1	.72	1.75	.930	.837	
25	1500	10	17.0	0	0	9.5	1.6	1.30	1.30	See Micro's Macro's +EPMA
26	1800	6	2.5	50	0	.12	1.3	.150	.075	See Micro's + EPM
27	"	"	6.5	45	0	.28	1.85	.370	.203	
28	"	"	13.0	60	0	.50	2.0	.600	.240	Keyholing. See Micro's
29	"	8	2.5	50	0	.13	1.35	.190	.950	
30	"	"	5.0	30	0	.30	1.7	.30	.217	
31	"	"	6.5	20	0	.32	1.75	.385	.308	
32	"	"	9.5	10	0	.50	1.8	.630	.567	Keyholing (slight)
33	"	"	13.0	20	0	.60	1.9	.730	.584	Keyholing (slight)
34	"	"	16.0	30	5	.75	2.1	.970	.679	
35	"	10	2.5	50	0	.15	1.4	.160	.800	
36	"	"	6.5	10	0	.35	1.6	.390	.351	
37	"	"	13.0	10	35	.70	1.8	.900	.810	Porosity: See Macro

FIGURE 5.3.

The relationships between production parameters and finished product. [Valve cladding]

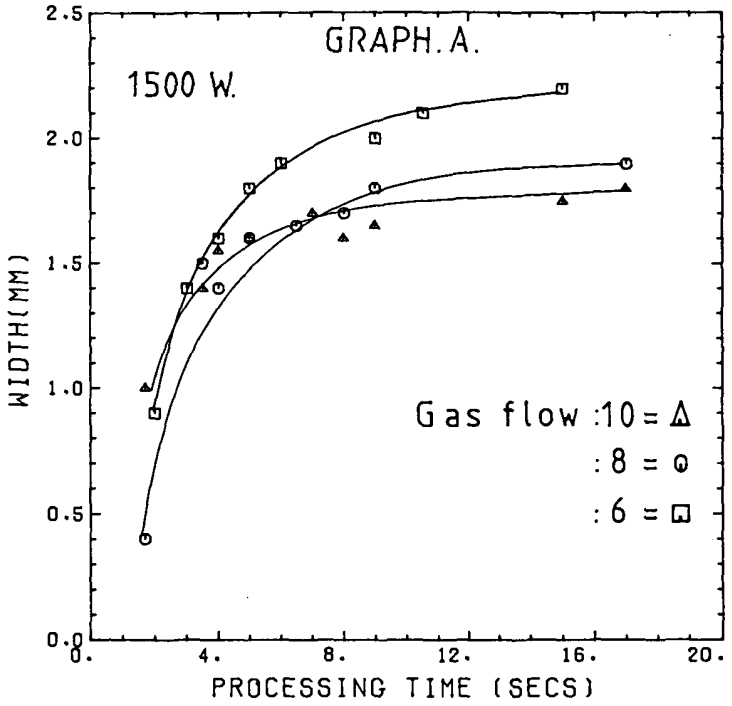

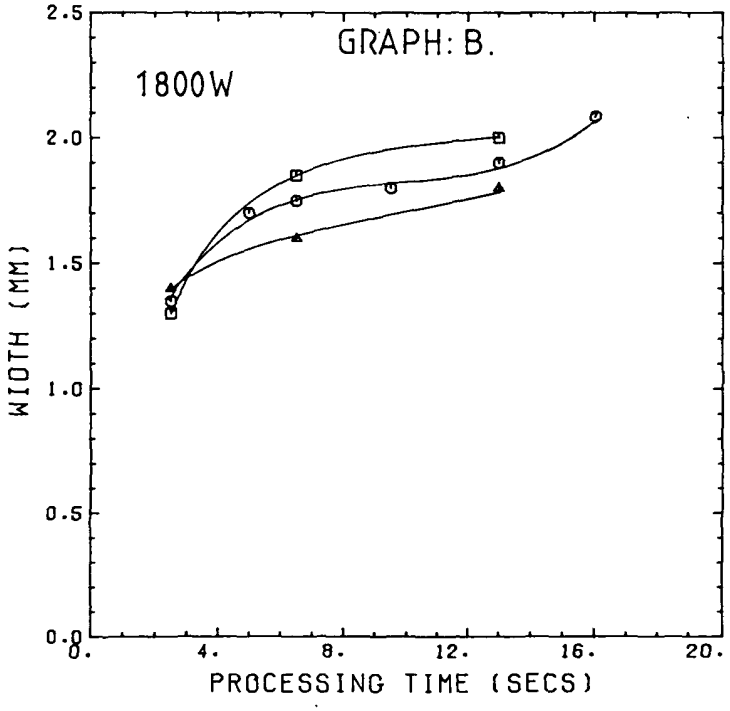

FIGURE. 5.3. (Cont)

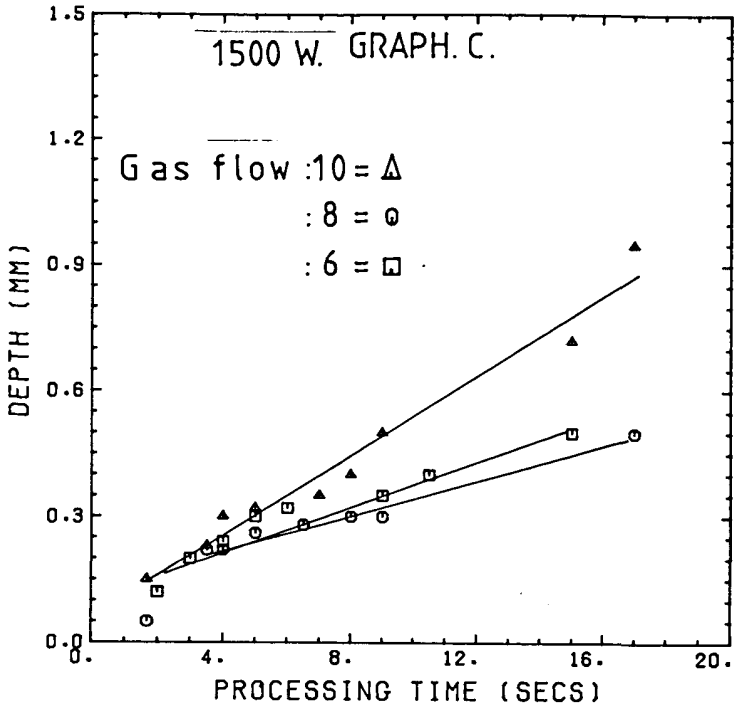

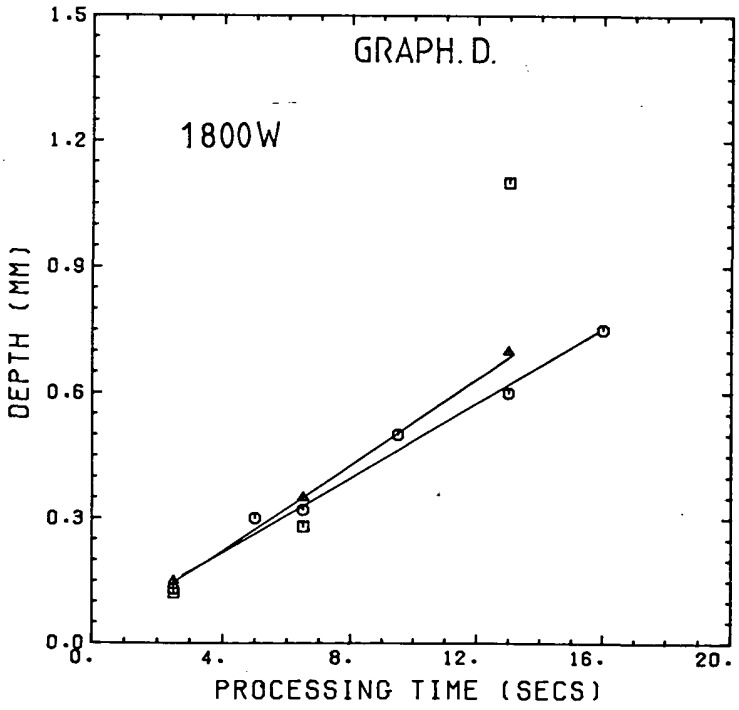

FIGURE 5.3. (Cont)

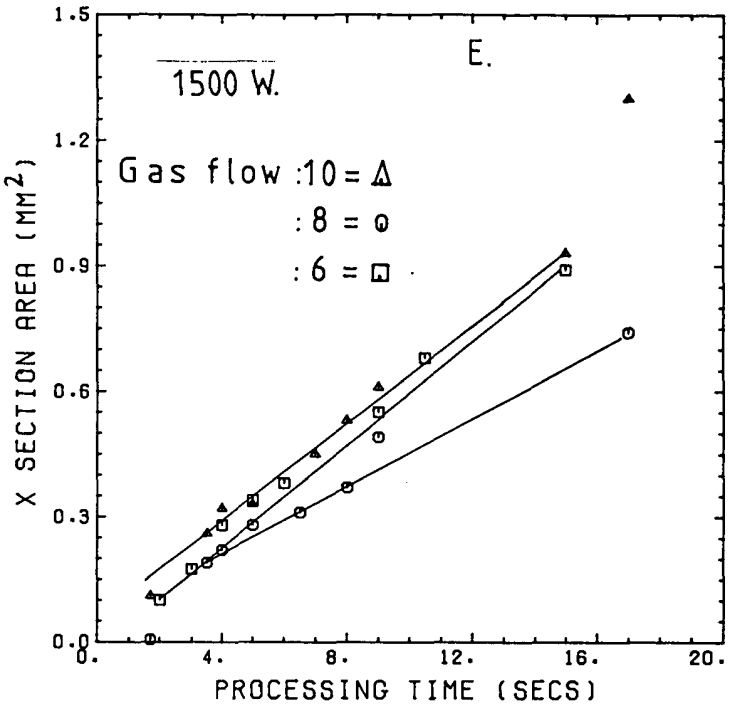

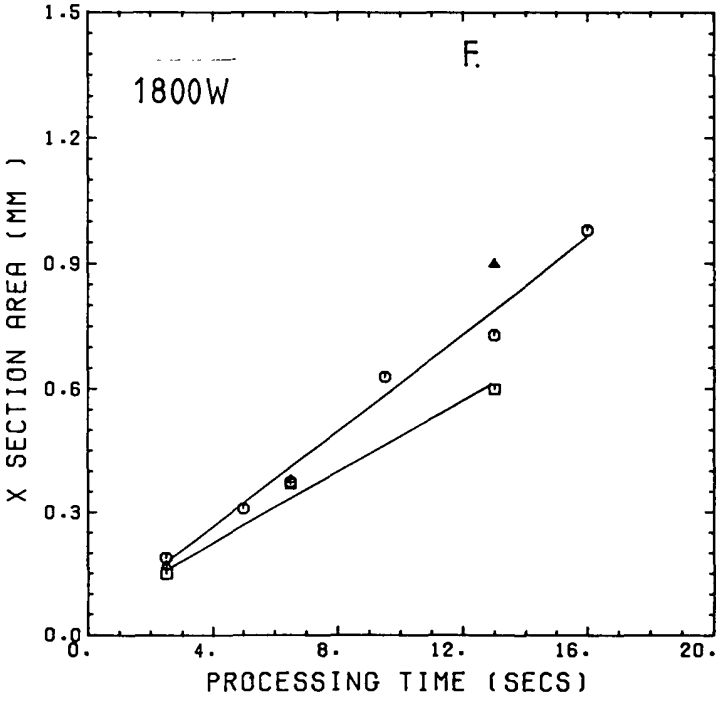

FIGURE.5.3. (Cont.)

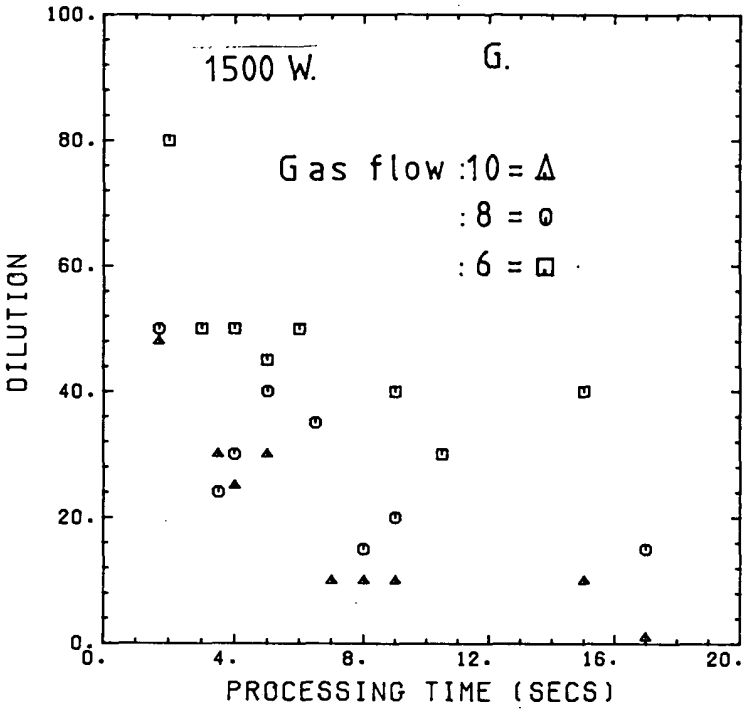

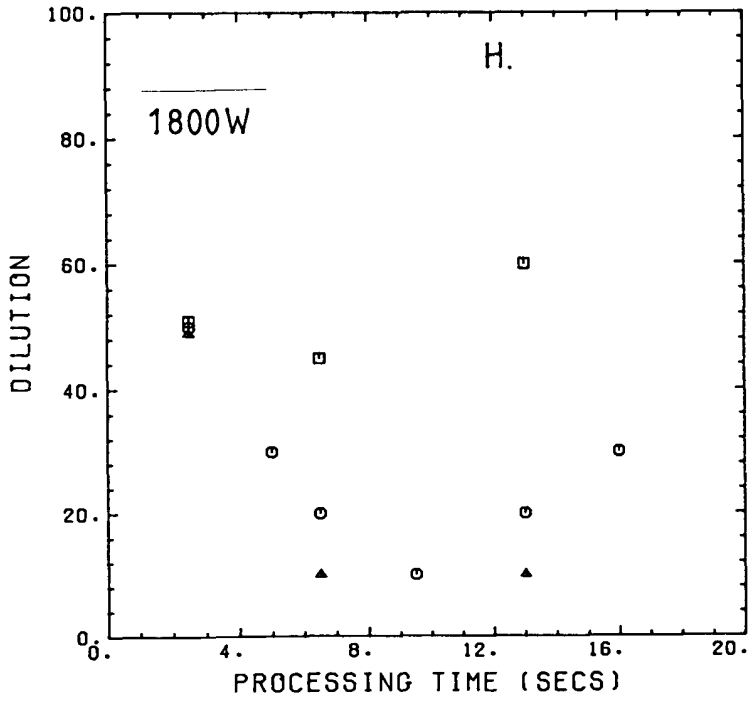

FIGURE.5.3. (Cont.)

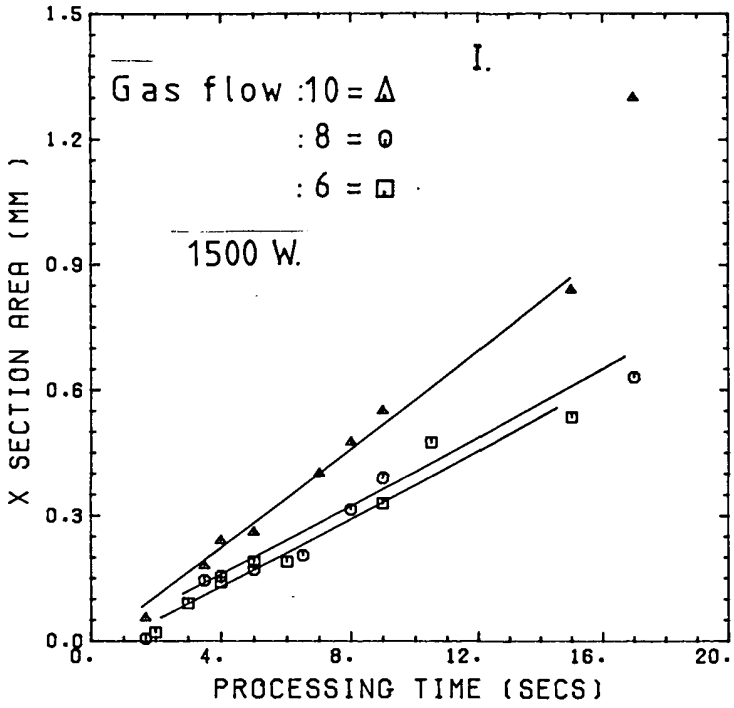

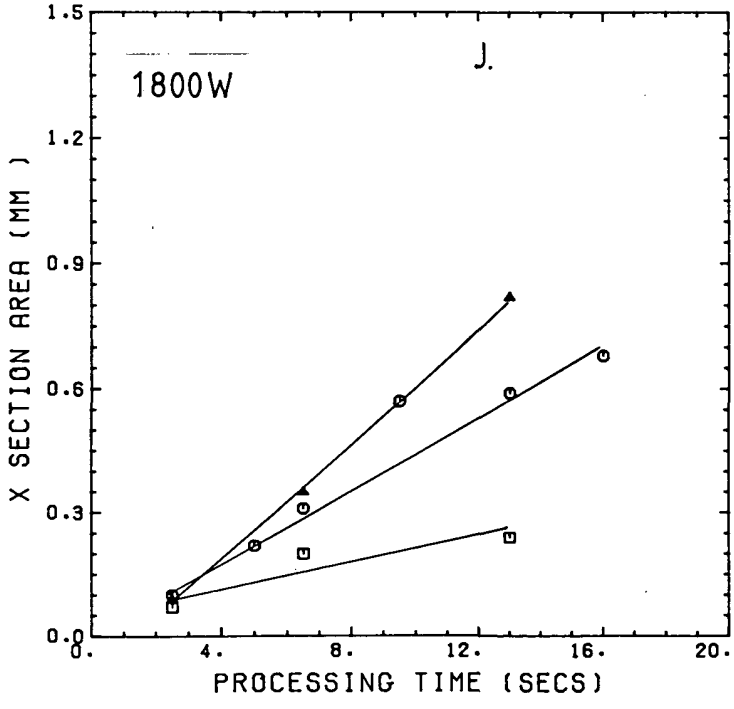

Figure 5.4. Macrographs of selected clad valves

A.(laser:1500 Watts)
(Gas flow: 8)

B.(laser:1500 Watts.)
(Gas flow:10)

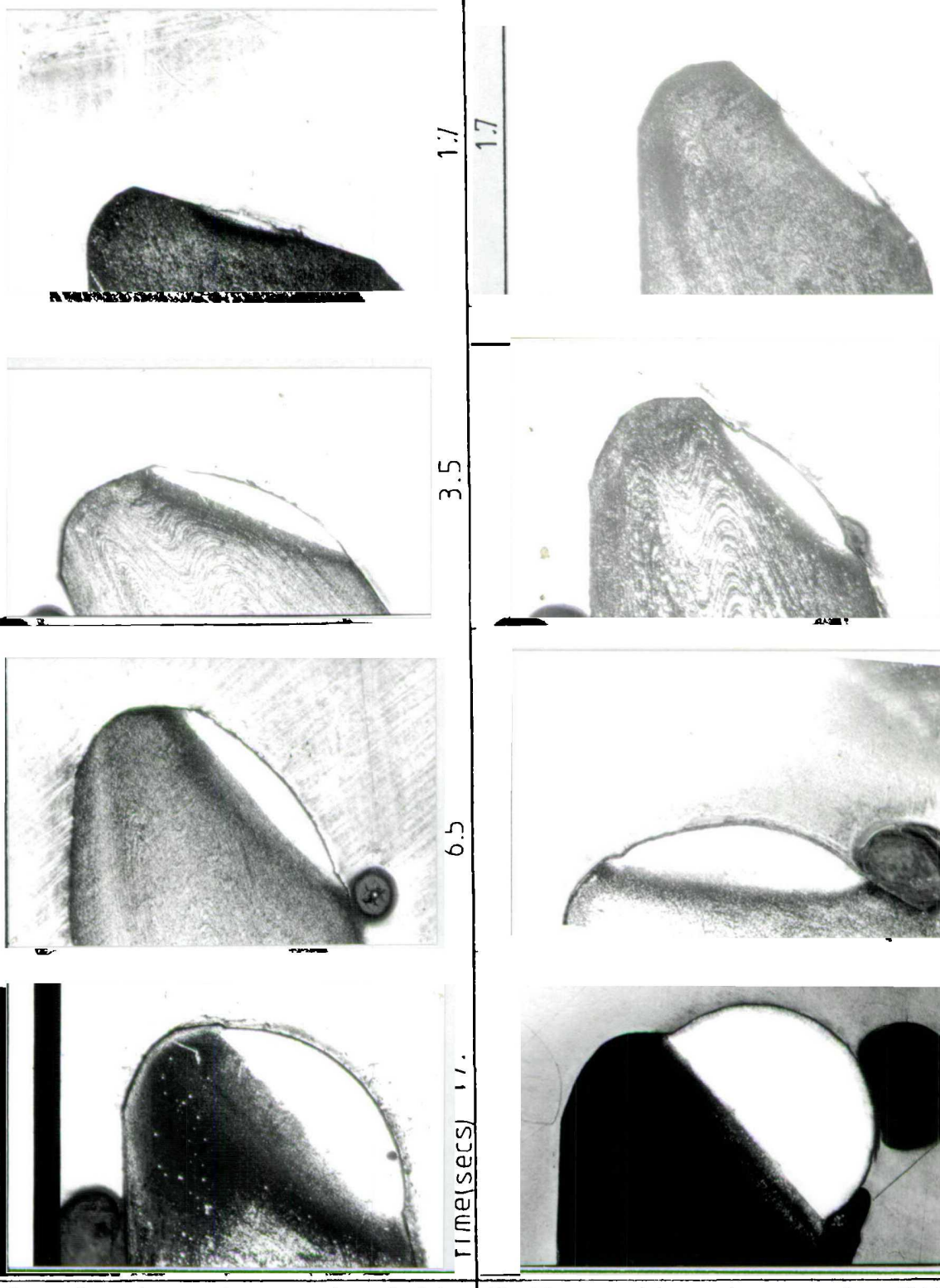

C.Keyholing. (sample 28)

D Porosity. (sample 37)

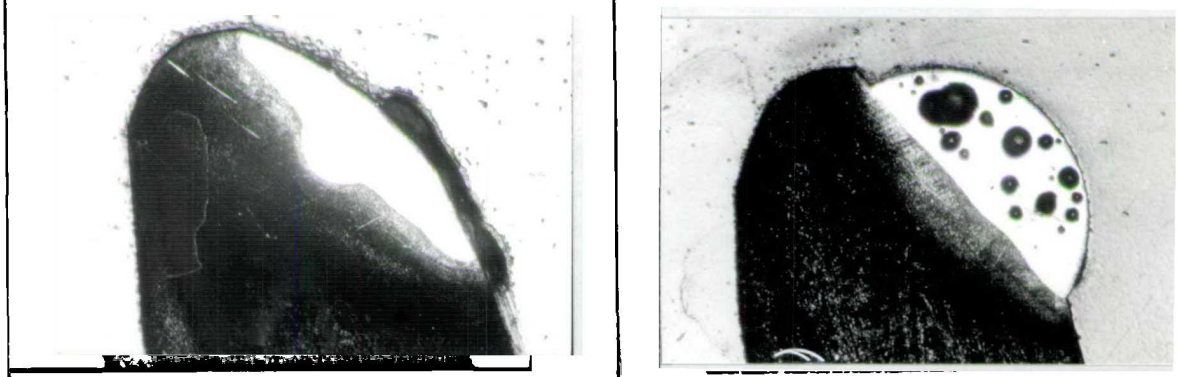

FIGURE. 5.5. GRAPH.1. (Heavy deposit)

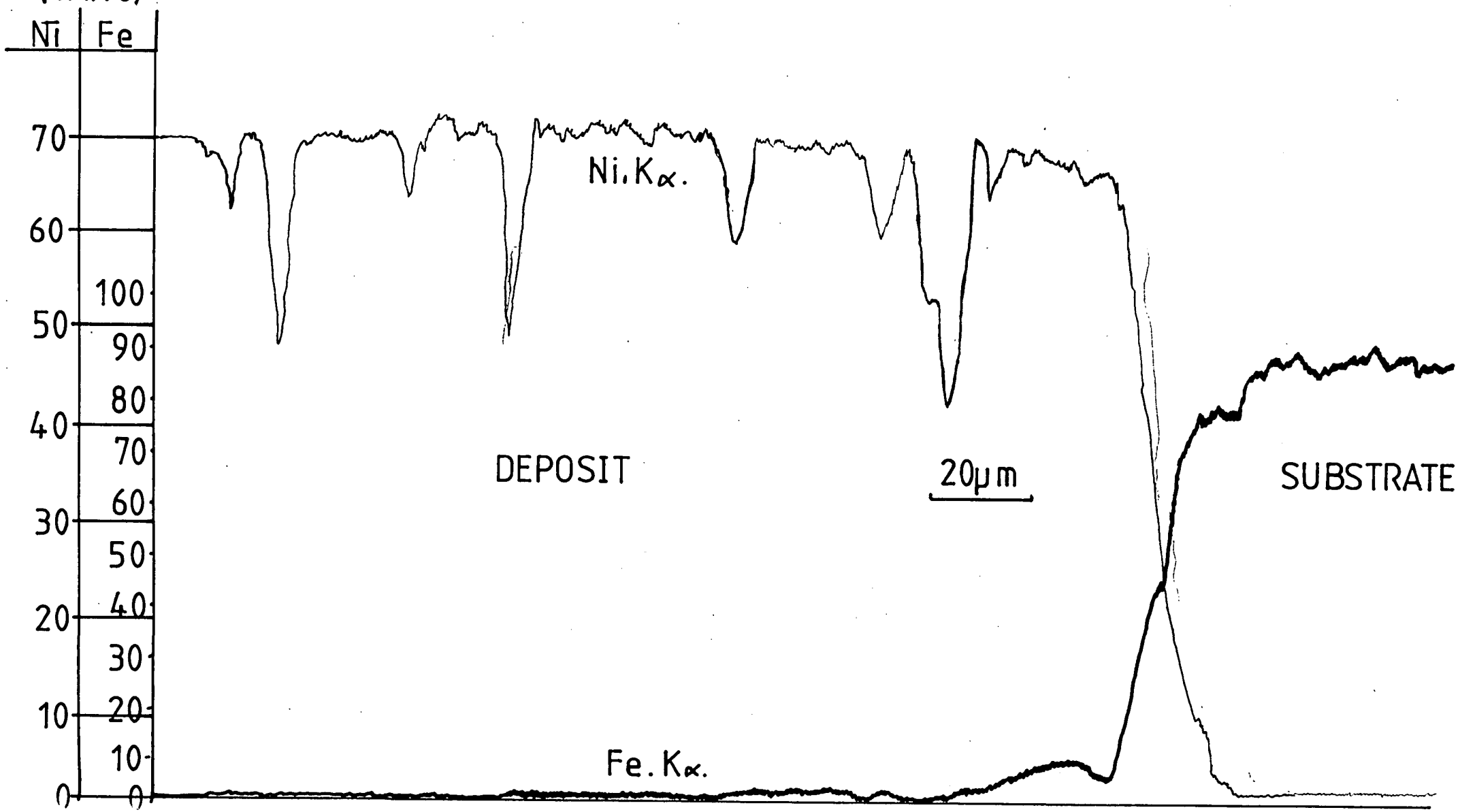

FIGURE.5.5. GRAPH.2. (Heavy deposit)

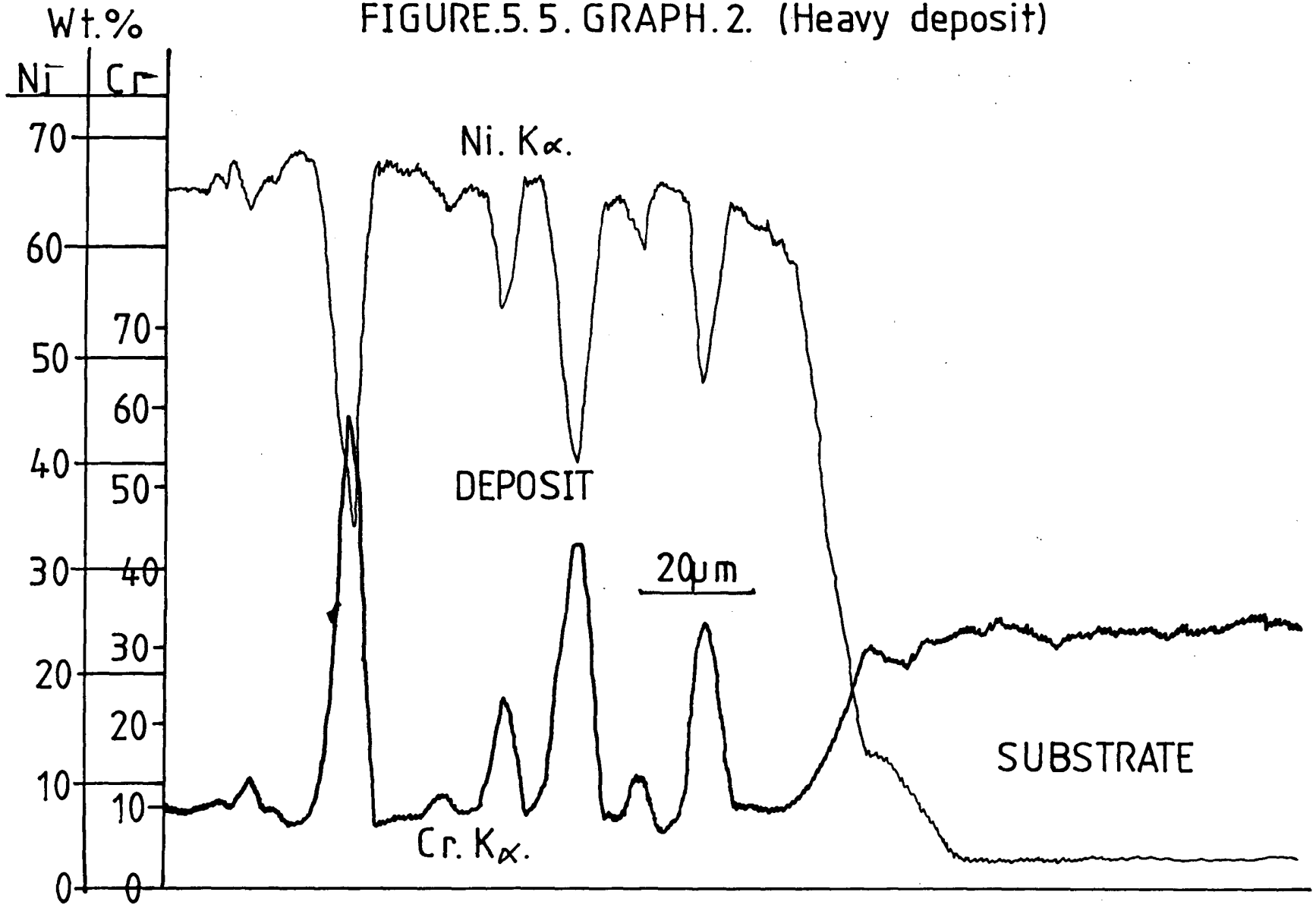

FIGURE.5.5. GRAPH.3. (Moderate deposit)

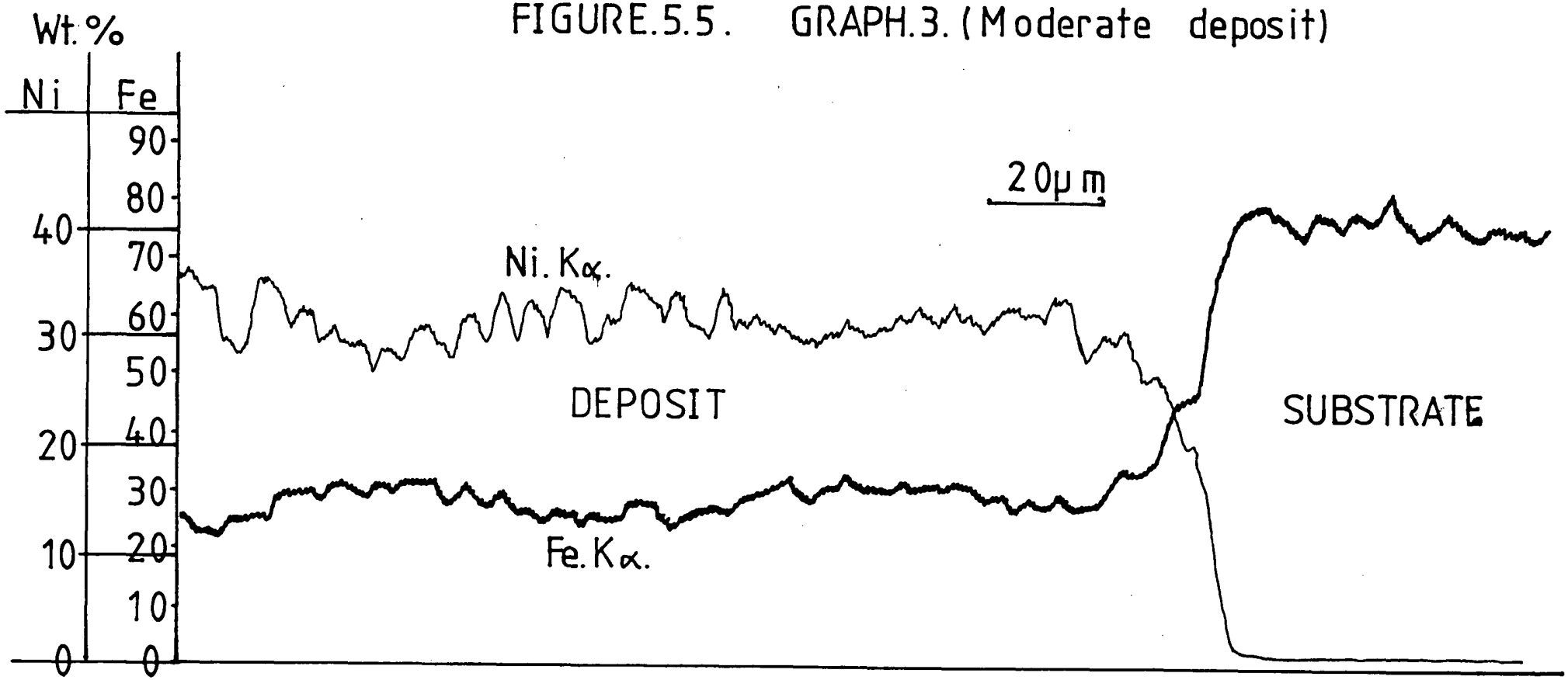

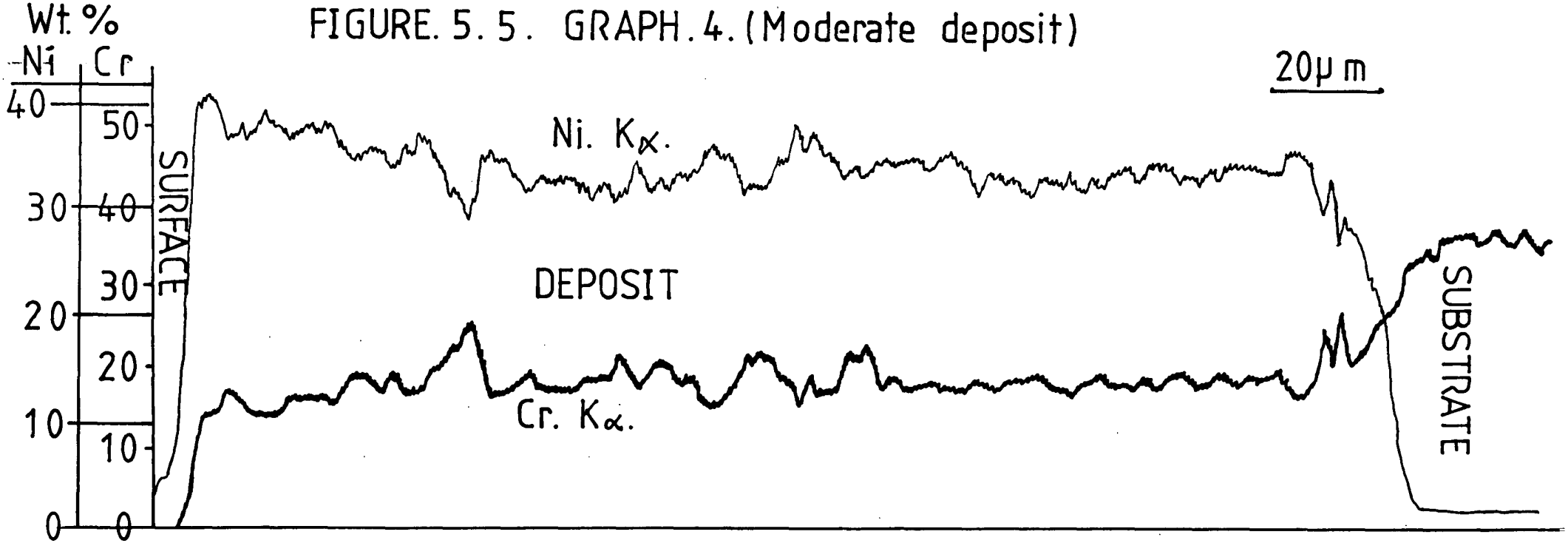

FIGURE. 5. 5. GRAPH. 4. (Moderate deposit)

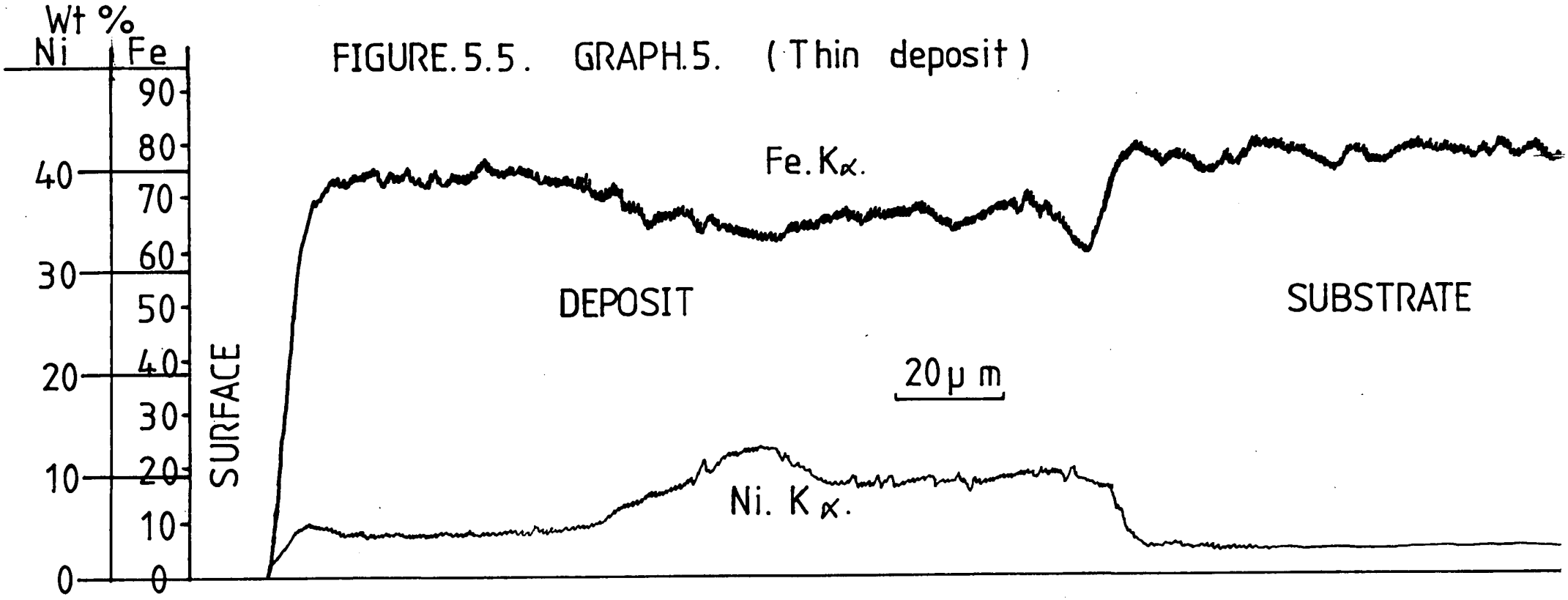

FIGURE.5.5. GRAPH.5. (Thin deposit)

FIGURE.5.5. GRAPH.6. (Thin deposit)

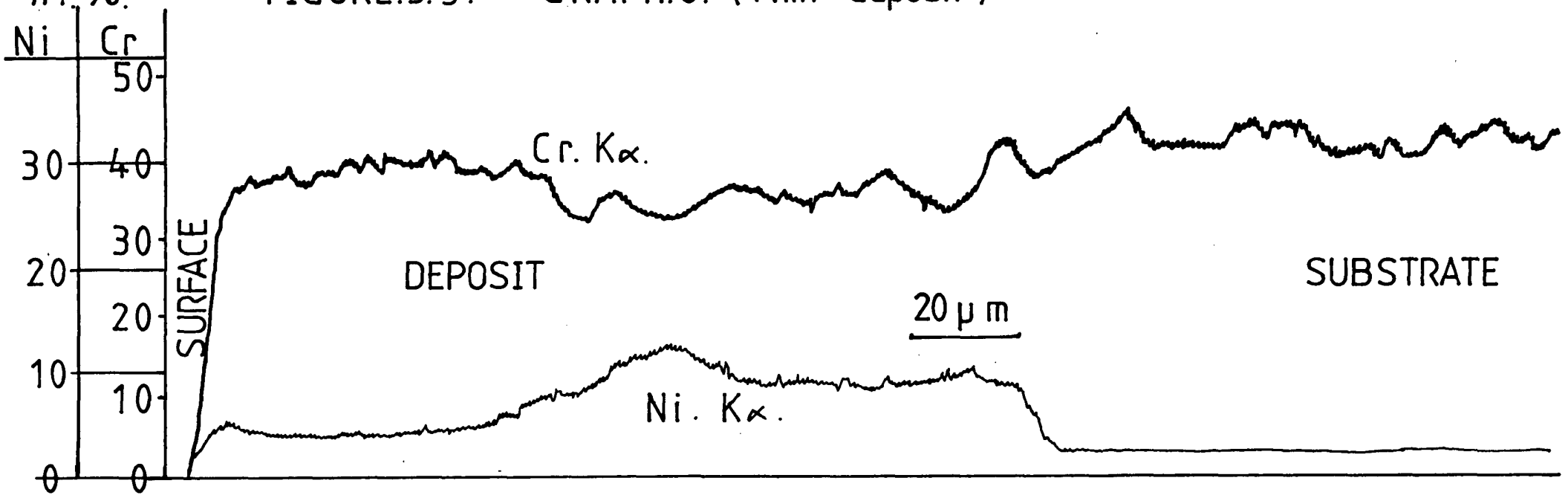

FIGURE 5.6 Micrograph investigation of selected clad valves.

Micrograph. 1. Sample. 25. (Heavy deposit)

(× 127.5)

The direction of solidification towards the top of the deposit follows the movement of the weld pool. (i.e. into page)

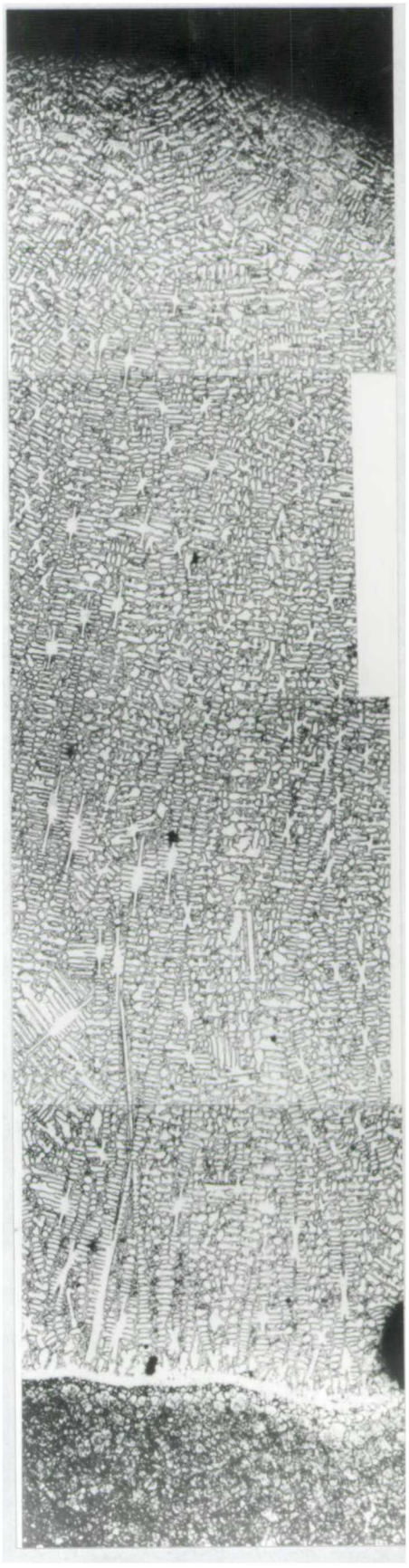

Vertical solidification towards the clad-substrate interface. (chill cast type)

FIGURE. 5.6.(Continued)

Micrograph .2. Sample 10. (Moderate deposit)
(×

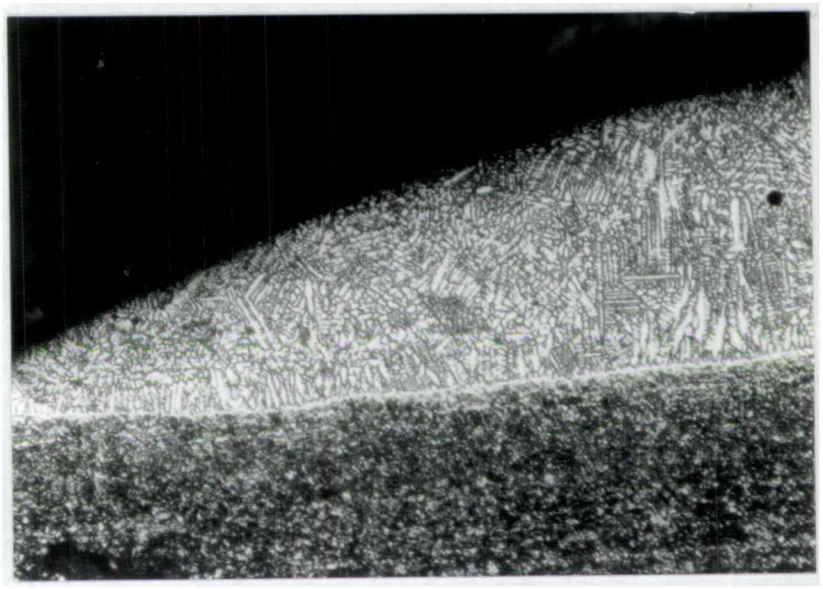

Micrograph.3. Sample.26. (Slight deposit.)
(×)

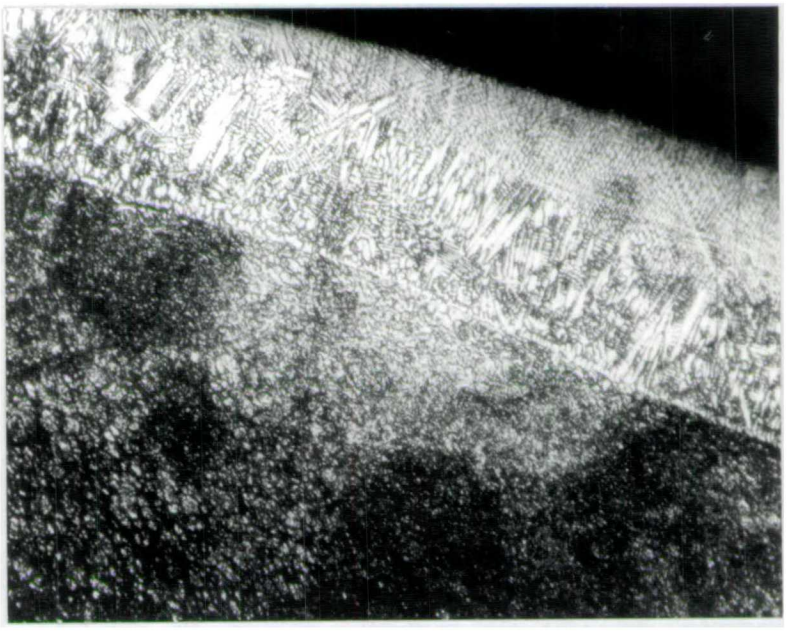

5.3 DISCUSSION OF RESULTS OF SF4O CLADDING ON TO VALVES

5.3.1 THE RELATIONSHIPS BETWEEN THE PRODUCTION PARAMETERS AND THE 'DEPOSIT' GEOMETRY

5.3.1.1 DEPOSIT WIDTH VARIATIONS

The variation of the deposit width ('Deposit referring to all the material melted during processing) with; the speed of processing. Argon and powder flow and laser power is presented in graphical form in graphs A and B of Figure 5.3.

5.3.1.1.1 WIDTH VARIATION WITH SPEED OF PROCESSING

The deposit width changes in a very similar manner with duration of processing in all cases. The general trend being a sharp rise in deposit width until the processing time reaches between four and five seconds.

Processing time in excess of five seconds show a much more gradual rise in deposit width with decreasing cladding speed (Obviously; Processing time $\propto$ (cladding speed)$^{-1}$)

The levelling out of the increase of molten zone width is attributable to a large extent to the characteristics of the incident laser beam. The partially focussed beam has an approximately gaussian power distribution which means that increasing the laser-material interaction time results in an increased diameter of weld pool, this increase being affected primarily by the increasing radius of energy

density capable of initiating melting, and secondarily by conduction of the 'surplus' energy within the weld pool to surrounding areas. The nature of a gaussian power distribution means that a linear increase in interaction time results in a rapid increase in molten pool diameter to begin with as the beam is more effectively coupled with the surface at increasing melting-threshold energy densities. Further increases in interaction time will increase the diameter of the 'melting threshold energy density' only very slowly and conduction of heat from the overheated weld pool will begin to be the dominant factor. This conduction-limited increase in weld pool diameter has only a minor effect because the weld pool itself has a very short 'lifetime' in any specific area; ie even at a processing time of 15 seconds for the 3cm diameter weld pool will move through 2mm in less than one third of a second. Figure 5.7 illustrates the fact, that the radius of a nominated energy density increases rapidly at first and then more slowly with increasing laser-material interaction time. For the purpose of the illustration it has been assumed that an increase in the laser-material interaction time is proportioned to an increasing laser power at constant processing speed. From the equation for the power distribution in a truncated gaussian beam:

$$P_r = \frac{P_{TOT}}{\pi r_b^2} \exp\left(\frac{-r^2}{r_b^2}\right)$$

the radius r_i can be found of a nominated power density

$$r_i = \sqrt{\left[\ln\left[\frac{P_r \pi r_b^2}{P_{ToT}}\right]\right]\left[-r_b^2\right]}$$

If a Pr is chosen as the limiting energy density capable of melting the material, then the variations of r_i with P_{tot} is shown in graph A of Figure 5.7. In this case the series of lines on the graph represent the growth of the radius of various energy densities with increasing PTOT for a laser beam with a radius of 1 mm. This principle was used to develop a similar plot for the practical conditions investigated in this set of experiments. As a starting point it was assumed from the experimental data that a 1500 W beam with a 3.5 radius melted a weld pool of radius 1.2 mm (see graph A Figure 5.3). From this assumption a limiting energy density for melting was calculated to be 9.75×10^7 W/m^2. The decrease in the radius of this energy density is shown in graph B of Figure 5.7 where it can be seen that the slope of the curve is similar to the practical results illustrated in Figure 5.3 graph A and B. The major difference in these graphs is the gradient of the curves towards the right of the graph. In the case of increasing processing times the curves level out more than the sister curves showing the effect of increasing PTOT. This effect can be explained by recognition of the fact that as the radius of the named power density is increased with increasing power, the power density gradient at that point is being made more and more shallow.

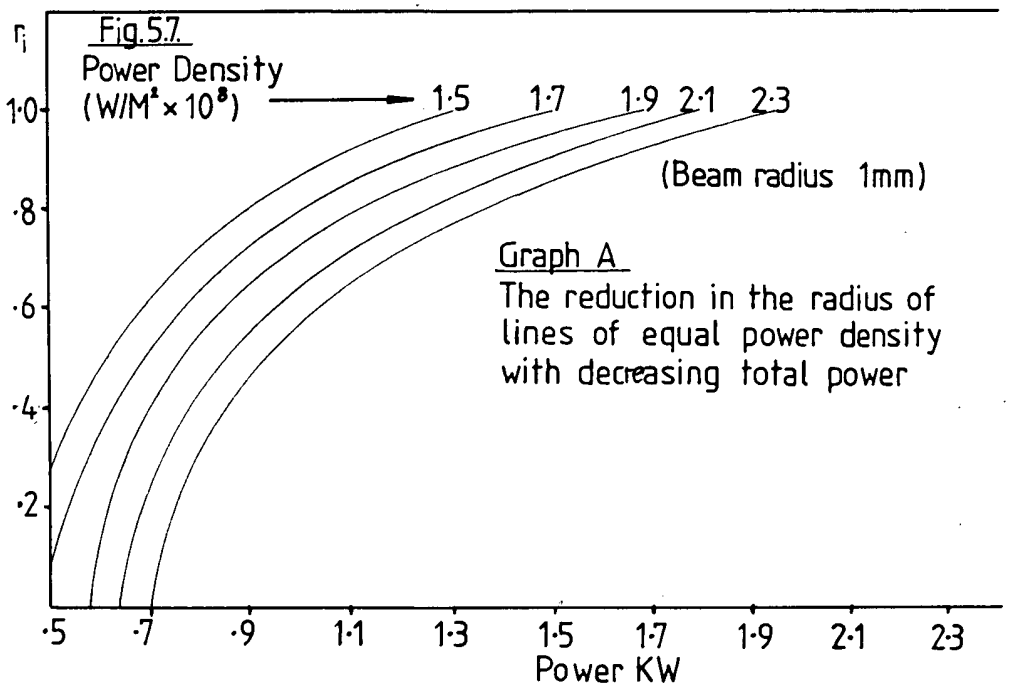
Fig.5.7
Power Density
(W/M² × 10⁸)
1·5
1·7
1·9
2·1
2·3
(Beam radius 1mm)
Graph A
The reduction in the radius of lines of equal power density with decreasing total power
ri
1·0
·8
·6
·4
·2
·5
·7
·9
1·1
1·3
1·5
1·7
1·9
2·1
2·3
Power KW

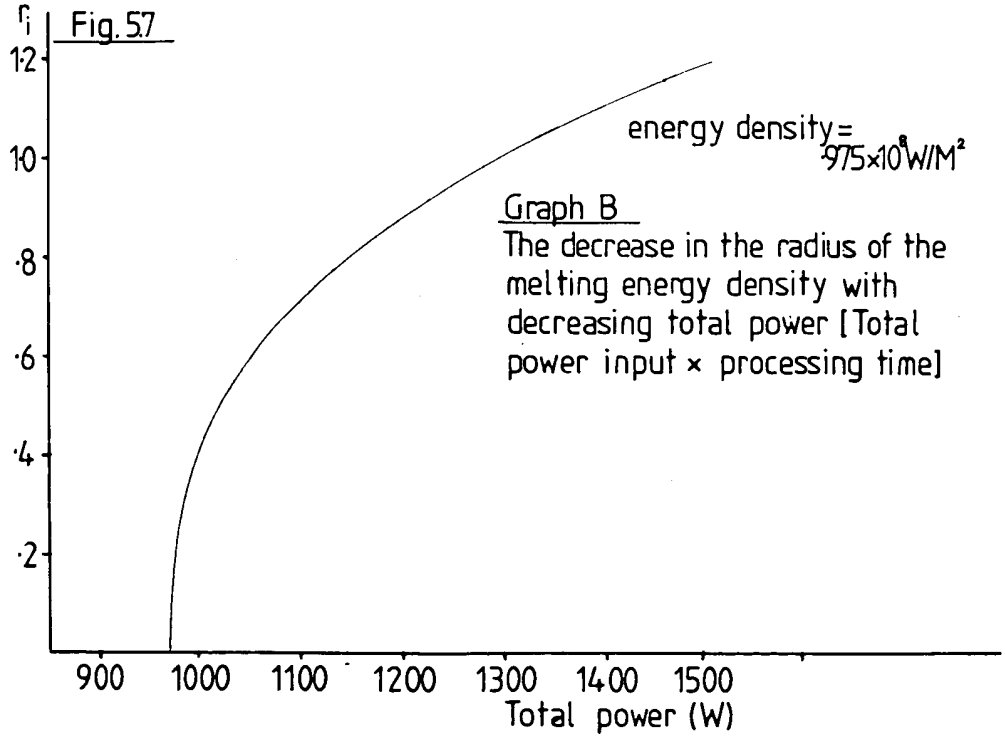
Fig. 5.7
ri
1·2
1·0
·8
·6
·4
·2
energy density = 975×10⁶W/M²
Graph B
The decrease in the radius of the melting energy density with decreasing total power [Total power input × processing time]
900
1000
1100
1200
1300
1400
1500
Total power (W)

It can be assumed therefore that the extent of melting is related to a combination of power density and power density gradient at the edge of the molten pool.

5.3.1.1.2 WIDTH VARIATIONS WITH ARGON/POWDER FLOW

As a clarification to the following discussion Figure 5.8 shows both the simple principle of operation of the gravity fed powder blowing gun and a typical calibration chart of Powder and Argon flows against Rotameter readings. Observation of this figure makes it clear that the powder flow increases with gas flow which means that the resultant powder cloud approaching and to some extent, covering the weld pool becomes denser and faster moving if the Rotameter reading is increased.

Dissatisfaction with the use of this type of powder blowing gun results from the fact that it is impossible to increase the mass flow of the particles without increasing their average velocity. This increase in particle velocity decreases the particle-laser interaction time and reduces the efficiency of the process, also, the fast moving particles are not easily trapped in the weld pool. Two further complaints are the fact that the guns can only be used with expensive, free flowing, spheroidised powder and that the mass flow rate-gas flow rate relationship changes if the gun as a whole is tilted at a different angle (tilting the gun towards the vertical increases powder flow rates and a tilt towards the horizontal can result in sporadic flow of powder as powder pours to fill the gas flow conduit until

Fig. 5.8

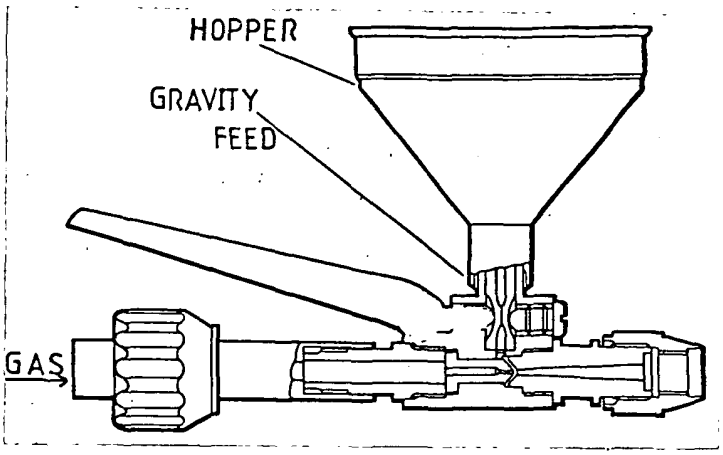

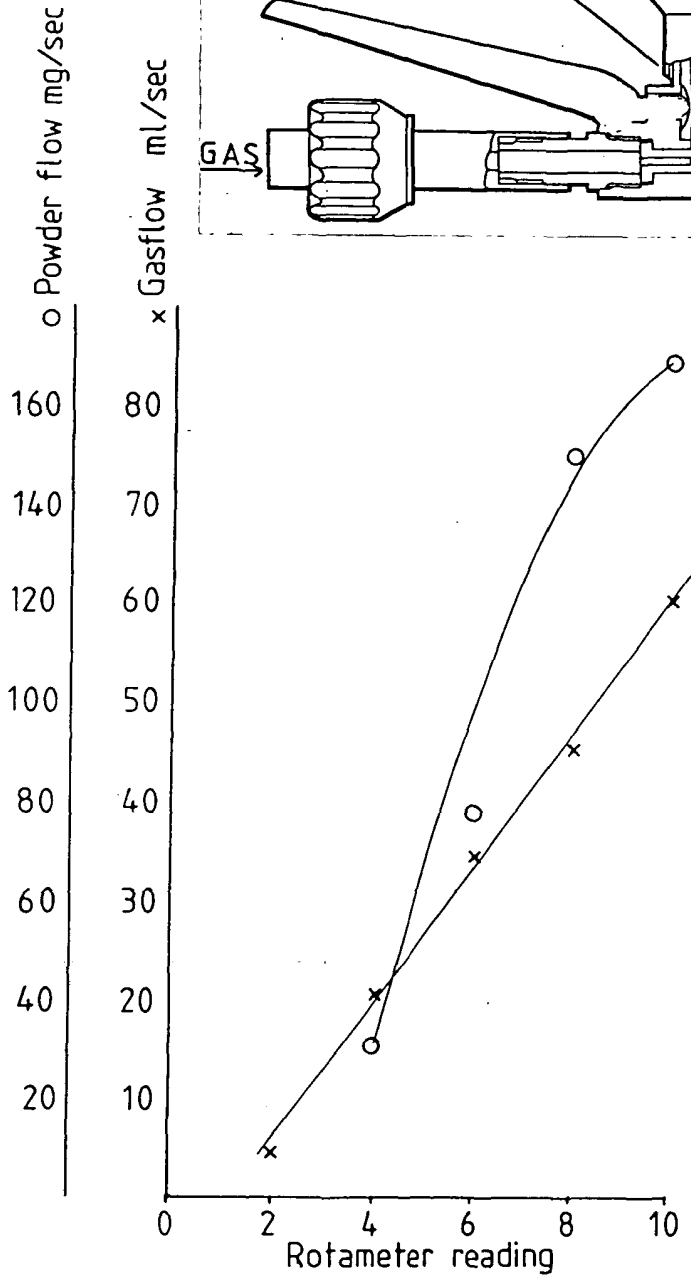

FIGURE. 5.9. The increasing powder catchment area of the weld pool with increasing deposit depth.

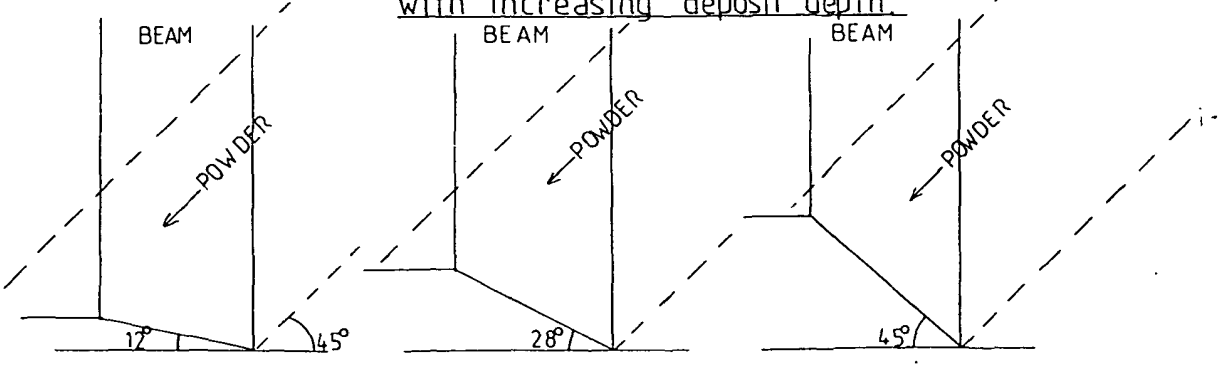

sufficient pressure has built up to blow the blockage clear, in a cyclic manner). It is for this reason that the flow calibration chart can only be referred to as 'typical'. Finally, another difficulty is that the powder has to travel up to 2cm from the end of the gun to the weld area, (if the gun is nearer than 1cm away the reflected heat can result in the gun becoming clogged with softened powder) the particles travel in an arc the shape of which is affected by their momentum. This in effect means that is the powder gun is tilted to feed powder directly into the weld pool at a rotameter reading of 8, a reading of 10 can lead to a disproportionate amount of over shooting,the reverse being true with a reading of 6. It was mentioned earlier that re-tilting the gun to provide the best powder trafectory for each gas flow causes important mass flow discrepancies. In view of these drawbacks any resultant trend in finished product characteristics will tend to be a complicated optimisation of the various variables described. (NB. Please see Appendix B)

Considering the graphs of Figure 5.3 A and B, it can be seen that the general trend for processing times in excess of five seconds is that the higher the rotameter reading the narrower is the melted zone width. This effect can be attributed to three factors:

a. Increased cooling from the powder transport gas jet
b. Increased cooling from an increase in incoming powder
c. Increased shielding of the weld pool by the denser powder.

The trend is a small one because these factors are only minor components of the energy balance (see Chapter 3).

When processing times of less than five seconds are being considered the picture is rather more confused. The information available in graph B is unfortunately too slight to be very instructive in itself but it does re-inforce the information in graph A. The graph indicates that several effects of comparable influences are conflicting, the overall effect of which is to present a confused picture which is best described by merely listing the various influences:
Considering an increasing gas flow rate;

a. The speed of the particle cloud is increased - the laser particle interaction time is decreased.

b. The cloud density above the weld pool is increased thereby reducing the amount of laser output energy reaching the weld pool.

c. The increased gas flow over the weld pool will act as a cooling agent.

d. Several optima exist for different particle trajectory-weld pool geometry combinations.

e. It is possible that due to the increased velocity of the particles an increase in the proportion of particles injected into the weld pool could occur in the cases of 'direct hits'.

f. In some cases the high density of impinging particles on the weld pool surface will aid the absorption of laser energy - a rough surface being a worse reflector than a smooth one.

g. Oxide contamination of the surface of the weld pool will be reduced due to the increased argon cover.

5.3.1.1.3 WIDTH VARIATION WITH INCIDENT POWER

Considering the graphs in Figure 5.3 A and B a general trend of increasing width with power can be seen. The only anomaly would appear to be sample 28 (representing Power 1800, gas flow 6 and processing time 13 seconds) which is 2.0mm wide when, to follow the usual trend, a value of 2.2 or more would be expected. This apparently odd result is explained by the fact that it is the only sample to have a definitely keyhole type weld cross section, indicative of a different sort of energy transfer into the material. Keyholing as a phenomenon will be explained in section 5.3.2.2 when the macrographs are being discussed.

Although the comparison of the two graphs can only describe a trend, the actual percentage increase is of come interest:

Power increase from 1500 W to 1800 W = 20%

Average increase in value of "gas flow 8" widths = 5.5%

Average increase in value of "gas flow 10" widths = 2.0%

(NB Only processing times of 5 seconds or more considered)

Extrapolation would be unreasonable but these increases do at least follow the expected path.

A full discussion of the theoretical expectations of increasing power appears in the earlier section 5.3.1.1.1 and the practical results implied by that discussion ie that an increase in PTOT for varying processing times would mean a shift in the curves position towards the left, are evident in graphs A and B Figure 5.3.

5.3.1.2 DEPOSIT DEPTH VARIATIONS

are presented in graphs C and D of Figure 5.3.

5.3.1.2.1 DEPTH VARIATION WITH PROCESSING SPEED

Observation of graphs C and D (Figure 5.3) shows the basically linear relationship between the depth of melted material and the duration of processing. One exception to this trend is sample 28, the 'keyhole' sample already noted in the previous section.

Suffice it to say here, that if a limiting P/VD * value is exceeded for a particular laser material interaction, the energy is no longer absorbed into the material by simple conduction from the hot surface but by a more direct process which leads to deep penetration weld pool formation.

*NB P = Laser power

V = Laser-material relative velocity

D = Laser spot diameter

Deep penetration is, in general, something to be avoided when cladding or surface alloying because it leads to gross dilution of the clad weld pool by the substrate material, which reduces the effectiveness of the cladding material in improving the material surface durability.

The reason why sample 28 experienced keyholing is directly related to the effective energy density $\left[P/vd \right]$ it experienced. Inspection of the operating parameters show that it was exposed to 1800 W with a processing time of 13 seconds with an Argon rotameter reading of 6. The gas flow reading of 6 meant that there was less gas flow, cooling, and less cloud cover of incoming particles over the weld pool than was

the case with the gas flow 8, (which experienced slight key-holing effects with the same parameters) and the gas flow 10 (which did not 'keyhole'). This reduction in the weld pool powder shielding meant, in effect, that the weld pool of sample 28 was exposed to the highest effective $^{P}/_{VD}$ value.

Two mechanisms constitute an increase in melted zone depth, these are;

a. Increase in depth of substrate melted and

b. Increase in the amount of new cladding material melted. Although the general relationship between increasing $^{P}/_{VD}$ by decreasing V) and in increasing depth of weld pool is a a linear, proportional one, the molten material itself need not necessarily be uniform but will change as the weld pool geometry acts as a superior or an inferior powder catchment area.

5.3.1.2.2 DEPTH VARIATION WITH ARGON/POWDER FLOW

The two methods of increasing molten pool depth just mentioned (section 5.3.1.2.1) are very important when considering the depth variation with argon/powder flow. On the one hand an increase in the powder cloud density above the weld pool shields and cools the weld pool, and thus inhibits deep melting but on the other, the powder cloud itself absorbs more laser energy which leads to an increase in the height of the new deposit above the original substrate surface position. The conflict between these two effects and the resultant outcome can clearly be seen in graphs C and D of Figure 5.3 and in the macro graphs in Figure 5.4. Considering, for the sake of simplicity, graph C alone, the trends can be described as follows:-

1. Between the curves for the argon flow readings of 6 and 8 there is a general drop in the molten pool depths due to increasing powder cloud cover and gas cooling over the weld pool which effectively reduces $^{P}/_{VD}$.

2. Between the curves for the argon flow readings of 6 and 10 or 8 and 10 there is a general increase in molten pool depths due to more powder being melted and included into the weld pool, swelling its size rather than increasing the depth of penetration,

This entrapment of more powder is to some extent attributable to the molten weld pool surface geometry and its relationship to the direction of travel of the incoming powder jet.

This relationship is best described with the help of the diagram which constitutes Figure 5.9. Taking the simplified view that the molten or solid phase condition of the surface is dependant on the incident energy profile which remains unchanged, it can be assumed for the purpose of clarity that the diameter of the weld pool does not change in the X direction. It can be seen therefore that an increase in the cladding weld pool height above the substrate surface has the following two effects:-

a. The weld pool size increases making it into a better powder catchment area

b. The weld pool surface becomes more perpendicular to the direction of travel of the incoming powder, again increasing the efficiency of the entrapment process.

Ignoring, for the moment, the obvious flaws in this theoretical model (no attempt will be made to quantify the variations) It can be seen that the efficiency of the process is improved as the cladding weld pool is thickened. This trend is backed up by

the practical evidence in graph D (Figure 5.3) which shows, in the case of a gas flow of 10, an acceleration in clad depth with reducing cladding speed. This acceleration is attributable to the fact that if sufficient incoming powder is available, the efficiency of powder entrapment is increased with increasing cladding depth above the substrate surface.

5.3.1.2.3 DEPTH VARIATION WITH INCIDENT POWER

Comparison of graphs D and C (Figure 5.3) shows the expected trend towards greater melting with increasing $^{P}/_{VD}$.

The keyholing observed in the case of three of the samples (28 - severe and 32 and 33 - slight) is directly attributable to the increased power densities experienced by the 1800 W processed specimens. It will be noted that increasing the power has a greater effect at the slower processing times due to the more substantial powder melting taking place and the tendency to change from conduction-limited to keyhole welding with long laser-materials interaction times.

5.3.1.3 DEPOSIT CROSS SECTIONAL AREA VARIATIONS

The variation of the deposit cross sectional area with the production parameters is shown in graph E and F of Figure 5.3.

The cross sectional area of the welded pool is, of course, directly related to the width and depth of that pool, already thoroughly discussed in the previous sections. For this reason analysis of graphs E and F will refer back to previous arguments rather than re-iterating them.

5.3.1.3.1 CROSS SECTIONAL AREA VARIATION WITH SPEED OF PROCESSING

The relationship between cross sectional area of molten pool and speed of processing is a basically linear one - see graphs 5.3. E and F.

The only point which does not comply to this linear rule is that relating to specimen number 25. This ties in with earlier comments which concluded that in certain cases the efficiency of the cladding process is improved as deeper deposits are laid down. The expected anomalies due to the keyholing of certain welds were slight because although keyholing dramatically increases the maximum depth of deposit this new depth is restricted in width and so, increases in overall cross sectional area are not large. (NB Keyholing - see specimen 28 laser power 1800 W, gas flow 6 and rotation time 13 seconds).

In general, weld pools created during this experimental programme were developed by simple absorption from the material surfaces and conduction within the materials (both the powder and substrate). It is reasonable therefore to relate the linear nature of the increase in weld pool cross sectional area directly to the increasing $^{P}/_{VD}$ value concommitant with reducing V (or, increasing the processing time).

5.3.1.3.2 CROSS SECTIONAL AREA VARIATION WITH ARGON/ POWDER FLOW

Two conflicting effects caused by increasing the powder flow are the overiding factors in determining the cross sectional area: Argon/powder flow relationship. These effects are the shielding

of the weld pool by an increase in airborne powder combined with with increased Argon flow cooling which tends to reduce the amount of material melted and the introduction of more powder into the weld pool which tends to swell its size. This new powder is readily melted into the weld pool because the energy distribution of the laser beam leads to overheating of the central portion of the weld pool (as compared, for example, with the temperature gradient across a solidifying casting molten pool). If this was not the case, extra incoming powder would tend to cool the weld pool to below melting temperatures, a limiting condition not reached within the bounds of this experimental programme.

The following review uses the mathematical analysis in Chapter 3 section 3 with the actual experimental values used in this investigation.

Rotameter Reading	Mass flow (mg/sec)	Particle radius (mm)	Gas flow (m/sec.)	Voidage (ε)	Max power density for P_{TOT} 1500 (W/m^2)	Max power density with powder cloud (W/m^2)	% of the beam penetrating the cloud
6	77	.05	34	.99975	1.56×10^8	1.53×10^8	98%
8	150	.05	46	.999635	1.56×10^8	1.52×10^8	97.3%
10	170	.05	61	.999689	1.56×10^8	1.525×10^8	97.7%

Particle radius = 05

depth of powder cloud above weld = 5 (the largest value observed)

The review deals only with the energy conditions at the centre of the beam as it impinges on the weld pool the voidages calculated were all in excess of .999 and thus the skewing of the gaussian distribution can be disregarded (see Figure 3.3.2.A). As a close approximation it can be stated that the beam impingent upon the weld pool is gaussian in character and, in this case, retains 97 +% of its original power after penetrating the powder cloud. The velocities of the particles through the laser beam were of the order of 1.0 m/s and the values relating to the particles were fed into the computer model to reveal that the maximum temperature reached by the particles was 925°C. This temperature was that reached by any particle which travelled all the way through the beam along the centre line thus arriving at the X,Y position 0.0 (see Figure 3.3.1).

Figure 5.9 THE TEMPERATURE ARRAY OF POWDER PARTICLES

(all values taken from experimental data)

Temperature in °C

Y Direction Distance from Focus

X direction distance from the leading edge of the beam (mm)

	0	.2	.4	.6	.8	1.0	1.2	1.4	1.6
0	925	903	898	790		Beam	Absent	in Area	this
.35	862	849	842	751	680	594	482		
.75	777	761	754	672	618	535	443	355	
1.15	667	651	640	574	525	455	377	323	208
1.55	537	53[illegible]	510	466	419	359	296	261	151
1.95	400	39[illegible]	374	343	310	262	258	195	92
2.35	270	26[illegible]	250	230	203	169	148	122	34
2.75	160	158	144	131	113	87	58	27	20
3.15	74	71	64	54	43	25	20	20	20
3.5	20	20	20	20	20	20	20	20	20

The particles then can be considered to have a cooling effect on the weld pool and consolidation is brought about by conduction from the overheated weld pool lying beneath the approximately gaussian distribution laser beam. The particles themselves tend to skew the energy distribution towards the X = 0 line by carrying the heat absorbed by them in that direction, the hottest particles arriving nearest the X = 0 line but this effect, involving the skewing of less than 3% of the total input energy can be ignored.

5.3.1.3.3 CROSS SECTIONAL AREA VARIATION WITH INCIDENT POWER

Graphs E and F show that the increase in laser power of 20% from 1500 W to 1800 W has resulted in the expected slight increase in the amount of material melted in most cases. Anomalies to this trend are caused either by the onset of keyholing in high power runs (leading to a deep, narrow weld pool) or the increasing efficiency of the process already noted in the slower speed, laser power 1500 gas flow 10 runs. The increase in molten material noted between the values for gas flows of 8 can be taken to represent the usual case.

5.3.2 DEPOSIT COMPOSITION CHARACTERISTICS

5.3.2.1 MACROGRAPHIC ANALYSIS OF DILUTION OF THE DEPOSIT

Graphs G and H of Figure 5.3 show the trends in dilution levels* of the deposits. In-depth analysis of these trends is made difficult by the complex inter relationships between the variables affecting the level of dilution in any weld pool.

The readings are taken from a computer aided analysis of the macrographs carried out with an Apple computer and a 'digipad' which gives a reading of the area within any traced line.

(*NB a 65% dilution level means that 65% of the weld pool consisted of substrate material).

Graphs I and J of figure 5.3 describe the varying amount of SF40 cladding powder incorporated into the weld pools, this trend is linear, strongly resembling the graphs showing the total amount of material melted (Graphs E and F). It is the relationship between these two sets of graphs which is illustrated by graphs G and H.

The general trends are as follows:

A. Dilution is decreased with decreasing speed of processing.

B. Dilution is decreased with a greater powder flow.

C. Dilution appears to be not greatly affected by the change in laser power

Discussing these in turn, a decrease in dilution with decreasing speed of processing is related to the improvement of the weld pool as a powder catchment area as it becomes thicker (see Figure 5.9, section 5.3.1.2.2). The weld pool at the higher processing speeds is small in diameter and lies almost flush with the substrate, catching very little powder. At lower speeds the deposit is built up and the weld pool lies at an angle to the substrate and tends towards perpendicularity with respect to the direction of approach of the incoming powder, thus more effectively 'capturing' incoming particles.

Dilution is decreased with greater powder flows because more powder is being injected into the weld pool. An increase in powder flow increases the mass transfer rate and also the velocity of the particle cloud. The increase in cloud density obviously causes the weld pool to be made up of more incoming powder than hitherto but the increase in velocity has two conflicting effects:

A. Fast moving particles impinging upon the weld pool can be more easily submerged and incorporated into the pool.

B. Fast moving particles are cooler on arrival at the weld pool due to their short previous exposure to the laser radiation, they therefore cool the pool more effectively and thereby reduce further powder melting capability. Also, fast moving particles which strike the weld pool surface at a glancing angle are more likely to bounce out of the area than their slow moving counterparts.

Although the cooling effect of the powder injection can limit the capability of the weld pool to melt more powder it also reduces the conduction of heat into the substrate and this reduces the level of dilution.

The lack of any trend in dilution with increasing power within the limited range (1500 + 1800 W) investigated can be attributed to the similar increases in the degree of melting of incoming powder and the weld pool cross sections as a whole (compare graphs I and J with E and F).

The increases in dilution after an initial drop for the lines corresponding to gas flow of 6 and 8 with laser power 1800, are linked to the onset of keyholing as the processing times are increased. Keyholing is a deep penetration welding phenomenon and as such results in a sudden increase in the amount of

substrate melted during the process without affecting the degree of powder melting.

5.3.2.2 DISCUSSION OF SELECTED MACROGRAPHS

Figure 5.4 (page142) shows a selection of the many macrographs which form the basis of this investigation.

5.3.2.2.1 GENERAL CASES

The two sets of four macrographs Figure 5.4 A and B illustate the points examined at length in the earlier sections of this chapter. A short reference list of the major points to observe may be of help at this stage;

1. Increase of weld pool size with increasing processing time.
2. Increase of deposit and reductions in dilution with increasing powder flow.
3. Increase of pool width up to a limiting value with increasing processing time.
4. Low levels of porosity and the presence of conduction limited heating only (shown by the absence of keyholing).

5.3.2.2.2 KEYHOLING

Section 2.2 considered the fundamental interactions of lasers and materials within the usual energy density limitations imposed upon the cladding process. If the energy density above the weld pool is sufficient however, the mechanism of heat transfer changes from conduction - convection to keyholing.

As a moving molten weld pool begins to boil as a result of the incident laser energy, the vapour improves the energy coupling which leads to further boiling. As the boiling rate is increased

a local surface depression is created in the weld pool. This depression becomes a hole which acts as a black-body absorber with near zero reflectivity.

Once the keyhole has been established, a dynamic situation exists between the vapour holding the keyhole open, and the molten metal which attempts to close the hole using the combined forces of surface tension and gravity.

The subject of keyholing is a large one and an in-depth investigation would be out of place in this present work as keyholing is, in general, to be avoided when cladding.

In summary, keyhole welding can be considered to involve a line source moving through a material with the energy from the laser being pled first to the metal vapour within the keyhole and thence to the molten surface which lines the hole.

Macrograph C in Figure 5.4 shows the cross section of sample 28 which shows signs of the keyholing process. This keyholing is not severe in the context of welding but should not be present at all in the laser cladding process. It is a clear indication that the energy density above the weld pool is too great, this can be reduced by many methods ie increasing processing speeds, increasing powder cloud density or reducing laser power.

5.3.2.2.3 POROSITY

Macrograph D of Figure 5.4 shows a cross section of sample 37 (laser power 1800, gas flow 10, processing time 13.0). This sample was the only one in this group of experiments to exhibit

gross porosity. The generally spherical nature of tne pores indicates that they existed as bubbles of gas trapped in the liquid pool. The possible mechanisms of porosity formation are numerous but the mechanism relevant to this sample would appear to be the consolidation of much smaller pores trapped when the relatively high density, high velocity powder cloud was arrested, melted and frozen in the short time available in laser processing. The reason why this porosity played such a small part in other cross sections was a combination of the following porosity inhibiting factors:

a. smaller amount of powder melted

b. slower processing speeds

c. slower moving gas cloud

d. higher energy density over weld pool

Porosity in clad deposits is always to be avoided but because it is caused by the correct (or incorrect!) juxtaposition of many variables it is difficult to judge when it will, or will not, be a serious problem. The presence of porosity can deleteriously effect the performance of a clad surface whether its major function is physical or chemical protection.

5.3.2.3 ELECTRON PROBE MICRO ANALYSIS AND MICROGRAPHIC EXAMINATION OF SELECTED DEPOSITS

Samples 25, 10 and 26 underwent Electron probe micro analysis and micrographic examination, their production parameters etc were as follows:-

Sample	Laser Power	Gas Flow	Processing Time	X Sect area	% Dilution
25	1500W	10	17 secs	$1.3mm^2$	0
10	1500	8	3.5 secs	$.195mm^2$	25
26	1800	6	2.5 secs	$.150mm^2$	50

The specimens were chosen for their wide range of processing variables and the possibilities they afford for the analysis of dilution.

Figure 5.5 shows the EPMA scans across the interface between the substrate and the solidified clad weld pool in each case and Figure 5.6 presents the micrographs. EPMA was carried out for the iron, nickel and chromium content over a distance of approximately .25mm , situated near the centre of the weld where the most typical conditions can be found.

Examination of Figure 5.5 graphs 1 and 2 together with Figures 5.6 micrograph 1, which deal with sample 25 reveals the very narrow dilution layer present at the deposit - substrate interface. The changeover between substrate composition and stellite composition takes place within thirty microns. The sudden decreases in nickel content in the stellite correspond with sudden increases in the chromium content. Subsequent investigation showed ((68) 'electron probe micro analysis) that the chromium content of the stellite varied in sympathy with the carbon content, which explains the variations as evidence of the presence of chromium rich carbides.

Micrograph 1 of Figure 5.6. shows the following important features:

a. The narrow heat affected zone in the substrate.

b. The narrow white phase dilution area.

c. The dendritic nature of the deposit.

d. A small amount of porosity.

e. The slight coarsening of the deposit dendritic arm spacing as the distance from the interface increases.

The reasons behind this coarsening lie in the analysis of the heat flow in the solidifying and cooling weld pool. Although heat is radiated from the surface of the weld pool and conduction-convection heating of the surrounding air does take place, the major heat transfer method is by conduction into the cold substrate material. The situation is analagous, to some extent, to the solidification of a casting from its mould contacting walls inwards. The quenching effect near the deposit-substrate interface is therefore more severe than at the deposit-interface. As the rate of solidification and cooling is increased the dendrite arm spacing is decreased although this effect cannot be expected to be very profound when considering such a shallow weld pool and such a small amount of substrate material. (The smaller the bulk of substrate, the less effective it is as a heat sink).

Graphs number 3 and 4 of Figure 5.5. together with micrograph 2 of Figure 5.6. constitute the information relevant to specimen 10 and show a marked degree of dilution. The presence of the chromium rich carbides seems to have been reduced, an effect which can be attributed to the increased carbon solubility in the 'deposit' which contains a good deal of iron. The interfacial distance between the deposit and the substrate is still approximately 30 microns but the deposit is considerably dilued with substrate material. The graphs indicate that there is a great deal of turbulence in the weld pool by showing the eveness of distribution of the dilution.

Convection in laser weld pools was first analysed by Antony and Cline[69] and more recent work has been carried out by Copley et al[70] and Chan and Mazumder[71]. The work was carried out to explain ripples in the surface of laser surface melted materials but the conclusion and principles are applicable to the different

geometry cladding weld pools. For the sake of simplicity, the principles will be explained considering surface melting weld pools:

The energy distribution of the beam and the nature of weld pools themselves means that there is a large thermal gradient across the molten pool. This thermal gradient results in a surface tension gradient across the weld pool, the surface tension of a molten metal decreasing with increasing temperature. At the point of impingment of the laser beam the temperature is highest and the surface tension lowest. The surface tension increases along a line from the impingment point to the edge of the weld pool (see Figure 5.10). Thus any volume element of the surface experiences a force parellel to the surface causing it to move from the centre to the edge of the weld pool. This causes the liquid-vapour interface to assume a concave curvature if viewed from above. The difference in static pressure on volume elements resulting from the curvature produces a return flow deep in the melt pool from the melt pool edge to the impingment point.

Copley et al demonstrated this principle by producing weld pools in a camphene - tricyclene alloy. This alloy is transparent and allowed high speed photography to verify the theory. This principle of surface tension induced stirring, translated to the different geometry of a clad weld pool, explains the very even distribution of diluents in a solid diluted laser weld pool satisfactorily although other mechanisms may play a part eg mechanical stirring induced by the impingment of incoming powder particles.

Micrograph 2 shows the material to be of a finer grain size than

FIGURE. 5.10.

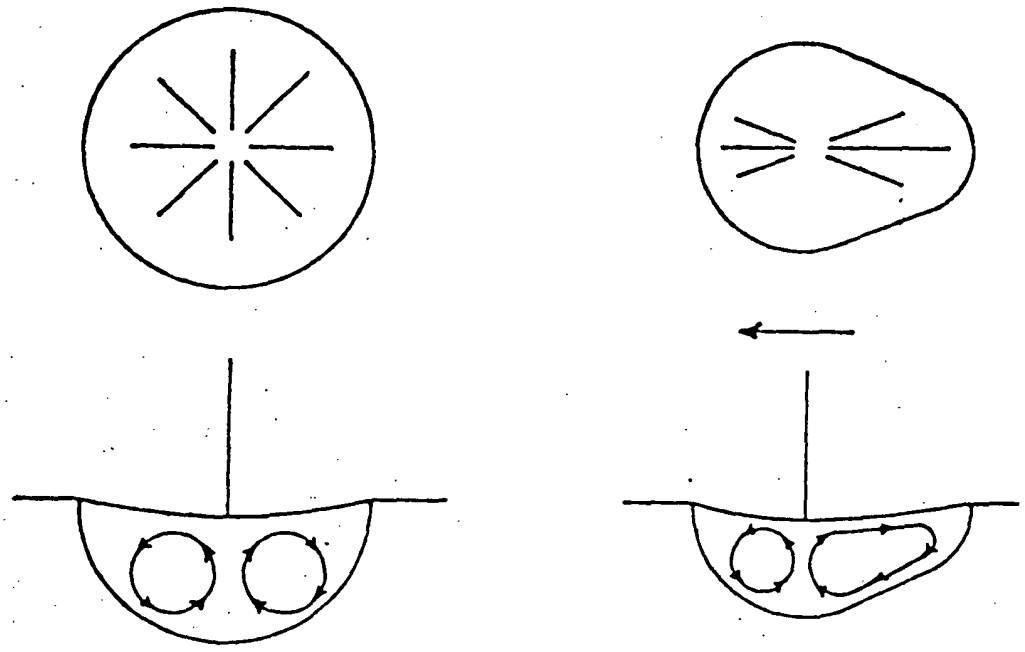

Convection patterns in laser melted pool:
(a) scan velocity equals zero; and
(b) scan velocity not equal to zero

sample 25 (micrograph 1). This is to be attributed, in part, to the difference in processing time which changes the range of cooling rates experienced by the sample. A reduction in processing time from 17 to 3.5 seconds reduces the amount of material melted but increases the heat sinking ability of the substrate and thus increases the cooling rates. This increase in cooling rate results in a finer grain structure than could be found in heavier deposits attempting to sink their heat into a small substrate, in which case a valve can often glow orange hot for a few seconds. Changes in grain size cannot be wholly attributed to changes in cooling rate however, because the actual composition of the weld pool has been changed by dilution.

The final EPMA results and micrograph show the information relevant to sample 26 and these show the expected trends. The EPMA results show a narrow interfacial area with a well mixed weld pool. The distribution of the alloying elements is unusual in that there appears to be less dilution in the central portion of weld than near the surface. This distribution could be a physical manifestation of the stirring process being 'frozen' in mid cycle by the rapid processing speed experienced by this sample. In this case the initially SF40 rich, top part of the weld pool, would only have had time to be 'surface tension stirred' until it lay beneath its original position when the removal of enough heat to freeze the material led to solidification before the cycle was complete. Once again, the rapid cycling of the specimen (2.5 secs) has led to a fine microstructure although in this case the weld pool should really be considered as a substrate weld pool diluted with SF40 rather than an SF40 weld pool diluted with substrate.

5.4 GEOMETRICAL CONSIDERATIONS FOR FUTURE WORK

A study of the macro and micrographs shows that cladding onto a flat surface results in a deposit with a curved, convex cross section. This curvature is related to the wetting and surface tension properties of the molten weld pool (see chapter 4) and necessitates post cladding grinding to give a flat surface to the finished product. This grinding operation is obviously time consuming and expensive. Pilot experiments have shown that the properties of the liquid weld pool can be utilised to give a good flat finish to the clad product if a change in the surface geometry is effected. This flatter finish reduces the need for post cladding grinding to a minimum and allows accomodation of deeper, less dilute weld pools.

The principle depends upon the use of the cladding process to fill up a groove in the substrate. The macrographs in Figure 5.11 show that the process holds great promise for the future but the difficulty in preparing valves with different grooves for experimentation meant that a full investigation would require too much time to be included in the present work. The grooved valve clad here (Figure 5.11) is of a larger size than the ones used in the earlier experiments and therefore no direct comparison is available. The principle of swinging round the balance of forces until an almost flush deposit is achieved is demonstrated in Figure 5.1 2 and an in-depth analysis of the principle and its practical outcome will be very useful to further work.

FIGURE.5.11 Macrograph of a valve which has been prepare to give a flush clad deposit.

(×9)

prepared

clad

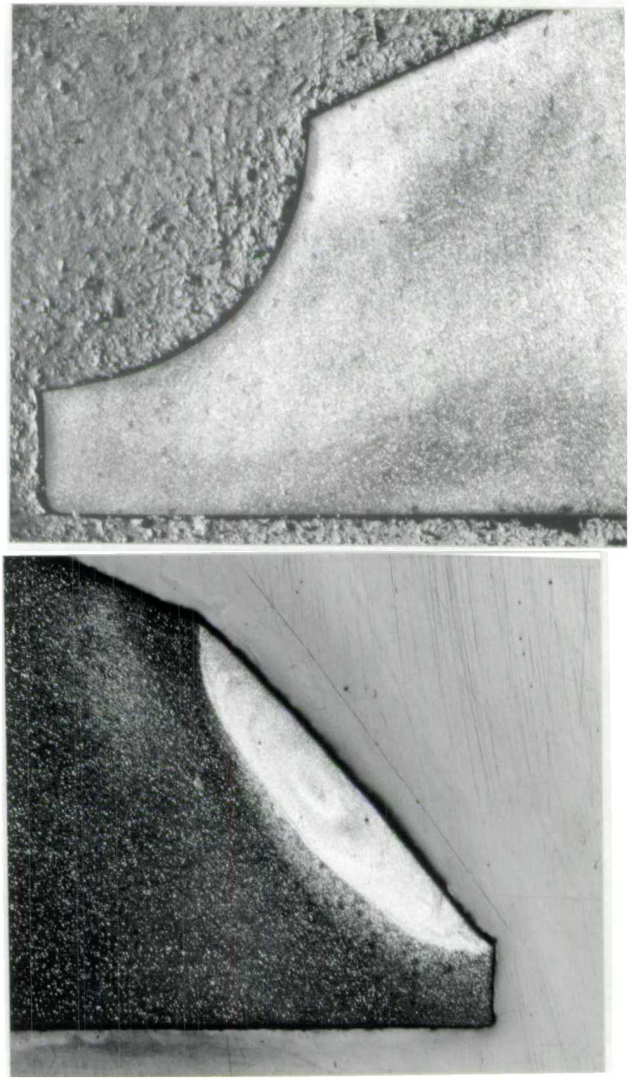

Figure 5.12. Balance of interfacial forces.

$\gamma_{as} = \gamma_{ls} + \gamma_{la}\cos\theta$

$\gamma_{as} = \gamma_{la} + \gamma_{ls}\cos\alpha$

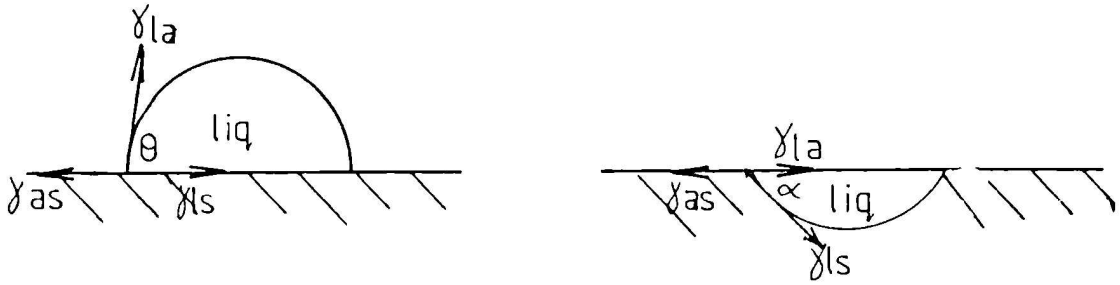

γ_{la} = interfacial energy liqued-air

ls = " " liqued-solid

as= " " solid-air

5.5 SUMMARY

The cladding of valves by the laser melting - blown on powder method results in a wide range of possible deposits. Dilution levels, grain sizes and deposit dimensions all vary with the numerous processing parameters in a complex relationship based on the inter-dependence of these parameters.

Basically, it can be said that if a given finished product is specified there is a range of processing parameters over which that product can be produced (eg in certain cases it should be possible to increase the laser power, the speed of processing and the rate of incoming powder to produce the same sample faster).

Judicious choice of the substrate geometry can lead to the deposition of a deep, undilute deposit with an almost flat surface and this should be the direction taken by further work.

CHAPTER 6

VIBRO LASER CLADDING

6.1 GENERAL INTRODUCTION

Vibro laser cladding is the name given to the process of cladding by the blown on powder technique whilst simultaneously vibrating the substrate material and weld pool by means of ultrasonic transducers. The process, which gave improved cladding quality, has already led to the publishing of two papers[76,77] and a patent[78] by the present author. A copy of the patent application is added to this thesis as appendix F. The original idea and development of the VLC process was the result of a combination of factors.

a. Stress levels in cooling laser clad tracks often resulted in crack formation.

b. Porosity in many blown on cladding deposits.

c. Attainment of low dilution deposits was difficult if the good wetting needed for a sound interface was to be achieved.

Fundamental consideration of the cladding process led to the hypothesis that a vigourously shaken weld pool would reject pores and wet the substrate better. A review of the subject of vibratory stress relief supported the assumption that ultrasonic vibration of the solidifying and cooling deposit would help to reduce stress levels in the final product[72,73].

Although improvements in the wetting and porosity characteristics of the clad deposit were easily identified by optical micrography, a more advanced monitoring technique was needed to show changes in deposit stress levels. Acoustic emmission monitoring of the

cooling deposit was employed and a close correlation was found to exist between the noise generated by a cooling deposit and the density of micro and macro cracks observed therein.

6.2 EXPERIMENTAL PROCEDURE

6.2.1 GENERAL

Figure 6.1 shows the basic experimental set up used during this investigation. Vibration of the Mild Steel (en3) substrate was made possible by clamping it to an aluminium plate attached to four powerful ultrasonic transducers working in phase. This specialised ultrasonic vibration equipment was supplied by C J Electronics Limited who built it specifically for this project under direction from the author. A grease layer was placed between the aluminium plate and the mild steel substrate for better vibration propogation and the bases of the transducers were set in rubber as they could not be clamped without damaging them.

The vibration experienced by the substrate was of an amplitude of 20 microns at a frequency of 25kHz. Deep (2mm) deposits of Deloro stellite SF40 or S6 were then clad onto the substrate by the blown on powder process described in Chapter 5. SF40 is a nickel base hard facing alloy of composition; Ni 85.2%, Cr 7.5%, Fe 1.5%. B 1.5%, Si 4% Co 3% and S6 is a cobalt based alloy of composition; Co 66%, Cr 26%, W 6%, C 1%.

Clad deposits were laid in identical pairs with the only changed parameter between the runs in any pair being the use of ultra-

FIGURE 6.1. Vibro Laser Cladding

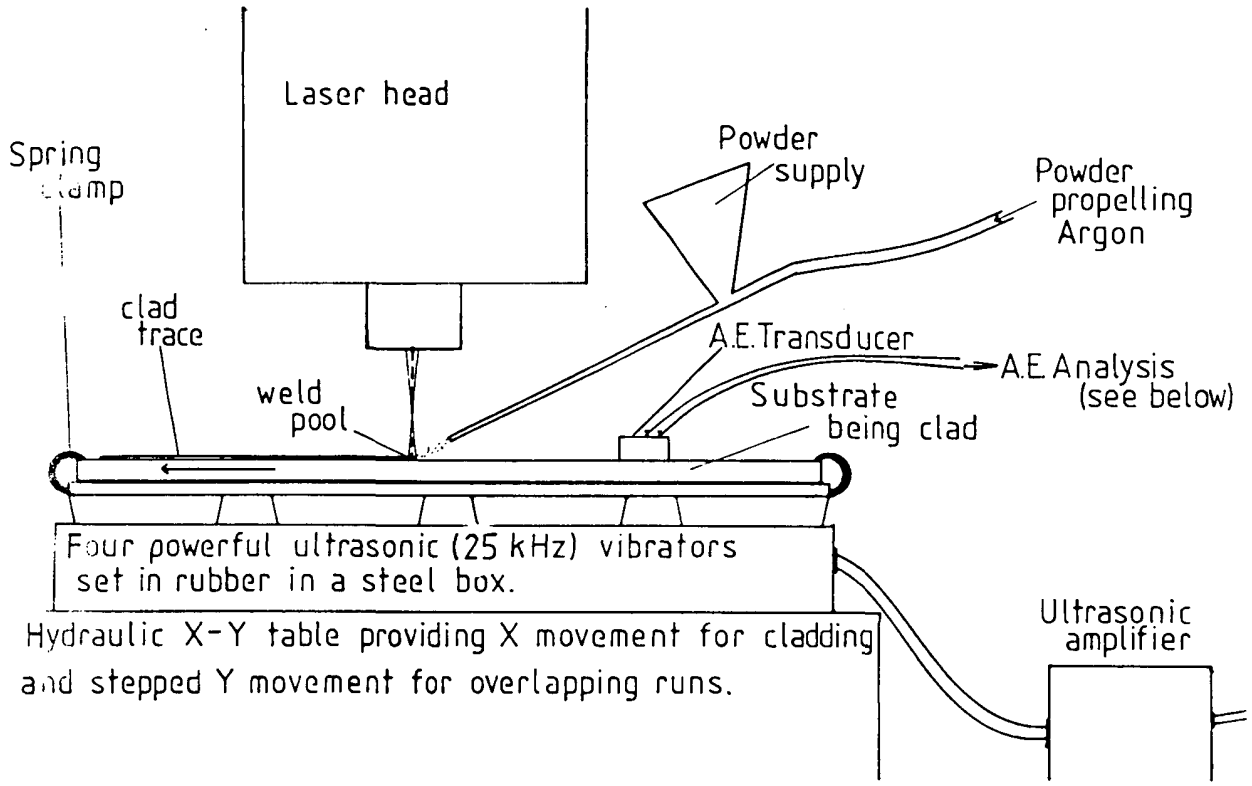

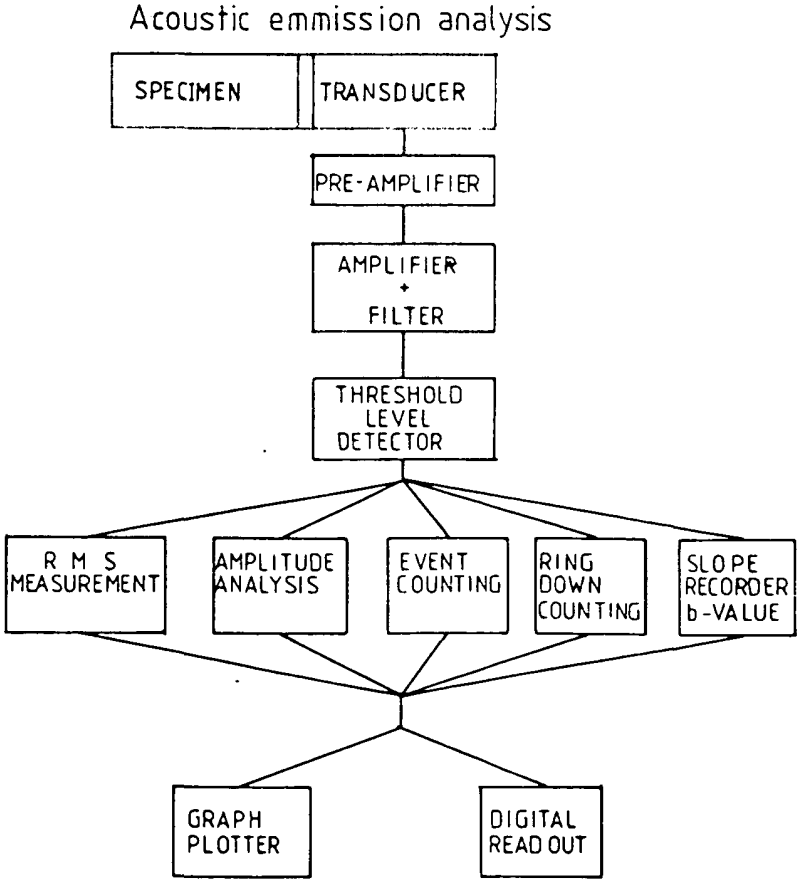

sonic vibration. The runs were of standard length and at the instant the cladding process was terminated the transducer feeding information to the Acoustic Emission equipment was turned on. Acoustic Emmission in itself a large and complex subject and so some words are needed here to explain the principles.

6.2. ACOUSTIC EMISSION

When a dynamic process such as cracking, dislocation motion or a martensitic transformation occurs in a material some of the released elastic strain energy can generate stress waves, ie vibration within the material. These stress waves propogate through the material and eventually reach the surface, so producing small, temporary, surface displacements. In extreme cases, for example, in the well known cracking of ice, the stress waves may be of high amplitude and low frequency and audible. However, in most cases, the stress waves are low amplitude and high frequency and sensitive transducers are required to detect and amplify the very small surface displacements. The transducers which are generally used are piezo-electric crytsals which convert a surface displacement into an electrical signal. The electrical signal is subsequently amplified and, as the crystals are left undamped, the signal resulting from a single surface displacement will be similar to that shown in Figure 6.2. In the idealised case the voltage V versus time T relationship for such a signal approximates to a decaying sinusoid(74)

$$V = V_p \left(\sin(2\pi ft)\right) \exp\left(-t/\tau\right) \qquad (1)$$

Where f is the resonant frequency of the transducer, τ is the decay time and V_p is the peak voltage. The problem is then one of quantifying the numerous signals which may be detected during a test. A number of signal analysis techniques are used but only

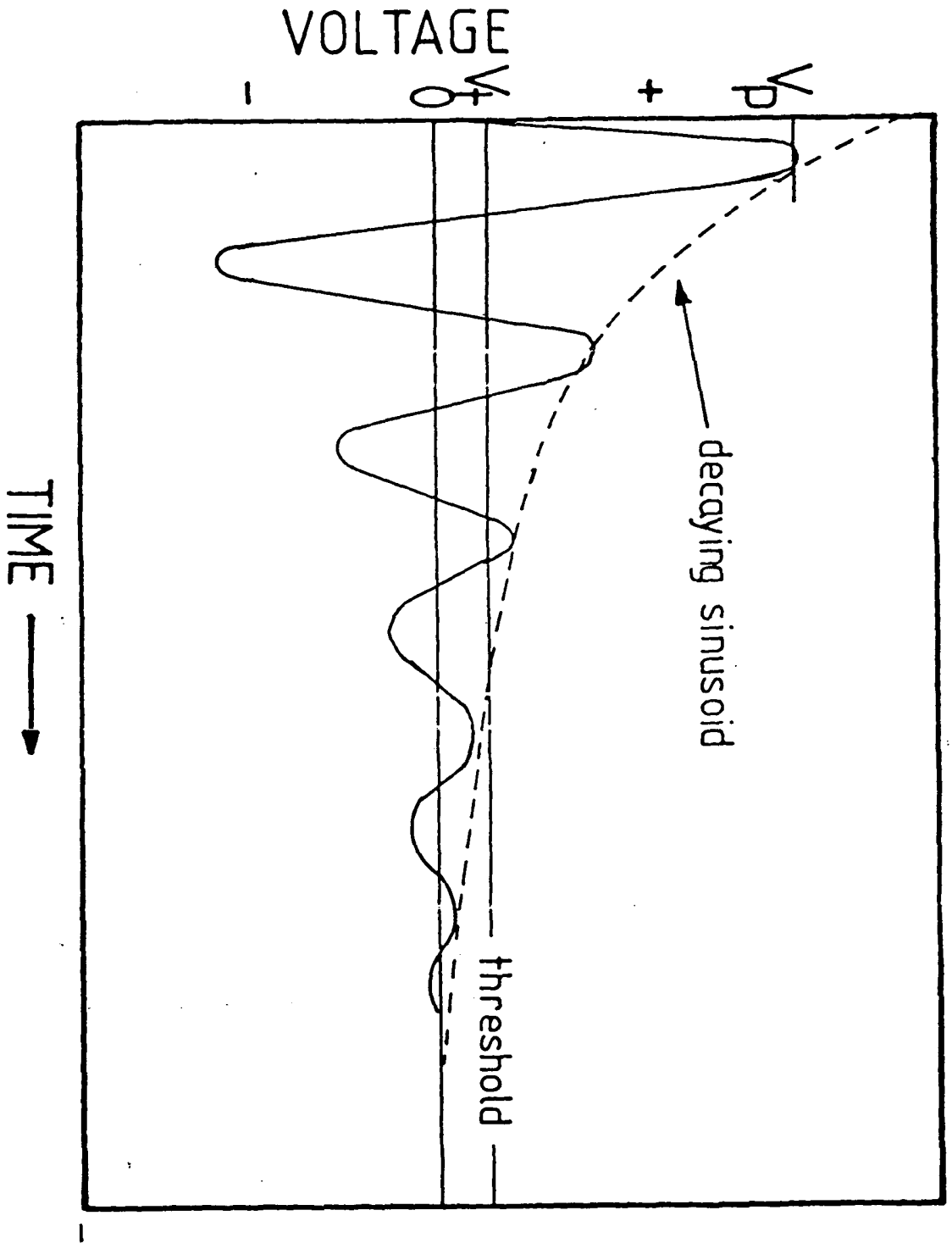

FIG.6.2. SIGNAL FROM A PIEZO-ELECTRIC TRANSDUCER. THIS SIGNAL WOULD CORRESPOND TO ONE EVENT COUNT AND THREE RING-DOWN COUNTS

those employed in the present study will be described.

The simplest method is to count the number of amplified pulses which exceed an arbitrary threshold voltage V. This is ring-down counting. The signal in Figure 6.2 would correspond to 3 ring-down counts. If the signal approximates to a decaying sinusoid equation it follows that the number of ring-down counts N_R depends on the peak voltage and is given by:

$$N_R = f\tau \ln \frac{V_p}{V_t} \qquad (2)$$

As the signal shown in Figure 6.2 was produced by a single surface displacement, which in turn may be assumed to be the consequence of a single source event inside the material, it is sometimes convenient to record a count of unity rather than the multiple count obtained by ring-down counting; this mode of analysis is known as event counting.

The peak voltage is a function of the acoustic emission energy E and for a resonant transducer with narrow band instrumentation, the appropriate relationship is:

$$E = gV_p^2 \qquad (3)$$

where g is a constant. The acoustic emission energy is related to the energy of the source event although the exact partition function is generally not known.

Because of the relationship between V_p and E, and as more ring-down counts are recorded the greater V_p (equation 2), the ratio of ring-down counts to event counts is a measure, albeit crude, of the acoustic emission energy. However, it is clear that more detailed and comprehensive information on the acoustic energy emitted over a period of time may be obtained from histograms

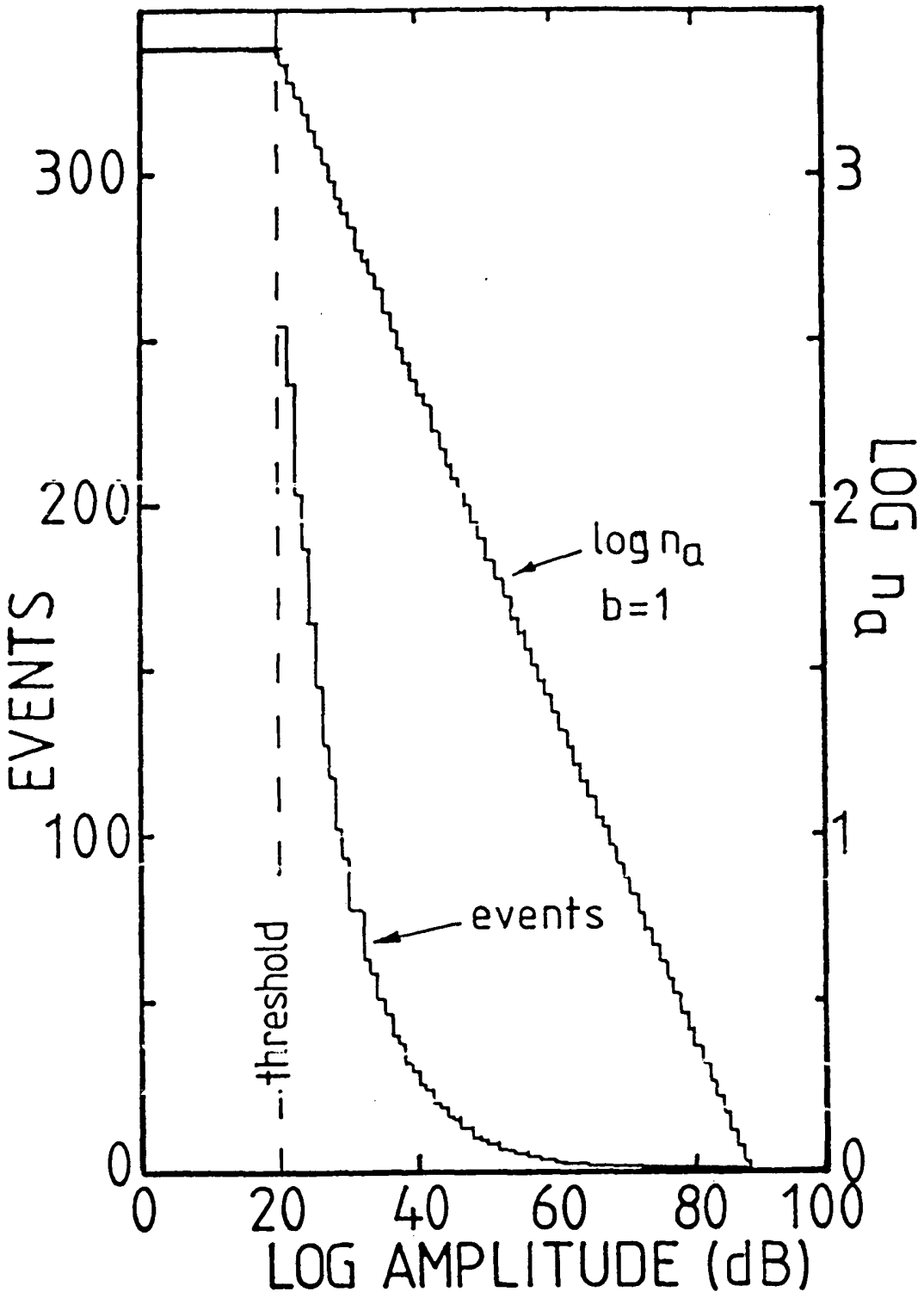

FIG.6.3 THE AMPLITUDE DISTRIBUTION AND THE CORRESPONDING LOG-LOG PLOT TO OBTAIN THE b-VALUE (SEE EQUATION 4). IN THIS PARTICULAR EXAMPLE b IS EQUAL TO UNITY

of the number of events against peak voltage (Figure 6.3). In practice, the amplitude of the emission is normally quoted in dB:

$$dB = 20 \log (V_p/V_r)$$

where V_r is a reference voltage. This is shown in Figure 6.3. If only one type of source event is occuring over the monitoring period the histogram or amplitude distribution is often found to obey a power law namely.

$$n_a = \left[\frac{V_a}{V_o}\right]^{-b} \qquad (4)$$

where n_a is the fraction of the emission population whose peak voltage exceeds V_a, V_o is the lowest detectable voltage and the exponent b is a constant which characterises the distribution. The amplitude distribution is replotted as log n_a versus log V_a and yields a single straight line of slope -b, in accordance with equation (4) (see Figure 6.3).

In certain situations, the source events are taking place so rapidly that the acoustic signals overlap and in extreme cases an almost continuous signal may result. Significant overlapping of signals can lead to errors with the previously described counting modes, particularly if the signals are of low energy (low V_p). In these circumstances the measurement of the root mean source voltage (RMS) is advisable provided the voltage is changing relatively slowly with time as the response time of most RMS meters is of the order of 100 ms. The RMS of a time dependent voltage $V_{(t)}$, over the time interval 0 to T, is given by:

$$RMS = \left[\frac{1}{\tau}\int_0^T V^2(t)dt\right]^{\frac{1}{2}}$$

The deposits were monitored for ten minutes after the cladding had been completed and were found to be acoustically active over this period. The rate of emission was such that counting techniques and not RMS voltage measurements were appropriate and examples of the output from the AE equipment will be shown in the results.

6.3 Results and discussion

6.3.1 The change in deposit quality brought about by VLC

Table 6.1 sets out representative results taken from this series of experiments. The variation between pairs defies graphical analysis but comparison of the vibrated samples with their vibrated counterparts invariably shows a reduction in porosity, cracking and acoustic emission if VLC is employed.

The complexity of the relationships between pairs is easily understood if all the effects contributing to stress and porosity within the deposit are considered. For example, reducing the table traverse speed would have the following effects:

A. More material will be melted, which will tend to generate more noise.

B. More heat will be put into the system reducing the cooling rates and thus reducing the stress on cooling and the noise associated with it.

C. The level of dilution will change altering the cooling stress levels.

D. The shape of the melt-substrate interface will change, altering the cooling rate (semi circular contact in cross section being a more effective quenchant for a constant melt volume than a straight linecontact with the same width).

E. The melt will have had more time to generate cooling noise prior

TABLE. 6.1 Typical results from V.L.C. experiments

SAMPLE	PROCESSING SPEED (MM SEC)	DEPOSIT CROSS SECTION (MM^2) (AV)	CLAD MATERIAL	WRT/SEC	NET	LENGTH OF FLAWS PER UNIT LENGTH DEPOSIT	HARDNESS (VPN)	CONTACT ANGLE (SUBSTRATE-DEPOSIT)	AR POWDER FLOW (SEE PAGE 156)
A	19.25	4.1	SF 40	35.75	1095	2.02	579	90	6
AV	19.25			53.5	648	0.64	633	86	6
B	31	1.3		10.15	171	.4	513	129	6
BV	31			5.8	120	.24	552	118	6
C	31	3.2		46.75	588	1.06	590	97	8
CV	31			44	448	.97	640	92	8
D	50	1.2		10.77	139	.2	565	102	8
DV	50			4.0	74	.18	589	93	8
E	25	1.5	S6	8.7	129	1.7	448	109	7
EV	25			6.2	105	.85	503	107	7
F	21	1.8		37.9	651	3.8	279	151	7
FV	21			21.55	367	2.1	268	140	7
G	32	1.0		14.9	314	1.5	210	160	7
GV	32			14.2	300	.8	307	145	7

Slight increase in hardness for vibrated samples. This is probably a result of increased cooling rates due to better wetting of the substrate.

Differences between pairs are due to varying levels of dilution with the substrate which softens the deposit.

to A.E monitoring - an important point when considering the fact that the majority of the noise recorded was emitted in the first few seconds of cooling.

Combining all these factors it is obvious that comparison between pairs is invalid at the moment although various interesting points can be raised if each pair is examined seperately and the group viewed as a whole.

Figure 6.4 shows the type of results generated by the A.E equipment, groups A and C referring to specimen A and graphs B and D referring to its vibrated twin AV. The unvibrated specimen "A" generated far more noise during the first ten minutes of cooling than its vibrated counterpart. (The values of NET total being 1059 and 648 respectively). It can be seen that most of the noise was generated in the first minute of cooling as might be expected (cracking or movement becomes more difficult as the clad trace cools and becomes stronger). The N_{RT} curve for specimen A increases disproportionally with the increase in N_{ET} showing a higher level of ring down counting or countable signals per event. This implies that the events counted had a high proportion of large amplitude signals, indicative of gross movement within the material (ie cracking).

Comparison of graphs C and D support this idea and reflect the higher level of signal in the 50 d B range. The correlation between the NET and NRT signals and the extent of imperfection in a deposit is very clear and figure 6.5 compares the signals with the extent of cracking and porosity which was measured by optical microscopy. LT is the proportion of length of fault per unit length of deposit. The macrographic analysis later in this chapter demonstrates the

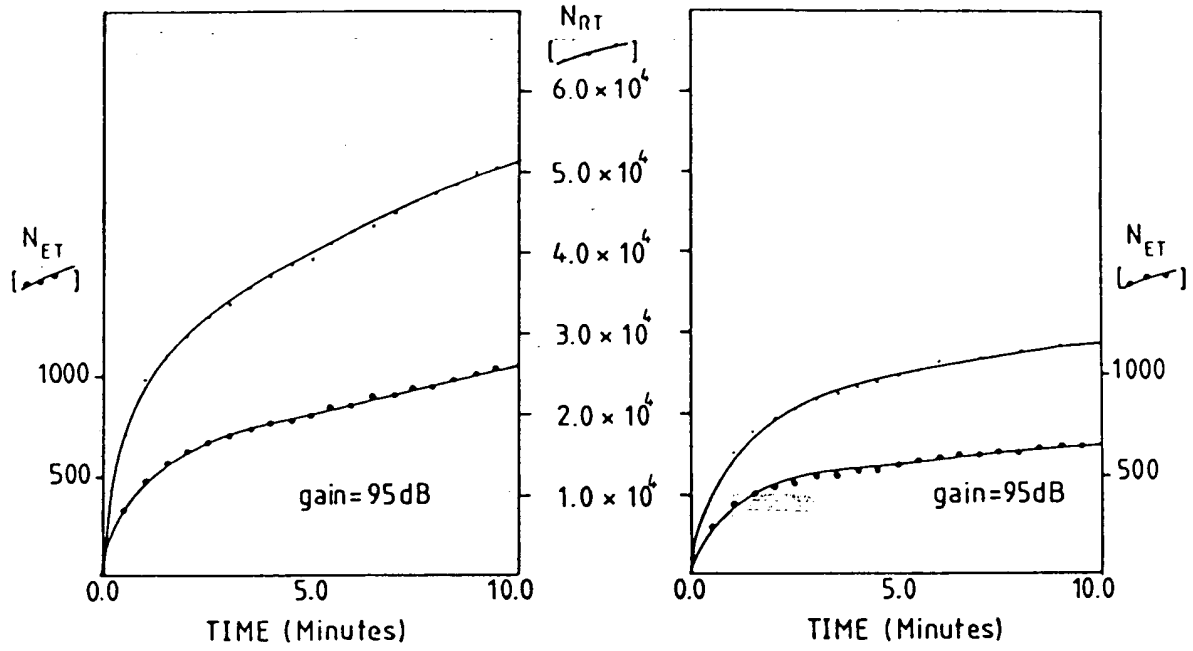

Graph A.
(Normal laser clad specimen)

Graph B.
(Vibro laser clad specimen)

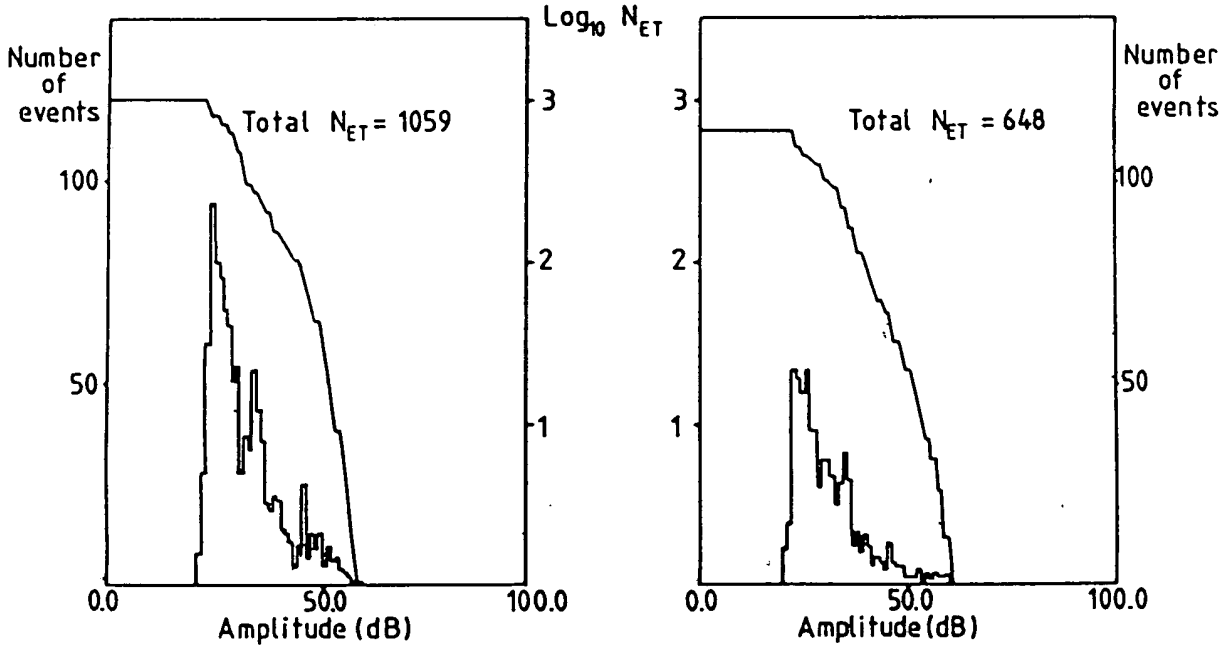

Graph C.
(Normally clad)

Graph D.
(Vibro laser clad)

FIG.6.4 - A sample of the results of the acoustic emission survey

FIGURE. 6.5 The relationship between the acoustic emmision of deposits and the flaw length per unit length. (L_T).

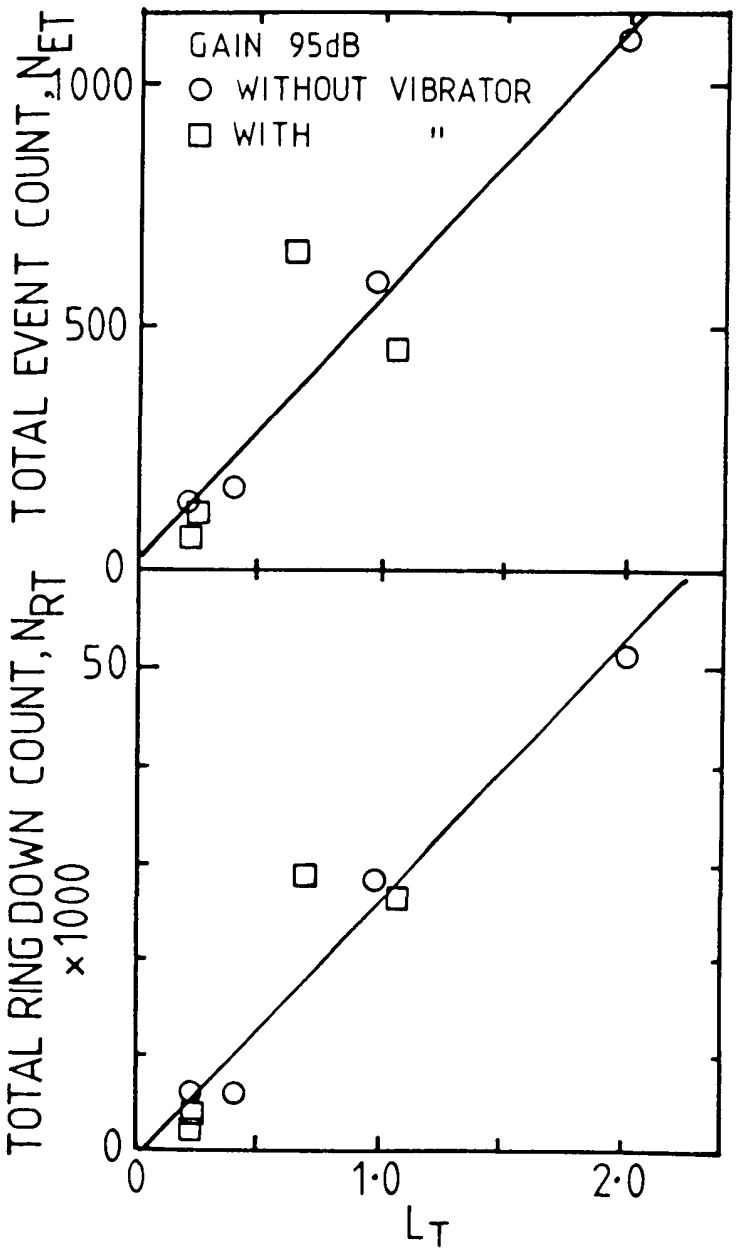

difference between pairs of runs and in one of the examples shown a macro crack can easily be seen. Macro and micro cracks were always more plentiful in the unvibrated sampels than in their vibrated counterparts.

6.3.2 POROSITY

Porosity within the deposits is created by a number of different mechanisms. The interfacial porosity noted in many cases (see photos - Figure 6.7) was a result of poor wetting of the cladding weld pool to the substrate. Micro and macro porosity within the deposit is a result of the trapping in the solid state of bubbles formed in the liquid state. This creation of bubbles can be brought about by the rejection of a dissolved gas from solution or the reaction of dissolved gas. Bubbles will form in liquid metals when the partial pressure just exceeds one atmosphere (79).

Rejection of dissolved gas:

The solubility of gasses in liquid metal is an order of magnitude higher than in solid metals. This solubility increases steadily from the melting point to a maximum just below the boiling point. (79). On cooling, the equilibrium gas content of a weld pool drops and a supersaturated solution will form eventually leading to bubble formation.

The magnitude of the change in solubility at the freezing point leads to high gas concentrations at the solidification front which forms a good bubble nucleation site. Gasses are absorbed at the weld pool surface by being dissociated into their monatomic form and then

being dissolved. Unusually high gas concentrations found in some cases can be the result of gas absorption at a high rate at the hottest part of the weld pool surface followed by convective stirring transporting the gas to cooler parts of the melt.

Other methods of gas injection into the weld pool include the reduction of the oxides on the particle surface and encorporation of the propellant gas (usually Argon) as the particles impinge upon the molten surface.

Reaction of dissolved gasses:

The nitrides and oxides of Nickel, Cobalt Iron are susceptable in weld pool to the following reactions:

$$MO + 2H = M + H_2O$$

$$MO + C = M + CO$$

$$2MN = 2M + N_2$$

The susceptability is attributable to the rather unstable nature of the oxides and nitrides of Ni, Co and Fe when compared with, for example Ti and Al. (See Figure 6.6).

A rather high level of metal oxide will be incorporated into the laser clad welds as a result of the high surface to volume ratio experienced by small particles. A further source of metal oxides will, of course, be the surface to the clad.

These reduction reactions lead to the creation of gas bubbles in the melt which consolidate to give rise to porosity.

Vibro laser cladding did not attempt to reduce the amount of porosity

FIGURE.6.6

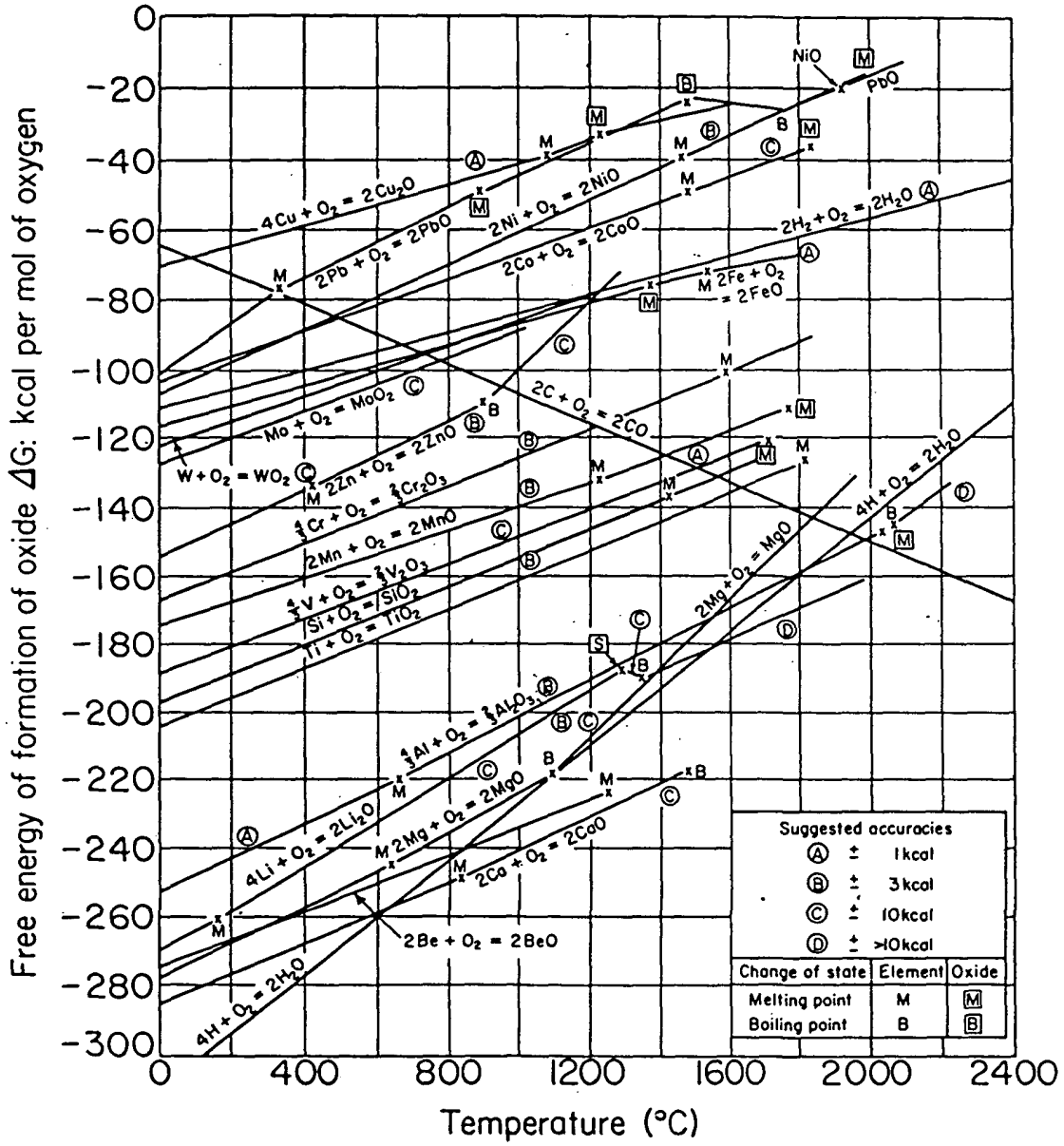

Free energy of formation of various oxides, based on the original diagram by Ellingham. (D. R. Milner, *Brit. Welding J.*, 1958, 5, 97)

evolved but to improve the mobility of the pores. This principle of mobility improvement was demonstrated by the following simple experiment:

Two small, identical containers were filled with a mixture of slow setting transparent resin with 100g of tungston powder in each. The mixture in each container was vigorously stirred and the resulting aerated metal suspension was allowed to solidify. One of the containers was allowed to solidify whilst resting on a stationery steel plate but its partner was supported by the ultrasonically vibrating substrate. This experiment was carried out four times giving almost identical results each time. Figure 6.7 shows the cross sections of such a pair of specimens. It can be clearly seen that the porosity of the vibrated sample has been reduced and the consolidation of the W powder improved. (The increase in density of the W consolidate was approximately 5% in each case).

Work carried out by Shukl et al (75) on the solidification of aluminium alloy castings showed that in many cases the level of porosity in the castings could be reduced by vibration. The work can be considered to be a macro sized version of the present work because the cooling rates were much lower the vibration was subsonic and the molten pools were much larger than the laser cladding weld pools.

The increase in mobility of the pores and W particles in the solidifying resin discussed earlier implies an increased fluidity of weld pool and this was substantiated by a decrease in interfacial porosity between the deposit and the substrate. This improved wetting of the substrate by the weld pool had a further beneficial effect, that of a decrease in the contact angle between the deposit and the substrate. Although

FIGURE 6 7.

The cross sections of solidified aerated suspensions of W powder in slow setting resin.

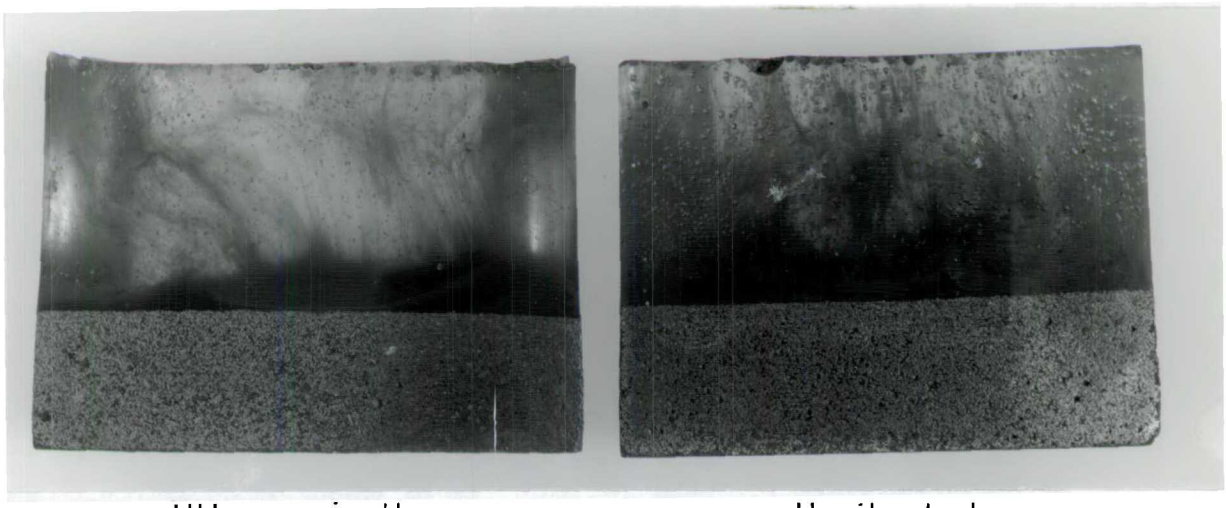

Ultrasonically vibrated during solidification

Unvibrated

the decreases were small (~5%) they were enough in some cases to eliminate the undercut which leads to inter run porosity when overlapping tracks are employed to cover an area of substrate. An example of this reduction in undercut is given in Figure 6.8. Acoustic emission monitoring of these multi run deposits was not practical because of the length of time needed to complete the cladding.

6.3.3 Cracking

The reduction in cracking on cooling of the vibrated specimens can be attributed to three factors:

A. The reduction in porosity (both micro and macro) meant a reduction in stress raisers and thus a reduction in crack initiation sites.

B. The disruption of the surface of the weld pool damped out any cyclic influences on the weld bead formation and produced a flatter deposit with less severe changes in cross section (see Figure 6.7)

C. The improved wetting led to a more even cooling rate distribution (interfacial pores act as insulators) and reduced undercut which is a stress raising influence.

Cracks in the deposits were invariably associated with stress raisers of the types mentioned above and so it is postulated that although vibrating stress relief does play a part in the improved quality of the welds, the reduction in cracking is strongly influenced by the increased tensile strength of the deposit as a result of the reduction in the population of stress raisers.

6.3.4 Macrographic examination

The following photographs illustrate various points raised in this discussion.

They are in the main, self explanatory and so rather than a written discussion, footnotes are appended to the photos were required.

FIGURE. 6.6.

MACRO ,1,
Sample A (× 13)

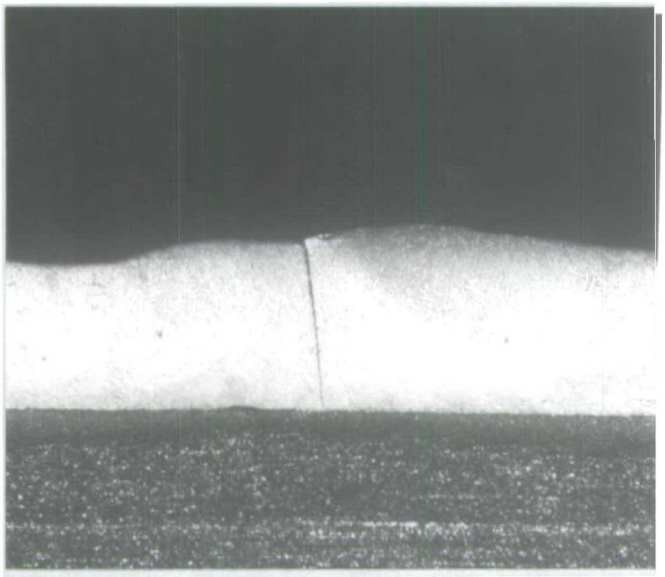

Note: interfacial porosity and crack associated with change in cross section

MACRO ,2,
Sample AV

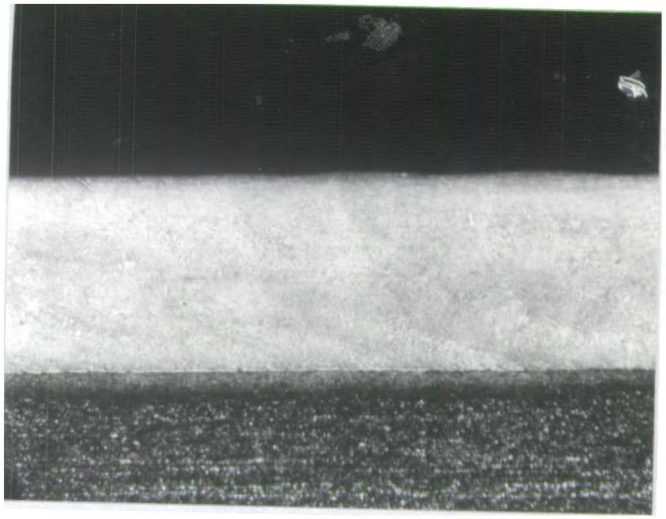

MACRO, 3,
Sample (× 10)

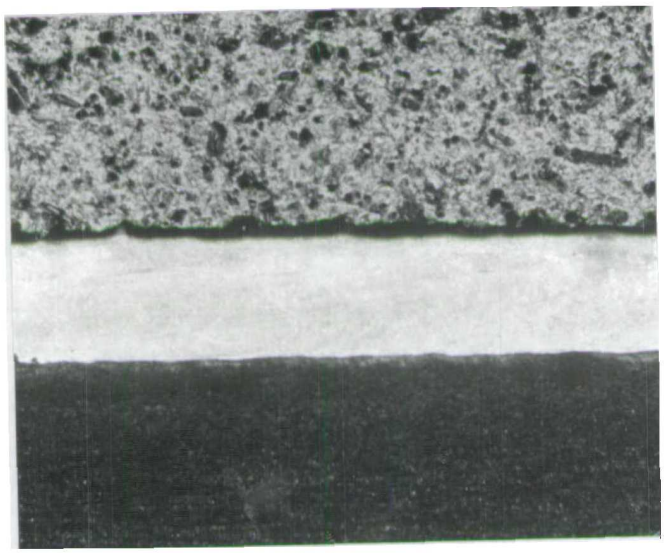

MACRO, 4,
Sample V

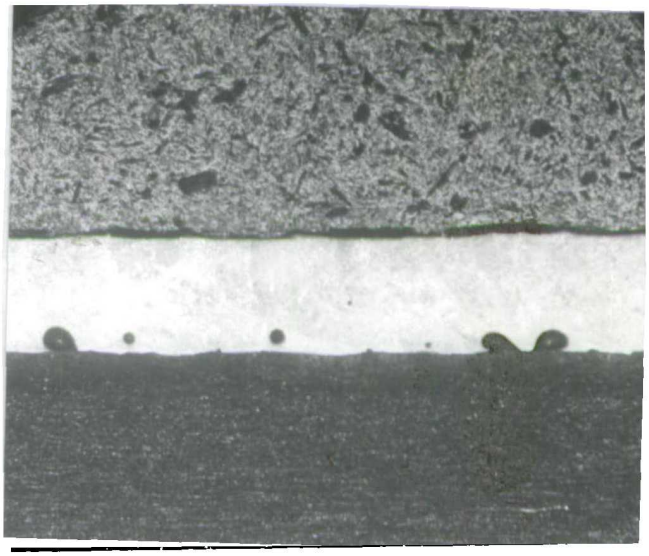

Note the improvement in wetting and reduction in porosity in the "V" (vibrated) sample.

MACRO, 5,
Transverse section through cladding made up of overlapping tracks. (×75)
(Unvibrated)

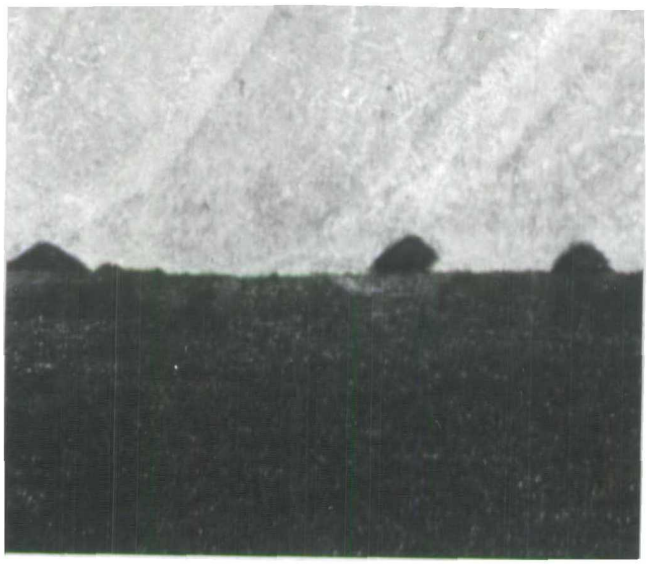

MACRO 6

Vibrated twin of macro 5 specimen.

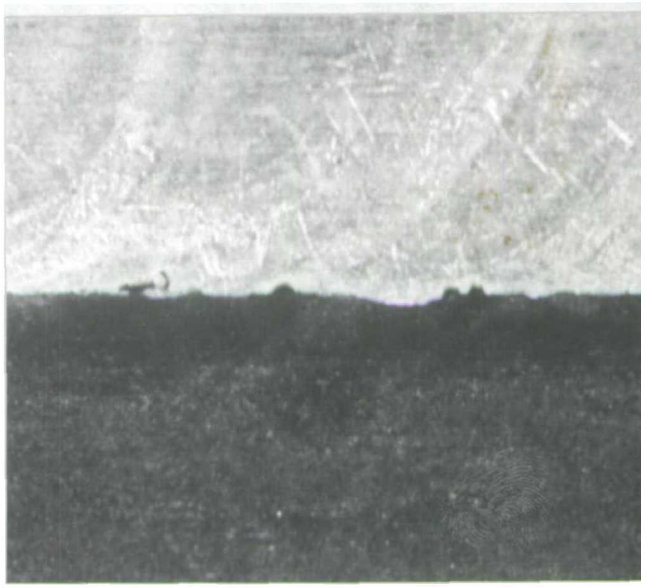

Note the reduction in inter run porosity due to improved wetting.

6.4 Conclusions

Although the investigation is only in the qualatitive stage as yet the following fundamental claims can be made:

A. VLC gives reduced porosity in laser clad deposits by increasing the pore mobility.

B. VLC increases the fluidity of the weld pool giving improved wetting characteristics and reducing undercut.

C. VLC reduces cracking in laser clad deposits by stress relief and reducing the population of stress raisers.

CHAPTER 7 CONCLUSIONS

7.1 General.

As this is the first thesis investigation of the subject of laser cladding the conclusions to be drawn from the theoretical and practical work are of a fundamental nature.

The major influences on deposit morphology and quality (dilution, porosity, cracking and wetting) have been identified and it is clear that laser cladding by the preplaced or blown on powder methods has a great deal to offer industry. Preplaced powder cladding suffers from the disadvantages of:

A. Powder positioning and retention of position prior to laser irradiation.

B. Difficulty in overlapping tracks to clad a continuous surface.

C. Difficulty in keeping the powder bed of constant depth and density.

The more easily automated process of blown on powder cladding suffers from dilution in many cases but this should become less of a problem when a satisfactory method of producing the correct powder mass/velocity flow into the weld pool (see Appendix B) is developed. Massive (.5mm + deep) deposits of clad material deposited on a substrate as a contin uous surface tend to crack and also thermally distort the substrate.

In the context of cladding for wear resistance, the results accrued from the practical experimentation imply that it should be possible (by either cladding method) to fill a prepared groove with cladding metal to provide a hard wearing surface to protect the substrate surface as a whole. Correct choice of groove cross section could lead to the production of almost flat, flush deposits requiring only a minimum of grinding, thereby saving machining time and cladding material.

7.2 Conclusions

7.2.1 Preplace Powder Cladding.

A. The use of a defocussed or focussed unrastered beam produces a deposit suffering from undercut when depositing thick (.5mm +) undilute deposits.

b. Use of a rastered beam results in wide clad tracks the morphology of which is governed by the X- section of the melt prior to substrate contact.

C. Weld cross sections are controlled by conflicting influences of surface tension and incident energy distribution.

D. There is up to an order of magnitude difference between the maximum and minimum parameters capable of giving an undilute clad deposit.

7.2.2 Blown on Powder Cladding

A. Deposit morphology is dependent on incident beam energy distribution, powder feed rates and speed of processing.

B. The amount of molten substrate incorporated into the weld pool increases with; increasing incident energy, decreasing processing speed, and decreasing powder input.

C. The incoming powder has a cooling rather than heating effect on the weld pool even after direct exposure to the beam.

D. When the ratio of partic les to transporting gas is 1 to 1,000+ (by volume) the beam can be assumed to be unattenuated on impingment with the weld pool.

7.2.3. Vibro Laser Cladding.

A. Ultrasonic vibration of the weld pool decreases the pore content on solidification by increasing the pore mobility.

B. Ultrasonic vibration of the weld pool decreased the number of cracks in the deposit.

C. Vibration of the weld pool increases the liquid substrate wetting by increasing the fluidity of the weld pool.

7.3 Suggestions for future work.

1. Continue the development of an adequate powder feed device (see appendix B).
2. Investigate cladding prepared grooves
3. Continue the development of an inert gas shroud (see appendix C)
4. By means of electron diffraction analyse the stress levels in laser clad deposits and the relaxation thereof by vibro laser cladding.
5. Compare sinusoidally rastered beams and their effect on preplaced powder cladding with line rastered beams (line rastering has no dwell time and is carried out by rotating a multifaceted mirror).

There is of course a great deal of work to be carried out in the field of laser cladding. These suggestions are of particular interest and should indicate more clearly the direction for future work.

APPENDIX : A.

Laser Surface Treatment

W.M. STEEN and J. POWELL

Department of Metallurgy and Materials Science, Imperial College, London SW7

Introduction

In recent years the laser has become an accepted and useful tool in the fields of welding and cutting. These spectacular uses of light radiation have not only kindled the imaginations of fiction writers but have gained the laser a position in the forefront of these fields where high quality cuts and welds are important. A 2kW laser can cut and weld material up to about 4mm thick at rates faster than those of most other processes with minimal heat affected zone sizes. In welding the laser is comparable to an electron beam without the inconvenience of having to work in a vacuum or of generating X-radiation. In cutting the laser is in a class of its own especially for profile cutting.

To suggest using such a device for merely heating a surface, possibly without making full use of its ability to be focussed to a very small spot size, seems to be a corruption of a refined, precise, energy source. It is the intention of this article to show that this view is far from the truth.

The laser beam has qualities which make it superior to other surface heaters, consider:

(a) The energy is pure, monochromatic, electromagnetic radiation. It is thus absorbed by most metals and many non metals within 2 or 3 atomic diameters. This very small interaction depth means that it is a true surface heater with effectively no depth of penetration (c.f. induction heating).
(b) The energy is chemically clean, unlike flame heaters.
(c) It is easily, quickly and precisely shaped without the use of coils and there is no heat spillage as with all jet heating systems (flame, plasma etc.).
(d) The beam is not deflected by magnetic fields, nor is it possible for a laser beam to generate X-rays.
(e) It does not need to work in a vacuum as in the case of electron beam heaters.

With all these advantages it is not surprising to find that the laser is used in various ways to treat surfaces, that there is considerable research interest in this subject and that already, after only a decade, there are numerous industrial installations in production, for example; General Motors [1], Rolls Royce[2], Fiat[3] and Saginaw[4].

The ways in which a laser is currently being used in the surface treatment of metals are listed below:

Technique	Principal Use	Useful reference
Transformation hardening	Surface harden certain alloys e.g. steel	5
Surface homogenisation	Refine surface microstructure to avoid corrosion, wear, etc.	6
Laser glazing	Production of ultrafine microstructures or glasses. Metallurgical advantages not fully understood as yet.	7
Cladding	Different surface material. Surface welded onto substrate.	8
Surface alloying	Similar to cladding but with greater mixing with the substrate.	9

Each of these will now be discussed in turn.

Transformation Hardening

At certain specific temperatures between ambient temperature and the melting point of a metal, the three dimensional arrangement of the atoms undergoes a change or transformation. These transformations result in a new crystal structure which, if cooled slowly, will degenerate back to the old pre-transformation structure because the new structure is metastable below the transformation temperature. If a transformed, heated, structure is cooled rapidly enough, the atoms will not have time to move back to their previous low temperature stable position or configurations and a metastable phase will be formed. The formation and retention of these phases can be aided by the locking effect of an alloying element which inhibits movement in the lattice (e.g. carbon in steel). These

metastable phases are intrinsically highly stressed and are therefore usually hard and brittle. A common example of such a phase is martensite, this distorted tetragonal matrix is formed by rapidly cooling the face centered cubic lattice of steel heated into the austenitic region. These hard, corrosion resistant phases are very useful as surface layers on many metallic engineering components and the laser's unique ability to produce such layers without heating up the whole body of material and risking distortion on cooling is the subject of this present discussion.

The cooling rates necessary for the production of, for example, martensite from steel heated into the austenitic region can be predicted with the help of a T.T.T. (Time Temperature Transformation) diagram (Figure 1). A line

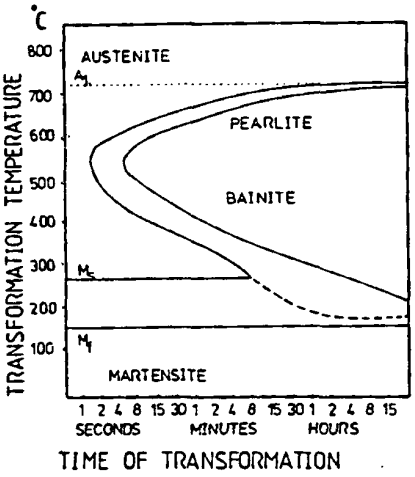

Fig. 1. The T.T.T. diagram for a 0.8% steel. This graph shows that a cooling rate of 10^4 °C. per second is well inside the range for transformation directly to martensite.

showing a typical laser heat treatment cooling rate (10^4 °C/sec) would be well to the left of the 'nose' of the curve, indicating transformation directly to martensite. The cooling rates possible after laser heating can be calculated with the aid of a mathematical model. The results of a finite difference solution[10] for a moving gaussian source are shown in Figure 2. The wide range of control over the cooling rates obtainable with the help of a laser means that localised control of the microstructure is relatively easy to achieve.

Figure 3 shows a good, typical example of the localisation possible. Producing single hard tracks on a

Laser power = 2kW. Beam radius = 3.0mm. Reflectivity = 0.4
Traverse speed = 42.5mm/s.
1. = Depth of 0.0mm.
2. = Depth of 0.22mm.
3 = Depth of 0.60mm.
4. = Depth of 1.69mm.

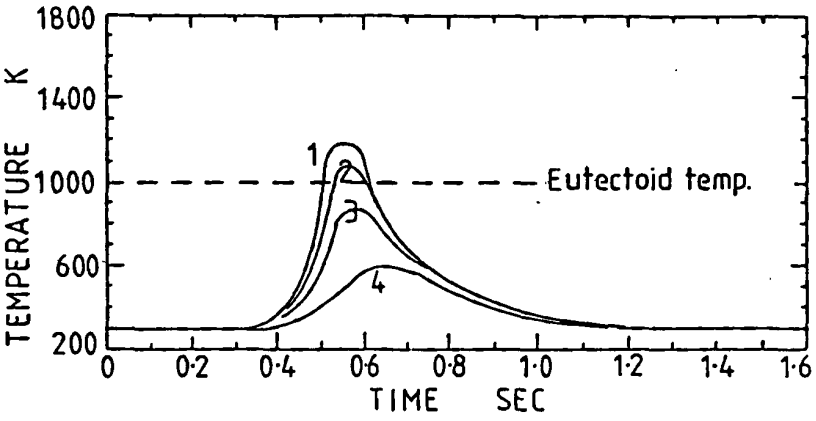

Fig. 2. The thermal cycle during laser heating of EN8. steel (Finite difference solution for a moving Gaussian source).

bearing surface has become a common feature in the field of laser heat treatment. The financial advantages of only covering a small area instead of a large area are obvious but one unexpected advantage is found in the fact that the worn depressions on each side of the hard ridge form good reservoirs for lubricants and also good "dumps" for wear particles produced in service.

There are three principal operating variables in laser processing: laser power, beam spot size on the surface of the workpiece and traverse speed. The numerous other process variables are mainly properties of the work-

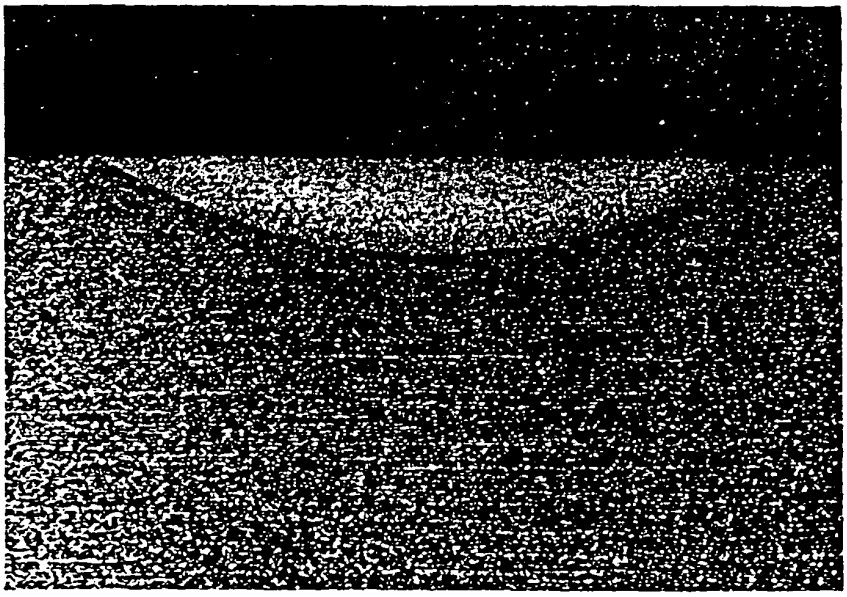

Fig. 3. Macrograph showing a section through a hardened trace (Magnification is x 18) Etchant is 2% nital, Beam power = 2kW, Beam diameter = 5.3mm, Speed of traverse = 8mm/s.

piece i.e. surface relectivity, thermal conductivity, melting point, boiling point etc.

Considering the three principal variables it is possible to plot laser processing structure diagrams as in Figure 4. For specific cases, e.g. the transformation hardening of En8 Steel,

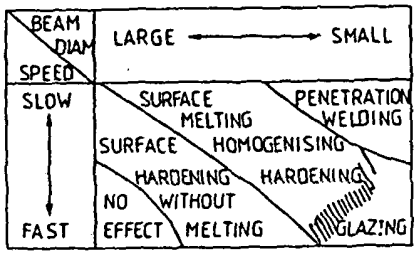

Fig. 4. Laser processing structure diagram for a constant power.

it is possible to draw operating curves based on experimental results as shown in Figure 5. The maximum depth of the hardened zone possible when using a laser to surface harden a metal is limited by the onset of surface melting of that metal. The operating 'window' (i.e. the variability of the three major variables) becomes progressively smaller as the required depth of hardening increases (Figure 6). Maximum depth of hardening has, of course, a strong dependence on the physical properties of the metal being treated. Depths of 0.5mm can be easily achieved in carbon steels with a maximum depth of approximately 1.0mm. Cast iron can be transformation hardened using a laser but, as might be expected considering the very fast thermal cycles involved,

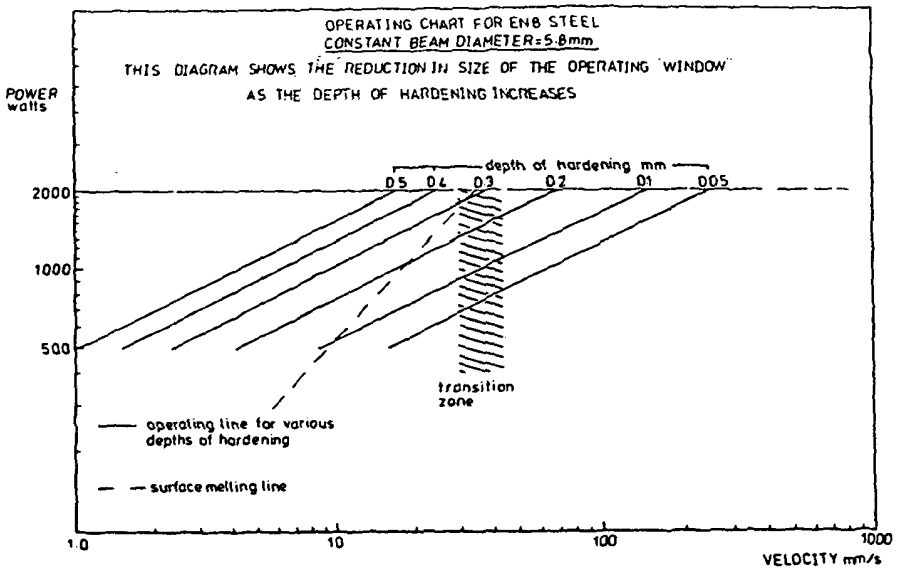

Fig. 6. Operating chart for EN8 steel constant beam diameter = 5.8mm.

there is insufficient time available for the graphite flakes or nodules to diffuse into solution and they remain in almost their original state in the new, hardened material. A typical laser transformation hardening thermal cycle is shown in Figure 2 and a transformation hardened cast iron is shown in Figure 7.

In summary, the laser is capable of transformation hardening the specific areas of a component which require it. No longer is it necessary to heat the whole article and subsequently quench it, a process which inevitably leads to a certain loss of product through thermal distortion. The process is quick, clean and could be carried out on the same lathe on which the component is produced if a laser beam is available as another tool of the lathe.

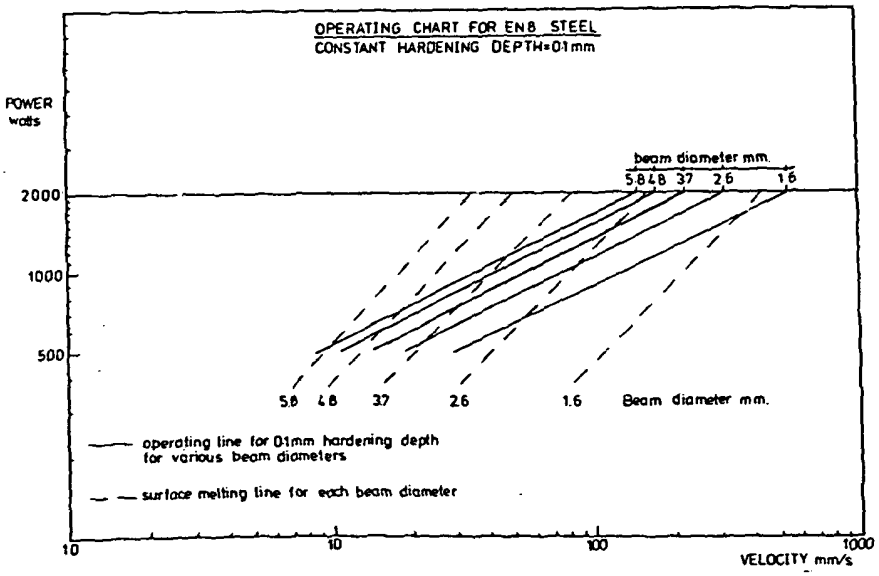

Fig. 5. Operating chart for EN8 steel constant hardening depth = 0.1mm.

Surface annealing of semiconductors

The mechanism of ion implantation of semiconductors is a highly energetic one which results in a great deal of damage to the substrate. This damage is due to the rapid injection of the deposit ions and the defects caused are normally removed by furnace annealing at between 900 and 1100°C in times of from thirty minutes to an hour. Very good results have been observed in a flood of recent papers (e.g. see American Institute of Physics Conference 50) on the subject of laser annealing. Two different types of annealing have been identified, they are (a) accelerated solid state epitaxial growth at elevated temperatures, (b) liquid phase epitaxial growth (the growth, of course, being from the underlying undamaged material).

The time scale for both these processes is in the millisecond or microsecond range. Although there is a general agreement between the workers in the field as regards the excellent quality of the finished product, there is widespread disagreement about the alteration in the deposit concentration profile produced by laser annealing.

Laser Glazing

Laser glazing is an extension of the transformation hardening technique wherein a thin surface layer of the metal being treated is allowed to melt.

Fig. 7. Micrograph of a laser transformation hardened cast iron.

This technique usually utilises the focussed beam travelling swiftly ($\sim$ 1ms^{-1}) over the surface of the workpiece. The molten trace thus produced self quenches on the substrate at rates in the order of 10^6 ^{o}C s^{-1} or higher. This extremely high quench rate will almost always result in the production of a metastable structure in the surface layer.

In some alloys (Pd/Cu/Si eutectic) metallic glass layers have been reported with a fully non crystalline (amorphous) structure[7]. The production of these layers is obviated in the case of most alloys because of the propensity of the solidifying melt to grow crystals epitaxially from the underlying unmelted zone. This epitaxial growth effect is clearly seen in the 'glazed' trace on a Nimonic alloy (Figure 8). Some alloys have quench structures built up of submicron dendrites (Figure 9). As cooling rates are increased the solidified trace becomes more homogeneous i.e. phase separation is prevented or minimised and the dendritic structure of the alloy is either eliminated or refined. The effects of these changes in the structure of the surface are usually:

1. improved corrosion resistance.
2. improved wear resistance
3. increased hardness

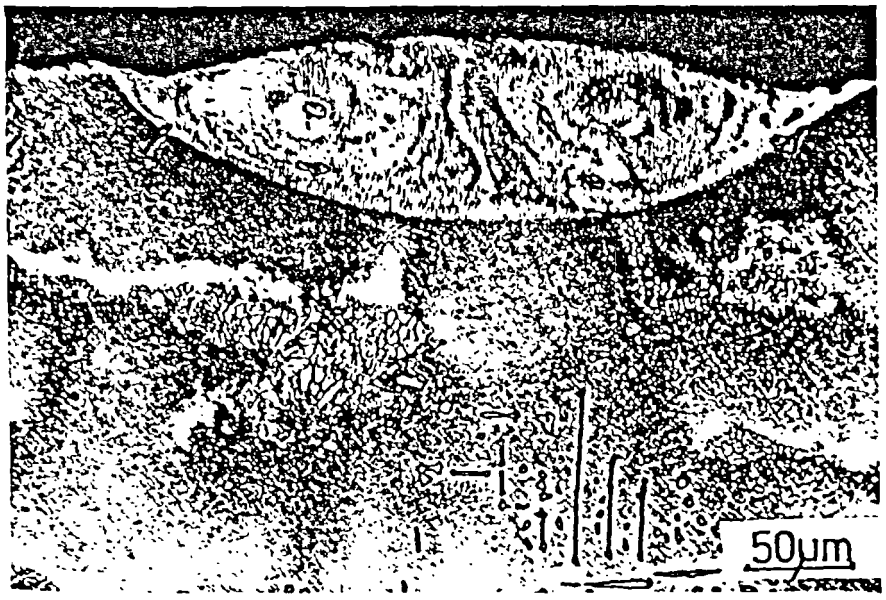

Fig. 8. A laser 'glazed' trace on a nimonic alloy.

It has become apparent that this process is capable of generating new structures in metals which have either not been studied before, or have never before been available in a useful form firmly adhering to a mechanically sound substrate. The laser has thus opened up a new area of metallurgy for nearly every metal.

The flow structure of these traces and those produced during surface homogenisation has been studied by Copley et al[11] in a series of elegant experiments investigating the convective flow in a moving melt pool in a camphene-tricyclene transparent alloy.

Figure 10 from some work at Imperial College[12] shows that a different flow pattern might develop at higher powers and speeds in that flow around both sides of the laser hotspot appears to take place. The convection currents in the molten pool also leave a slightly rippled surface on the solidified trace.

It may appear that glazing a very narrow trace of approximately 1.0mm width rules out this process as one applicable to the treatment of large areas but at 1.0m s^{-1} the covering rate is 1000 mm^2 s^{-1}. Allowing for an 80% overlap to increase homogeneity the area covering rate becomes 200 mm^2 s^{-1} which is .72 m^2 hr^{-1}.

Surface Homogenisation

This process is very similar to laser glazing but is usually slower and requiring more energy input i.e. P/VD must increase (P = laser power, V = velocity of workpiece relative to the laser beam, D = beam diameter at the workpiece surface). The aim of this process is to melt a reasonably deep layer, dissolve all phases and quench rapidly so that they do not separate out again. The example of Anthony and Cline[6] is of a sensitised stainless steel which is susceptible to intergranular corrosion. After laser homogenisation, Strauss tests indicated a complete resistance to intergranular corrosion. Mechanical testing at strains less than 15% showed that laser surface melting had indefinitely extended specimen life in a stress corrosion environment. At strains above 15% the laser scanned layer was breached by cracks. Mechanical tests also showed that the laser surface melted layer had a yield strength which was approximately ten times that of

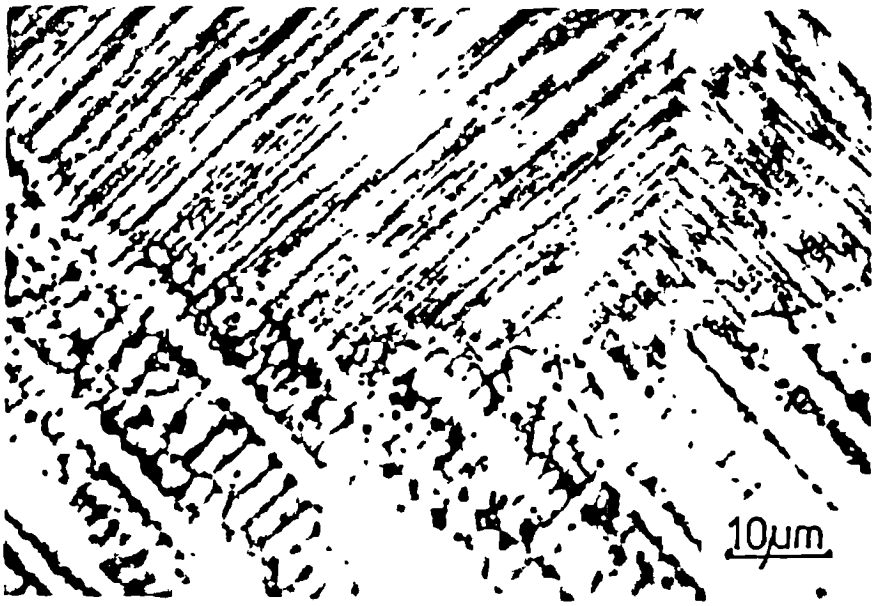

Fig. 9 Micrograph showing submicron dendrites in a 'glazed' Nimonic alloy.

the rest of the sample. These results were shown to be compatible with the observed appearance of martensite in the homogenised surface layer.

Cladding

The laser can be used to surface weld a different material to the surface of a substrate by one of several methods e g.

1) powder fusion by preplaced powder or blown powder[8]
2) vapour deposition[13]

The experimental arrangement for cladding by preplaced powder is shown in Figure 11.

The advantages of using a laser are:

a) very low dilution
b) chemical cleanliness
c) high degree of localisation
d) homogenised fine microstructure in the clad layer

Some graphs describing the relationship between the operating parameters of the process and the resultant clad traces are shown in Figures 12 and 13.

The size and shape of the cross section of the clad track is a function of the surface tension of the molten material, the power and diameter of the incident laser beam, the speed of travel of the substrate relative to the laser beam, the powder feed rate, and in some cases the surface to volume ratio of the grains of powder. Typical maximum track depths without undercut are approximately 2mm. Undercut can lead to interrun inclusions and pores between overlapping runs (Figure 14). Adherence of clad tracks to substrates is usually very good as would be expected from a process

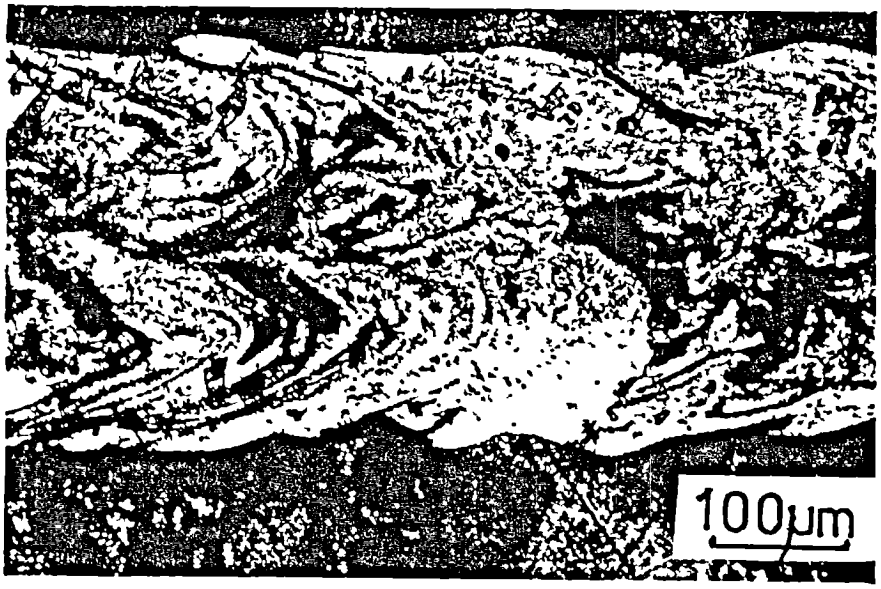

Fig. 10 Macrograph showing flow patterns on the surface of a glazed trace.

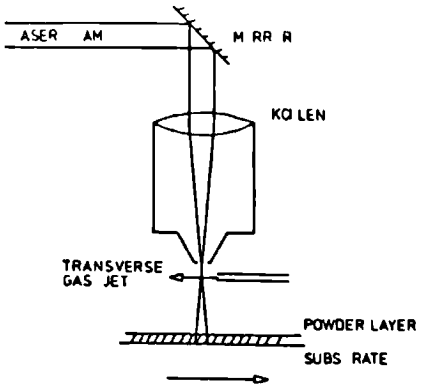

Fig. 11 Arrangement of apparatus for cladding by the preplaced powder technique.

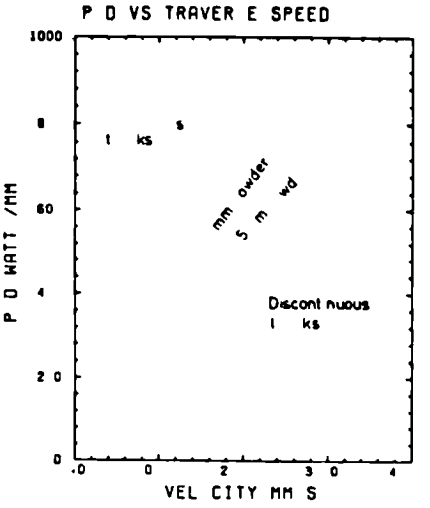

Fig. 12. Operating parameters of cladding.

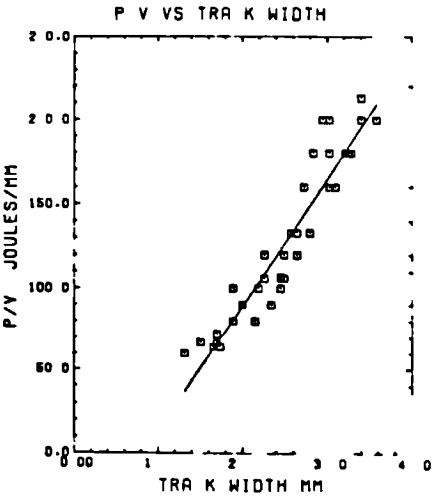

Fig. 13. Operating parameters of cladding.

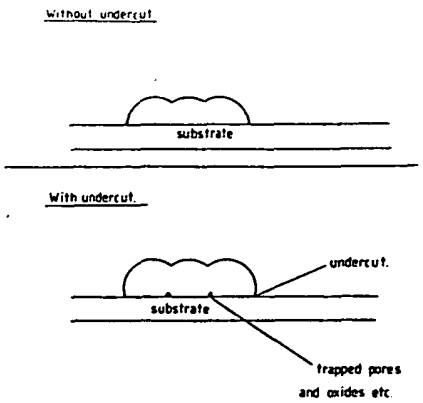

Fig. 14. The effect of undercut on overlapping runs.

which welds the two together but this is not the case when bonding non metals to metals. Dilution varies depending upon how much substrate is allowed to melt but can be confined to a 100μm thick region at the interface as shown in Figure 15 more recent work has reduced this figure to less than 25μm. Figure 16 illustrates the dependence of dilution on energy per unit area. Heat treating the substrate can be advantageous in cases where the residual thermal stresses in the clad

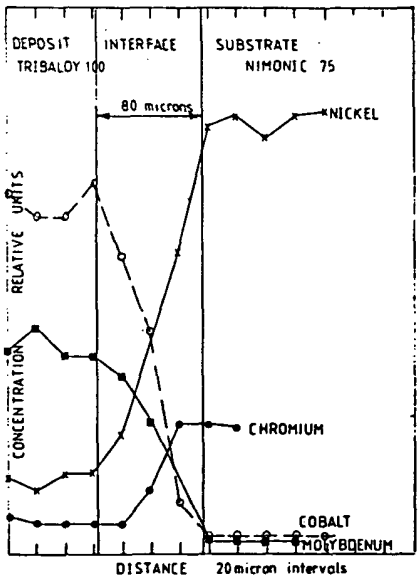

Fig. 15. Electron probe micro analysis of the substrate - deposit interface.

track cause cracking. In the same way as laser transformation hardening can be general over a surface or confined to small areas where it is most needed, laser cladding a hard, corrosion resistant alloy onto a less serviceable substrate can be used over the whole surface of a component or, more probably, only in restricted areas saving time and material.

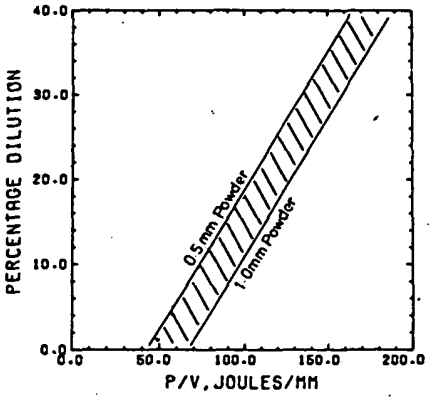

Fig. 16. Dilution vs P/V for 2.0mm beam diameter.

Surface Alloying

Surface alloying with a laser is a similar process to cladding except that the specific energy of the process is higher, allowing more substrate to melt. It is usually advisable to operate in the region where the laser evaporates a small keyhole into the substrate as the resulting turbulence allows better mixing of the alloying layer.

Boronising has been successfully carried out by this method as has the fusing of electroplated layers of a number of metals. It is also possible to achieve very shallow alloyed layers by surface melting in a reactive gas such as ammonia.

Conclusion

Surface treatment with a laser has become one of the principal areas of laser material processing research. It has opened up a new metallurgical field in rapidly quenched surface layers, and new engineering possibilities in the cladding or transformation hardening of only the areas if a component that need it. The cost savings the processes offer have in some cases paid for the laser installation in under a year.

References

1. G.H. Harth, W.C. Leslie, V.G. Gregson and B.A. Saunders, Laser Heat Treating of Steels. Journal of Metals, April 1976.
2. Rolls Royce. private communication.
3. A.V. La Rocca, H. Walther and P.C. Cappelli, Development activities for the industrial application of high power lasers to metal working. International seminar on laser processing of engineering materials June 30th, 1977.
4. Charles Wick Laser Hardening Manufacturing Eng. June 1976.
5. C. Courtney and W.M. Steen, The Surface heat treatment of En8 steel using a 2kW CW CO_2 Laser. Metals Technology, December 1979 pp 456-62
6. T.R. Anthony and H.E. Cline, The normalisation of sensitised stainless steel by laser surface melting J. Appl. Phys. Vol. 49, No. 3, March 1978.
7. B.H. Kear, E.M. Breinan, L.E. Greenwald and C.M. Banas, Laser Glazing - a new process for production and control of rapidly chilled metallurgical microstructures. S.M.E. Technical paper M.R. 76-867, 1976.
8. W.M. Steen and C.G.H. Courtney, Hard facing of Nimonic 75 using a 2kW Continuous Wave CO_2 laser. Metals Technology 7, (6) 232-237, June 1980.
9. F.D. Seaman and D.S. Gnanamutha, Using the industrial laser to surface harden and alloy Met. Prog. 108 (3) 67-74 August 1975.
10. J. Mazumder and W.M. Steen, Heat transfer model for C.W. Laser material processing. J. Appl. Phys. 51 (2) February 1980.
11. S.M. Copley, D. Beck, O. Esquivel, M. Bass, Laser Melt quenching and alloying American Institute of Physics Conf. 50 pp 161-171.
12. K. Lipscombe, W.M. Steen and D.R.F. West, The laser glazing of a cast Nickel based super alloy and an alpha plus beta Titanium alloy.
13. W.M. Steen, Surface coating using a laser. Advances in surface coating technology – International Conference Paper 3. February, 1978.

APPENDIX B. THE DEVELOPMENT OF A POWDER FEEDING SYSTEM FOR BLOWN ON POWDER CLADDING

A.B.1. THE NEED FOR A POWDER FEED SYSTEM

The cladding investigated in chapters five and six of this thesis was carried out using spherodised powder in a gravity fed powder spray gun. Spherodised powder is very expensive and this of course reduces commercial interest in the process but it is the dependance of the powder mass flow rate on the gas flow rate which is the major drawback to the use of this type of gun. If large (ie grams per second) powder mass flows are to be realised to reduce dilution and speed up the cladding process (see Chapter 5) these must be accompanied by moderate gas flow rates just capable of transporting the powder. The very high gas flow rate needed to supply powder at a rate of for example, one gram per second, into the laser interaction area with the gravity fed gun results in the weld pool being spattered all over the surface of the substrate. Another drawback to the use of this kind of gun is the difficulty of calibration and reproducability as mentioned in Chapter 5.

As the work progressed it became more and more obvious that the design of a powder feed device capable of feeding a variable moderate gas flow with a variable powder mass flow (of non spherodised powder) was an important consideration and several devices were designed and investigated.

AB.2. ARCHIMEDES SCREW DEVICES

Figure AB.1. shows the first type of powder feed device designed and built. The archimedes screw provides a positive drive to the powder feed and was found to be capable of delivering sufficient powder but with the following major drawbacks:-

a. the mass flow rate was cyclic, the cycle corresponding to the cycle of the screw. This led to the deposition of a clad trace of cyclicly varying cross section.

b. if the archimedes screw was a good fit in its surrounding tube the small hard powder particles tended to jam the movement by coming between the two: If, on the other hand the clearance was increased to prevent this effect the powder would flow down the sides sporadically.

c. in some cases the propellant gas would exit the system by bubbling through the archimedes screw and hopper powder.

These serious defects were combated by sealing the top of the powder hopper and by changing the axis of drive of the archimedes screw. Re-designing the feeder to make the screw drive the powder in the horizontal direction and, as a further refinement, horizontally and upwards at an angle of 45° with a sealed hopper, helped to solve some of these problems but even the best design which used a double entry screw driving upwards and sideways from a sealed hopper suffered from jamming and cyclic effects due to the leading edges of the screws.

The design effort was now concentrated upon the main problem,

FIGURE. A.B.1. Archimedes screw powder feeder.

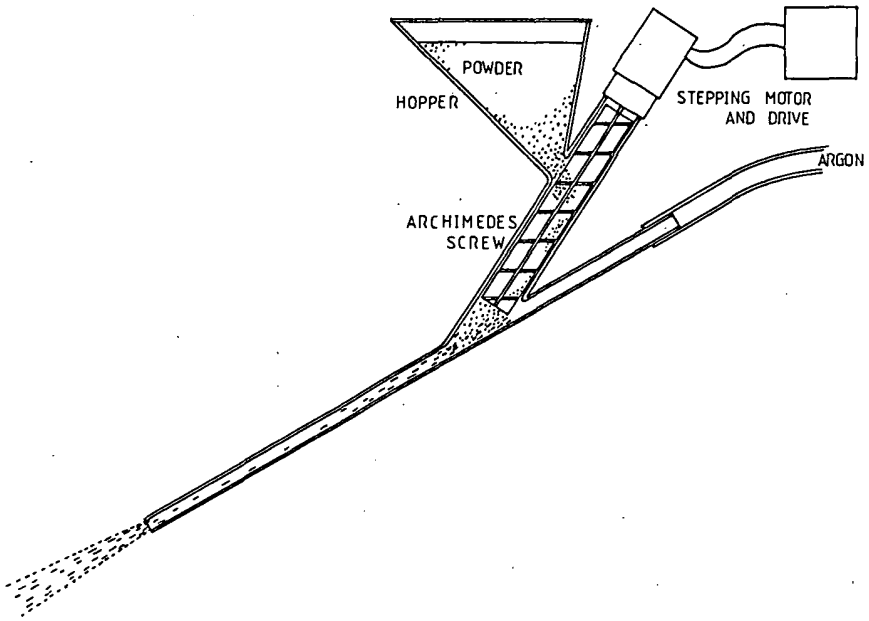

FIGURE.2. The principle of operation of a conveyor belt assisted powder spaying gun.

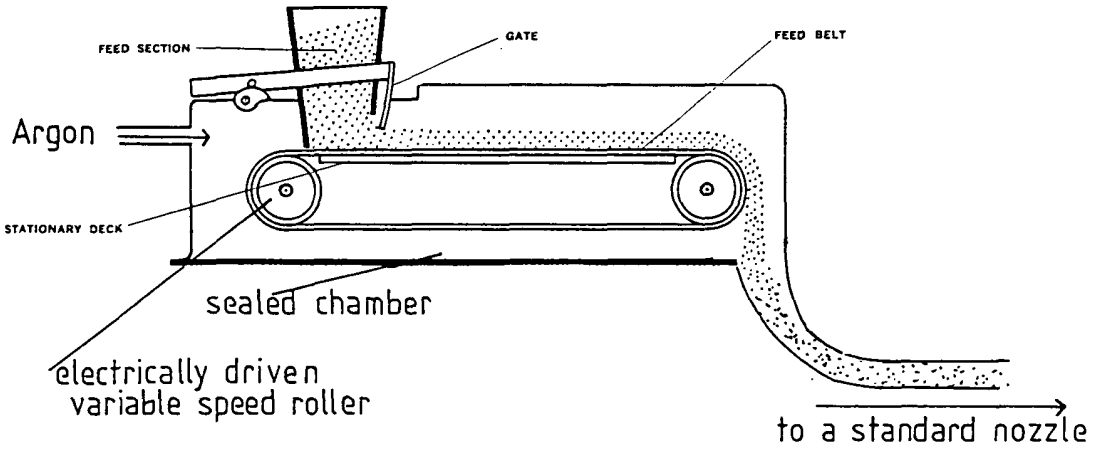

the achievement of a linear powder flow.

A.3 CONVEYOR BELT DEVICE

A powder feed device which utilised a conveyor belt to transport the powder to the output is shown in figure 2. The powder is dragged from the bottom of the hopper through an orifice of controllable dimensions and is thus metered. The belt then transports the powder to the outlet where it falls into the gas stream to then be propelled towards the weld pool. The difficulty with this device lay in three areas : a. If the metering gate was almost closed to allow the small mass flow rates needed (1 →5g / sec), the powder experienced a great deal of friction on leaving the hopper and the powder feed was sporadic. b. The whole device had to be gas sealed and thus involved tightly fitting components and sealed bearings. The high torque, low rotation speeds needed for the correct mass flow were difficult to obtain without the electric motor juddering. c. The powder tended to inbed itself into the belt and also interferred with all moving parts causing changes in the operating conditions of the device.

This powder feed device was found to be best suited to larger mass flow rates than were needed for this application. At higher mass flow rates (eg 25g/sec plus) the drawbacks mentioned lose their importance and flow can be said to be steady.

A. 4 ROTATING BASE DEVICE

After investigation of other principles of metering low mass

flows (eg bleeding off a proportion of a fluidised bed of powder) to no avail, the design work returned to the problem of attaining a linear flow from a cyclic motion. The most promising design is shown in figure A.8.3 which utilises a scoop on the rotating base of a powder column. The rotating portion of the base is small in comparison to the whole base to prevent jamming of the movement and to increase the friction on the powder column so that the scoop moves through it not with it. The smallest orifice the powder moves through is the entrance to the scoop. This prevents powder build up and clogging. The scooped off powder is directed to the centre of rotation to eliminate any cyclic effects and then dropped down the hollow drive shaft into the gas flow. The principle is simple and although an imperfect prototype gave better results than has been attained before, a correctly engineered device was not built during the course of this work because of time considerations. Future work should include the development of this design as one of the present limitations on laser cladding has nothing to do with either lasers or materials but is simply the lack of a metering device capable of feeding an independantly controlled gas supply with a metal powder at rates of between 0 to 10 grams per second.

Fig. A.B.3.

Rotating base powder feeder

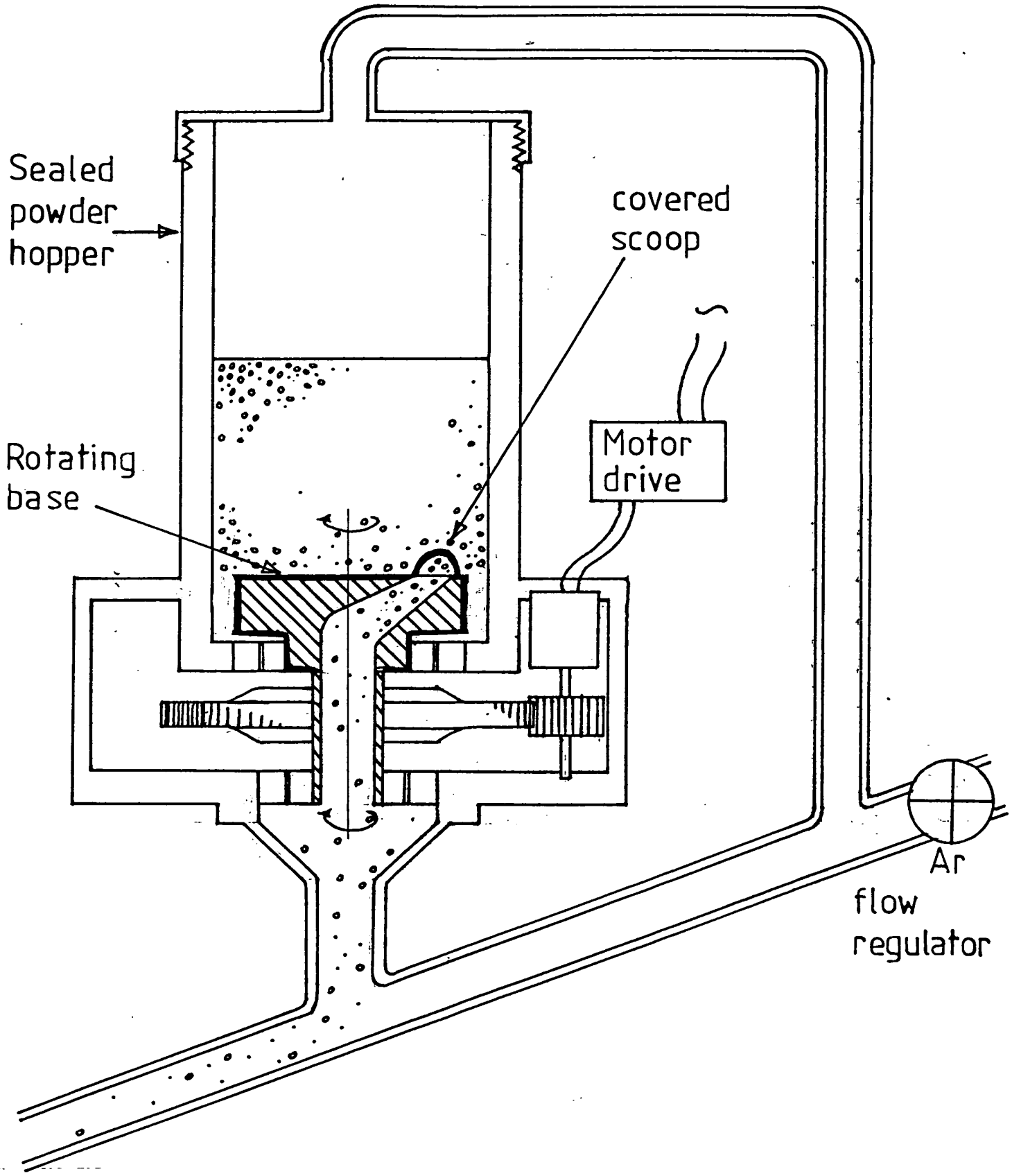

APPENDIX.C.

The Development of a non contact gas shield

One great difficulty encountered when attempting to laser clad any substrate with any blown on powder is adequate gas shielding of the weld pool and the cooling metal. The conventional method of gas shielding when using a laser ie. blowing Argon onto the heated area through the same nozzle as the laser beam comes through is impractical in the case of blown powder cladding because the Argon blows the incoming powder out of the area of the weld pool. A new approach to this problem has been under investigation at Imperial College. The idea is to trap a slowly replenished volume of Argon above the general area of the weld pool and cooling metal using a wall of moving compressed air. The principle of operation of the shroud is shown in Figure A.1. Compressed air blown into the apparatus shown leaves the bottom annular orifice as a divering, hollow, conical jet of compressed air. This cone rebounds off the substrate travelling away from the central axis (see diagram). If the area inside the cone is first purged and then fed with a slow bleed of Argon, that area will be free of oxygen and the Ar will sweep away fumes through the base of the cone where the turbulent cone of compressed air meets the substrate. This invention works on the principle that a gas will only move from an area of high pressure to an area of low pressure. As the pressure anywhere within the moving hollow cone of compressed air is well above one atmosphere, the outside air will not cross the cone and nor will the Argon inside except to relieve itself of the slight extra pressure exerted by the cleansing Argon 'bleed' which will result in a slow flow outwards at the air cone/substrate interface. The cladding and some of the cooling can take place within this cone of Argon without the turbulence at the edges of the cone of

FIGURE.C.1.The principles of operation of the new cladding gas shield.

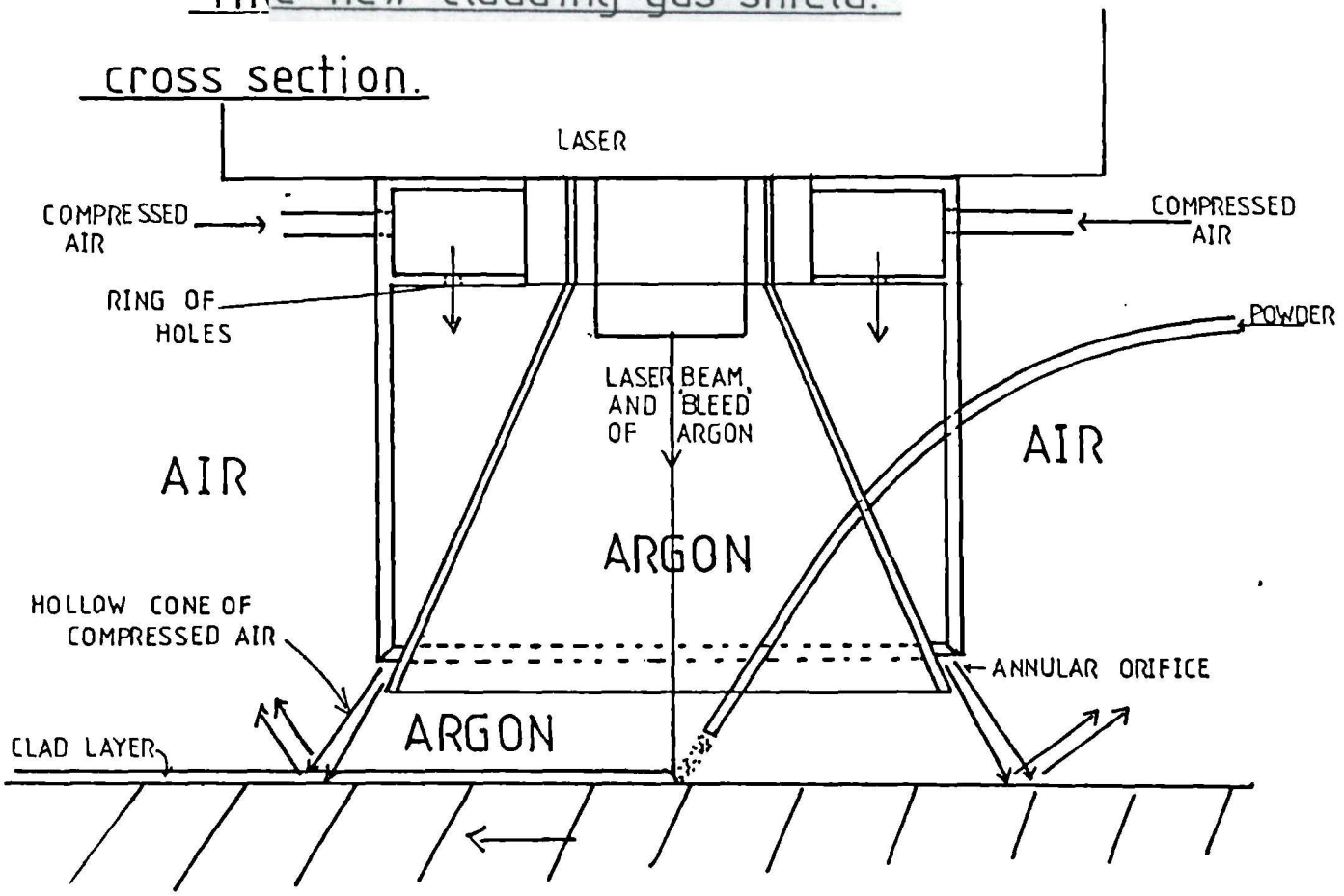

Cross section of a powder feed tube which could be pushed through the hollow cone of compressed air without disturbing its seal.

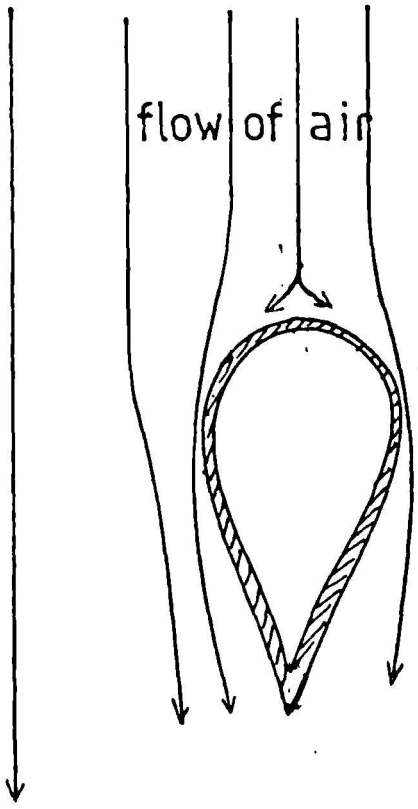

compressed air affecting the almost tranquil inner cone of Argon. The powder can be fed into the weld pool by passing the tube carrying it through the metal body of the apparatus as shown or by shaping a special cross-section tube (see diagram) to pierce the compressed air cone without causing too much turbulence as a circular cross-section tube would certainly do. This compressed air cone has been shown to produce a tranquil internal cone in the following way: a model was built from the basic design in Figure 9 (2½" high 3½" diameter) and the central hole which would normally be blocked by the laser nozzle was blocked. Chalk dust was spread out on a table and the apparatus was rested on the table and then lifted approximately half an inch from its surface. The compressed air was turned on and the chalk dust outside a circle of a slightly bigger diameter than that of the apparatus was blown away. The dust within this circle remained absolutely stationery and stayed so as the cone device was raised to a height of two inches from the table. Above this height the area under the cone device began to experience turbulence due to the divergence of the hollow compressed air cone along its cross-section. This apparatus, when incorporated into the machinery used to laser clad, could be of great value.

The principle of operation of the shroud device was examined By building a cross-section model out of perspex and using ink and water to represent the Argon and Air flows respectively. It was shown that for a rather large range of flow combinations the central portion of the cross-section could be kept pure but break down could occur under some conditions eg water (Ar) flow being too low. Figure C.2 shows photographs of the flow experienced

within this fluid flow model.

Work is still being carried out to make this gas shroud device capable of producing non oxidised processed material.

A fully adjustable version of the device has been built but trials have led to dissapointing results so far, the problems being associated with turbulence. Although the device does not yet work well if it is used as originally intended,very good results have been found if Ar is passed through both gas transport systems. The central portion of the atmosphere remains pure and tranquil and even the surface melting of titanium has been carried out with no oxidation.

FIGURE C.2. Fluid flow model

stable condition

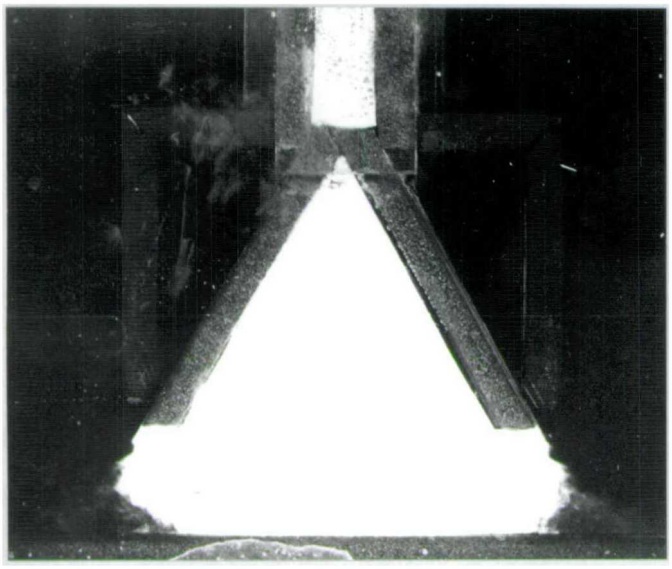

instability due to insufficient water (Argon) bleed.

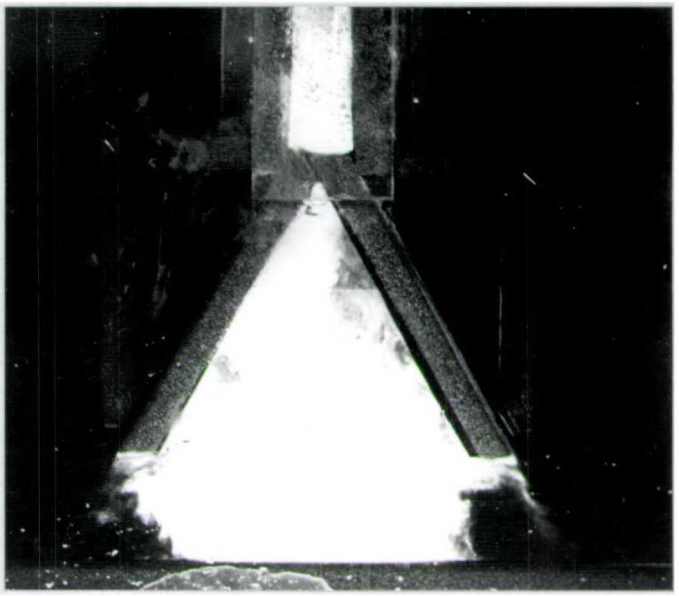

APPENDIX . D.

Computer program for pre placed powder cladding (see chapter 4)

```
      REAL MPT
      DIMENSION T(50)
      COMMON/C1/DENS,COND,SPHT
      COMMON/C2/MPT,BPT,VM,VB,QMEL,QVAP
      COMMON/C3/CM,CV,CS
      COMMON/C4/CPM,CPV,CPS
      DATA MPT,VM,QMEL/1812.,5.,269000./
      DATA BPT,VB,QVAP/3000.,5.,9000000./
      DATA SPHT,COND,DENS/438.,80.0,7860./
      DATA NP,N/11,21/
      EMF=E(MPT+VM)
C
C  SET POWER DENSITY
C
      WRITE(6,1)
    1 FORMAT(/,4X,"ENTER BEAM POWER,RADIUS,AND TRAVERSE SPEED")
      READ(5,*)PT,RB,U
C
      P=PT/(3.14159*RB**2)
      WRITE(6,4)P
    4 FORMAT(4X,"POWER DENSITY=",G12.5," W/M**2")
      TLIMIT=RB/U
      WRITE(6,5)TLIMIT
    5 FORMAT(/,4X,"INTER-ACTION T=",F7.5,"S")
C
C    INITIALISE ARRAY
C
      DO 100 I=1,N+1
  100 T(I)=300.
      WRITE(6,2)
    2 FORMAT(/,4X,"ENTER POWDER LAYER THICKNESS")
      READ(5,*)D
      DX=D/FLOAT(NP-1)
      WRITE(6,6)DX
    6 FORMAT(4X,"ELEMENT SPACING=",F8.6,"M")
      A=COND/(SPHT*DENS)
      DELTIME=(DX**2)/(10.*A)
      SIGMA=5.67E-08
      T3004=300.**4
C
C  SET CONSTANTS TO BE USED
C
      CPS=DELTIME/(SPHT*DENS*DX)
      CPM=DELTIME/( (SPHT + QMEL/VM)*DENS*DX)
      CPV=DELTIME/( (SPHT + QVAP/VB)*DENS*DX)
      WRITE(6,*)"CPS=",CPS,"CPM=",CPM,"CPV=",CPV
C
      CS=COND*DELTIME/(DENS*SPHT*DX**2)
      CM=COND*DELTIME/(DENS* (SPHT +QMEL/VM)*DX**2)
      CV=COND*DELTIME/(DENS* (SPHT +QVAP/VB)*DX**2)
      WRITE(6,*)"CS=",CS,"CM=",CM,"CV=",CV
C-----------------------------------------------------------------
C
C        CARRY OUT INITIAL MELT-THROUG OF POWDER LAYER
C
C-----------------------------------------------------------------
      IPRINT=10
      ICOUNT=0
      TIME=0.0
C
      WHILE( T(NP).LT.MPT .AND. TIME.LT.TLIMIT)DO
C
      ICOUNT=ICOUNT+1
      TIME=TIME+DELTIME
      DO 200 I=1,NP,2
        IF(I.EQ.1)THEN
        TA=T(I)
          IF(T(I).LT.MPT)THEN
          TB=TA + CP(TA)*P-SIGMA*CP(TA)*(TA**4-T3004)
          T(I)=TCOR(TB,TA)
          ELSE
          TB=TA + CP(TA)*P-SIGMA*CP(TA)*(TA**4-T3004) + (T(I+1)-TA)*C(TA)
          T(I)=TCOR(TB,TA)
          ENDIF
        ELSEIF(T(I-1).GT.MPT .AND. T(I+1).LT.MPT)THEN
        TA=T(I)
        TB=TA + C(TA)*(T(I-1)-TA)
        T(I)=TCOR(TB,TA)
        ELSEIF(T(I-1).GT.MPT .AND. T(I+1).GT.MPT)THEN
        TA=T(I)
        TB=TA + C(TA)*(T(I-1)+T(I+1)-2.*TA)
        T(I)=TCOR(TB,TA)
        ENDIF
  200 CONTINUE
```

```
00 DO 300 I=2,NP-1,2
50    IF(T(I-1).GT.MPT .AND. T(I+1).LT.MPT)THEN
00    TA=T(I)
50    TB=TA + C(TA)*(T(I-1)-TA)
00    T(I)=TCOR(TB,TA)
50    ELSEIF(T(I-1).GT.MPT .AND. T(I+1).GT.MPT)THEN
00    TA=T(I)
50    TB=TA + C(TA)*(T(I-1)+T(I+1)-2.*TA)
00    T(I)=TCOR(TB,TA)
50    ENDIF
00 300 CONTINUE
50C
00 IF(ICOUNT.EQ.IPRINT)THEN
50 IPRINT=IPRINT+40
00 WRITE(6,3)TIME,(T(I),I=1,NP)
50 3 FORMAT(1X,"TIME=",F6.4,":",15F5.0)
00 I=1
50 WHILE(I.LT.NP+1 .AND. T(I).GT.MPT+VM)DO
00 I=I+1
50 ENDWHILE
50 IF(I.EQ.1)THEN
00 WRITE(6,15)
50 15 FORMAT(2X,"NO MELTING PRESENT")
00 ELSE
02 I=I-1
50  EE=E(T(I))
00 EP=E(T(I+1))
50 X= FLOAT(I)*DX
00 XM=X-DX*(EP-EMF)/(EP-EE)
50 WRITE(6,16)XM*1000.
00 16 FORMAT(2X,"MELT INTERFACE DEPTH=",F6.3,"MM")
50 ENDIF
00 ENDIF
50C
00 ENDWHILE
50 WRITE(6,3)TIME,(T(I),I=1,NP)
00 WRITE(6,9)
50 9 FORMAT(/,10X,"POWDER MELT SECTION COMPLETE",/)
00 IPRINT=ICOUNT+1
50C
00C-------------------------------------------------------------------
50C
00C      EVALUATE MELT BACK VS TIME , IF TIME < TLIMIT
50C
00C-------------------------------------------------------------------
50C
00 IF(TIME.LT.TLIMIT)THEN
50C
00 WHILE(TIME.LT.TLIMIT)DO
50 ICOUNT=ICOUNT+1
00 TIME=TIME+DELTIME
50C
00 DO 210 I=1,N,2
50    IF(I.EQ.1)THEN
00    TA=T(I)
50    TB=TA +P*CP(TA) + C(TA)*(T(I+1)-TA)
00    T(I)=TCOR(TB,TA)
50    ELSE
00    TA=T(I)
50    TB=TA + C(TA)*(T(I-1)+T(I+1)-2.*TA)
00    T(I)=TCOR(TB,TA)
50    ENDIF
00 210 CONTINUE
50C
00 DO 310 I=2,N-1,2
50    TA=T(I)
00    TB=TA + C(TA)*(T(I-1)+T(I+1)-2.*TA)
50    T(I)=TCOR(TB,TA)
00 310 CONTINUE
50C
00 IF(ICOUNT.EQ.IPRINT)THEN
50 IPRINT=IPRINT+40
00 WRITE(6,11)TIME,(T(I),I=1,N)
00 11 FORMAT(1X,"TIME=",F6.4,":",21F5.0)
50 I=1
00 WHILE(I.LT.N+1 .AND. T(I).GT.MPT+VM)DO
50 I=I+1
00 ENDWHILE
 0 IF(I.EQ.1)THEN
 0 WRITE(6,15)
 0 ELSE
 2 I=I-1
 0  EE=E(T(I))
 0 EP=E(T(I+1))
```

```
      XM=X-DX*(EP-EMF)/(EP-EE)
      WRITE(6,16)XM*1000.
      ENDIF
      ENDIF
C
      ENDWHILE
      ENDIF
      STOP
      END
C
C     FUNCTION FOR LATENT HEAT VARIATION IN SURFACE INPUT
C
      FUNCTION CP(T)
      COMMON/C2/MPT,BPT,VM,VB,QMEL,QVAP
      COMMON/C4/CPM,CPV,CPS
      IF(T.GT.BPT .AND. T.LT.BPT+VB)THEN
         CP=CPV
      ELSEIF(T.GT.MPT. AND. T.LT.MPT+VM)THEN
         CP=CPM
      ELSE
         CP=CPS
      ENDIF
      RETURN
      END
C
C    FUNCTION FOR GENERAL ALOOWANCE FOR LATENT HEAT
C
      FUNCTION C(T)
      COMMON/C2/MPT,BPT,VM,VB,QMEL,QVAP
      COMMON/C3/CM,CV,CS
      IF(T.GT.MPT .AND. T.LT.MPT+VM)THEN
         C=CM
      ELSEIF(T.GT.BPT .AND. T.LT.BPT+VB)THEN
         C=CV
      ELSE
         C=CS
      ENDIF
      RETURN
      END
C
C  LATENT HEAT TEMPERATURE TRAPS
C
      FUNCTION TCOR(TB,TA)
      COMMON/C2/MPT,BPT,VM,VB,QMEL,QVAP
      COMMON/C3/CM,CV,CS
      IF(TB.GT.BPT .AND. TA.LT.BPT)THEN
        TCOR =BPT+(TB-BPT)*CV/CS
      ELSEIF(TB.GT.MPT .AND. TA.LT.MPT)THEN
        TCOR =BPT+(TB-BPT)*CM/CS
      ELSEIF(TB.LT.BPT+VB .AND. TA.GT.BPT+VB)THEN
        TCOR=BPT+VB+(TB-BPT-VB)*CV/CS
      ELSEIF(TB.LT.MPT+VM .AND. TA.GT.MPT+VM)THEN
        TCOR=MPT+VM+(TB-MPT-VM)*CM/CS
      ELSE
        TCOR=TB
      ENDIF
CIF(TCOR.GT.BPT+VB)TCOR=BPT+VB
      RETURN
      END
      FUNCTION E(T)
      COMMON/C1/DENS,COND,SPHT
      COMMON/C2/MPT,BPT,VM,VB,QMEL,QVAP
      IF(T.LE.MPT)THEN
      E=SPHT*T
      ELSEIF(T.LT.MPT+VM)
      E=SPHT*T +(T-MPT)*QMEL/VM
      ELSEIF(T.LE.BPT)THEN
      E=SPHT*T + QMEL/VM
      ELSEIF(T.LT.BPT+VB)THEN
      E=SPHT*T + QMEL/VM +(T-BPT)*QVAP/VB
      ELSE
      E=SPHT*T + QMEL/VM + QVAP/VB
      ENDIF
      RETURN
      END
```

APPENDIX. E.

Computer program for blown on powder cladding.

(see chapter 5.)

```
0100 PROGRAM TEMPS(INPUT,OUTPUT,TAPE5=INPUT,TAPE6=OUTPUT,TAPE7,TAPE10,
0110+TAPE55)
0120 REAL LM,LHV
0130 COMMON/CGEN/PTOT,RB
0140 COMMON/CARRAY/XP(21),XPDS(21),YP(11),YPDS(21),DT(21,11)
0150 COMMON/CSTATE/TMS,TME,TBS,TBF,GM,GV,RMPT,BPTK,SPHT,QMEL,QVAP
0160 DIMENSION CX(21),CY(11),UV(3),RPV(3),ANGLE(3),EV(3)
0170 DIMENSION IN(3,3),IS(4),IDMP(4),DZV(3)
0180 DATA PTOT,RB/1500.,.0010/
0190 DATA CP,DENS,R/483.0,.7870,.0.05/
0200 DATA RMPT,BPTK/1536.,2960./
0210 DATA QMEL,QVAP,SPHT/272000.,6100000.,483./
0220 DATA PI/3.14159/
0230 DATA LM,XS,DZ/8.,-1.,1./
0240 DATA UV(1),UV(2),RPV(1),RPV(2)/500.,1000.,.1,.05/
0250 DATA EV(1),EV(2),ANGLE(1),ANGLE(2)/.90,.95,30.,60./
0260 DATA DZV(1),DZV(2)/1.,2./
0270 DATA ((IN(I,J),J=1,2),I=1,2)/2HJ1,2HJ2,2HJ3,2HJ4/
0280 DATA IS(1),IS(2),IS(4)/6HXPLACE,.7HTAPE50=.4H,N4./
0290 TMS=RMPT
0300 TME=RMPT+QMEL/SPHT
0310 TBS=BPTK+QMEL/SPHT
0320 TBF=BPTK+(QMEL+QVAP)/SPHT
0330 GM=100.
0340 GV=100.
0360 DO 405 I=1,2
0370 UV(I)=UV(I)/1000.
0380 RPV(I)=RPV(I)/1000.
0390 DZV(I)=DZV(I)/1000.
0400 ANGLE(I)=ANGLE(I)*(PI/180.)
0410 405 CONTINUE
0420 LM=LM/1000.
0430 XS=XS/1000.
0440 DO 888 N1=1,2
0450 U=UV(N1)
0460 DO 888 N2=1,2
0470 RP=RPV(N2)
0480 DO 777 N3=1,2
0490 E=EV(N3)
0500 DO 777 N4=1,2
0510 THETA=ANGLE(N4)
0520 DO 777 N5=1,2
0530 DZ=DZV(N5)
0540C
0550C   EVALUATE XF,BL AND PHI
0560C
0570 BL=-(ALOG(1.5*E-0.5)/RP)
0580 XF=XS+(LM-DZ)/TAN(THETA)
0590 PHI=ATAN(TAN(THETA)*DZ/(LM-DZ))
0600C
0610 WRITE(60,201)BL,XS,XF,THETA*180./PI
0620 201 FORMAT(3X," ANALOGUE WILL RUN WITH THE FOLLOWING VALUES",/,
0630+5X,"BIER LAMBERT COEFICIENT=",F10.4,/,5X,"CLADDING STARTS AT X=",
0640+1X,F7.5,"M",/,5X,"CLADDING FINISHES AT X=",F7.5,"M",/,
0650+5X,"ANGLE OF POWDER FLOW=",F5.1," DEGREES")
0660C
0670 WRITE(60,30)RMPT,RMPT+GM,BPTK+GM,BPTK+GM+GV
0680 30 FORMAT(/,1X," NEW IMPROVED VERSION ALLOWING FOR MELTING AND BOILING",/
0690+3X," MELTING STARTS AT ",F7.1,"C FINISHES AT",F7.1,"C",/,
0700+3X," BOILING STARTS AT ",F7.1,"C FINISHES AT",F7.1,"C")
0710C::::::::::::::::::::::::::::::::::::::::::::::::::::::::::::::::::::::::
0720C     START MAIN CALCULATION
0730C
0740C::::::::::::::::::::::::::::::::::::::::::::::::::::::::::::::::::::::::
0750 C1=0.75*(1.0-R)*PTOT/(CP*U*DENS*RP*RB**2*PI*COS(THETA))
0760C
0770C                      ;FORM SURFACE GRID
0780C
0790 XTENT=XF-XS
0800 XD=XTENT/20.0
0810 DO 1 N=1,21
0820    XP(N)=XS+XD*FLOAT(N-1)
0830  1 CONTINUE
0840C
0850 YD=RB/5.0
0860 DO 2 N=1,11
0870    YP(N)=FLOAT(N-1)*YD
0880 2 CONTINUE
0890C
0900C
0910C          ; SET CX & CY ARRAYS
0920 DO 3 N=1,21
0930    CX(N)=EXP(-(BL*LM*(XF-XP(N))/(XF-XS)))
0940 3 CONTINUE
0950C
```

```
0960 DO4 N=1,11
0970  CY(N)=EXP(-(YP(N)/99)**2)
0980 4 CONTINUE
0990C
1000C                ;EVALUATE TEMPERATURE FOR ALL POINTS
1010C
1020 DO 5 K=1,21
1030     XINT=XINTEG3(-RB,YP(K))
1040 DO 5 I=1,11
1050    DT(K,I)=C1*CX(K)*CY(I)*XINT
1060 5 CONTINUE
1070C                ;EVALUATE "MELT ZONE"
1080 CALL XTRAP
1090C                 ; ALLOW FOR PHASE CHANGES
1100 DO 7 K=1,21
1110 DO 7 I=1,11
1120     IF(DT(K,I).GT.RMPT)DT(K,I)=STATE(DT(K,I))
1130 7 CONTINUE
1140C::::::::::::::::::::::::::::::::::::::::::::::::::::::::::::::::::::::::
1150C                 END OF MAIN CALCULATION ; PRINT OUTPUT
1160C::::::::::::::::::::::::::::::::::::::::::::::::::::::::::::::::::::::::
1170 WRITE(10,*)PTOT,U,THETA*(180./PI),LM,XS,XF,RB,RP,PHI
1180 WRITE(60,202)U,LM,XS,XF,DZ,RP,PHI*(180./PI)
1190 202 FORMAT(//,2X,"SURFACE PARTICLE TEMPERATURE ARRAY",//,
1200+4X,"POWDER SPEED =",F6.4,"M/S",/,4X,"POWDER DEPTH=",F6.4,"M",/,
1210+4X,"X_POSN CLAD START =",F6.4,"M",/,4X,"X_POSN CLAD FINISH =",F6.4,"M",/
1220+4X,"CLAD DEPTH=",F6.4,"M",/,4X,"PARTICLE RADIUS=",F6.4,"M",/,
1230+4X,"CLAD FACE ELEVATION=",F6.2,"DEGREES",//)
1232 WRITE(60,220)E,PTOT,RB
1234 220 FORMAT(/,4X,"POWDER VOIDADGE=",F5.2,/,
1236+4X,"BEAM POWER=",F6.0,"W",/,
1238+4X,"BEAM RADIUS=",F7.4,"M")
1240 WRITE(60,203)(YP(N),N=1,11)
1250 203 FORMAT(1X,"X_POSN,"50X,"Y_POSN",//,7X,11(1X,F7.5,2X),/)
1260C
1270 DO 6 K=1,21
1280    WRITE(60,204)XP(K),(DT(K,I),I=1,11)
1290    WRITE(10,205)(DT(K,I),I=1,11)
1300 6 CONTINUE
1310 204 FORMAT(F7.5,11(1X,F7.1,2X))
1320 205 FORMAT(11F10.2)
1330 WRITE(60,208)
1340 208 FORMAT(/,15X,"MELT ZONE : (X_POSN, MOLTEN POWDER TRACK WIDTH)",//)
1350 WRITE(60,207)(XPOS(K),2.0*YPOS(K),K=1,21)
1360 207 FORMAT(7("(",F7.5,",",F7.5,")"))
1370 777 CONTINUE
1380 IS(3)=IN(N1,N2)
1390 REWIND,60
1400 CALL PFREQ(IS,IERR)
1410 CALL PFREQ("RETURN,TAPE60",IERR)
1420 888 CONTINUE
1430 STOP
1440 END
1450 SUBROUTINE XTRAP
1460 COMMON/CARRAY/XP(21),XPOS(21),YP(11),YPOS(21),DT(21,11)
1470 COMMON/CSTATE/TMS,TMF,TBS,TBF,GM,GV,RMPT,BPTK,SPHT,QMEL,QVAP
1480C
1490 DO 1 K=1,21
1500     XPOS(K)=XP(K)
1510     YPOS(K)=0.0
1520     IF(DT(K,1).LT.RMPT)GO TO 1
1530C
1540      N=1
1550      2 N=N+1
1560      IF(DT(K,N).LT.RMPT.OR.N.EQ.11)GO TO 3
1570      GO TO 2
1580C
1590      3 NM=N-1
1600      YPOS(K)=YP(NM)+(RMPT-DT(K,NM))*(YP(N)-YP(NM))/(DT(K,N)-DT(K,NM))
1610C
1620 1 CONTINUE
1630 RETURN
1640 END
1650 FUNCTION XINTEG3(X1,X2)
1660 COMMON/CGEN/PTOT,RBEAM
1670 F(Z)=EXP(-((Z/RBEAM)**2))
1680 R=100.
1690 S=(X2-X1)/(2.0*R)
1700 P=S*2.0
1710 XOD=X1+S
1720 XEV=X1+P
1730 SOD=0.0
1740 SEV=0.0
1750 RC=1.0
1760 XINTEG3=0.0
```

```
      IF(X1.EQ.X2)GOTO 844
  841 CONTINUE
      SOD=SOD+(F(XOD)*2.0)
      SEV=SEV+(F(XEV)*4.0)
      RC=RC+1.0
      XOD=XOD+P
      XEV=XEV+P
      IF(RC.GT.P+2.0)GO TO 844
      IF(XOD-X2)841,842,842
  842 CONTINUE
      XINTEG3=(S/3.0)*(F(X1)+F(X2)+SOD+SEV)
  844 CONTINUE
      RETURN
      END
      FUNCTION STATE(T)
      COMMON/CSTATE/TMS,TMF,TBS,TBF,GM,GV,PMPT,BPTK,SPHT,QMEL,QVAP
      IF(T.LE.TMF)GO TO 1
      IF(T.LE.TBS) GO TO 2
      IF(T.LE.TBF)GO TO 3
      GO TO 4
C-----------------------------------------
    1 T=TMS+(T-TMS)*GM/(TMF-TMS)
      GO TO 10
    2 T=T+GM-(QMEL/SPHT)
      GO TO 10
    3 T=BPTK+(T-TBS)*GV/(TBF-TBS)+GM
      GO TO 10
    4 T=T+GM+GV-(QMEL/QVAP)/SPHT
   10 CONTINUE
      STATE=T
      RETURN
      END
```

(12) UK Patent Application (19) GB (11) 2 090 873 A

(21) Application No 8200418
(22) Date of filing 7 Jan 1982
(30) Priority data
(31) 81/00644
(32) 9 Jan 1981
(33) United Kingdom (GB)
(43) Application published
21 Jul 1982
(51) INT CL³
C23C 1/00
(52) Domestic classification
C7F 1L 2T 4K 5A
(56) Documents cited
GB 1562583
GB 846808
GB 808831
GB 806677
GB 713566
(58) Field of search
C7F
(71) Applicants
Control Laser Limited,
9 Royal Oak Way South,
Daventry, NN11 5PJ,
Northamptonshire
(72) Inventors
William Maxwell Steen,
John Powell
(74) Agent
J. B. King,
Kings Patent Agency
Limited, 146a Queen
Victoria Street, London
EC4V 5AT

(54) Fusing cladding material to a substrate

(57) In fusing a cladding material, in the form of a powder as example, to a substrate using a laser which tracks across the substrate producing a fusion zone into which the powder is fed, ultrasonic vibratory energy is applied to the substrate. The stresses formed in the fusion zone and inclusion of pores are thereby reduced significantly.

GB 2 090 873 A

The drawings originally filed were informal and the print here reproduced is taken from a later filed formal copy.

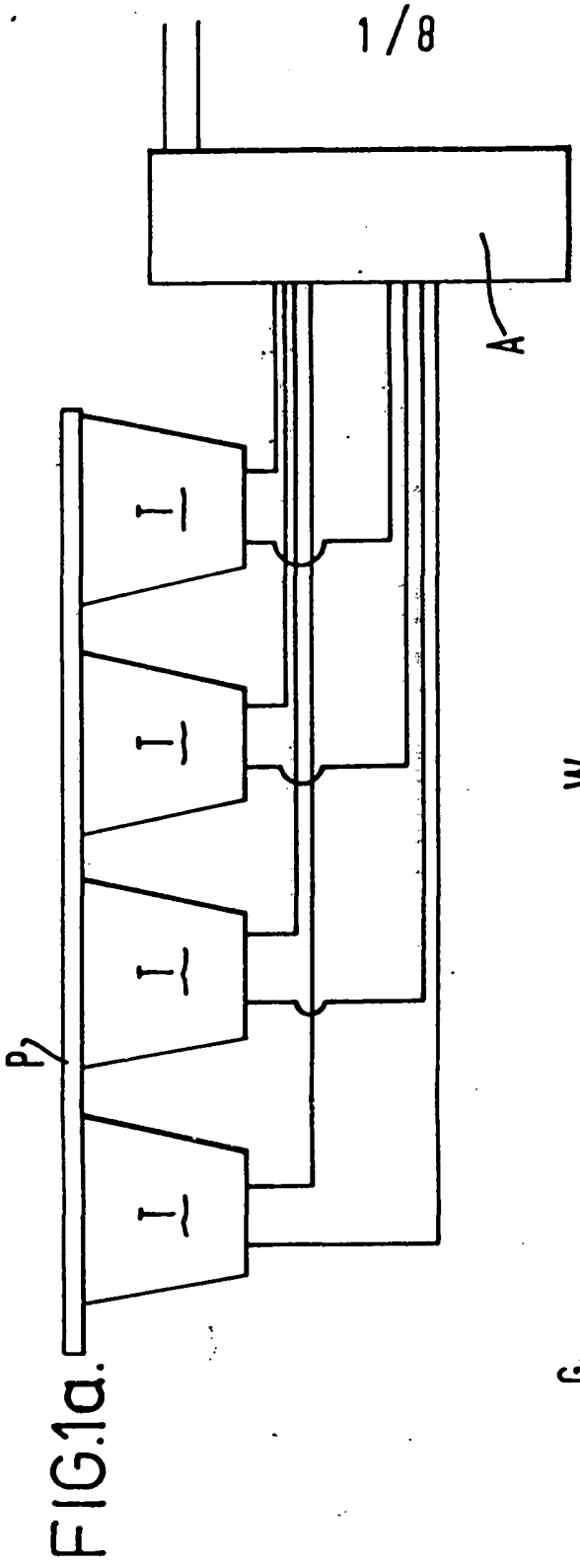

FIG.1a.

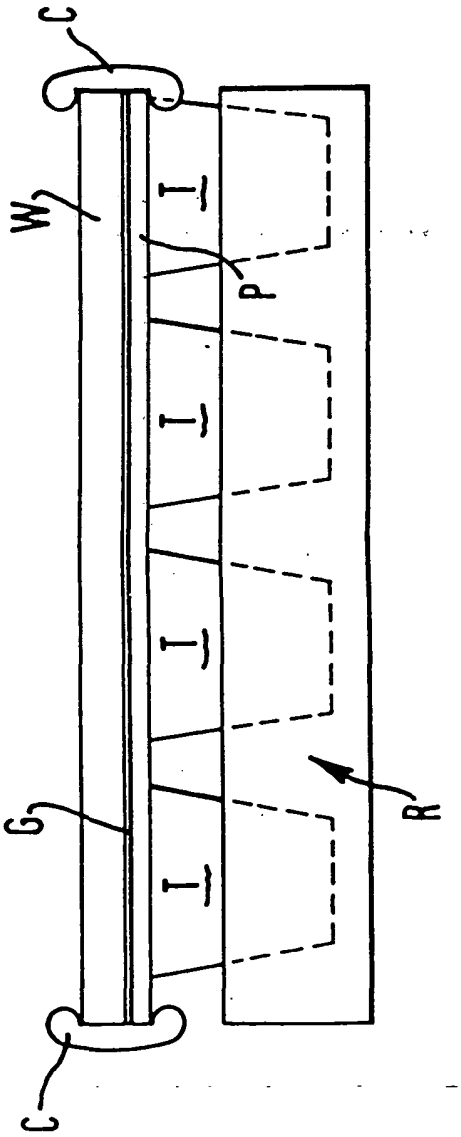

FIG.1b.

FIG. 2a.

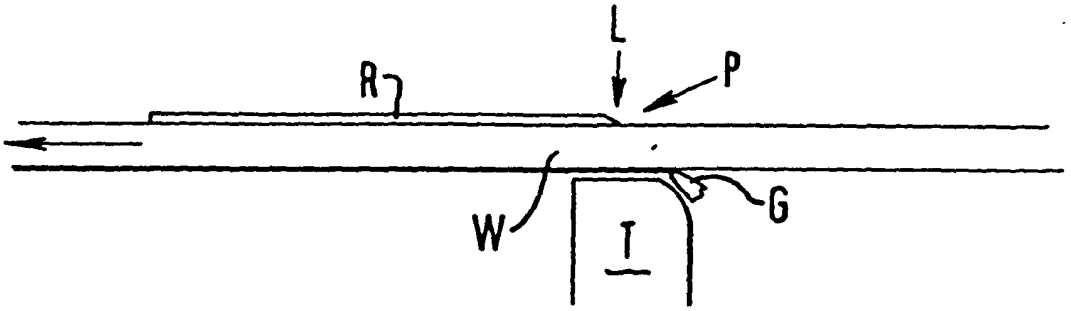

FIG. 2b.

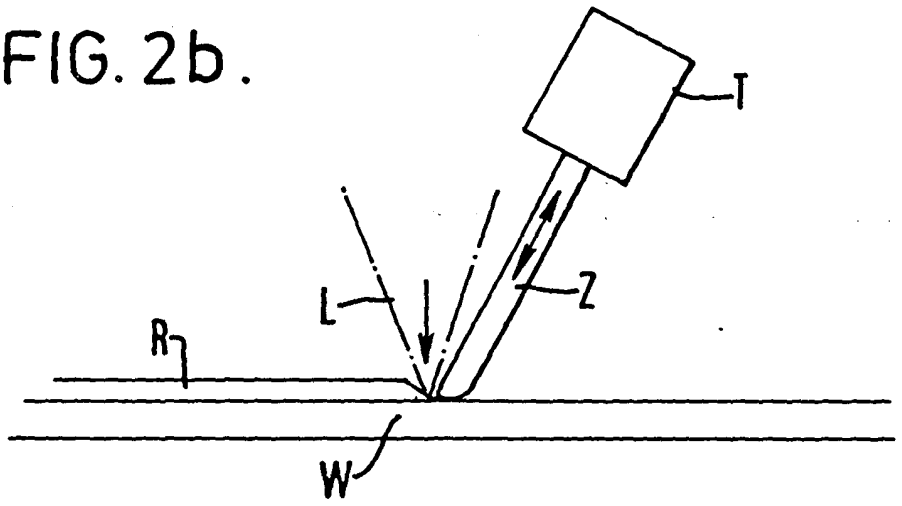

FIG. 2c.

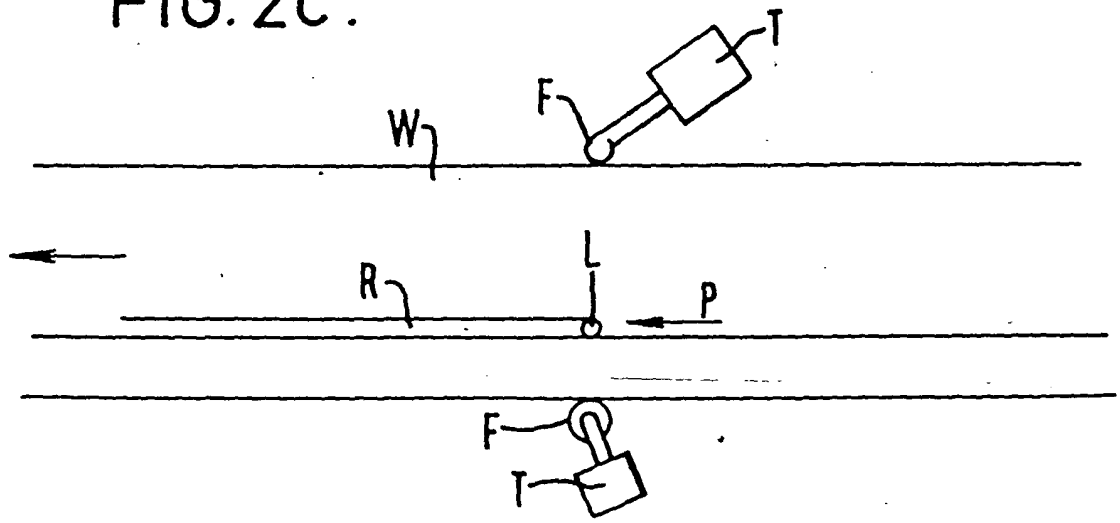

FIG. 3b.

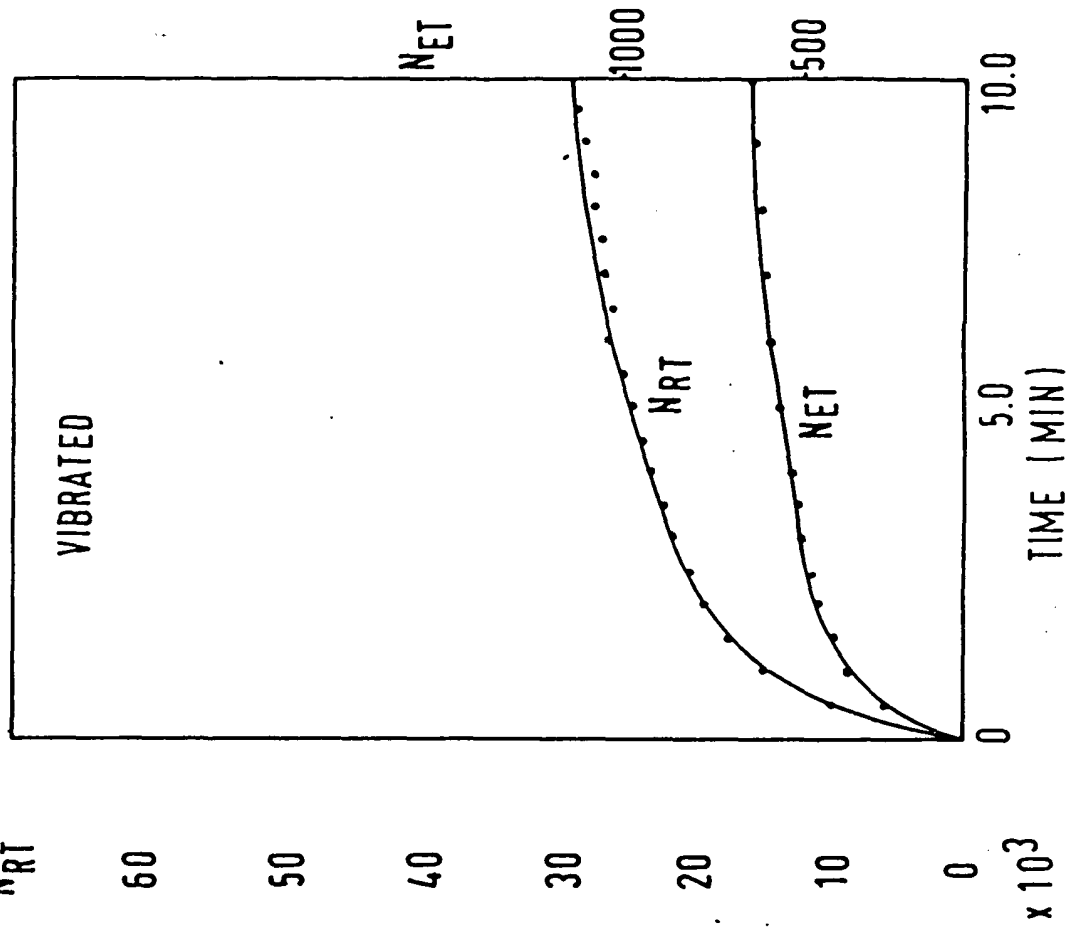
VIBRATED
N_{ET}
1000
500
N_{RT}
N_{ET}
0
5.0
10.0
TIME (MIN)

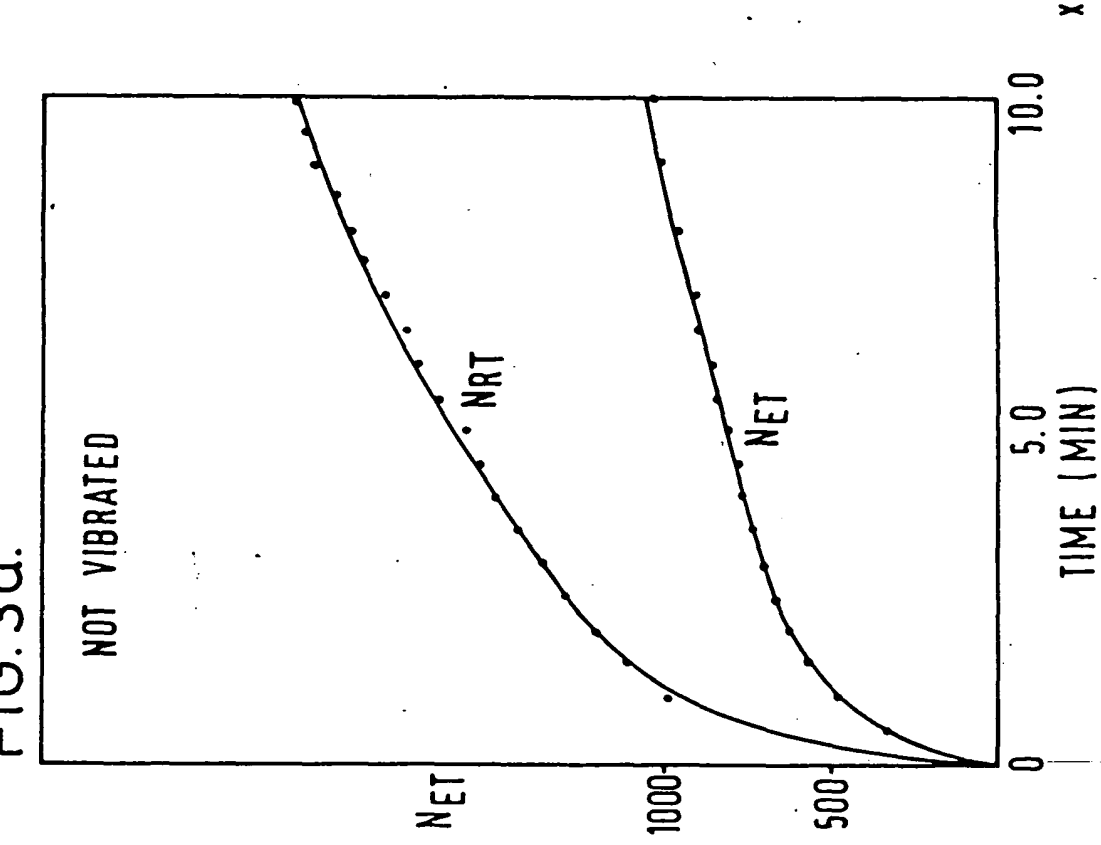
N_{RT}
60
50
40
30
20
10
0
$\times 10^3$

FIG. 3a.

NOT VIBRATED
N_{ET}
1000
500
N_{RT}
N_{ET}
0
5.0
10.0
TIME (MIN)

FIG.4a.

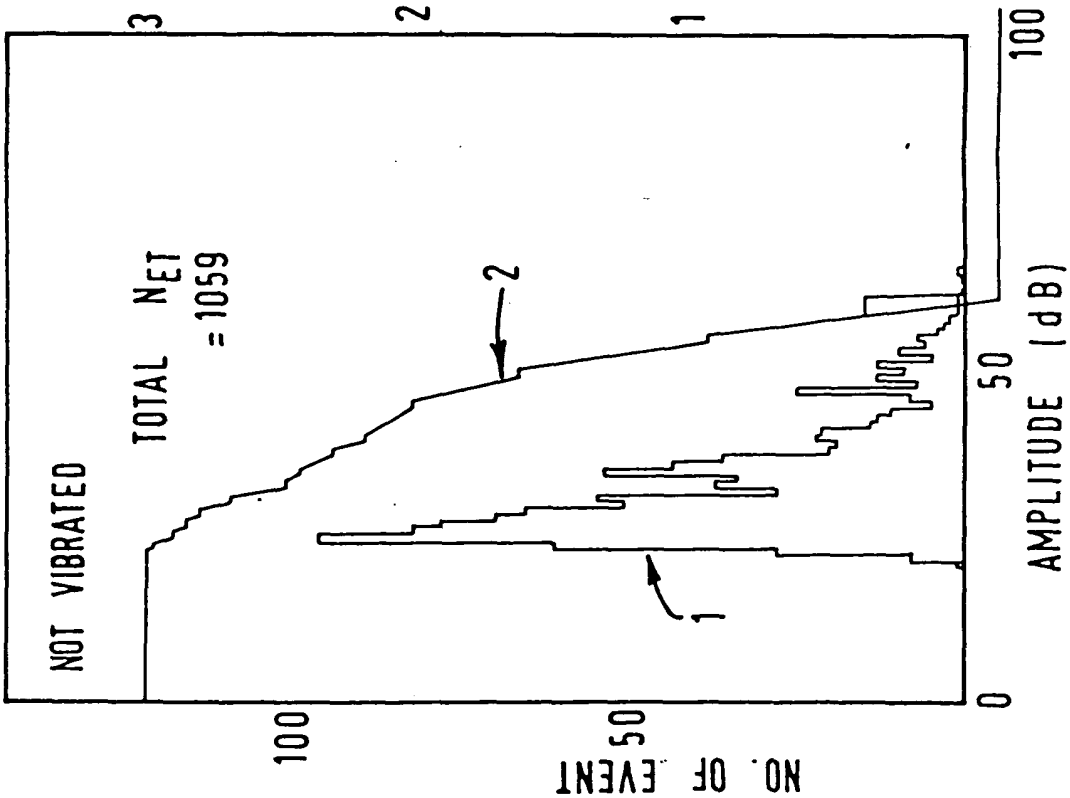
NOT VIBRATED
TOTAL NET
=1059
1
2
NO. OF EVENT
100
50
0
AMPLITUDE (dB)
100
50
0
LOG 10 (NET)
3
2
1

FIG.4b.

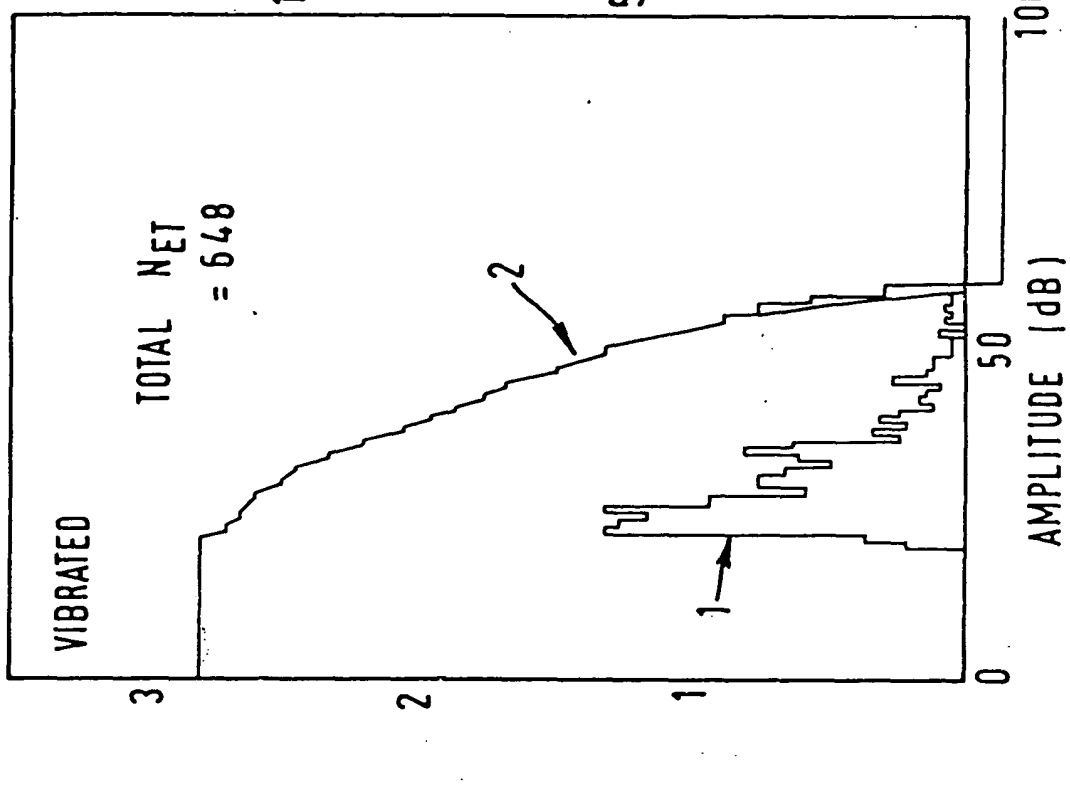
VIBRATED
TOTAL NET
=648
1
2
NO. OF EVENT
100
50
0
AMPLITUDE (dB)
100
50
0
3
2
1

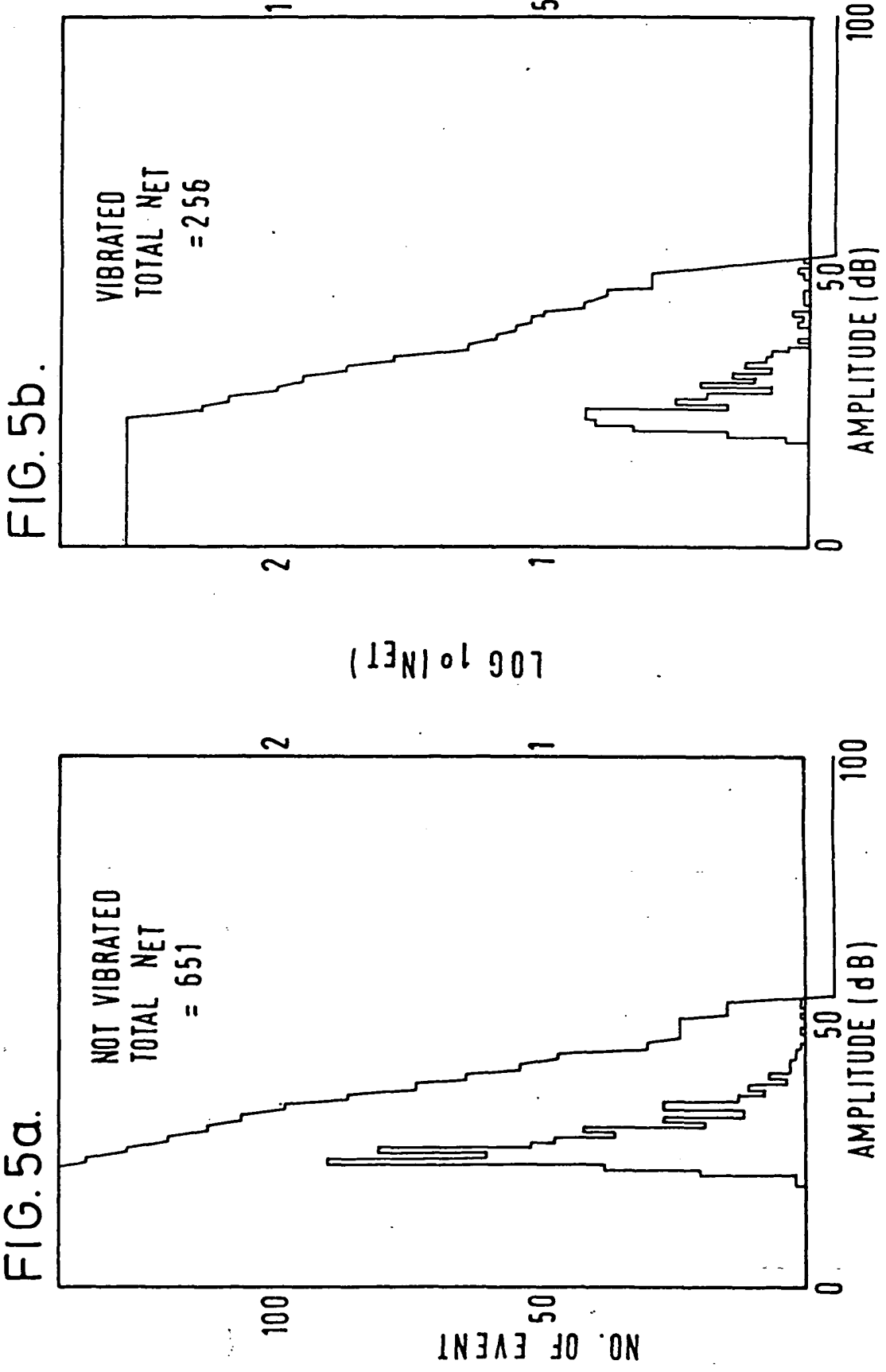
NOT VIBRATED
TOTAL NET
= 651
VIBRATED
TOTAL NET
=256
NO. OF EVENT
LOG 10 (NET)
AMPLITUDE (dB)
AMPLITUDE (dB)
100
50
0
2
1
100
50
0
2
1

FIG. 5a.

FIG. 5b.

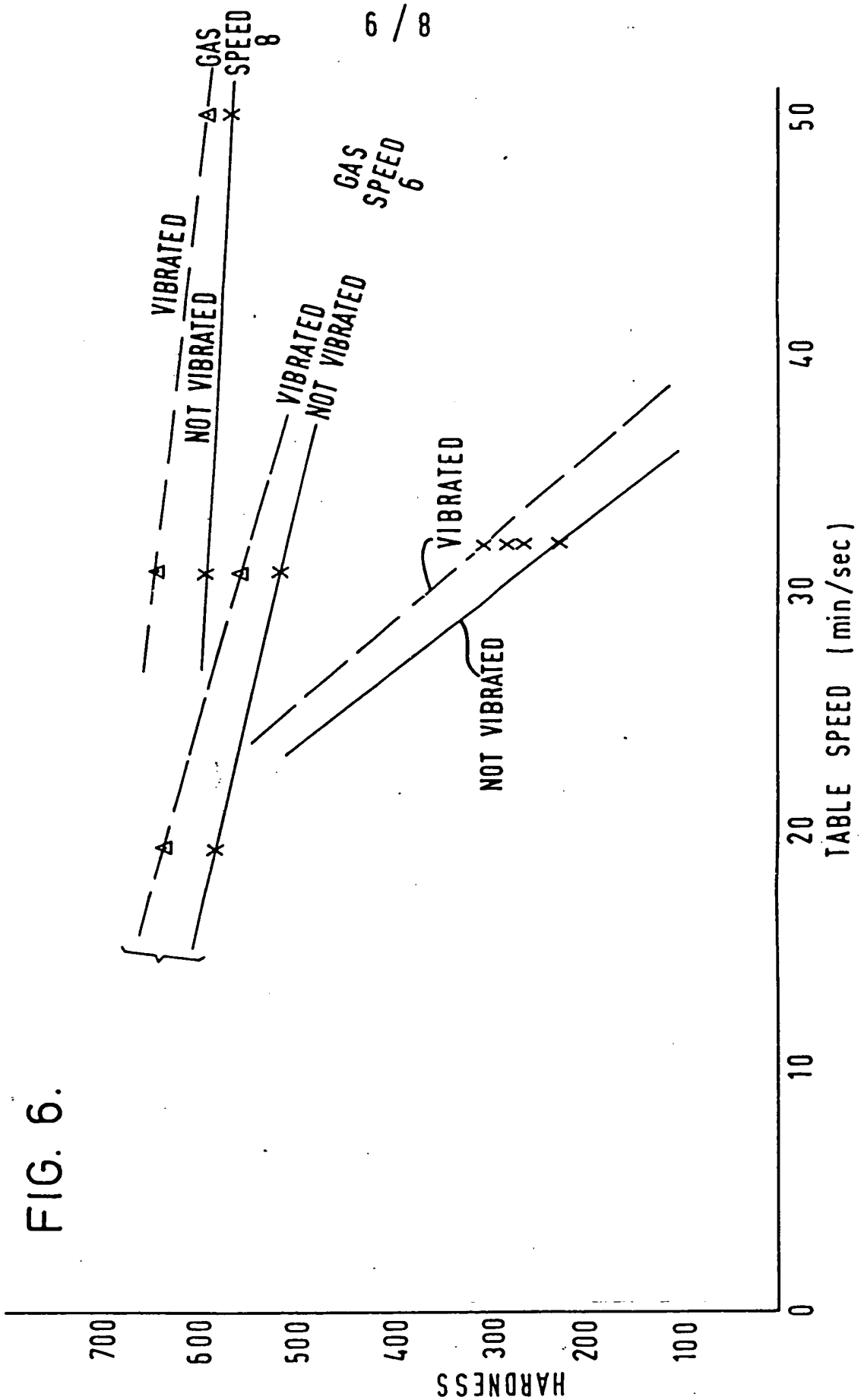
GAS SPEED 8
VIBRATED
NOT VIBRATED
GAS SPEED 6
VIBRATED
NOT VIBRATED
VIBRATED
NOT VIBRATED
HARDNESS
700
600
500
400
300
200
100
0
10
20
30
40
50
TABLE SPEED (min/sec)

FIG. 6.

FIG. 7.

Increase in:	Gas speed	Table speed	Deposit vol.	With u/s VRS
Cracks and pores	↑	↓	↑	↓
N_{RT}, N_{ET}	↑	↓	↑	↓
Contact angel	↓	↑	—	↓
Hardness	↑	↓	—	↑
Deposit vol.	↑	↓	—	—

↑ increase

↓ decrease

— no effect

FIG. 6.

(a)

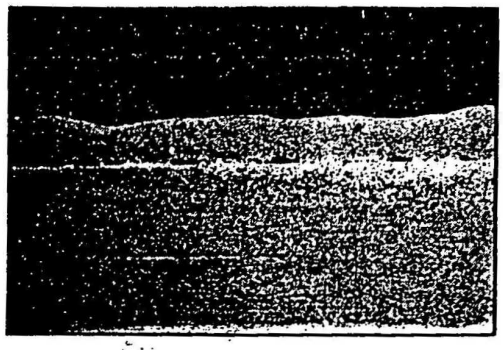

(d)

(c)

(d)

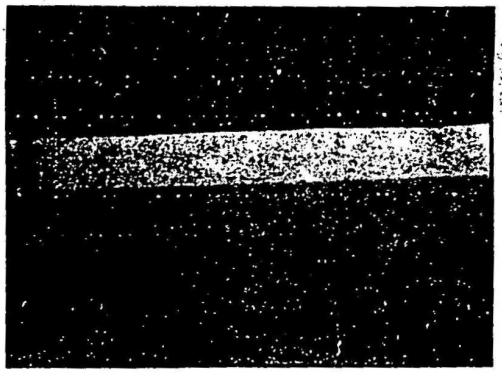

(e)

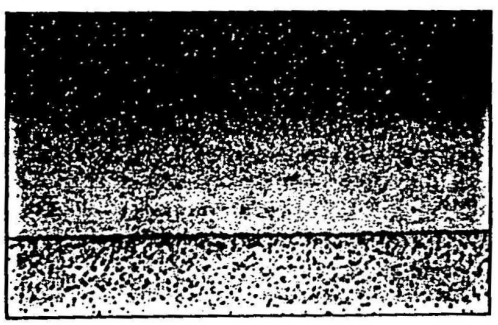

SPECIFICATION

Method and apparatus for fusing a cladding material to a substrate

This invention relates to a method of fusing a cladding to a substrate and to an apparatus for carrying out the method.

This invention is primarily concerned with the reduction or avoidance of stresses, inclusions and voids normally occurring in a method of cladding a metal with a metal coating using a high power laser to fusibly bond the coating, which may be applied as a powder, preferably forcibly blown, into an area subject to high intensity heating by the laser.

The cladding of steel and other substrate metals with a thin layer of a hard and/or corrosion resistant metal, usually expensive, is known and one of the most effective ways of producing a clad article is by traversing a molten spot area across the surface of a substrate and blowing the cladding metal in powdered form onto this spot so that it melts and fuses with the substrate. The molten spot conveniently is produced using a high power (1 kW+) laser.

The method, however, has drawbacks and two principle ones are the formation of pores in the track of cladding metal and the risk of the clad layer and/or underbead cracking due to the high thermal stresses incurred in rapid thermal cycling (cooling rates of the order of 10^6 °C/sec or more).

Broadly this invention seeks to provide an improvement in processes of the aforementioned kind whereby residual stresses and porosity may be reduced.

According to this invention there is provided, in a method of fusing a cladding material to a substrate, the step of applying vibratory energy to the substrate at least at the zone of active fusion.

The frequency of the vibratory energy may be in the sonic or ultrasonic range and typically would have a lower limit of 50 Hertz. It is preferred to use ultrasonic frequencies such as those of the order of 25 kHz.

The vibratory energy may be applied from the lower surface of the substrate using one or more transducers in effective vibratory transmissive contact therewith, and where a plurality of transducers are used these may be driven in or out of phase. Conveniently the transducers will be bonded to a plate which is brought into contact with and firmly attached to the substrate constituting the workpiece with the interposition of grease or other substance to establish a good contact.

Alternative and further preferred methods comprise a transducer with a contact member brought into effective engagement with the top or bottom of the workpiece and as close as practical to the point of active fusion, the transducer being arranged to track with the moving fusion zone. Contact can be effected using a runner wheel or contact finger. In another arrangement the transducer is contacted against a side surface of the workpiece. Vibration is effected continuously during the cladding operation.

The method of this invention is broadly applicable to a wide range of cladding processes and whilst the method is primarily for use with a laser heat source it can be employed usefully with flame electric arc or plasma techniques alone or in combination with a laser. Likewise many arrangements for the application of the cladding material can be used such as free fall powder, blown powder, slurry and paste applied powder or preform shapes. Multiple laser beams and/or rastering may be used with the cladding trace being as wide as the vibrated zone.

Substantial improvements have been observed in comparison with the same cladding method not using vibration. The method of this invention:—

a) reduces the creation of stresses during the intense temperature changes at the fusion zone, thereby rendering the underbead and the cladding less likely to crack,

b) increases hardness of the deposit,

c) provides a metallurgically cleaner interface between substrate and deposit,

d) reduces pore diameter,

e) reduces and relieves stresses, and

f) causes less overall distortion due to the cladding.

The method is effective during the deposition and fusion to reduce stress creation and is to be contrasted with known post-weld treatments designed to relieve already created stresses.

The method of this invention together with apparatus for carrying out the method are described further in conjunction with the accompanying drawings, wherein:—

Figures 1*a* and 1*b* show one arrangement for applying vibratory energy,

Figures 2*a* to 2*c* show three further arrangements for supplying vibratory energy,

Figures 3*a* and 3*b* show comparative acoustic emission results (ring-down count) from clad substrates without and with vibration applied during fusion,

Figures 4*a* and 4*b* show comparative results in a way related to Figure 3,

Figures 5*a* and 5*b* show comparative results as in Figure 4, but of a different trace,

Figure 6 shows comparative hardness results,

Figure 7 shows results of changing various work parameters, and

Figures 8*a* to 8*e* show comparative photo micrographs of the interface region.

Referring to Figures 1 and 2, these illustrate schematically methods of imparting vibratory energy to the workpiece. In Figure 1 four ultrasonic transducers T are bonded to an aluminium plate P using a resin adhesive, as example, and each transducer is driven in or out of phase by an amplifier A delivering power at 25 kHz. As shown in Figure 1*b*, a steel plate W forming the workpiece to be clad, is attached to plate F by means of clamps C using an interposed grease layer G in order to obtain good transmission. The transducer T will preferably be set in a rubber matrix R enclosed in a steel box.

The laser and the powder blowing equipment are set up in the usual way and the assembly clamped to an X—Y work table. As the clad trace is being desposited the transducers are turned on and the plate P and workpiece W vibrate at the ultrasonic frequency of 25 kHz. This vibration creates a highly energetic, turbulent weld pool which is incapable of retaining many pores and thus the porosity of the solid deposit is almost completely pore free. The vibrational energy supplied to the solidifying metal atoms also helps them to achieve stable and more unstressed configurations than is possible without the supply of kinetic energy through the transducers.

Reducing the stress in the deposit inhibits cracking and reduces the occurrence to a minimum. Known post cladding heat treatment is not effective to change the presence of numerous cracks because although stress in the deposit can be eliminated, such heat treatment can do nothing to heal already formed cracks. The ultrasonic vibration is a method of stress reduction or avoidance and thus reduces the initiation of cracks and the need for post cladding heat treatment. This arrangement further provides, as a comparison of vibrated and unvibrated specimens shows, (a) an increase in the hardness of the deposit by approximately 10%, and (b) the interface between the deposit and the substrate is a great deal cleaner metallurgically. This is probably because the oxides present on the substrate are floated off to the surface by the turbulence of the weld pool; previously these oxides could form a distinct visible interfacial layer. In a series of experiments the following two results are relevant to show practical effects:—

1. Crack length per unit deposit length reduced by: 76.4%, 24%, 28%, 41% and 93% (Average 52.5%).

2. Pore diameter per unit deposit length reduced by: 57%, 61%, 94%, 31%, 92%, 36% (Average 61.8%).

Figure 2 shows other arrangements for applying vibratory energy by way of further example. In Figure 2*a* the transducer T is in sliding contact with the lower surface of the workpiece W and grease G is fed between the mating surfaces. The transducer is below the point of impingement of the laser beam L and powdered metal P which produce the clad trace R. The vibration in this version is thus limited to the area under the laser and multiple lasers or rastering could be used to produce a trace having a width comparable to the transducer, i.e. about 2.5 cm.

In Figure 2*b* the ultrasonic transducer T acts through a transmission means Z on the zone of impingement of the laser L. Figure 2*c* shows an arrangement in plan view wherein the transducer T (two in this case) act on each side of the workpiece W through a contact finger or roller F abeam the laser zone L.

Figures 3*a* and 3*b* show two graphs produced with the help of acoustic emission equipment which was turned on immediately after the laser clad trace was deposited, using apparatus as shown in Figure 1. Two identical traces (vibrated and non-vibrated) were produced and the ring down counts (N_{RT}) were recorded for ten minutes as well as a count of super threshold events (N_{ET}). The two graphs show a dramatic drop in both N_{RT} and N_{ET} when the specimen is vibrated, i.e. the final value of N_{RT} without vibration is 51 and this drops to 29 if the specimen is vibrated ultrasonically during the cladding; the drop of N_{ET} is from 840 to 660. This pair of graphs is typical of the results obtained from approximately twenty such pairs of laser clad runs. N_{RT} and N_{ET} are measures of the noise emitted by cooling clad trace and are very closely related to the internal stress in the finished product. These graphs show a decrease in this acoustic emission when vibro laser cladding is used and this reflects a decrease in internal stress in the deposit and a decrease in the number of micro and macro cracks in the deposit.

Figures 4*a* and 4*b* show two graphs closely related to the graphs in Figures 3*a* and 3*b* in that they give information about the N_{ET} against the amplitude of the signals produced by the internal noise in the deposit. This amplitude distribution was presented in two forms:

1. in the normal linear mode, the histogram of the N° of events versus their amplitude,

2. in the sum log mode, the events of each successive element were added to the higher elements for display on a log scale.

Figures 5*a* and 5*b* differ from Figure 4 in that they show another pair of traces; both Figures 4 and 5 indicate that the distribution of amplitude is not greatly affected but that the number of events is greatly reduced when a vibrating specimen is clad.

Figure 6 shows a graph of the effects of workpiece traverse speed (table speed), powder-flow rate (gas speed) and ultrasonic vibration on the hardness of the deposits. For the present purpose it need only be noted that the hardness of the deposit increases when ultrasonic vibration is employed during the cladding process, this being clearly shown.

Figure 7 is a self explanatory tabular summary of the results of varying the various work parameters in a series of tests to compare identical runs produced by laser cladding and vibro laser cladding.

Figure 8 shows photomicrographs of the workpiece to laser cladding interface and Figures 8*a* to 8*c* show unvibrated specimens in longitudinal section. Porosity and trapped oxides in the interface are clearly present and in addition some macro pores were observed, although not shown here. A prominent crack is shown in Figure 8*c*. In contrast Figures 8*d* and 8*e* show specimens obtained with the use of vibration but under otherwise similar conditions, and illustrate a considerable reduction in porosity and cracking.

Multiple trace deposits may also be made and flame, electric arc or plasma heating may be employed as well as laser. A further advantage in the method of this invention resides in the melt

trace passing through any surface layer such as electroplate, carburising, nitriding, boromising or flame sprayed finish.

CLAIMS

1. In a method of fusing a cladding material to a substrate, the step of applying vibratory energy to the substrate at least at the zone of active fusion.

2. A method in accordance with Claim 1, wherein the cladding material is fused using energy from a laser source.

3. A method in accordance with Claim 1 or 2, wherein the cladding material is fused using a flame source.

4. A method in accordance with Claim 1 or 2, wherein the cladding material is fused using an electric arc.

5. A method in accordance with Claim 1 or 2, wherein the cladding material is fused using a plasma.

6. A method in accordance with any preceding Claim, wherein the cladding material is applied as a gravity fed powder, a blow powder, a slurry, a paste or a preformed shape.

7. A method in accordance with any preceding Claim, wherein the frequency of the vibratory energy is sonic or ultrasonic.

8. A method in accordance with Claim 7, wherein the frequency is between 50 Hz and 50 kHz.

9. A method in accordance with any preceding Claim, wherein the frequency of the vibratory energy is 25 kHz nominal.

10. A method in accordance with any preceding Claim, wherein the vibratory energy is applied from the lower surface of the substrate.

11. A method in accordance with any preceding Claim, wherein the vibratory energy is applied through a plurality of transducers bonded to a plate in intimate contact with and firmly attached to the substrate.

12. A method in accordance with Claim 11, wherein the transducers are driven in phase.

13. A method in accordance with any one of Claims 1 to 9, wherein the vibratory energy is derived from a transducer having a vibration transmissive contact member which is brought into effective engagement with the top or bottom of the workpiece, close to the point of active fusion, the transducer and contact member being arranged to track with the moving fusion point.

14. A method in accordance with Claim 13, wherein the contact member comprises a runner wheel or contact finger.

15. A method in accordance with any preceding Claim, wherein the vibratory energy is applied from the side of the substrate or from the side of a plate connected therewith.

16. A method in accordance with any preceding Claim, wherein vibratory energy is applied continuously during fusion.

17. A method in accordance with any preceding Claim, wherein the zone of active fusion progresses as a track across the substrate, a plurality of tracks being laid in juxtaposed relationship across the substrate.

18. A method of fusing a cladding material to a substrate as described herein and as exemplified with reference to the drawings.

19. Apparatus for use in fusing a cladding material to a substrate broadly as herein described and with reference to Figure 1, or Figures 2*a* to 2*c* of the drawings.

20. Apparatus for applying a cladding material to a workpiece forming a substrate, the apparatus comprising:—

a) a workpiece support bed movable in both X and Y directions of a horizontal plane,

b) ultrasonic transducer means on the bed capable of being brought into ultrasonically transmissive contact with the workpiece,

c) means for supplying electrical energy at ultrasonic frequency to the workpiece,

d) a laser beam receiver arranged to direct a beam from a laser onto a workpiece on the bed,

e) a cladding material supply means arranged to direct cladding material powder onto the workpiece at the point of impingement of the laser beam thereon, and

f) drive means to effect steady controlled traverse of the work bed in one direction.

Printed for Her Majesty's Stationery Office by the Courier Press, Leamington Spa, 1982. Published by the Patent Office, 25 Southampton Buildings, London, WC2A 1AY, from which copies may be obtained.

Appendix G. Previous methods of Cladding.

APPENDIX : G

PREVIOUS METHODS OF CLADDING

G.1. GENERAL

Cladding, i.e. the coverage of one metal with another, can be divided into two major regimes of application: A) Hard facing for wear resistance and B) Corrosion resistance. Hard facing applications include excavation machinery, aero engine components, forging dyes and rolling mill rolls etc. Cladding for corrosion resistance is often utilised in the chemical and petroleum industries where the corrosion environments are very severe.

Many cladding alloys combine hard facing and corrosion resistant properties and hard facing in general can be defined as (1) 'The application of hard, wear resisting material to the surface of a component by welding, spraying or allied processes for the main purpose of reducing wear or loss of material by abrasion, impact, corrosion, galling and cavitation'. Hard facing by this definition has been known for many years; perhaps the first materials used in this way were the Co-Cr-W alloys developed in the late 1890's.

One way to combat wear is to produce the components from a material which can withstand the working conditions. This practice is generally very expensive both in materials cost and in the cost of machining such durable materials. Also, it is unusual that excellent wear resistant properties are required anywhere other than on the surface and even then rarely over all the surface.

In some cases, making the whole article of a hard abrasion resistant material can itself cause problems elsewhere on that component in its interaction with other components. The desirable practice, therefore, is to select a cheaper base material and to cover its critical areas with a material having superior properties.

To provide a context for the present subject of research, laser cladding, a review of existing cladding methods has been compiled. This is useful in that it shows the difficulties and advantages associated with the established processes of producing a new surface on a substrate with inadequate surface properties. The large number of metal surface treatments has meant that not all of them can be included in a review of this limited length, for example, thermochenical treatments of the carburising and nitriding type have been classed as being not relevant enough to the discussion to warrant inclusion. Heat treatments are, of course, very important methods of altering the surface properties of metals but to give the literature review greater cohesion and to keep the length reasonable, only those methods which involve the application a new 'clad' surface have been reviewed.

These cladding processes include:-

a) Cladding by electric arc welding methods.
b) Explosive cladding.
c) Electroplating.
d) Hot dipping.

e) Cladding by rolling.

f) Thermal spraying techniques.

g) Chemical vapour deposition.

h) Physical vapour deposition.

i) Ion Implantation.

G.2. CLADDING BY ELECTRIC ARC WELDING METHODS

There are four electric arc cladding methods:

G.2.1. MANUAL METAL ARC

The use of basic electrodes is extensive as they are capable of producing welds having very low hydrogen content. This reduces the tendency to cracking of both weld and substrate. Improved arc stability of modern electrodes minimises the loss of expensive alloying elements as they are transferred through the arc.

G.2.2. FLUX COVERED WIRES

Semi automatic non shielded welding with a hand held gun gives a considerably increased output compared to manual metal arc welding and, therefore, the down time of equipment being re-claimed by cladding can be reduced.

G.2.3. AUTOMATIC OPEN ARC AND SUBMERGED ARC PROCESSES

The introduction of flux-cored wire in continuous coil form has increased the application of mechanised welding to surfacing. The brittleness of many hard facing alloys prevented their production in the form of solid wires. Automatic submerged arc hard facing was thus carried out with plain carbon or low alloy steel wires and alloy-enriched submerged arc fluxes. The introduction of cored wires has changed the situation dramatically and many differenct alloys can now be deposited by automatic or mechanised welding procedures. A development in submerged arc welding has been the introduction of the Bulkhead process (1) (developed by Texas Alloys Products U.S.A.) in which a layer of powdered alloy underneath the flux burden increased deposition rates and reduces dilution.

G 2.4. INERT GAS SHIELDED ARC PROCESSES

Both the tungsten arc and metal arc processes are being applied in the field of surfacing. One of the most interesting applications of argon tungsten-arc welding is in facing components with an overlay of tungsten carbide, which is introduced into the molten pool in the form of granules fed through a tube. (There is a similar process of 'particle injection' used in a laser surfacing treatment discussed later). The process is automatic, faster than oxy-acetylene welding and the carbides do not melt as in the case of manual metal arc welding.

These four methods of cladding are all well established methods of fusing on a new metal surface utilising the energy output of an electric arc struck between an electrode and the substrate to be clad. Deposition rates can be as high as 10kg/h for semi automatic metal inert gas (M.I.G.) welding and 70kg/h for the fully automatic submerged arc process. (2) Coating thicknesses can also be high particularly with the utilisation of overlaying techniques. Figure A1. gives typical values of coating thickness for various techniques and it is obvious that arc welding processes are only applicable where a coating thickness of more than 2mm is required. Problems associated with arc welding cladding are the expected ones from such a turbulent, energy intensive process, i.e. Dilution, thermal distortion and residual stress on cooling, non-smooth surfaces and porosity.

The nature of a welding arc is such that the substrate must be substantially melted, any clad layer is therefore bound to be diluted with substrate metal and the electro-magnetic lorenz forces associated with the arc produce a stirring effect which distributes this diluent throughout the clad layer. The effect of this dilution on the cladding alloy is to alter its physical properties in a manner usually deleterious to the quality of the finished product. A common effect is that of a reduction in the hardness value of the hard facing deposit. Dilution is generally considered to be undesirable in cladding applications because it makes prediction of the properties of the clad layer very difficult.

Due to the localised nature of the thermal cycles which it experiences, including cooling rates of the order of hundreds of °C per second (3), the weld zone is inevitably subjected to non-uniform expansion and contraction during welding, Since this will be constrained by the body of the material, associated stress and strain cycles, will be generated particularly in the region of the weld itself. The effects which are produced are obviously complex and vary according to the particular process and application, but they can be summerised as follows:-

1) Plastic and elastic strains during welding, the former arising principally from the reduced yield stress at elevated temperatures.

2) Thermal stresses during the welding cycle due to the restraint of dimensional changes by the surrounding metal.

3) Residual stress after the cladding is completed.

4) Distortion of the clad area and parent material.

G.3. EXPLOSIVE CLADDING

1) METHOD

Explosive cladding, as carried out by, for example, I.C.I. Kelsmet (4), employs explosive power to clad a large number of combinations of metals. The cladding metal is placed at a controlled distance from the thicker substrate, than a uniform layer of explosive is spread across the cladding plate and detonated (see figure A 2).

The explosion progressively bonds the cladding plate to the backing metal forming a metallic jet at the point of impact. The effect of this jet is to remove the contaminated surface of both metals. The virgin surfaces behind the jet make molecular contact under very high instantaneous pressure giving an intermetallic bond.

2) ADVANTAGES

Explosive cladding offers a wide range of metals bonded to one or both sides of carbon, low alloy or stainless steels, or non ferous metals if required and has been carried out using: Aluminium, Nickel, Copper, Titanium and their alloys. There are no problems with dilution with this process as no thermally induced melting takes place(even though the pressure during bonding is in the order of 10^7 p.s.i. the temperature at the interface on bonding is well below 100 °C and is typically 60-70°C). Obviously this low temperature also ensures that no metallurgical changes take place in either metal.

FIGURE 2.

EXPLOSIVE CLADDING

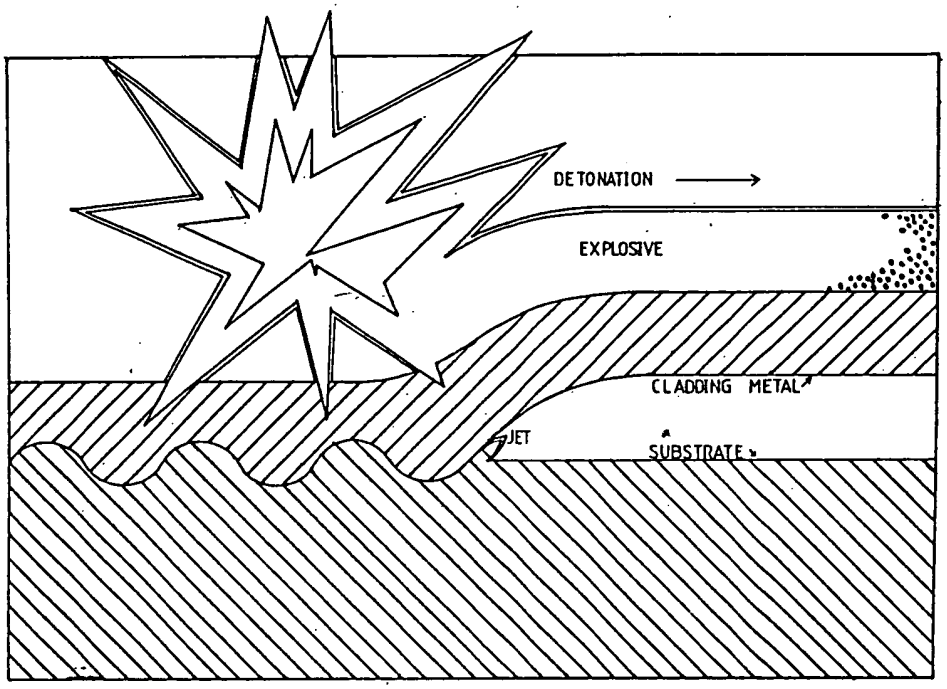

The ripple type cross section shown figuratively in figure two, is a result of the mechanics of the explosion propogation. This ripple is an asset in that it increases the surface area of the bond contact, and thereby improves bonding. The bond sheer strength is generally stronger than that of the weaker metal. The process is obviously an extremely quick one once the explosive 'sandwich' has been prepared.

3) DISADVANTAGES

When explosive bonding is employed as a method of cladding plates there is a tendency towards poor joining at the edges of the 'sandwich', due to the easy dissipation of the explosive energy in this region. Another area where poor bonding is found is at the initiation corner of the plate (the explosion is usually started at one corner of a rectangular plate) because the collapse angle and jet (see figure two), have not yet been formed.

After the explosion the plates need flattening and machining, which is costly and wasteful of cladding metal. The distortion in the plate as a whole being caused by the effects of the explosion reaching the corners of a plate in a staggered manner. The process uses a great deal of expensive explosive, this can be up to two tonnes for a twenty tonne clad plate, only 20% of this explosive energy is utilised by the actual bonding process.

This cladding method is restricted to the cladding of rather heavy cross section steel and should never be used when the substrate thickness is less than 15mm.

G.4. ELECTROPLATING

The basic principle of electroplating is a simple one: A metallic object, in a suitably cleaned condition, is made cathodic in an aqueous solution of a metal salt, a predetermined current is passed for a given time to deposit the required metal thickness and the component is subsequently rinsed and dried.

Chromium is the most widely used of the hard coatings (5). This metal is deposited from corrosive electrolytes containing chromic acid and sulphuric acid. The electrolyte is notorious for its poor efficiency and rather poor covering power. Chromium can be deposited at high hardness values (up to 1000 Vickers (6)) and possesses excellent wear properties. For heavy engineering applications both high current densities and long plating times are required. The adhesion of chromium plate to the substrate is often greater than the tensile strength of the coating itself.

More recently, electroless nickel coatings have been shown to possess very good wear resistance in a variety of applications.

Electroless plating is not strictly an electroplating process and essentially consists of promoting autocatalytic deposition of nickel from a meta-stable solution of one of its salts onto a suitable substrate. No current passage is involved in the process although in other ways it is similar to electroplating. Because no current is required, there is no preferential build-up of coating metal at sharp points as there is with normal electroplating and the coating is deposited uniformly over the surface of the substrate. The properties of electroless coatings are unique; rather than the pure metal, a proportion of nickel phosphide or boride is deposited (the plating solution consists of: a nickel salt, an organic hydroxy acid and sodium hypophosphite at acid pH-4.5 or alkaline borohydride (7)

The as-plated coating is quite hard and suitable low temperature heat treatment can yield a vikers hardness value of apporximately 800 (8).

A recent advance in coating technology in the field of electroplating is the co-deposition of particles with electro-deposits or, more recently, electroless deposits. This method involves having a suspension of hard particles (eg Aluminium or chromium carbide) dispersed in the electrolyte solution.

By this method, a uniform distribution of these hard particles are caught up in the flow of plating metal towards the substrate and are distributed throughout the finished electroplated deposit.

One of the major restrictions of electroplating as a cladding method, is the necessity for stringent substrate preparations, Ideally the condition of the surface prior to entering the plating electrolyte should be as follows:(9)

1) Completely free from grease and oil.
2) Free from significant oxide and other surface films,
3) Free from gross surface defects.
4) Of Uniform appearance.
5) Having a smooth surface.
6) Free from severe work hardening.

Certain conditions regarding the bulk metal quality are also required:

7) Free from excessive inclusions.
8) Free from porosity.
9) Free from excessive amounts of dissolved gas.

Electroplating is a well established,extensively used method of metal cladding and it is of course, only possible to talk in very general terms about the process in a short review of this sort.

The technique is generally used for thin coatings (see figure 1) and difficulties are often associated with high stress levels in deposits, particularly in the case of chromium which tends to crack (the science of chromium plating makes use of a technique of depositing deliberatly micro-cracked or micro-porous chromium in cases where the natural macro cracking is to be avoided).

Electroplating as a process, lends itself mosteffectively to the field ofcorrosion protection where tne 'state of the art' has advanced from simple cladding of one metal with another, to the complex multilayer plating used extensively in the motor car industry for the protection of zinc die cast 'trim'. The zinc is protected by a layer of copper electroplate, a layer of nickel and a thin top coat of chromium (usually micro-porous or micro'cracked). The galvanic corrosion cell set up tends to slowly corrode away the intermediate nickel layer so that the zinc and the outside chromium surface remain unblemished.

Another difficulty associated with electroplating is concerned with the unavoidable fact that the electrical charge density on the surface of an electrode (the substrate) varies with the geometry of that electrode (10).

These differences in charge density result in changes in the depth the depth of deposit over the surface of the electroplated object. This effect is particularly noticeable at sharp changes in cross section, for example, notches tend to be

Smoothed out of a surface because a notch attracts more plating metal to itself than does the surrounding flat area.

G.5. HOT DIPPING

G.5.1. GENERAL

In hot dipping, the component to be coated is immersed in a bath of the molten coating metal. Reactions then take place between the component and the coating metal to form a layer of intermetallic compounds (generally known as the 'alloy layer') the thickness of which is governed by the nature of the metals involved and the time and temperature of the process. When the component is finally withdrawn from the bath, a layer of molten coating metal remains on its surface. The thickness of this layer is dependant on the melt viscosity, surface tension and solidification rate.

Three general rules given by Gorbunov (11) indicate whether or not a satisfactory coating can be applied to a given substrate: a) The atomic diameters of the coating and substrate metals must differ by no more than 15-16%.
b) The metals of the coating system must have some mutual solubility at temperatures down to room temperature.
c) There must be physical contact between coating and substrate metals during the dipping operation. (ie surface oxides and contaminants must be removed).

The four most commonly produced hot dipped coatings are:-

G.5.2. GALVANISED COATINGS

Zinc coatings are anodic with respect to steel so, unless a barrier layer of corrosion products is produced, as when zinc carbonate is formed in moist air, the life of a coating will be approximately proportional to its thickness. Galvanised coatings vary in thickness from about 25 μm for sheet grades to 50 → 150 + μm on fabricated steel. As corrosion rates for zinc vary from about 1-6 μm/annum depending on the severity of the environment, some indication of the protective lifetime of a coating may be obtained. It should also be noted that the electrochemical current generated by the zinc-iron cell is generally sufficient to protect uncoated regions and cut edges. Applications of galvanising include items such as bridge structural members and power transmission pylons.

G.5.3. ALUMINISED COATINGS

Aluminised steel has good high tempertature oxidation resistance and atmospheric corrosion resistance.

The aluminium-iron phase diagram indicates that at commercial dipping temperatures (-700 C) the aluminium coating and a steel base should be separated by layers of ζ ($Fe\ Al_2$), η ($Fe_2\ Al_5$) and θ ($Fe\ Al_3$), in practice the only phase detected (11) is η which grows rapidly in a characteristic serrated form.

This phase is extremely hard and brittle and coatings produced from 'pure'aluminium baths therefore have some restrictions to their formability. This type of clad material is known as Type 2 aluminised steel,

The addition of between 9.5 and 10.5% of silicon to the melt reduces the depth of the brittle alloy layer and also changes its morphology from serrated to flat. This product has much improved formability and is known as Type 1. Another effect of the silicon addition is to reduce the micro-hardness of the alloy from 900 to 300 HV.

The corrosion protection afforded by aluminised steel arises essentially from its covering of aluminium oxide. This film is tenacious, not easily ruptured and prevents access of oxygen tothe base metal. Its one drawback is the way in which it empedes the sacrificial action of aluminium at cut edges, except in chlorine environments.

Type 1 aluminised steel is used extensively for motor vehicle exhaust systems where its combination of heat and atmospheric corrosion resistance is particularly useful.

Type 2 aluminised steel finds widespread application as an architectural material.

G.5.4. TIN COATINGS

Tin is non-toxic and corrosion resistant and so it is not surprising that its major application as a coating is in the food industry. The coating is also very soft and can aid fabrication in subsequent forming operations. The alloy layer which forms on hot dipped tinplate is $FeSn_2$, the extent of coverage of the steel by $FeSn_2$ is important because within a can of tinplate, anaerobic conditions may exist which can make the tin coating anodic with respect to the steel base. Because of the high price of tin, much tinplate is now produced electrolytically rather than by hot dipping where the coating thickness is larger.

G.5.5. TERNE COATINGS

Lead and Iron together do not form any intermetallic compounds and are almost completely insoluble in each other in the solid and liquid states. It is therefore neccessary to add a third element which reacts with iron to the lead melt to promote wetting. Tin or antimony, which form intermettalic layers on iron of FeSn and FeSb respectively, are both capable of performing this function and 'terne' coatings containing up to 25% tin or 7% antimony are available commercially.

Additions of arsenic, cadmium and zinc to lead-tin, lead antimony or lead-tin-antimony melts have also been claimed to improve coating performance.

The terne coatings are soft and can enhance formability of the product in the same way as tin coatings do. Major applications of terne coated steels are found in the car industry in the production of petrol tanks and under-bonnet fittings. Terne coatings are incapable of providing sacrificial protection to a steel base but the formation of insoluble sulphates, sulphides, carbonates and oxides assist in the blocking of coating pores and slows down the rate of attack.

The primary object in hot dip coating steel is to improve its corrosion resistance. The process lends itself well to mechanisation and production line techniques. Hot dip coating is the oldest coating technology, it remains one of the most important for the protection of ferrous metals from their environment.

G .6 Cladding by Rolling

The mechanism of roll cladding obvious; the cladding material and the substrate are initally joined by welding along their edges and then repeatedly rolled to a combined thinner section, the pressure and interfacial friction resulting in an interfacial bond.

The 'Colclad' process used by B.S.C. (12) uses just this principle to produce large sheets (11m x 3.3m x 5cm for example) of mild steel clad in a number of materials including stainless steels and nickel alloys. Applications include brewery equipment and water turbines. The bond produced at the substrate caldding interface is a result of mechanical working on that interface and so there is no dilution problem associated with the product but the degree of bonding is poor in comparison with other cladding processes. The colclad product comes in three grades A,B and C, and these have differing amounts of permissable area percentages of unbonding; 10% 4% and 2% respectively. These figures for permissable interfacial porosity are rather high in comparison with other cladding techniques. One further disadvantage of the process is the time involved in production, the whole process takes several weeks for each plate which, of course, renders the finished product rather expensive.

G .7. THERMAL SPRAYING TECHNIQUES

G 7.1. GENERAL

The four main types of thermal spraying techniques are (13):

a) Flame spraying
b) Arc spraying
c) Detonation spraying
d) Plasma spraying

Although they differ in detail, all generally involve three features:-

1) The material to be sprayed is heated and this becomes substantially molten.
2) The molten material is projected onto the base material.
3) The projected material adheres to the substrate to give the required cladding.

The four main types of thermal spraying are shown in figure 4 and will now be discussed separately.

G.7.2. FLAME SPRAYING

The bulk of commerical production is based on flame spraying, using oxygen-gas mixtures as the fuel and powder or, more usually, rod or wire as the feed.

In all metal spraying, adhesion is generally acheived by a mechanised keying action so the substrate needs to be prepared to have a clean, uniformly rough surface. Various abrasives may be used. Flint and steel being common for the removal of the bulk of the scale, Flame cleaning is used to remove grease and dirt and to reduce the last of oxide on the surface. If the spraying is being used on worh out parts of machinery, then further preparation may be required, including acid pickling and etching. With proper precautions, a fairly dense and reasonable adherent coating can be produced. Bond strength and density can be increased by melting and consolidating the sprayed on layer (see section 2.3.2.3.) the coating material may contain fluxing additions to facilitate this. The equipment for flame spraying is cheap and consiquently, capital costs are low.

The process suffers from two major limitations:
Firstly, the flame temperature is too low to melt the more refractory metals and many ceramics; secondly, the substrate tends to be heated by the flame and this may cause difficulties with workpiece distortion, as well as theuse of low melting point substrates.

G 7.3. ARC SPRAYING

A complementory process to the flame method is arc spraying in which the material to be sprayed (which must be available as rod or wire and be electrically conductive) forms the consumable electrodes of the gun (see figure A4). The molten particles are blown, usually by an air blast, against the

substrate and since the gun can reach a higher temperature than the oxy-acetylene flame, marginally denser coatings are produced. Arc spraying has a higher capital cost than flame spraying but running costs are claimed to be lower. (13)

G .7.4. DETONATION SPRAYING

The high quality requirements of the aircraft, aerospace and electronics industries have stimulated the development of spray processes which give superior results to flame and arc spraying. The detonation process was developed from studies of flame propogation in tubes. The coating powder amd carrier gas are fed into an oxy-acetylene gas chamber in which detonation occurs some four times per second; this produces high velocity impingement and gives very dense coatings with excellent adhesion. However, the process is the most expensive of all the thermal processes and has more geometrical limitations on the substrate than the others.

G.7.5. PLASMA SPRAYING

To create plasma conditions a suitable gas is passed through a high current arc; at sufficiently high temperatures, the gas becomes ionised and collisions between electrons and ions generate radiant energy. In a plasma torch, the thermal balance is changed by constricting the arc, and this raises the temperature substantially, usually to 15,000 - 20,000 K. The very high temperatures in the plasma torch allow any material to be sprayed, provided it melts without significant

dissociation and a practical temperature interval exists between its melting and boiling points. The absence of direct substrate heating minimises the problem of work piece distortion and allows the use of low, as well as high, melting point bases. The process is thus remarkably versatile; it may be used to spray metals and alloys, ceramics, cerments and plastics, while the substrate may be of metal, ceramic or plastic. Plasma deposits can vary in thickness from less than 0.03mm to more than 2.5mm; normally being in the 0.10 - 0.60 range (13). Due to the high particle temperatures and the rapid impingement on the target, the coatings are usually dense and adherent, porosities as low as 1% being common. The presence of an inert gas atmosphere minimises oxidation of the coating. Within limits, the properties of the deposit can be varied to suit particular applications, eg. a controlled degree of porsity may be incorporated to enhance oil retention for bearing applications.

Plasma coatings are being increasingly used for wear and abrasion resistance, electrical conduction, thermal and electrical resistance, reclamation of worn parts, repair of wrongly machined components and, in certain cases, corrosion resistance. In addition to surface treatment applications, the process is also finding growing use for the production of free-standing shapes in which case steps are taken to prevent the deposit adhering firmly to the substrate.

Plasma spraying has been successfully employed as a means of hard facing the shoulder of internal combustion engine

exhaust valves (14). Advantages over arc or oxy-aceylene surface welding processes included the promotion of rapid and highly directional solidification from the weld interface to the deposit surface. This effect is due to the concentration of the heat of the process into the deposit. The deposits are consequently free of micro-shrinkage and have smooth as welded surface. Dilution effects were, of course, much reduced and the finished product had superior qualities in general.

In summary, table 2 shows various advantages and limitations of the various thermal spraying processes.

FIGURE .4.

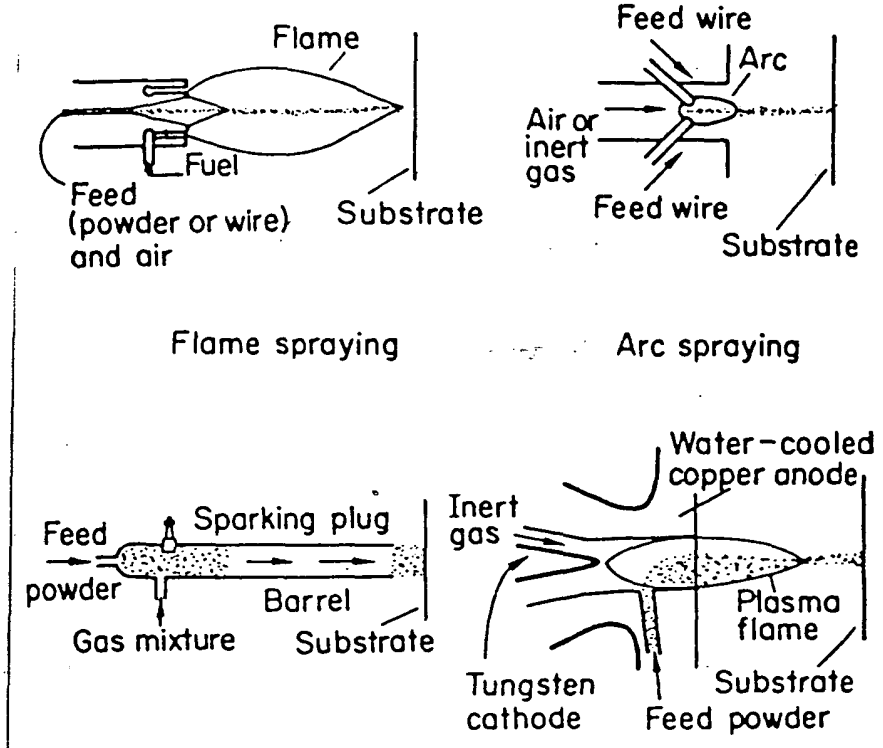

Features of thermal spraying processes.

TABLE 2

Features of thermal spraying processes

PROCESS	FLAME	ARC	PLASMA	DETORATION
Imp ingement speed m/sec	100	100	150	800
Temp K. (Approx)	3,000	5,000	20,000	4,000
Typical Deposit Poronty %	10-15	10-15	1 - 10	1 - 2
Typical Adherence MN/M^2	7	10	30	60
Advantages	Cheap High Deposition rates	Cheap Low Contamination Cool substrate	Low Porosity Good Adhesion Versatile Cool substrate Low Contamination	Very low Porosity very good adhesion Cool Substrate
Disadvantages	Normally high porosity Inferior adhesion Heats work piece Limited	Only electrical conductors normally high porosity	Fairly Expensive	Very Expensive Low Efficiency

G.8. CHEMICAL VAPOUR DEPOSITION

G.8. GENERAL

Chemical Vapour Deposition (CVD) may be described as the ntrolled precipitation of material brought about through an induced vapour phase chemical reaction (15).

A plating vapour or mixture of plating vapours is led, under controlled mass flow and at a defined pressure, into a plating chamber which contains the article to be coated. The plating chamber may be maintained at a suitably elevated temperature, or the article may be heated independently of the chamber, eg by induction heating. An essential requirement of the CVD method is the availability of an appropriate vapour source and of a suitable chemical reaction whereby these sources can be made to yield the chemical coating product. Examples of vapour sources of acceptable volatility include halides, carbonyls, carbonyl halides, oxychlorides and organo-metallics. Of these the halides are the most widely employed, primarily because they generally give better quality coatings than other sources.

Many of the chemical reactions employed in CVD have features in common and can be grouped together into reaction types:

G.8.2. HYDROGEN REDUCTION OF HALIDES

The first and most important group of reactions includes those involving metal halide vapours, which are reducable by hydrogen at practical temperatures of interest, eg:

Element	Reaction	Deposition Temp ^{o}C
B	$BCl + {}^{3}/_{2}\ H_2 = B + 3HCl$	1200 - 1500
Mo	$MoF_6 + 3H_2 = Mo + 6HF$	700 - 900
1r	$1rF_6 + 3H_2 = 1r + 6HF$	700 - 900

Other coating materials include:

Elements: Si, V, Nb, Ta, W, Re, and Pt.

Compounds: AL_2O_3, BN (hex), B_4C, BP, $B_{13}P_2$, SiC, Si_3N_4, TiC, TiC/TiN and W_2C.

The extensive use of halides in reduction reactions arises from their ready availability, ease of volatilisation, reductability and low cost, coupled with their effectiveness in producing coatings of an acceptable quality. The majority of reduction reactions require temperatures above the softening points of most steels, which is a severe limitation for many potential applications in engineering. The deposition of tungsten carbide (W_2C) from tungsten hexafluoride, hydrogen and carbon monoxide (16) or benzene (17) (at temperatures of between 500 ^{o}C and 600 ^{o}c) is an exception which is now under development.

G.8.3. THERMAL DECOMPOSITION REACTIONS

A second important group of reactions comprises those from which coatings are produced as a result of the thermal decomposition of plating vapour. The temperatures of decomposition vary widely. The carbonyls, organometallics and some of the hydrides can be decomposed at low temperatures, well below the softening point of steels. For example, Aluminium coatings can be obtained from the aluminium alkyles (eg tri-iso butyl-

aluminium) at a temperature of approximately 250°C (15).

However, thermal decomposition of hydrocarbons is frequently conducted at temperatures above 2000°C in order to produce well orientated pyrolytic graphite deposits.

Coating materials include:

Elements: B, Al, C Si, Mo, W, Cr, Ti, Zr, Hf and Pt.

Compounds: Al_2O_3, BN, SiC and Si_3N_4.

Future CVD processes based upon thermal decomposition reactions appear to have considerable scope once the major constraints currently limiting their successful application have been overcome. This is particularly true in the case of organo-metallics, some of which are able to form coatings at temperatures in the range 50°C to 150°C. Current constraints include the contamination of metal with carbon eg carbon in Chronium deposits, inadequate adhesion and co-hesion, availability and cost.

G.8.4. CHEMICAL TRANSPORT REACTIONS

A third important group includes those reactions where de-position occurs as a result of chemical trans port. This may be illustrated by reference to the following equilibria:

$$SiCl_4(g) + Si\ (c) \rightleftharpoons 2Si\ Cl_2(g) \qquad (18)$$

$$BF_3\ (g) + 2B(c) \rightleftharpoons 3BF\ (g) \qquad (19)$$

At suitably high temperatures, silicon tetrachloride vapour will react with silicon to produce a gas mixture containing a proportion of silicon dichloride vapour. The extent of conversion increases with increasing temperature and decreasing pressure. If this vapour mix is sufficiently cooled, reversal of the reaction will occur and silicon will be precipitated.

The chemistry of transport reactions and their applications have been studied extensively by Schafer (20), who has derived ground rules as an aid to determining the feasability of transport and the conditions under which transport is best carried out. A major application of transport reactions has been in the vapour phase growth of electronic materials, and the production of quartz-halogen lamps.

G.8.5. CVD PROTECTIVE APPLICATIONS

Chemical vapour deposition can be can be carried out at rates ranging from micrometers to millimeters per hour of coating depth. The deposition rates are closely related to the thermodynamics and kinetics of the reactions involved. The preparation of sub-micron coatings which are continuous is generally limited by the grain size of the crystalline deposit. Within a process, grain size shows a dependence upon process parameters, increasing temperature and decreasing pressure tending to favour a larger grain size, but generally wide control of grain size has so far not been achieved.

CVD usually operates in a pressure range around 1 torr to 1 atmosphere, which provides good 'throwing power' for the coating of complex shapes and internal surfaces. CVD coating of long narrow holes is routinely practised.

Under controlled deposition conditions CVD coatings are usually free of voids and since the vapours used are of high purity the coatings are, in general, very pure themselves. In the development of coatings for corrosion protection both these features are very advantageous because they result in a very low permiability. CVD tantalum has excellent corrosion in acid media and has been used on the base of steel tubes, on valves and thermowells. Pure aluminium from metal alkyds has been applied to steel, nonferrous metals and high temperature stable plastics for corrosion resistence.

Steel tools coated with a hard facing if CVD titanium carbide and other hard CVD compounds (TiN, TiC/TiN) are well known as are CVD metallised coatings produced by aluminising, chromising, siliconising andcoronosing.

Adhesion of CVD coatings shows considerable variation. In many diffusion-type coatings, adhesion is good. Also in many high temperature halide processes, where a small amount of diffusion between coating and substrate is possible, acceptable bonding can be achieved. Brittle diffusion interfaces can however, produce failure. At medium and low temperatures ($600^{o}C$ to $300^{o}C$) many CVD coatings are only poorly bonded to substrates. This has been ascribed to various factors (21), including in particular, the formation or presence of corrosion layers on the substrate surface. Improved adhesion has been achieved by the use of interlayers to which the CVD coating is more strongly bonded.

Many CVD coatings show an oriented columnar growth with grain sizes in the range 0.01 to 10 micrometer. The presence of

columnar growth in brittle materials represents a structural weakness and attempts have been made to deposit more equiaxed structures but so far success has been very limited.

G.9. PHYSICAL VAPOUR DEPOSITION

G.9.1. VACUUM DEPOSITION

The development of vacuum technology has made it possible to commercially utilise hard vacuums ($< 1\mu m$ mercury) in order to evaporate a cladding material with the aim of depositing the vapour onto a substrate. The method is most satisfactory for cladding metals of low melting point and high vapour pressure. The evaporating metal is resistence heated inside the vacuum chamber. The deposition rate depends on the cladding metal but for Cd or Zn, 0.01 mm can be built up in 10 mins, while for Cu, Al or Pt it may take almost an hour (22). Good control of thickness and distribution is possible and deposits are usually smooth, coherent and highly reflecting. Alloy formation can be completely avoided and the corrosion resistence may be twice as good as the same thickness of electrodeposit by virtue of reduced porosity. There is considerable interest in the application of vacuum vapour deposition to the continuous coating of steel strip to a thickness of about 10^{-4} cm (ie tinplate thickness) (23). Both aluminium and aluminium-zinc co-deposits have been assessed, but by comparison with tinplate the porosity would appear to be too high at the equivalent thicknesses. There is a 'sister technique' to straight forward physical vapour deposition which should be summarised at this point.

6.9.2. CATHODIC SPUTTERING

This technique does not involve the use of such a hard vacuum, 10-100mm being sufficient. Low vapour pressure materials are clad in this way by making them the cathode in a 400V (approx) arc. The cathode disintegrates on the pressure and voltage as well as on the atmospheric gas in the chamber. Heavier inert gases may increase the rate by ten times or more and also obviate oxidation. The deposits tend to be fine grained, adherent and coherent and at about 10-3mm thickness are essentially pore free. Interest in superior sputtering techniques has been quickened by the electronics industry, the requirements being to develop epitaxially grown semi conductor films and to deposit thin metal films on plastics. Low energy ion sputtering techniques enable both metals and ceramic materials to be deposited on any substrate and by superimposing radio frequensies on a cathode type process the rates of deposition can be increased tenfold or more.

Both of these cladding methods produce good quality results at a rather high cost and thus, industrial applications tend to be in those fields where economics is a secondary consideration. It may also be noted here that these two vacuum deposition processes are only relevant to the deposition of thin films, generally much thinner than 0.1mm.

6.10. ION IMPLANTATION

6.10. GENERAL

Ion implantation provides a means of introducing chosen atomic species into the surface layers of a material or component without the need for heating. Atomic species which impart

protection against corrosion, such as nickel, chromium or rare earths can be implanted. Atoms which form strong inter-atomic bonds, such as nitrogen or carbon, will harden a metal surface and improve wear resistence. Various mechanisms result in a protective layer which far exceeds in thickness the range of the implanted ions.

The chosen atomic species are first ionised and then accelerated in an electric field, to energies which usually range from a few tens to a few hundred kilo electron volts in a moderatly hard vacuum (10-5 torr), towards the workpiece.

The accelerated ions penetrate the surface of the workpiece and lose energy by collisions with the atoms of the substrate and by electrobic excitation processes, coming to rest in an approximalty gaussian distribution about a mean penetration depth (24). The penetration depth is very shallow eg 100mm depth for nitrogen ions of 100KeV energy implanted into ion. (25).

G .10.2. CORROSION RESISTENT SURFACES

Small amounts of beneficial alloying species can have a profound effect upon the corrosion behaviour of a metal. Ion implantation introduces the dosen metallic species into the surface layers of the substrate without interferring with the bulk properties. The alternatives eg electroplating, galvanising etc all have a distinct substrate-surface layer interface which is acceptable to corrosion once the coating is pierced. Ion implanation is effective in inhibiting both thermal and aquerous corrosion, subjects which should be discussed seperately.

6.10.2. THERMAL OXIDATION PROTECTION

The initial stage of oxidation of a metal is a chemical interaction between it and the gaseous environment, in which surface migration and the nucleation of the oxide film are very important. This stage is usually very rapid, and may indeed be complete before the ion bombardement begins. The number of nucleation sites involved can determine the grain boundary distribution and degree of epitaxy of an oxide and it is by modification of these surface conditions that a long term reduction in oxidation is achieved. Vacancy clusters and dislocation networks are the chief result of heavy ion bombardment in metals, and the final state of the material is not unlike that which would result from cold working. (26).

The second stage of oxidation is a progressive thickening of the oxide by processes which involve either the transport of oxygen inwards, to interact with the metal, or of metal cations outwards, to interact with oxygen at the outer surface. Since this matter transportation is usually by means of charged ions, there must be a corresponding flow of electronic charges in the form of electrons or 'holes'. Corrosion protection by ion implanation is achieved either by hampering the movement of ions through the oxide or, in the rarer cases in which electronic transport is rate determining by reducing the mobility or number of such carriers.

Yetrium and rare earth elements have been shown (27) to bring about useful reductions in the high temperature oxidation of hrmium containing steels. Normally these elements would

degrade the ductility and tensile strength of the alloy but when they are ion implanted into the surface layer a long lasting protection is achieved without impairing the bulk properties.

The yetrium is found to be carried forward, near to the metal oxide interface and probably acts by formation of the perovskite YCrOz which may serve as an impermiable barrier to chromium out-diffusion.

Another example of this effect is that the thermal oxidation of titanium was reduced (27) by implantation of alkaline earth and rare earth species. Ion size emerged as a significant parameter as well as electronegatiority. It seems that in this case perovskites ($SrTiO_2$ and $EuTiO_2$) were again the corrosion inhibiting phase, achieving their end by blocking pathways which normally allow rapid ion transport.

6.10.2.2. AQUEOUS CORROSION

A research group at U.M.I.S.T. has investigated the effects of ion implantation into iron and aluminium. Chromium (28) has a beneficial effect in iron, behaving in the same manner as in a bulk alloy of the same surface composition. Tantalium, normally insoluble in iron, has an even stronger effect, as had been expected. Molyldenum ions were found to inhibit the pitting corrosion of both stainless steel and of aluminium. This is an interesting result since it suggests that it is a direct consequence of the Mo, and not an indirect effect of formation of intermetallic inclusions during alloying.

G.10.3 WEAR RESISTENT SURFACES

The basic principle in this application is to introduce into the surface of a metal a fairly high concentration of species which will form strong inter-atomic bonds with the host atoms and which will also impede the movement of dislocations. This, of course, is precisely the function of conventional nitriding ot carburising and it is not surprising that implanted N^+ or C^+ ions have a similar effect in ferous alloys.

In a normal wear situation, the load is not carried by the whole bearing surface but by many small asperities, and the true area of contact is only a minute fraction of the surface area. Frictional work dissipated at these asperities will result in significant temperature rises of up to several hundred degrees centigrade (29). Since the peak Hertzion stresses lie a little below the surface this is where dislocations are most readily formed and it is also in this region that the temperature will be at a maximum. Mobile inter species such as nitrogen or carbon will tend to migrate towards this zone and associate themselves with the dislocations and thereby impede their movement.

This process, creating what has been referred to as a 'Cottrell atmosphere' has been proposed as the explanation of strain ageing in steel (30). Thus, during wear, mobile implanted atoms will tend to diffuse into the dislocated region and will harden it, an effect which can be expected to improve wear resistence in precisely the zone in which it is needed.

Conventional nitriding and carburising operate rather differently by formation of hard nitrides and carbides in a steel matric. In the ion implantation case this is not necessary, since the interstitial dissolved nitrogen or carbon is effective by itself. It is this difference which makes it possible to improve the wear resistence of even gas nitrided steel by nitrogen implantation.

Ion implantation equipment is costly and sophisticated even though it is not necessary to achieve as high a beam purity or uniformity when ion implanting for corrosion or wear resistence as it is when ion implanting semi-conductors for specific electrical properties.

The implantation of semi-conductors is the most widely used application of the technique and the amending of such implanted devices is a recent industrial application of lasers (see section on laser surface treatments).

A major limitation on the use of ion implantation as a method of corrosion or wear resistence is the need for a hard vacuum which reduces the suitability of the process to industry considerably.

References

1. D R Andrews and R Sharma. 'Surfacing of forging dies and tools by welding'. Metallurgia September 1978. 591

2. T C Wells 'An introduction to surface coatings and treatments. Surface treatments for protection. Inst of metallurgists Series No 3 No 10 April 1978.

3. M F Jordan. 'Weldability of materials'. Chapter 5 of Soldering Brazing Welding and Adhesives. Ed D R Andrews : 1 Prod E.

4. 'Kelomet, metal clad by explosive'. ICI. Nobels Explosive Company Limited. Commercial literature and private correspondence.

5. BS 4641, 1970 Electroplated coatings of chronium for engineering applications.

6. IRA Christie. 'Electroplating : a brief review' Surf treat for protection. Inst Met Series 3 No 10 1978.

7. A Brenner and G Riddell., Proc Amer Electroplaters Society 34 156.

8. C Baldwin and T E Such. Trans Inst Metal finishing 1971 49 105.

9. E H Reid and W Goldie., Gold plating technology. Electrochem Pub 1974 105.

11. R D Jones. 'Hot dip coating processes. Surf treat for protection. Inst Met Series 3 No 10 42-55

12. 'COLCLAD' British Steel Corporation literature.

13. R F Smart and J A Catherall. 'Plasma Spraying'. M & B technical library TL/ME/3.

14. W M Matlock J F Nocis and A T Vitcha 'plasma arc hard facing exhaust valves with an iron base alloy'. Metal Progress. May 1978.

15. C Hayman. 'An introduction to chemical vapour deposition'. Surf treat for protection. Inst of Met Series 3 No 10.

16. D A Tarver. US Patent 3574672. 1971.

17. R H Lewin and C Hayman. Brit patent: No 1326769 (1973) US Pat No 3814625 (1974).

18. W A Bryant J Mat Sci 12. 1285. 1977.

19. K K Yee. Int Metals Rev No 226. 1. 19.

20. J H Burston and J D Fleming: 'Proceedings of Conf on CVD Amer Nuc Soc. Hinsdale Il USA 1967. 57.

21. M R James Metallurgist, 1977. 9. 483.

22. D R Gabe. 'Principles of metal surface treatment and protection'. Perga,on Press.

23. W N Jenkins. Sheet Metal Industry. 1968. 45. 329.

24. G Dearnaley and P D Goode. 'ion implantation for combating wear and corrosion'. Surf treat for protection. List of Met. Series 3. No 10.

25. J Lindhard., M Scharff and H E Schistt. 1963 Kgl Danske Vid Selsk., Matt - Figs Medd. 33 No 14.

26. P D Goode. List of Phys. Conf Series No 28. 154 1976.

27. J E Antill. et al. 'Ion implantation in semi conductors and other material'., ed B L Crowder, Phenum Press. 1972.

28. V Asworth et al. 'Ion implantation in semi conductors' ed S Nambra, Phenum Press. 1975.

29 G Dearnaley and P D Goode. 'Ion implantation for combating wear and corrosion'. Surf treat for protection. List of met Series No 3. No 10.

30. A Cottrell. 'Introduction to Metallurgy'. Arnold. London

31. J E Harry. 'Industrial lasers and their applications'. McGraw Hill.

32. I J Spalding. 'High power lasers for processing of materials' - a comparison of available systems. Optics and laser tech. Feb 1978.

33. N Bloembergen. 'Fundamentals of laser-solid interactions'. AIP conf proc No 50. 1978.

34. J F Ready 'Industrial applications of lasers'. Academic Press 1978.

35. W W Duley 'CO_2 lasers effects and applications'. Academic Press.

36. E V Locke and D S Gnonamuthu'. SME Technical paper MR 74 - 706. 1974.

37. J M P C Megaw and A S Kaye. Proc Laser 77 opto-electronics conf Munich.

38. C D Desforges. Proc laser 78 conf London.

39. F D Seaman and D F Granamuthu. Met Progress Aug 1975. 108

40. Caterpillar tractor Co. 'Method and apparatus for fusibility bonding and coating material to metal article. Patent No 1482044.

41. UK Patent application GB 2 052,566A. 'Laser application of hard surface alloy'. 1980.

42. W M Steen and C G H Courtney. 'Hardfacing of Nimonic 75 using a 2KW CW CO_2 laser. Metals Tech June 1980. 232.

43. D S Gnanamuthu. 'Laser surface treatment'. Proc conf. Applications of lasers in materials processing. 1979. Amer. Soc. for Metals.

44. Koji et al. Rhenium film preparation by laser melting. J Appl Phys 51 (5) May 1980. 2903.

45. R J Schaefer and J D Ayers. 'Laser spraying' US Patent 4,200,669. April 1980.

46. S M Copley, D Beck, O Esquivel and M Bass. 'Laser melt quenching and alloying'. AIP conf 50. 161

47. F D Seamon and D S Gnanamuthu. 'Using the Industrial laser to surface harden and alloy. Metals prog 1975. 108 (8) 67-74.

48. D A Belforte. 'High power laser surface treatment'. SME Paper No 1077-373.

49. M Bennett and W M Steen. 'A preliminary study of surface alloying using a laser'. Final report of an investigation for Rolls Royce Oct 1976.

50. J D Ayers and R J Schaefer. SPIE vol 198 'Consolidation of plasma sprayed coatings by laser remelting'. Lasers Applications in materials processing.

51. G C Irons. 'Laser fusing of flame sprayed coatings'. Weld J Dec 1978. 29.

52. D S Ganamuthu US Patent No 3952180. 1976.

53. R J Shaefer, T R Tucker and J D Ayers. 'Laser surface melting with carbide particle injection'. Laser and electron

beam processing. eds: C A White and R S Peercy. Academic Press.

54. J D Ayers, T R Tucker and R J Schaefer. 'Wear resisting surfaces by carbide particle injection'. Rapid solidificarion processing, principles and technologies: eds B H Kear and M Cohen. Claitors publishing division. 180.

55. J D Ayers, T R Tucker and R C Bowers: 'A reduction in the coefficient of friction for Ti-GAI-4V'. Scripta Metallurgia vol 14 pp 549-550. 1980.

56. J D Ayers and T R Tucker. 'Particulate-TIC-hardened steel surfaces by laser melt injection'. Thin solid films, 73 (1980) 201.

57. J Mazumder and S D Allen. 'Laser chemical vapour deposition of titanium carbide'. SPIE. vol. 198. Laser applications in materials processing (1979) 73.

58. T Takahashi and M Itoh. J Electrochem Soc. Vol 124. 1977. pp 797.

59. S D Allen. 'Laser chemical vapour deposition of metals and insulators'. 1979 IEEE/OSA Conf on laser engineering and applications. Session 7.

60. W M Steen. 'Surface coating using a laser'. Paper 3 Conf. Advances in surface coating technology, Welding Inst. London, Feb. 1978.

61. M S Hess and J F Milkosky. 'Vapour deposition of platinum

using C W laser energy. J Appl Phys. Vol 43 No 11 4680.

62. G Hass and J B Ramsey. 'Vacuum deposition of dielectric and semi-conductor films by a CO_2 laser. Applied optics Vol 8 No 6. 1115.

63. J T Cox and G Hass. 'Physics of thin films'. eds: G Hass and R E Thurn. Academic Press Inc Vol 2. 239.

64. J F Hall Jr. J Opt Soc Amer 47. 622. H M Smith and A F Turner. Appl Opt 4, 147.

65. S V Gapanov et el. 'Morphological features and strucure of films condensed from a laser plasma. Sov Phys Solid State 19 (10) Oct 1977.

66. B V Bondarenko and A A Shchuker. 'Resistivity and structure of tungsten, molybdenum and chronium films prepared by laser evaporation. Fiz metal metalloced. 30. No 1. 207-210. 1970.

67. J Kamalu. Laser cutting of mild steel. Ph.D. thesis, 1981, Imperial College.

68. S Murphy. E.P.M.A. of Laser clad valves. Aston University, private communication.

69. T Anthony and H Cline. J. Appl. Phys. 48, 9 (1977), 3888.

70. S Copely, D Beck, O Esquivel and M Bass. Proc. Conf. 'Lasers in Metallurgy', A.I.M.E., Chicago, 1981.

71. A model for surface tension driven fluid flow in laser surface alloying. C Chan, J Mazumder (to be published).

72. A A Grudz et al 'Reducing the welding stress in plates by vibration' Aut Svarka 1972, No.7, 75.

73. G G Saunders, V.S.R. A current state of the art appraisal. paper 29, page 173.

74. W M Steen and R Rawlings 'Acoustic Emission in Monitoring of surface hardening by laser' to be published.

75. D P Shukla et al 'Effect of Vibration on the formation of porosity in Al ingots. Metallurgical transactions, vol.11B, March 1980, 166.

76. J Powell and W M Steen 'Vibro Laser Cladding' "Lasers in Metallurgy" conf. proc. A.I.M.E., Chicago, 1981.

77. J Powell and W M Steen 'Recent advances in laser cladding quality' Opto electronic conf. proc., Munich, 1981.

78. Fusing Cladding material to a substrate. U.K. Patent application G.B. 2090873A.

79. J F Lancaster. The Metallurgy of welding, brazing and soldering. G Allen and Unwin (pub).

Acknowledgements

The author would like to thank the following people for their invaluable assistance in the production of this work.

Dr. W.M. Steen

Paul Henry

Clem Young

Trish Clarke

Rolls Royce Aero Engines.

Deloro Stellite Limited. British Steel and British Leyland.

The technical and academic staff of the J. Percy Group. (especially Jim, Pam, Alec, Russell and Roy)

All members of the Imperial College

Laser applications group (past and present)

And of course my family and friends (especially Di Morgan)

Can I go home now?